



Durham E-Theses

The engineering properties and mechanical behaviour of fibre reinforced clay

WANG, JIANYE

How to cite:

WANG, JIANYE (2020) *The engineering properties and mechanical behaviour of fibre reinforced clay*, Durham theses, Durham University. Available at Durham E-Theses Online:
<http://etheses.dur.ac.uk/13589/>

Use policy

The full-text may be used and/or reproduced, and given to third parties in any format or medium, without prior permission or charge, for personal research or study, educational, or not-for-profit purposes provided that:

- a full bibliographic reference is made to the original source
- a [link](#) is made to the metadata record in Durham E-Theses
- the full-text is not changed in any way

The full-text must not be sold in any format or medium without the formal permission of the copyright holders.

Please consult the [full Durham E-Theses policy](#) for further details.

Academic Support Office, Durham University, University Office, Old Elvet, Durham DH1 3HP
e-mail: e-theses.admin@dur.ac.uk Tel: +44 0191 334 6107
<http://etheses.dur.ac.uk>

The Engineering Properties and Mechanical Behaviour of Fibre Reinforced Clay

Jianye Wang

Thesis submitted as partial consideration towards the degree of
Doctor of Philosophy



Sustainable Infrastructure Group

Department of Engineering

Durham University, Durham

United Kingdom

March 2020

The Engineering Properties and Mechanical Behaviour of Fibre Reinforced Clay

Jianye Wang

ABSTRACT

Embankment slope failure due to insufficient strength, weak bearing capacity, excessive deformation and desiccation cracking of problematic soils is commonly observed on the UK road network, and this leads to huge expenditure in the maintenance and repair of highway projects every year. It is necessary to reduce these engineering problems and economic losses through environmentally and economically friendly methods.

Previous studies have shown that randomly distributed fibres can significantly improve various soil properties. However, there is a lack of comprehensive study on the engineering properties of fibre reinforced high plasticity clay. Also, limited mechanical models have been proposed for predicting the shear strength behaviour of fibre reinforced clay.

In order to investigate these problems, a series of laboratory investigations including compaction, bearing capacity, one-dimensional consolidation, linear shrinkage, desiccation cracking, direct tensile strength, triaxial compression tests were conducted on unreinforced and polypropylene fibre reinforced London Clay. A mechanical model was proposed for predicting the shear strength of fibre reinforced clay.

The experimental results showed that fibres can significantly improve the engineering properties of London Clay. As fibre inclusion ratio increased, the bearing capacity, coefficient of consolidation, tensile strength and shear strength of the soil increased; the compression index, swelling index, linear shrinkage and desiccation cracking area of the soil decreased. As fibre length increased, the bearing capacity and desiccation cracking area of the soil decreased; the tensile strength and shear strength of the soil increased. The mechanical model was proposed based on the conception of equivalent confining stress and the predicted stress-strain-pore water pressure response and stress path behaviour of fibre reinforced soil were compared with the experimental results. The comparisons showed that the model was capable of predicting the shear strength behaviour of fibre reinforced clay.

TABLE OF CONTENTS

ABSTRACT	ii
TABLE OF CONTENTS	iv
LIST OF SYMBOLS	vii
DECLARATION	ix
SATEMENT OF COPYRIGHT	x
ACKNOWLEDGEMENTS	xi
1. INTRODUCTION	1
1.1 Background of study	1
1.2 Aims and objectives	2
1.3 Scope of the study	4
1.4 Structure of the thesis.....	5
2. LITERATURE REVIEW	7
2.1 Soil reinforcement	7
2.2 Laboratory investigations of fibre reinforced soil.....	9
2.2.1 Shear strength	11
2.2.2 Tensile strength	28
2.2.3 Unconfined compressive strength	29
2.2.4 Compaction.....	31
2.2.5 Bearing capacity	33
2.2.6 Swelling and consolidation	34
2.2.7 Shrinkage and cracking	36
2.2.8 Summary	39
2.3 Full scale tests and engineering applications	39
2.3.1 Pavements.....	40
2.3.2 Foundations	41
2.3.3 Embankments	42
2.3.4 Seismic applications	43
2.3.5 Summary	43

2.4 Modelling fibre reinforced soil	44
2.4.1 Analytical models of fibre reinforced soil	44
2.4.2 Numerical models	58
2.5 Chapter summary	62
3. EXPERIMENTAL TESTING PROGRAMME	64
3.1 Introduction	64
3.2 Materials	65
3.2.1 London Clay	65
3.2.2 Fibres	67
3.3 Soil mixing	70
3.4 Testing program	72
3.4.1 Compaction tests	72
3.4.2 CBR tests	73
3.4.3 Consolidation tests	74
3.4.4 Linear shrinkage tests	76
3.4.5 Desiccation cracking tests	77
3.4.6 Direct tensile tests	80
3.4.7 Triaxial tests	82
3.4.8 Summary	85
4. COMPACTION AND CONSOLIDATION PROPERTIES OF FIBRE REINFORCED CLAY	86
4.1 Compaction tests	86
4.2 CBR tests	88
4.3 Consolidation tests	91
4.4 Chapter summary	97
5. DESICCATION CRACKING AND TENSILE STRENGTH OF FIBRE REINFORCED CLAY	98
5.1 Linear shrinkage tests	98
5.2 Desiccation cracking tests	101
5.2.1 Image analysis processing	101
5.2.2 Crack intensity factor and cracking initiation	102

5.2.3 Crack development and crack patterns	107
5.3 Direct tensile tests	115
5.3.1 Tensile strength improvement	115
5.3.2 Stiffness behaviour	119
5.3.3 Failure patterns	124
5.3.4 Suction behaviour	126
5.4 Chapter summary	128
6. SHEAR STRENGTH BEHAVIOUR OF FIBRE REINFORCED CLAY	130
6.1 Data processing	130
6.2 The effect of fibre on deviator stress and pore water pressure behaviour of soil	134
6.2.1 Effect of fibre inclusion ratio	134
6.2.2 Effect of fibre length	142
6.2.3 Effect of cell pressure	149
6.3 The effect of fibre reinforcement on stress paths of soil	154
6.3.1 Effect of cell pressure	154
6.3.2 Effect of fibre inclusion ratio	159
6.3.3 Effect of fibre length	164
6.4 The effect of fibre reinforcement on failure mode of soil	169
6.5 Chapter summary	173
7. TOWARDS A PREDICTIVE MODEL OF THE SHEAR STRENGTH BEHAVIOUR OF FIBRE REINFORCED CLAY	175
7.1 Basis of the model	175
7.1.1 Assumptions	175
7.1.2 Definitions	176
7.1.3 Equivalent confining stress in a CU triaxial test	177
7.2 Model derivation	179
7.2.1 The tensile force carried by a single fibre	179
7.2.2 Total tensile force of all fibres	181
7.2.3 Total equivalent confining pressure	186
7.2.4 Model calibration	188
7.2.5 Predicting stress-strain behaviour using the model	192

7.3 Comparison of predicted and experimental results	195
7.3.1 Stress strain behaviour	195
7.3.2 Pore water pressure behaviour	199
7.3.3 Stress path behaviour	203
7.4 Chapter summary	207
8. CONCLUSIONS AND RECOMMENDATIONS	209
8.1 Thesis and discussion and conclusions	209
8.2 Implications of the research in civil engineering applications	211
8.3 Recommendations for future work	212
REFERENCES	215

LIST OF SYMBOLS

Symbol	Definition
A_f^1	cross section area of single fibre
A_f^θ	total cross section area of fibres in θ
c	cohesion of the soil
C_s	swelling index
C_c	compression index
c_v	coefficient of consolidation
D_{50}	median diameter of soil
d_f	diameter of fibre
e	void ratio
E_f	elastic modulus of fibre
$F_{rf}^1(\theta)$	tensile force in radial direction carried by single fibre
$F_{rf}(\theta)$	total tensile force in radial direction carried by fibres in θ
F_{rf}	total tensile force in radial direction carried by all fibres
H	height of triaxial specimen
l_f	fibre length
m_s	mass of the fibre
m_f	mass of the dry soil
M	critical state stress ratio
$N(\theta)$	number of fibres in θ
p	mean stress
p_{ref}	reference pressure
p_f	equivalent confining pressure induced by all fibres
p_f^*	calibrated equivalent confining pressure
p'	mean effective stress
p'_0	effective consolidation pressure
q	deviator stress

R	radius of specimen
S_l	lateral surface of specimen
u	pore water pressure
V	total volume of fibre sphere
V_f	volume of fibres
V_t	total volume of specimen
V_f^θ	total fibre volume in direction θ
w	water content of the sample
$\alpha, \beta, \gamma, \chi$	parameters of the model
α_f	fibre-soil interaction factor
δ	surface friction angle of fibre
ε_a	axial strain
ε_r	radial strain
$\varepsilon_f^1(\theta)$	single fibre strain in fibre direction
η_f	fibre aspect ratio
η	stress ratio
θ_0	limit incline angle of effective fibres in specimen
v	specific volume
v_f	volumetric fibre inclusion ratio
v_f^{ref}	reference volume
ρ_f	gravimetric fibre inclusion ratio
$\rho(\theta)$	volumetric fibre concentration in direction θ
ρ_{ave}	average volumetric fibre concentration in sphere
σ_1	major principal stress
σ_3	minor principal stress
$\sigma_f^1(\theta)$	single fibre stress in fibre direction
$\sigma_{af}^1(\theta)$	single fibre strain in axial direction
$\sigma_{rf}^1(\theta)$	single fibre strain in radial direction
ϕ	internal friction angle of soil

DECLARATION

I hereby declare that the work presented in this thesis is based on the research carried out in the Sustainable Infrastructure Group, Department of Engineering of Durham University during 10/2016- 03/2020. All material in this thesis is original except where indicated by reference to other work. No part of this thesis has been submitted elsewhere for any other degree or qualification.

Parts of this work have been used or reproduced in the following:

Published Conference Papers

1. Wang, J.Y., Andrew Sadler, Paul Hughes, and Charles Augarde., 2018. Compaction Characteristics and Shrinkage Properties of Fibre Reinforced London Clay. In Proceedings of China-Europe Conference on Geotechnical Engineering, pp. 858-861. Springer, Cham.
2. Wang, J.Y., Hughes, P.N. and Augarde, C.E., 2019. CBR strength of London Clay reinforced with polypropylene fibre. In Proceedings of XVII ECSMGE-2019. doi: 10.32075/17ECSMGE-2019-0296.

Signed: _____

Date: _____

STATEMENT OF COPYRIGHT

The copyright of this thesis rests with the author. No quotation from it should be published without the author's prior written consent and information derived from it should be acknowledged.

Signed: _____

Date: _____

ACKNOWLEDGEMENTS

Firstly, I would like to extend my sincere gratitude to Prof. Charles Augarde and Dr. Paul Hughes for their supervision. They help me improving the outline of research, managing the timetable, correcting the errors and mistakes in my thesis and providing enlightening ideas. This thesis would not be possible without their knowledge, support and enormous encouragement.

Secondly, I am very thankful to the contributions of the Prof. David Toll, Dr. Ashraf, and Dr. Marti Lloret-Cabot. They providing kind and helpful advices in the reviews and reports. I gained a lot in every conversation with them.

Special thanks goes to technicians in the laboratory, Mr. Stephen Richardson and Mr. Kevan Longley. They gave me a lot of supporting in the laboratory equipment and operation in the past three years.

The financial support provided by the China Scholarship Council is grateful acknowledged. Thank you for believing and choosing my project and giving the opportunity to me. I would like to acknowledge the support of Mr. Mark Mitchell from ADFIL. Ltd, who supported the fibre used in this research.

I cannot forget the ones who have contributed in many ways on this thesis: Chu Xia, Lei, Kaizhou, Ben, Arash, Joe and all those who have lent me support. What you have given me is much more than you think!

Finally, and most importantly, I would like to thank my lovely girlfriend Yuanyuan and my parents, who have shown me unwavering love and support me during my Ph.D. Thank you for being there these years. You always give me courage and power to face any challenges.

Dedicated to my grandparents Wang Changshun and Zhang Shuying

Chapter 1

1. Introduction

1.1 Background of the study

With the growth of cities and industrial areas, the availability of land for construction with sufficient bearing capacity and low settlement potential is reducing. Suitable fill material is not readily available in many locations and is costly to transport over long distances.

Geotechnical engineers have no choice but to deal with the ground conditions they encounter. High plasticity clays (CH) are vulnerable to shrinkage and swelling, settlement and strength reduction when used as foundation or backfill material. As an example, compacted CH layers are susceptible to desiccation cracking when exposed to fluctuations in temperature and humidity when combined with shrinkage and swelling of fill material, this can lead to progressive failure (Figure 1.1) in infrastructure earthworks and is known to be a problem on the UK transport network (Dawson et al, 2018).



Figure 1.1. Cracking appears on the embankment shoulder in A801 Avon Gorge road, UK.

(from BBC News, 2018)

There are approximately 10000 km of rail, highway and waterway embankments totally in the UK. The repair of highway embankment and cutting slopes costs approximately £20 million per annum in the UK (Arup, 2010). Dealing with problematic ground conditions can add significantly to project costs. For example, subgrades with poor bearing capacity necessitate a greater pavement thickness resulting in higher construction cost and longer construction periods.

The improvement of problematic soils in construction can involve many different techniques including mechanical treatments (compaction), chemical treatments (the addition of cement or lime) or reinforcement (with geosynthetics or soil nails). In recent decades, the use of randomly distributed fibres as soil stabilisation has attracted increasing attention in geotechnical engineering as an alternative method of soil reinforcement and a number of investigations have been conducted to determine the effects of randomly distributed fibres on the behaviour of sandy soils. However, less attention has been paid to the engineering behaviour of fibre reinforced high plasticity clays from both an experimental and mechanical modelling perspective. This study attempts to address this knowledge gap through a series of laboratory investigations and model development.

1.2 Aims and objectives

The research aims to investigate the effect of polypropylene (PP) fibres on the engineering behaviour and mechanical properties of London Clay (a high plasticity soil prevalent in southern England). To achieve this aim the following 3 objectives have been identified:

Determination of the effect of polypropylene fibre on the compaction and consolidation properties of London Clay

- To determine the optimum moisture content and maximum dry density of unreinforced and fibre reinforced soil, and investigate the effect of fibres on the compaction behaviour of London Clay.
- To determine the effect of fibre inclusion ratio and fibre length on the bearing capacity of London Clay. To establish the effect of fibre reinforcement on the design thickness of the subgrade.
- To determine the effect of fibre reinforcement on the coefficient of consolidation and compressibility indices of London Clay.

To ascertain the effect of polypropylene fibres on the desiccation cracking and tensile strength behaviour of London Clay

- To determine the linear shrinkage of unreinforced and fibre reinforced soil, and establish the effect of fibres on the linear shrinkage behaviour of London Clay.
- To quantify the effect of fibre inclusion ratio and fibre length on the desiccation cracking behaviour of compacted London Clay. To investigate the cracking patterns and cracking development of unreinforced and fibre reinforced soil.
- To quantify the effect of fibre inclusion ratio and fibre length on tensile strength and stiffness behaviour of compacted London Clay under different water contents. To investigate the failure patterns of unreinforced and fibre reinforced soil.

To determine the effect of polypropylene fibre on the mechanical behaviour of London Clay

- To investigate the effect of fibre inclusion ratio and fibre length on the consolidated undrained shear strength behaviour of London Clay at different cell pressures.

- To propose a mechanical model in order to predict the stress-strain, pore water pressure-strain responses and stress paths of fibre reinforced clay.
- To calibrate the model based on the test results and evaluate the model by comparing the experimental results and predicted results.

1.3 Scope of the study

This study investigates the potential for using randomly distributed polypropylene fibres to reinforce clay road embankments. Consequently the laboratory study is limited to the investigations of compaction, volume change and mechanical properties. The scope of work also includes developing a mechanical model for predicting stress-strain-pore water pressure response of fibre reinforced soil. Hence the mechanical properties of soils were tested in the laboratory and the model was derived based on the test results. Despite a comprehensive research programme being developed, there were certain limitations of this study, as shown as follows:

- Initial dry density can exert significant influence on the properties of fibre reinforced soil. However, soil was mostly compacted at or close to the maximum dry density. Due to the time constraints, the initial dry density of the soil was not a variable in the laboratory testing programme, nor in the proposed model.
- The interface strength behaviour of fibre reinforced soil was not tested. Also, due to limitations of available testing equipment, the micro-mechanism of fibre-clay interaction was not evaluated and investigated through the tests, and was not considered in the model.
- Considering practicality of materials in engineering, the most commonly used fibre type (e.g. polypropylene fibre) was utilised in this study. The scope of the work was

limited to this type of fibre and the effects of different types of fibres (e.g. materials, shape, coating condition) were not considered in this study.

- This study only focused on the shear strength behaviour of fibre reinforced soil based on isotropic consolidated undrained triaxial compression tests. Consolidated drained tests, triaxial extension behaviour, and shear strength behaviour under different stress paths are not discussed in this study.

1.4 Structure of the thesis

The thesis comprises eight chapters. Chapter 1 is the introduction chapter and sets out the overall project.

Chapter 2 presents an overview of soil stabilisation techniques, followed by a review of previous laboratory investigations, field experiments and analytical and numerical works on fibre reinforced soil.

Chapter 3 describes the methodology of the study. It introduces the properties of the soils and fibres used in the study. A summary of sample preparation methods and testing procedures is also presented.

Chapter 4 presents experimental results from compaction testing, California Bearing Ratio tests and one-dimensional consolidation tests on unreinforced and fibre reinforced soil. The effect of fibres on compaction and consolidation properties of fibre reinforced soil is discussed.

Chapter 5 presents the results of linear shrinkage tests, desiccation cracking tests and tensile strength tests. The influence of fibre reinforcement on shrinkage restriction, cracking reduction and tensile strength improvement are evaluated and discussed.

Chapter 6 presents the results of consolidated undrained triaxial tests on unreinforced and reinforced soil. The influence of fibre inclusion ratio, fibre length and cell pressure on stress-strain, pore water pressure-strain responses and stress path behaviour are discussed. The failure patterns of specimens are also analysed.

Chapter 7 proposes a mechanical model for predicting the shear strength behaviour of fibre reinforced clay. The derivation process is described and results of the model calibration are presented. Then the predicted results are compared with the experimental results and the capability of the model is evaluated and discussed.

Chapter 8 presents a combined discussion of the findings detailed in previous chapters and draws conclusions for the entire research project based on the experimental and theoretical investigations performed. Implications for the use of fibre reinforced clay in engineering applications and recommendations for further research are presented.

Chapter 2

2. Literature review

This chapter begins with a brief history of soil reinforcement to present a general background to the research. A comprehensive review of previous research related to laboratory and full scale tests on fibre reinforced soil is then presented organised by test and behaviour type. This is then followed by a review of previous analytical investigations of fibre reinforced soil.

2.1 Soil reinforcement

In the modern engineering world, soil stabilisation techniques can be divided into two categories: additive and non-additive methods (Figure 2.1). The non-additive methods are usually conducted in three major ways: mechanical methods, thermal methods and electrical methods. Mechanical methods usually includes vibro-compaction (Baumann and Bauer, 1974) and heavy tamping (Lo et al., 1990), thermal methods contains ground heating (Wang et al., 1990) and freezing (Sanger, 1968), and electrical methods can be conducted by electro-osmosis (Bjerrum et al., 1967). Additive methods can be sub-divided into two categories by the type of additive: chemical materials and fibrous materials. The former includes deep in-situ mixing and surface soil stabilisation with cementitious materials which usually have a higher strength, lower permeability and lower compressibility than the soil, like cement (Sherwood, 1962), fly ash (Edil et al., 2006), lime (Brandl, 1981), gypsum (Kolay and Pui, 2010), silica fume (Kalkan, 2011) and microorganisms (Ivanov and Chu, 2008). Fibrous materials additive methods use fibrous materials with high tensile strength to improve a soil's mechanical properties, an approach generally called "soil reinforcement", a term first coined by Vidal in 1969 (Vidal, 1969). Since then, nearly 4000 engineering projects have been built in more than 37 countries by 2012 using this concept of soil reinforcement (Hejazi et al.,

2012). The conventional fibrous materials used are geosynthetics, which include but are not limited to geogrids (Alfaro et al., 1995), geotextiles (Guido et al., 1986), geomembranes (Fleming et al., 2006), geocells (Dash et al., 2001), geonets (Bazne et al., 2005) and geocomposites (Iryo and Rowe, 2005), all of which have been proven by different researchers to be effective reinforcements for various applications.

However, the use of discrete randomly distributed fibres, as soil reinforcement, has attracted considerable attention in recent years. As a soil reinforcement technique, fibre reinforced soil is not a new invention but can be traced back to ancient times. In nature, the roots of the trees spread as they grow and friction is created between the soil particles and the roots below the ground surface. The ability of trees to resist toppling over under the weight of their branches and strong winds comes from the friction interacting between the roots and the surrounding soil and the root embedment. It is likely that, given this observation, people in ancient times started to mix plant roots into mud blocks used for construction, and some of these constructions still exist today. The walls of the Ziggurat in Mesopotamia (1400 B.C.) were built using layers of soil mixed with roots, and some parts of the Great Wall of China (200 B.C.) were constructed of mixtures of clay reinforced with the branches of trees and wheat straw (Hejazi et al., 2012, Jaquin and Augarde, 2012). The Romans used earth-reinforcing techniques, as evidenced by the use of reeds to reinforce earth levees constructed along the Tiber River (1st Century B.C.).

In comparison with conventional geosynthetics, using discrete fibres as reinforcement has the following advantages: (1) randomly distributed fibres can reinforce soil isotropically, this can limit potential planes of weakness which could be formed parallel to oriented reinforcements (Maher and Gray, 1990); (2) preparation of fibre-soil composites is relatively easy, it only requires physical mixing and can be adapted to different working conditions; (3) fibres also have the potential to be a cost effective and environmentally friendly technique depending on

the source. Based on these advantages, it is believed that fibre reinforcement of this nature could be a potentially robust and environmentally friendly method to improve the engineering behaviour of a soil for specific purposes. An extensive range of studies has been reported in the literature on the investigation of discrete randomly distributed fibre reinforced soil. These investigations are based on laboratory experiments, field scale tests, analytical models and numerical simulations, and a comprehensive review of all is provided in the following sections. Notably, for this literature in some investigations, authors did not provide much detailed information about the soils and fibres used.

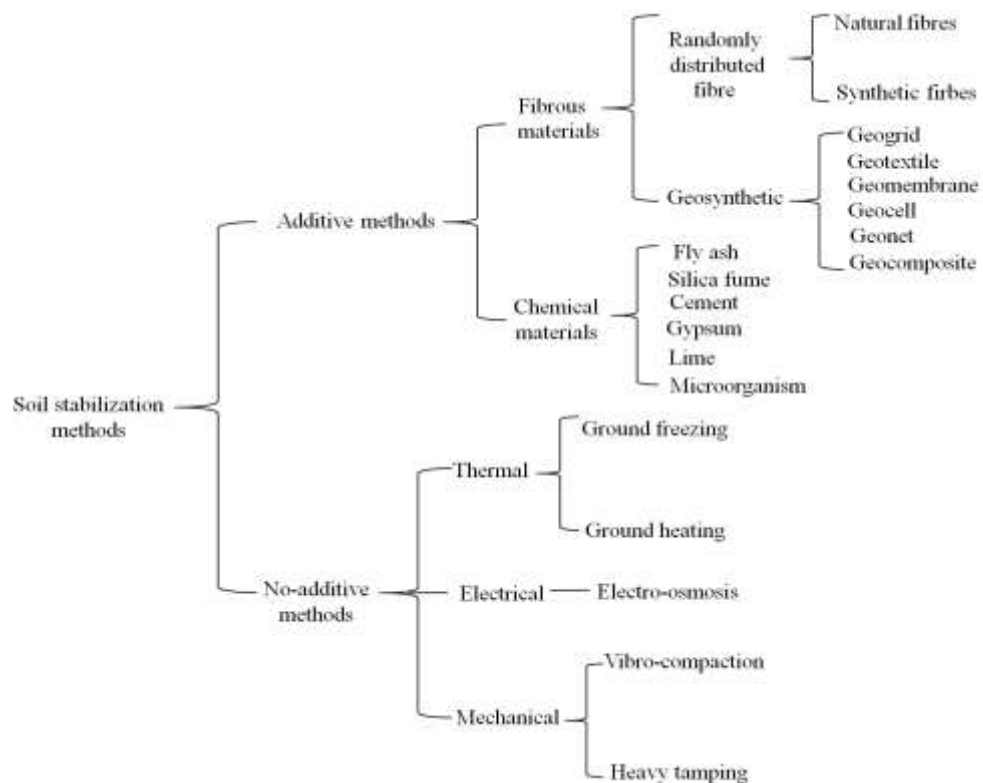


Figure 2.1. Different methods of soil stabilisation.

2.2 Laboratory investigations of fibre reinforced soil

The early experimental studies on fibre reinforced soil focused on soil-plant root systems, e.g. Gray (1978), Waldron (1977), and Wu et al., (1988), who reported that plant roots increase the shear strength of the soil and the stability of natural slopes. In addition, it is necessary to

mention that natural fibres have been used for a long time in developing countries in cement composites and earth blocks because of their availability and low cost (Ghavami et al., 1999 and Savastano et al., 2000). At the present time, there is a greater awareness of ecological balance and energy conservation, therefore as a potential environmentally friendly material, natural fibres like sisal (Mesbah et al., 2004), coconut (Pradani et al., 2017), jute (Hossain et al., 2015) and coir (Maity et al., 2018) have been the source of a great deal of interest for experimental studies on fibre reinforced soil. On the other hand, initial studies using synthetic fibres to reinforce soil have been conducted since the 1980s (Gray and Ohashi, 1983), and now some companies design and produce their own fibre-soil composites (TEXSOL, 2019 and FIBRESAND, 2019) as construction materials. Some other companies (TDP, 2019 and ADFIL, 2019) produce synthetic construction fibres for concrete and cement, which could be a potential future source of the fibres for fibre reinforced soil (Mitchell, 2019). In addition, recycled industrial wastes like plastic bottles (Choudhary et al., 2010) and tyres (Yaghoubi et al., 2018) could also be sources of synthetic fibres.

As a consequence of the above, laboratory studies of fibre reinforced soil can be divided into two major categories by the fibre type, i.e. natural and synthetic, each of which have their advantages and disadvantages. Natural fibres are usually more environmentally friendly and cheaper, but the organic ingredients in the fibres will experience microbial degradation and this might influence the long-term behaviour of the composite material. Synthetic fibres are industrial products so they are more uniform in specification and properties, and usually have better mechanical behaviour (e.g. tensile strength) than natural fibres. However, synthetic fibres are usually more expensive than natural fibres. Regardless of the fibre type used in tests, the fibre inclusion ratio and fibre aspect ratio are two parameters used in the majority of studies and they are defined below in Equations 2.1 and 2.2.

$$\rho_f = \frac{m_f}{m_s} \quad (2.1)$$

where m_f and m_s are the mass of the fibre and dry soil respectively

$$\eta_f = \frac{l_f}{d_f} \quad (2.2)$$

where l_f and d_f are the length and diameter of the fibre respectively.

As for the soil matrix, most work to date has concentrated on fibre reinforced sands, and less attention has been paid to fibre reinforced fine-grained soils (e.g. clays). Laboratory investigations of fibre reinforced soil are reviewed below.

2.2.1 Shear strength

Shear strength is a very important property of a given soil and is used by the designer to evaluate the bearing capacity of foundations, analyse the stability of slopes and design other constructions like dams and embankments. Accordingly, shear strength improvement is one of the major uses of (or reasons to use) fibre reinforcement. In laboratory studies, the most common test methods to measure shear strength of soils are the direct shear test and the triaxial test. The laboratory direct shear (shear box) test is a simple means of investigating the shear strength and the shear stress-strain behaviour of a soil. In the direct shear test a square in plan prism of soil is laterally restrained and sheared along a mechanically induced horizontal plane while subjected to a pressure applied normal to that plane (Figure 2.2). By carrying out tests on a set of specimens of the same soil under different normal pressures, the relationship between measured shear stress at failure and normal applied stress is obtained. Then by fitting a linear relationship between normal stress applied and shear stress at failure, one can obtain the internal friction angle (the slope) and the cohesion (the intercept) of the soil assuming a Mohr-Coulomb strength criterion as shown below:

$$\tau_f = \sigma \tan \phi + c \quad (2.3)$$

where τ_f is shear strength of the soil, σ is the normal stress, c is the cohesion and ϕ is the internal friction angle.

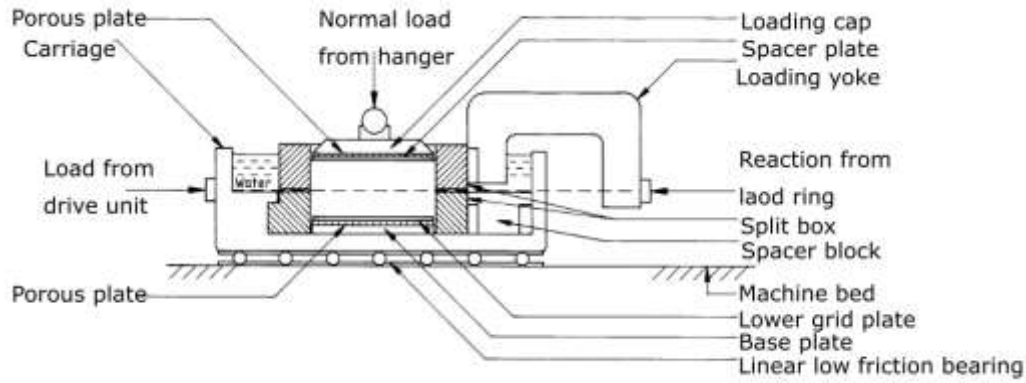


Figure 2.2 Typical general arrangement of shear box apparatus (from BS-1377-7, 1990).

By comparing the parameters c and ϕ of unreinforced and fibre reinforced soil with different fibre inclusion ratios and lengths obtained from direct shear tests, the effect of fibre on shear strength of the soil can be evaluated. In addition, one can also evaluate the effect of normal stress on the fibre reinforcement behaviour by introducing a parameter termed the stress ratio (η), which is defined as:

$$\eta = \frac{\tau}{\sigma_n} \quad (2.4)$$

where τ is the peak shear stress and σ_n is the normal stress.

As a method of evaluation of the shear strength behaviour of soil, the shear box is simple and efficient. However, according to Terzaghi's principle of effective stress (Terzaghi, 1936), the total stress of soil is consisted of effective stress and pore water pressure (Equation 2.5)

$$\sigma = \sigma' + u \quad (2.5)$$

Equation 2.3 can be expressed in the form of effective stress by using effective normal stress (σ'), effective cohesion (c') and effective internal friction angle (ϕ'). In shear box test, drainage conditions are hard to control and the measurement of pore water pressure is not convenient in the conventional shear box test, so the effective shear strength parameters of the soil cannot be obtained in conventional shear box test. In addition, the failure plane is forced to occur at the middle of the sample, which may not be the weakest plane, and the stress

distribution on the failure plane is not uniform. Consequently, the triaxial test is usually employed in many investigations of shear strength behaviour of soils. In the triaxial test, a sample is placed inside the triaxial cell (Figure 2.3) and is subjected to an all-round isotropic stress (σ_3) from the cell fluid. Once the sample is saturated and consolidated, the sample is compressed vertically with the displacement controlled and a vertical deviator stress is applied. The deviator stress (q) is defined as follows:

$$q' = q = \sigma_1' - \sigma_3' \quad (2.6)$$

where σ_1' and σ_3' are the effective axial stress and effective radial stress respectively.

During shearing, the drainage valves of the system can be kept either open or closed. With the valves closed, the volume of the sample will not change and the excess pore water pressure (u) generated in the sample can be measured. Such a test is usually called a “consolidated undrained (CU) test”. With the valves open, water is free to flow in the specimen and the volume change of the sample is measured, and this test is known as a “consolidated drained (CD) test”.

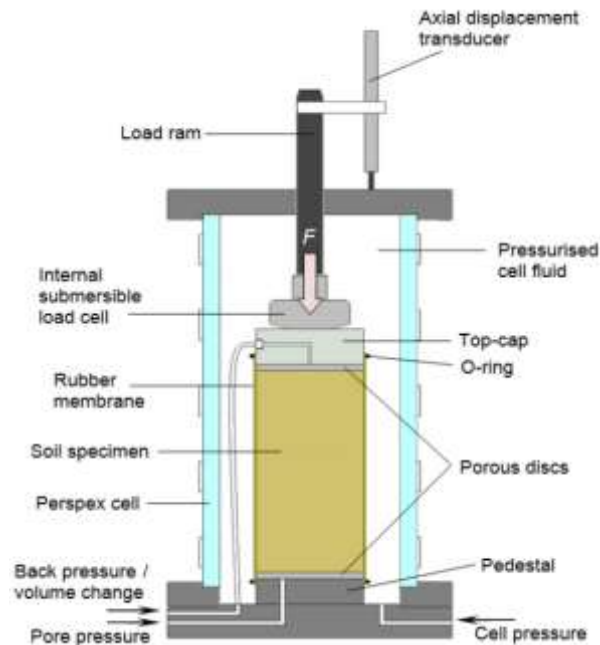


Figure 2.3 Essential features of a typical triaxial cell (from GDS, 2019).

Compared with the shear box test, the triaxial test not only monitors the complete state of stress at all stages, but also measures either volume change (drained condition) or pore water pressure change (undrained condition) of the specimen. Based on the triaxial test results, one can obtain the variation of mean stress p , mean effective stress p' (Equation 2.7), and deviator stress q applied to the soil sample during the test, and plot stress paths.

$$p - u = p' = \frac{\sigma'_1 + 2\sigma'_3}{3} \quad (2.7)$$

The stress paths represent the successive states of stress in a tested specimen under different loading (or unloading) conditions. The ratio of q to p' is called as “stress ratio” (η), which has the similar form in direct shear test (Equation 2.4), as shown in Equation 2.8

$$\eta = \frac{q}{p'} \quad (2.8)$$

In the idealised test condition, at large strains, further shear strains of the soil can occur with no changes in effective stresses or volume, this is termed the “critical state”, where the soil continues to deform and η in Equation 2.8 is a constant, termed as “critical state stress ratio” (M), and the void ratio (e) of soil is also a constant. The critical state is characterised by the Critical State Line (CSL), which is a straight line in $p': q$ plane passing through the origin with the slope equal to M (Figure 2.4a). In $\ln p': 1 + e$ plane the CSL is parallel to the normal consolidation line (NCL) of the soil (Figure 2.4b), and can be expressed by

$$1 + e = \Gamma - \lambda \ln p' \quad (2.9)$$

where λ is the slope of NCL, and Γ and N_p are the value of specific volume on CSL and NCL correspond to $p'=1$ kPa in Figure 2.4b. The CSL gives a prediction of the failure of initially isotropically consolidated soils when the stress state of the samples reaches this line, irrespective of the test path followed by the samples on their way to the critical state. Critical State Soil Mechanics (CSSM) is usually used to analyse the results obtained from triaxial tests and to discuss the soil behaviour. In addition, the triaxial test results can be interpreted

alternatively. For example, the relationship between failure major principal stress σ_{1f} and confining stress σ_3 can be used to draw a failure envelope to allow discussion of the behaviour under different confining stresses.

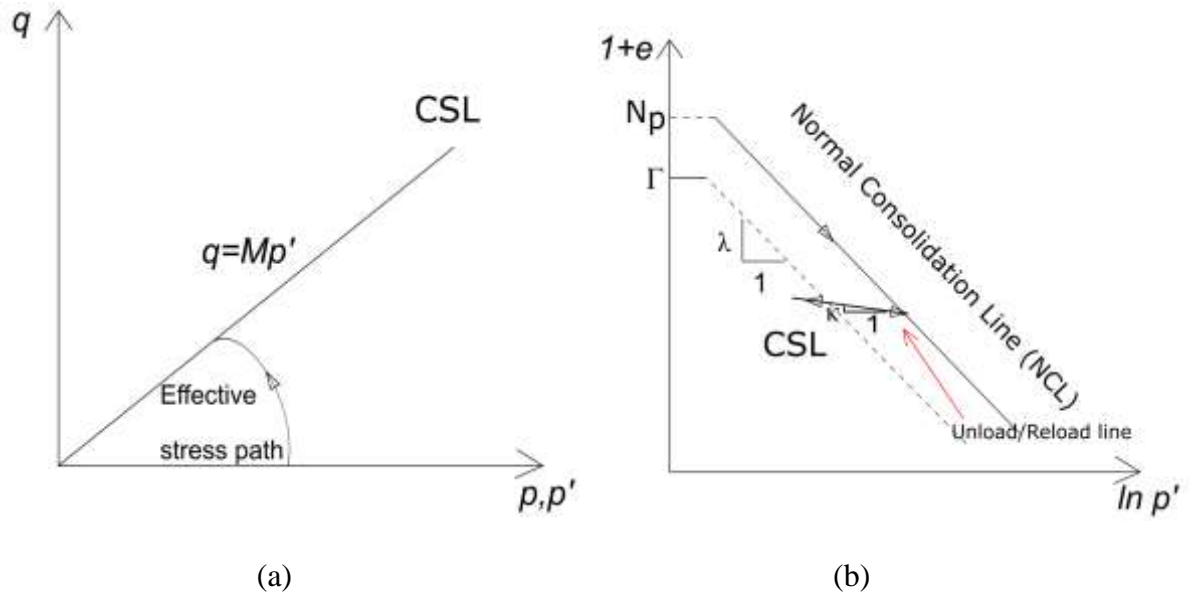


Figure 2.4. Stress paths and the critical state line in the (a) ($p': q$) plane (b) ($\ln p': 1 + e$) plane.

Many experimental investigations of the shear strength behaviour of sandy soil reinforced with randomly distributed discrete fibres have been conducted in the past few decades (e.g. Gray and Ohashi, 1983, Michalowski and Cermak, 2003, Consoli et al., 2007, Diambra et al., 2010, Yetimoglu, and Salbas, 2003, Ranjan et al., 1994, Sadek et al., 2010, Ahmad et al., 2010, Li and Zornberg 2012). These investigations indicate that the shear strength of soil can be improved by the addition of fibre as the reinforcement. Gray and Ohashi (1983) found that the relationship between peak shear stress and normal stress was bilinear, and deduced that there was a confining normal stress, below which fibres tended to slip or pull out. Yetimoglu and Salbas (2003) conducted direct shear tests on PP fibre reinforced uniform quartz river sand, and found that fibres leading to smaller loss of post-peak strength of the soil and a change in a brittle behaviour of the sand to a more ductile one. In addition, fibre reinforcement had no significant effect on the horizontal displacements at failure and initial

stiffness of the sand. Sadek et al., (2010) conducted a series of direct shear tests using black green line (BGL) coarse sand and Ottawa sand reinforced with nylon fibres. The authors found longer fibres resulted in a greater improvement in the shear strength of both soils. Also, for a fixed fibre aspect ratio, an increase in the length of fibres (from 7 to 27 mm) increased the extent of improvement in shear strength from 4 to 8%. It was also found that the reinforcing effect in fine (Ottawa) sand was more pronounced when the fibre concentration was small, whereas the relative increase in strength of coarse (BGL) sand was greater for larger fibre concentrations. These results are consistent with the grain-size effect reported by Michalowski and Cermak (2003) for fibre reinforced fine and coarse sands, which was based on triaxial drained tests. As for triaxial test investigations, Ahmad et al., (2010) conducted both CU and CD tests on palm fibre reinforced silty sand, and found that the dilation of the specimen decreased following an increase of the fibre inclusion ratio under drained conditions, and the pore water pressure under undrained conditions increased with an increase of the fibre inclusion ratio. According to the test results, palm fibres coated with acrylonitrile butadiene styrene (ABS) were more effective at improving shear strength of sand than natural palm fibres, because the layer of coating increased the diameter and surface area of the fibres, and consequently, interface friction of fibre and soil increased. Diambra et al., (2010) conducted both triaxial compression and tension drained tests on polypropylene (PP) fibre reinforced Houston sand, and reported that considerable increase of strength was induced by the presence of fibres in triaxial compression, while in extension tests the benefit of fibres was very limited. These results align with the findings of a previous study by the same authors on fibre orientation distribution which shows that the moist tamping technique generates preferential near horizontal orientation of fibres (Diambra et al., 2007). In addition, dense reinforced specimens had a much larger increase in strength than loose reinforced specimens. Previous published investigations, including those discussed above, of fibre reinforced sand

are summarised in Tables 2.1 and 2.2, which also include publications concerning fine-grained soils which are now discussed in detail.

A limited number of studies have focused on the shear strength behaviour of fibre reinforced clay via direct shear tests (e.g. Cai et al., 2006, Tang et al., 2007, Jiang et al., 2010, Qu et al., 2013, Pradhan et al., 2012, Falorca and Pinto, 2011) and triaxial compression tests (e.g. Ozkul and Baykal, 2007, Estabragh et al., 2011, Estabragh et al., 2012, Maliakal and Thiyyakkandi, 2013, Freilich et al., 2010, Ekinici 2016). These will be examined in more detail below.

2.2.1 a. Direct shear tests

Cai et al., (2006) investigated the effect of both (PP) fibres and lime on the shear strength of Nanjing clay by direct shear tests, and reported that cohesion (c) and internal friction angle (ϕ) of reinforced specimens at any particular lime inclusion ratio increased with increasing fibre inclusion ratio, and that the increase in strength of combined fibre and lime inclusions was much more than the sum of their individual increases. A similar trend was found by Tang et al., (2007) in a study of fibre reinforced cemented Nanjing clay. Qu et al., (2013), however, observed a different trend in tests on wheat straw fibre reinforced Shanghai clay. The authors found that for all the fibre lengths they tested, as the fibre inclusion ratio increased, the internal friction angle of the fibre reinforced soil (FRS) increased to an optimum maximum value and then decreased, while the cohesion of the FRS decreased to a minimum value and then increased. The authors attributed this to the interaction between the soil and fibres, but did not give a more detailed explanation for this uncommon phenomenon. In this study, both maximum increase in internal friction angle and minimum decrease in cohesion were found at 0.3% fibre inclusion ratio. Jiang et al., (2010) described the results of direct shear tests on fibre reinforced Nanjing clay finding that both cohesion and internal friction angle of fibre reinforced soil exhibit an initial increase followed by a rapid decrease with increasing fibre inclusion ratio and fibre length. The authors believed there to be two reasons for this

phenomenon: the large amount of fibres adhering to each other to form lumps, leading to an uneven distribution of fibres and deficient contact of fibres with soil particles, and for a certain fibre inclusion ratio, the fibre length increases meaning that the number of single fibres decreases, which reduces the entire reinforcement effect. Hence the optimal fibre inclusion ratio and fibre length were found to be 0.3% and 15 mm respectively in this study. Pradhan et al., (2011) reported that inclusion of randomly distributed PP fibres in Sambalpur clay increased both peak shear strength and residual shear strength (i.e. the shear strength which a soil can maintain when subjected to large shear displacement after the peak strength has been mobilised) in direct shear tests. For most cases, the peak and residual strength of the soil increased and then decreased with an increase of fibre length. The maximum increase in both peak and residual strengths occurred in this study for a fibre length of 20 mm at 0.4% fibre inclusion ratio. Falorca and Pinto (2011) investigated the influence of fibre texture and normal stress level in direct shear tests using PP fibre reinforced low plasticity clay. It was found that the stress ratio (Equation 2.4) decreased as the normal stress increased (Figure 2.5), which means that the fibre contribution was more significant at low normal stress levels. It was shown that no appreciable advantage was achieved by using crimped (texturised) fibres as far as shear strength is concerned, and in addition in that situation, creating a homogeneous mixture was harder than when compared with straight fibres. Scanning electron microscope (SEM) results presented in this reference revealed that the fibres did not rupture but stretched during the test, and some indentation damage occurred on the surface of the fibres. It was believed by the authors that damage mostly occurred during the compaction stage due to the high impact energy of the hammer in the Proctor type compaction procedure used.

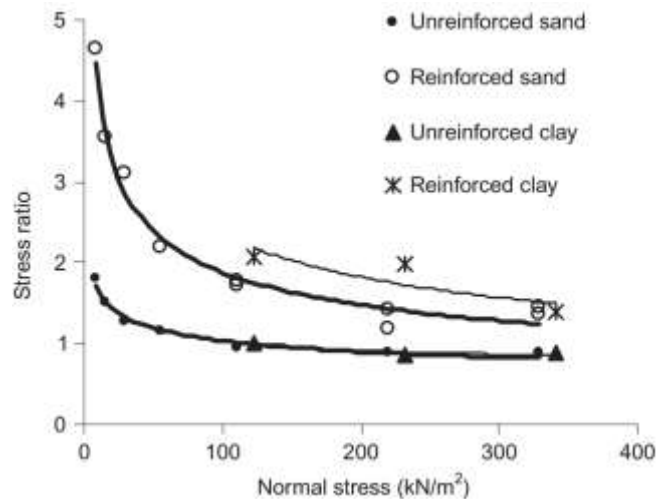


Figure 2.5 Stress ratio against normal stress for unreinforced and reinforced soil (from Falorca and Pinto, 2011).

Mirzababaei et al., (2017) and Mirzababaei et al., (2018) conducted a series of multi-stage reverse direct shear tests on monofilament propylene fibre reinforced high plasticity clay in Queensland. The tests were conducted on a single specimen under different effective normal stresses in order to ensure the identical homogeneous fibre distribution and initial void ratio. The specimen was consolidated at a normal effective stress of 600 kPa and subsequently unloaded to different normal effective stress and sheared in drained condition. The results showed that the effective internal friction angle (ϕ') of the soil was not significantly influenced by the fibre reinforcement, but the effective cohesion (c') of the soil was improved significantly. In addition, the effect of fibre reinforcement on the shear strength was evident at small normal effective stresses (i.e. 50 kPa) applied on clay soil samples with lower initial void ratio.

A brief summary of the direct shear tests mentioned above is listed in Table 2.1. According to these studies on fibre reinforced sandy and clayey soil, some conclusions can be reached: (1) the presence of the fibres can increase the both cohesion and internal friction angle of the soil, but an increase in fibre inclusion ratio and fibre length might lead to the degradation of these

two parameters; (2) fibres can lead to smaller loss of post-peak strength of the soil and can change the brittle behaviour of the soil to a more ductile one; (3) the fibre contribution is more significant at low normal stress levels, and (4) the increase in strength of combinations, i.e. fibres and other inclusions (e.g. lime, cement) is more than the sum of the increase caused by them individually.

Table 2.1. Summary of direct shear tests on fibre reinforced soil.

Literature	Soil type	Fibre type	Major conclusions
Gray and Ohashi (1983)	Michigan sand	Basket reed, PVC, palm and copper	Shear strength envelopes for fibre reinforced sand showed the existence of a threshold normal stress below which the fibres tended to slip or pull out. Increasing the length of fibre reinforcements increased the shear strength of the fibre-sand composite but only up to a point.
Yetimoglu and Salbas (2003)	uniform river sand	PP	Fibres could provide smaller loss of post-peak strength of the soil and change the brittle behaviour of the sand to a somewhat more ductile one.
Sadek et al., (2010)	BGL sand Ottawa sand	Nylon	Reinforcing effect in fine sand is more pronounced when the fibre concentration is small, and in coarse sand is greater for larger fibre concentrations.
Cai et al., (2006)	Nanjing clay with lime	PP	Cohesion and internal friction angle of reinforced soil at any particular lime inclusion ratio increased with increasing fibre inclusion ratio, with an optimum fibre inclusion ratio observed as 0.25% by the mass of dry soil.
Tang et al., (2007)	Nanjing clay with cement	PP	Increasing fibre inclusion ratio could decrease the stiffness and the loss of post-peak strength of cemented soil. The increase in strength of combined fibre and cement inclusions is much more than the sum of the increase caused by them

			individually.
Qu et al. (2013)	Shanghai clay	Wheat straw	With the fibre inclusion ratio increases, internal friction angle of FRS increases to optimum maximum value and then decreases, and the cohesion of FRS decreases to a minimum value then increases.
Jiang et al., (2010)	Nanjing clay	PP	Cohesion and internal friction angle of fibre reinforced soil exhibited an initial increase followed by a rapid decrease with increasing fibre inclusion ratio and fibre length.
Pradhan et al., (2011)	Sambalpur clay	PP	Fibres improve both peak shear strength and residual shear strength of the soil, the peak and residual strength of the soil increase and then decrease with the increase of the fibre length.
Falorca and Pinto (2011)	Low plasticity clay	PP	Fibre contribution is more significant for low normal stress levels, no appreciable advantage is achieved by using crimped fibres as far as shear strength is concerned
Mirzababaei et al., (2017) and Mirzababaei et al., (2018)	Queensland clay	PP	The effective internal friction angle of the soil is not significantly influenced by the fibre reinforcement, but the effective cohesion of the soil is improved significantly.

2.2.1 b. Triaxial tests

Previous investigations using triaxial testing of FRS has been conducted in both CD and CU conditions. Estabragh and co-workers carried out CU triaxial tests on a low plasticity clay reinforced with nylon fibres (Estabragh et al., 2011) and palm fibres (Estabragh et al., 2012) and the two studies led to the same conclusions. The pore water pressure generated in fibre reinforced soil were found higher than that in unreinforced soil, this is in agreement with the findings of Ahmad et al., (2010) and the authors believed this trend indicated the tendency towards contractive behaviour.

The friction angles in term of total stresses and effective stresses and the slope of the critical state line (M) increased with an increase in fibre inclusion ratio. Ozkul and Baykal (2007) investigated both drained and undrained strength of a commercially kaolinite rich clay reinforced with rubber fibres the results showing that the peak strength of the composite was comparable to or greater than that of unreinforced clay when the confining stresses were below 200- 300 kPa. Above this threshold scale, the presence of fibres tended to degrade the strength of the clay. In addition, pre-shear and post-shear permeability tests were also conducted for both unreinforced and reinforced soil. Shearing to large strains can cause increases in the permeability for both unreinforced and reinforced soil, however the study found that the pre-shear permeability of the clay was not significantly changed by the presence of rubber fibres. Maliakal and Thiyyakkandi (2013) discussed the shear strength of Kerala clay reinforced with coir fibres based on a series of CU tests. The results showed the coir fibres can significantly improve the shear strength of clay, but benefit of fibre reinforcement decreased if the confining pressure exceeds a critical value between 50- 100 kPa. A similar trend was observed with the variation of the fibre aspect ratio (when beyond 50- 100) and fibre inclusion ratio (when beyond 0.5%- 1%). In addition, the failure major principal stress (σ_{1f}) envelope exhibited a curvilinear variation with a transition at a confining stress (Figure 2.6), the authors of the study termed the “critical confining stress”. This trend coincides with the conclusions in Maher and Gray (1990) and Ranjan et al., (1996), and in agreement with the direct shear test results in Gray and Ohashi (1983).

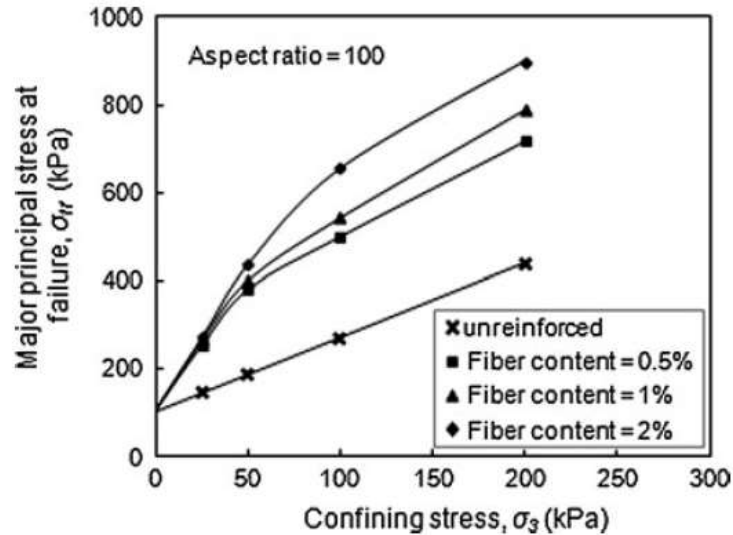


Figure 2.6 Principal stress envelopes for reinforced soil (from Maliakal and Thiyyakkandi, 2013).

In Ekinici (2016) and Ekinici and Ferreira (2012), the mechanical behaviour of fibre reinforced compacted Lambeth group clay investigated via CU and CD tests is reported. The tests were conducted on laboratory prepared specimens and “in-situ” specimens excavated from compacted unreinforced and reinforced slopes. The authors demonstrated that at low confining stresses (< 150 kPa), reinforced samples showed higher shear strength than equivalent unreinforced samples; for stresses higher than 150 kPa, the presence of fibres tended to degrade the shear strength and the unreinforced samples showed greater strength. Strain hardening behaviour during shearing was observed for both reinforced and unreinforced specimens, and in terms of observed failure modes, barrelling was seen in unreinforced samples at lower confining stresses (< 150 kPa) but seen in all fibre-reinforced tests. In the CU tests, for a given fibre inclusion ratio and confining stress, laboratory compacted reinforced samples showed higher peak deviator stress values and lower peak pore water pressure values than “in-situ” reinforced samples. Fibre alignment studies were also conducted for the reinforced samples by analysing fibre locations in dissected samples, finding that the majority of the fibres were aligned within $\pm 20^\circ$ of the horizontal plane and

greater than 50% within $\pm 10^\circ$; but the authors did not provide a clear idea of how these fibre alignment studies were actually conducted. This phenomenon, however, is in agreement with the conclusions in Diambra et al., (2007), in which the authors concluded that compacting the soil-fibre mixture during sample preparation led to a preferred near-horizontal orientation for the fibres. As for fibre orientation, Ibraim et al., (2012) concluded that moist vibration technique may provide less anisotropic orientations of fibre than moist tamping, and the fibre content did not have effect on the fibre orientations. Soriano et al., (2017) further discussed the fibre orientation of two sample preparation method through X-ray tomography, the results showed that for both methods the fibre orientation distribution appears to be axisymmetric with respect to the vertical axis of the sample, and preferential sub-horizontal directions. Freilich et al., (2010) compared the drained and undrained behaviour of PP fibre reinforced Eagle Ford clay and Silty Brown clay and found that fibres improved both drained and undrained strength and shear strengths of fibre reinforced soil obtained from CU tests were higher than for CD tests. The authors attributed this trend to the different drainage condition and strain rate of CU and CD tests, but did not provide a clear explanation. The pore water pressure generated in the fibre reinforced specimens were higher than that in unreinforced specimens. These trends indicated that the results obtained from CU tests may give a higher estimation on the effective results of fibre reinforced soil. In addition, the obvious failure plane can be observed on the unreinforced specimens after tests, while the reinforced specimens tended to bulge, indicating fibres increase the ductility (the deformation required to reach failure) of the soil.

A brief summary of the papers in which triaxial testing is used and which are mentioned above is listed in Table 2.2. According to these triaxial tests on fibre reinforced sandy and clayey soil, some conclusions can be drawn up: (1) the presence of fibres increases the peak shear strength and ductility of the soil; (2) fibres can restrict the dilation of the soil in drained

tests, this trend is reflected in an increase in pore water pressure of the soil in undrained tests; (3) as the fibre inclusion ratio increases, the shear strength of a reinforced soil might decrease and become even lower than its unreinforced equivalent; (4) there could be a “critical confining stress”, i.e. a point beyond which the presence of fibres tends to degrade the strength of the soil; (5) dense specimens tend to benefit more from fibre inclusion than loose specimens.

Table 2.2. Summary of triaxial tests on fibre reinforced soil.

Literature	Soil type	Fibre type	Major conclusions
Ahmad et al., (2010)	Silty sand	Palm	Volume dilation of the specimen decreases by increasing the fibre inclusion ratio under drained conditions, and the pore water pressure under undrained conditions increases due to increase of the fibre inclusion ratio. Coated fibres behave better than natural fibre as reinforcement.
Diambra et al., (2010)	Hostun sand	PP	Considerable increase of strength was induced by the presence of fibres in triaxial compression, while in extension tests the benefit of fibres is very limited. Dense specimens have a much larger increase in strength than loose specimens.
Michalowski and Cermak (2003)	Fine and coarse sand	PP	The reinforcing effect in fine sand is stronger compared to that in the coarse sand, when the fiber concentration is small (0- 0.5%). The relative increase in strength of coarse sand is greater for large fibre inclusion ratio.
Consoli et al., (2007)	Osorio sand	PP	The failure envelope of the FRS tested is independent of the stress path for triaxial compression tests. From the fibre length distribution after test, it can be seen that some fibres showing limited stretching and others

			possibly slipping under low confining stress, more pronounced fibre stretching but no breakage under high confining stress.
Ranjan et al.; (1994)	poorly graded fine sand	Plastic	The principal stress envelopes for fibre-reinforced sand are bilinear having a break at a confining stress, called critical confining stress. An increase in fibre aspect ratio results in a lower critical confining stress and higher contribution to shear strength.
Li and Zornberg (2012)	poorly graded sand	PP	The increasing soil density leads to an increase in peak shear strength for low fibre inclusion ratios, but has no influence for high fibre inclusion ratio. Soil with high fibre inclusion ratios can decrease post peak strength loss.
Estabragh et al., (2011); Estabragh et al., (2012)	Low plasticity clay	Palm and nylon	Fibres restrain the dilation, and a tendency of contraction of the soil tested leads to an increase of the excess pore water pressure in undrained tests. The friction angles in term of total stresses and effective stresses and the slope of critical state line (M) increased with the increase of fibre inclusion ratio.
Ozkul and Baykal (2007)	Kaolinite clay	Rubber	Peak strength of the composite was comparable to or greater than that of unreinforced clay when tested at confining stresses below 200- 300 kPa. Above this threshold scale, fibres tended to degrade the strength of the clay. The pre-shear permeability of the clay is not significantly changed by the presence of rubber fibres.
Maliakal and Thiyyakkandi (2013)	Kerala clay	Coir	Benefit of using coir fibres in clay as reinforcement is found to decrease if the confining stress increases beyond 50- 100 kPa. Similar trend was observed with the

			variation of aspect ratio and fibre inclusion ratio. The failure major principal stress (σ_{1f}) envelope exhibits a curvilinear.
Ekinici (2016); Ekinici and Ferreira (2012)	Over-consolidated London clay	PP	At low confining stresses, FRS showed higher shear strength than the unreinforced samples; for confining stresses higher than 150 kPa, the shear strength of the unreinforced samples is higher than FRS. Laboratory compacted FRS showed higher peak deviator stress values and lower peak pore water pressure values than field compacted FRS in CU tests.
Freilich et al., (2010)	Eagle Ford clay and Silty Brown clay	PP	Fibres can improve undrained strength of the clays significantly and drained strength of the clays slightly. Compared with unreinforced specimen (obvious shear plain), reinforced specimens tend to bulge, which indicating an increase in the ductility of the soil.

In addition, there are also some investigations which study shear strength of fibre reinforced soils by other test methods. Mandolini et al., (2019) studied the strength anisotropy of fibre-reinforced sands using a hollow cylinder torsional apparatus, the influence of the orientation of the principal stress directions on the fibre strengthening contribution was assessed. The results showed that the addition of fibres produces an anisotropic response and thus a distortion of the strength envelope. A deviatoric strength envelope in the multiaxial stress space was identified for fibre-reinforced sand. Also, unconsolidated undrained (UU) triaxial test (Qu et al., 2013, Abou Diab et al., 2016, Dasaka and Sumesh, 2011) is another common method. Since the pore water pressures are not measured during this test and therefore the results can only be interpreted in terms of undrained shear strength. Investigations on fibre reinforced soil based on this test method will not be further discussed in this review.

2.2.2 Tensile strength

The tensile strength of soil is a major mechanical parameter affecting the development of tensile cracking, which is commonly encountered in many earth structures (e.g. dams, hydraulic barriers, and highway embankments) especially when subjected to desiccation. Fundamentally, tensile stresses increase during soil drying and finally exceed the tensile strength of the soil resulting in the formation of a crack. It is therefore necessary to investigate soil's tensile behaviour to improve the understanding of the cracking behaviour of soil. Indeed, one of the positive aspects of fibre reinforcement is improvement of tensile capacity. A number of studies on the tensile strength characteristics of FRS have been conducted and can be classified by the test method used, i.e. indirect or direct tensile test. The most commonly used indirect methods are the Brazilian split tensile test (Maher and Ho, 1994, Consoli et al., 2011, Cristelo et al., 2017) and beam bending test (Thusyanthan et al., 2007, Viswanadham et al., 2010, Anggraini et al., 2015). Compared with indirect testing methods, tensile behaviour obtained from the direct tensile test is considered to be more reliable and precise. Tang et al. (2016) evaluated the direct tensile behaviour of PP fibre reinforced Nanjing clay. The results showed that the tensile strength was increased and the failure brittleness reduced. For unreinforced specimens, the tensile stress dropped to zero after failure, while for fibre reinforced specimens, some residual tensile stresses were remained after failure, and decreased gradually with increasing tensile displacement. The results also indicated that the fibre reinforcement benefit to tensile strength was more pronounced at a higher dry density of the soil. The trend is mainly because that a higher dry density leads to more contacts between soil particles, and also increases in the fibre-matrix interfacial resistance. A similar phenomenon was seen with cornsilk fibre reinforced cemented silt as described in Tran et al., (2019). Chebbi et al., (2017) conducted direct tensile tests on Thibar clay reinforced with two types of fibres. The results showed that sisal fibre and alfa fibre are more effective than nylon

fibres in improving tensile resistance and in addition, longer natural fibres were found to be more effective in improving the post-cracking behaviour of FRS than shorter natural fibres. Divya et al., (2013) carried out a series of direct tensile tests on polyester fibre reinforced Mumbai silt and used a digital image cross-correlation (DIC) system to obtain the strain field distribution on the surfaces of the specimens. The results indicated that as the fibre inclusion ratio and fibre length increased, there was an increase in the strain at crack initiation and a distinctly different strain field distribution for unreinforced soil and FRS was observed. Mesbah et al., (2004) conducted direct tensile tests on sisal fibre reinforced Lyon clay, and found fibre reinforcement to improve both ductility in tension and the inhibition of tensile crack propagation in comparison with unreinforced soil. Longer fibres were seen to behave better than shorter fibres as regards the properties mentioned above. However, the presence of fibres did not improve the peak tensile strength of the soil. Similar conclusions can be found in Oliveira et al., (2016).

Some common conclusions from the studies reported above are (1) fibres can improve the ductility of the soil, increase residual strength of the soil and inhibit the propagation of tensile cracking; (2) studies disagreed in whether fibres improved the peak tensile strength of soil to any significant extent although tensile strength was found to increase with the increase of dry density and the decrease of water content of the composite; (3) longer fibres have a better reinforcing effect when it comes to the tensile behaviour of soil.

2.2.3 Unconfined compressive strength

Kumar et al., (2006) conducted a series of Unconfined Compressive Strength (UCS) tests on polyester fibre reinforced light brown clay under different fibre inclusion ratios and mixed sand inclusion ratios. The results indicated that the UCS of clay increases with the addition of fibres and further increases when fibres were mixed in the clay-sand mixture. The strength was seen to increase with an increase of fibre length and fibre inclusion ratio, and crimped

fibres gave better results than plain fibres for a given fibre length and fibre inclusion ratio. Cai et al., (2006) conducted similar tests on PP fibre reinforced Nanjing clay but used lime as second mixture instead of sand. It was reported by the authors that the UCS of the soil increased with an increase of fibre inclusion ratio. In this study, the maximum value of the UCS of 0.88 MPa, was observed at 0.25% fibre + 5% lime inclusion ratio, which is 9.8 times that of the untreated specimen, 7.3 times that of samples with pure fibres and 1.3 times that of the samples with no fibres and pure lime which appears impressive. Mirzababaei et al., (2012) studied the UCS behaviour of a waste carpet fibre reinforced clay from northwest England and found that the relative benefit of improvement by fibres on UCS of the clay was highly dependent on initial dry unit weight and water content of the soil. In addition, fibres not only significantly enhanced the UCS of the soil, but also reduced post peak strength loss, and changed the failure behaviour from brittle to ductile. Similar conclusions were made in Tang et al., (2007) and Park (2011) in their research on fibre reinforced cemented clayey soil. Additionally, Ghazavi and Roustaei (2010) investigated the effect of freeze-thaw cycles on the UCS of PP fibre reinforced kaolinite clay finding that the inclusion of 3% PP fibres in clay samples increased the UCS of soil before and after applying freeze-thaw cycles by 60% to 160%.

Similar to the investigations on the tensile behaviour of fibre reinforced soil, researchers have not reached consistent conclusions on unconfined compressive strength improvement by fibre reinforcement: some studies showed that UCS of the soil increases with the increase of fibre inclusion ratio and fibre length, while some other studies reported the opposite. The contradictory conclusions may come from subtle differences in test conditions such as initial water content, density of the sample and type of the materials.

2.2.4 Compaction

Soil compaction is widely applied in geotechnical engineering practice. Higher dry density of the soil can reduce subsequent settlement under working loads and reduces the permeability of the soil. The durability and stability of structures are highly related to the appropriate compaction achievement. In addition, understanding the relationship between dry density and water content of a soil used in laboratory experimentation can guide the sample preparation procedures in further investigations. It is therefore necessary to investigate the compaction behaviour of fibre reinforced soil as currently understood in the publications that follow.

Naeini and Sadjadi (2008) conducted compaction tests on rubber fibre reinforced Iran clay and reported that the increase in fibre inclusion ratio results in a reduction of both the optimum moisture content (OMC) and maximum dry density (MDD) of the soil. Similar conclusions for fibre reinforced clayey soils can be found in Khan (2016), Senol (2012) and Abd (2013). Yaghoubi et al., (2018) and Estabragh et al., (2014) also found similar compaction behaviour with sandy soils. The decrease in densities reported is probably a result of the fibre filaments having less specific weight in comparison with the soil grains, and the fibres may act to block soil particles from approaching one another. However, some other investigations have found that an increase in fibre inclusion ratio causes a reduction in MDD, but an increase in OMC (Viswanadham et al., 2009, Hossain et al., 2015, Anggraini et al., 2015, Marandi et al., 2008 and Sarbaz et al., 2014). It is worth mentioning that most of the reinforcements used in these studies are natural fibres (e.g. jute, coir and palm) which have a greater water absorption capacity themselves than the surrounding soil and this could have an effect post mixing. Shukla et al., (2015) investigated the compaction behaviour of PP fibre reinforced Brickies sand and found fibre addition had almost no influence on the OMC of that soil. Some other studies (Soltani-Jigheh and Rasulifard, 2016, Malekzadeh and Bilsel, 2012 and Cetin et al., 2006) have experimentally confirmed similar conclusions in different soils

and using different fibre types. A summary is given here in Table 2.3. According to most of these investigations, the addition of fibres decreases the MDD of the soil, which is not expected in most geotechnical engineering. However, in general the decrease in the MDD of soil by fibres is not significant. In addition, the influence of fibres on the OMC of the soil may depend on the type of soil and fibre.

Table 2.3. A summary of studies on the compaction behaviour of fibre reinforced soil.

Literature	OMC	MDD	Fibre type	Soil type
Yaghoubi et al., (2018)	Decrease	Decrease	Tyre	Perth sand
Hossain et al., (2015)	Increase	Decrease	Jute	Clay in Chapai Nawabganj District
Shukla et al., (2015)	-	Decrease	PP	Sand
Khan (2016)	Decrease	Decrease	Waste plastic	CH (Subgrade soil)
Soltani-Jigheh and Rasulifard (2016)	-	-	Plastic chips	CL in East Azerbaijan
Sarbaz et al., (2014)	Increase	Decrease	Palm	Fine sand in Kerman
Anggraini et al., (2015)	Increase	Decrease	Coir	CH in Klang
Senol (2012)	Decrease	Decrease	PP	Sivas Clay+ Kangal fly ash
Malekzadeh and Bilsel (2012)	-	Decrease	PP	CH in North Cyprus
Mohamed (2013)	Decrease	Decrease	Hay	Silty clay
Estabragh et al., (2014)	Decrease	Decrease	PP Polyester	Silty sand

Cetin et al., (2006)	-	Decrease	Tyre	CL
Viswanadham et al., (2009)	Increase	Decrease	PP	CH in Pune
Marandi et al., (2008)	Increase	Decrease	Palm	Silty sand in Iran
Naeini and Sadjadi (2008)	Decrease	Decrease	Rubber	Iran clay

2.2.5 Bearing capacity

Improving the bearing capacity of soil is significant in civil engineering. The California Bearing Ratio (*CBR*) test is a method commonly used in laboratory investigations to evaluate the soil's bearing capacity. The *CBR* value is expressed as a percentage of the actual load causing the penetrations of 2.5 mm or 5.0 mm to the standard loads, as shown in the Equation 2.10:

$$CBR = \frac{N}{N_s} \times 100\% \quad (2.10)$$

According to the Design Manual for Roads and Bridges (England Highways, 2006), an increase in the *CBR* strength of subgrade can be used to justify a reduction in pavement thickness. This means lower project costs and higher efficiency in construction. A number of studies can be found on the *CBR* behaviour of FRS. In sandy soils, Sarbaz et al., (2014) found that increasing the fibre inclusion ratio led to an increase in *CBR* value of Kerman sand reinforced with palm fibres and some other laboratory studies (Chandra et al., 2008, Choudhary et al., 2010 and Kumar et al., 1999) reached similar conclusions for other sandy soils reinforced with different kinds of fibres.

As for clayey soil, Senol (2012), Chandra et al., (2008) and Hossain et al., (2015) also found that an increase in fibre inclusion ratio increases *CBR* values and Senol (2012) found that for a given fibre inclusion ratio, the effect on the *CBR* of a Sivas clay-fly ash mixture was greater for multifilament PP fibres compared with fibrillated PP fibres. This was thought to be a

result of the softer textured multifilament fibres being easier to hold/restrain soil particles when mixed with soil. In an unusual study, Butt et al., (2016), conducted *CBR* tests on human hair reinforced high plasticity clay and found *CBR* values also to increase with an increase of fibre inclusion ratio, reaching a maximum value, following which there was a decrease. Similar trends were reported in Fletcher and Humphries (1991), Zaimoglu and Yetimoglu (2012) and Masoumi et al., (2013). This phenomenon can be attributed to the fact that the increased fibre volume causes greater interaction between fibres, which tends to decrease the punching shear resistance of the composite. As for the effect of fibre length on the influence of *CBR* value of soil, Chore et al., (2011) and Pradani et al., (2017) conducted *CBR* tests on sandy soil reinforced with PP fibres and coconut fibres respectively and found that shorter fibres had better behaviour than longer fibres in improving the *CBR* value of soil, while Marandi et al., (2008) reached opposite conclusions for palm fibre reinforced Iran clay: i.e. longer fibres had greater benefit as regards *CBR* value. In addition, according to Maity et al., (2018), the *CBR* value of Kolkata clay reinforced with coir, sabai grass and jute fibres tended to increase with an increase of fibre length up to a maximum of 10 mm and beyond that exhibited a reduction in *CBR* value, and similar trends can be found in Masoumi et al., (2013). Investigations in Singh and Bagra (2013), Hossain et al., (2015) and Sonthwal and Sahni (2015) agreed that for a given fibre length and fibre inclusion ratio, the *CBR* value of soil increased as the fibre aspect ratio decreased.

2.2.6 Swelling and consolidation

Expansive soils swell when they absorb water and shrink when water evaporates from them. Due to the swelling and shrinkage behaviour, civil engineering structures (e.g. highway, railway, foundations, etc.) founded in these soils can be severely distressed and careful design is required (Phanikumar and Singla, 2016). On the other hand, high compressibility clayey soils cause a lot of problems in civil engineering. For example, constructions based on these

soils are often affected by stability and settlement problems. Naturally various researchers have considered fibre reinforcement as a solution to some of these issues.

Abdi et al., (2008) studied the consolidation settlement and swelling characteristics of a mixture of kaolinite and montmorillonite with inclusion of PP fibres. It was found that the addition of randomly distributed fibres resulted in a substantial reduction of the consolidation settlement of the soil. Fibre length was seen not to have a significant effect on these soil characteristics, whereas fibre inclusion ratio proved more influential and effective. The authors also concluded that the fibre inclusion ratio up to a certain value reduced the swelling pressure and the swelling potential of the soils significantly. Similar trends can be found reported in Viswanadham et al., (2009), Cai et al., (2006), Loehr et al., (2000), Phanikumar and Singla (2016) and Punthutaecha et al., (2007). The reason for this trend is believed to be due to the flexible fibres in the soil stretching when soil swelling occurs, and the tensile force mobilised in the fibres then resisting further swelling. When the fibre volume is higher, compaction is difficult and this leads to a larger void distribution in the FRS, which results in the increased swelling properties. Kar et al., (2012) studied the consolidation properties of Sambalpur clay reinforced with PP and coir fibres respectively via oedometer tests and found that the coefficient of consolidation increased with an increase in fibre inclusion ratio and fibre length. The compression index decreased with a rise in the proportion of polypropylene/coir fibres in the soil up to certain fibre inclusion ratio and increased thereafter. In addition, the compression index also decreased as the fibre length decreased. Deb and Narnaware (2015) studied the compressibility properties of synthetic fibre reinforced low plasticity clay also by oedometer tests. The authors found that the coefficient of consolidation of the soil increased due to the addition of the fibres, which indicates that fibres increase the rate of consolidation of the soil which could be an advantage practically. This study also observed that the compression index decreased as the fibre length increased, which is opposite

to the conclusion in Kar et al., (2012). A mechanical model was then proposed to determine the settlement of a granular fill-soft subgrade system. These authors concluded that the settlement of the system decreased at a decreasing rate as the thickness of the fibre reinforced zone increased. Based on the studies above, it can be concluded that the presence of fibres to a certain inclusion ratio can reduce the consolidation settlement and swelling potential, this means fibre reinforcement can be a potential stabilisation technique in embankment engineering.

2.2.7 Shrinkage and cracking

Reduction in the overall volume (volumetric shrinkage) along with the development of cracks is an inherent characteristic of compacted expansive soils subjected to drying (Yong and Warkentin, 1975). The shrinkage of soil in engineering applications is caused by evaporation and evapotranspiration, and desiccation cracks form due to the uneven shrinkage of soil layers as a reduction of moisture takes place. Based on these properties, soil structures constructed using clayey soils may exhibit desiccation cracks under seasonal changes when subjected to wetting-drying cycles. Hence, much effort has been expended to overcome the problems of desiccation cracking and volumetric shrinkage in geotechnical engineering. Conventional treatments for problematic soils include the addition of additives like lime, cement and fly ash (Leung and Vipulanandan, 1995; Omid et al., 1996; Mishra and Ravindra, 2016). However, it has been found that these additions often do not sufficiently suppress soil desiccation cracking when the initial water content is high. In addition, the presence of lime can cause the hydraulic conductivity to increase by a factor of 10 to 1000 which can be detrimental to the intended behaviour of the soil (George, 1970). A number of investigations have been conducted on the effect of randomly distributed fibres on shrinkage and desiccation cracking behaviour of clayey soil. Some studies focused on the shrinkage limit of soil, which is defined as the water content that the volume of the soil does not decrease when the water content is

reduced below this limit. Jayasree et al., (2014) found that the shrinkage limit of Ernakulum clay significantly increased as a result of increased coir fibre inclusion ratio and length, which indicated fibres can improve the shrinkage resistance of the soil. Abdi et al., (2008) reported similar results for PP fibre reinforced kaolinite and montmorillonite mixture. Dang et al. (2016) and Bouhicha et al., (2005) tested the linear shrinkage of sugarcane (bagasse) fibre reinforced Queensland clay and straw fibre reinforced Algeria clay respectively, and came to similar conclusions, i.e. linear shrinkage of fibre reinforced expansive soils reduced significantly as fibre inclusion ratio is increased. Ekinici and Ferreira (2012) studied the shrinkage behaviour of PP fibre reinforced Lambeth Group clay by compacting reinforced soil with different initial water content in a *CBR* mould. The results showed that an increase of fibre inclusion ratio led to a reduction of volumetric shrinkage, and more interestingly that the contribution of the fibres was more pronounced in vertical shrinkage compare to horizontal shrinkage. Puppala and Musenda (2000), Punthutaecha et al., (2006), Jayasree et al., (2014) evaluated the volume shrinkage of FRS by drying a fibre-expansive soil composite slurry in a standard Proctor mould. They all found that fibres reduced volumetric shrinkage strains of these expansive clays and once again there was a positive correlation between fibre inclusion ratio and a decrease in volumetric shrinkage strains. Jayasree et al., (2014) also found that the vertical shrinkage of the reinforced specimens was higher than that of diametrical shrinkage.

One area in which there is an increasing body of literature is concerned with the effect of fibre reinforcement on restricting desiccation cracking in soil. Different evaluation methods and indices were introduced and utilised in these studies to analyse the cracking behaviour of fibre reinforced soil. For example, crack development is often quantified using the Crack Intensity Factor (*CIF*) proposed by Miller et al., (1998), which is defined as the ratio between the area of the cracks and the total area of the specimen. Digital image processing has also been used

to accurately quantify desiccation cracks seen in FRS (Miller et al., 1998, Velde, 1999, Yesiller et al., 2000). Some studies investigated the desiccation crack resistance of initially saturated (slurry) FRS (Freilich et al., 2008, Tang et al., 2012, Chaduvula et al., 2017, Soltani et al., 2018). It was found in these studies that the *CIF* and the average length and width of cracks decreased with increasing fibre inclusion ratio. Tang et al., (2012) also considered crack network as a sequence of segments that intersect other segments, and these segments define the outline of the soil crack pattern. The authors reported that at low fibre content (< 0.2%), the segments intersect in “T” and “+” shape, and intersections were dominated by “Y” shape at high fibre content. The number of crack segments increases as the increased fibre content. Other researchers have investigated the desiccation cracking behaviour of unsaturated (compacted) FRS in order to investigate desiccation problems commonly encountered in landfill barrier material. Ziegler et al., (1998) assessed the feasibility of using PP fibres to reduce the development of desiccation cracking of synthetic clay, and reported that fibres to be effective in reducing the amount of desiccation cracking. However, when the soil in this study was subjected to wetting-drying cycles, the effectiveness of the fibres was not as evident. The authors did not give the explanation of this trend but it is inconsistent with Chaduvula et al., (2018), in which it was found the effectiveness of fibres on crack resistance was independent on the number of wetting-drying cycles. The conflicting conclusions might come from difference testing conditions. Unsaturated compacted cylindrical specimens were tested in the former research while saturated board-shaped specimens were tested in the latter research. Harianto et al., (2008) found that both the *CIF* and the volumetric shrinkage strain of compacted Akaboku silt specimens decreased with an increasing PP fibre inclusion ratio. Xue et al., (2014) investigated cracking resistance performance of Wuhan clay reinforced with straw fibres. The results showed that with increased fibre inclusion ratio, the *CIF*

decreased at relatively low fibre inclusion ratios and then increased at higher fibre inclusion ratios.

In summary, the results obtained from the studies mentioned above indicate that fibres can increase the shrinkage limit and decrease linear shrinkage and volumetric shrinkage of and amended soil. The presence of fibres can also improve the cracking behaviour of a soil by decreasing the width, length and area of the cracking. These conclusions suggest that fibre reinforcement could be a feasible method to suppress desiccation cracks and shrinkage encountered in road pavement and embankment.

2.2.8 Summary

The review of laboratory investigations mentioned above shows that there is a general consensus that fibre reinforcement (e.g. natural or synthetic fibres) can improve the behaviour of sandy and clayey soils in different aspects, which includes but is not limited to bearing capacity, shear strength, tensile strength, compression and swelling properties and crack resistance. However, there is no agreement on the optimum fibre length and fibre inclusion ratio for different properties of different types of soils. In addition, limited studies were focused on the effect of fibres on the properties of high plasticity clay. Since high plasticity clay has commonly been used in various types of construction (e.g. road embankment), a comprehensive study on the engineering properties and mechanical behaviours of fibre reinforced high plasticity clay appears necessary.

2.3 Full scale tests and engineering applications

Few well documented cases can be found on the utilisation of fibre reinforcement in engineering projects. However, in comparison with conventional laboratory tests, full scale tests can simulate the soil's condition in real engineering projects more accurately. Hence some researchers and engineers have chosen to conduct full scale tests to further prove the

practicability of fibre reinforcement in engineering applications. A brief discussion about these studies is introduced in the following.

2.3.1 Pavements

Santoni and Webster (2001) conducted field validation via truck traffic tests on a poorly graded sand pavement reinforced with 1% PP fibre (Figure 2.7). The fibres were mixed into the sand with the self-propelled rotary mixer then turned over using a front-end loader to ensure a uniform sand-fibre mixture. The test results indicating that a 203 mm layer of fibre reinforced sand with a tree resin spray-on surfacing could easily support 5000 military truck passes with a gross vehicle weight of 19.1 ton with very little damage to the pavement. A 102 mm layer of fibre reinforced sand could support over 1000 passes of a C-130 aircraft load with less than 41 mm of rutting. The authors also reported a new method of separating the individual fibres from the yarn: a handful of yarn fibres were placed in the bag with a few holes near the closed end, the bag was hand-held closed around an air nozzle, inverted, and air was blown through the fibres.



Figure 2.7. Traffic test with 13608-kg single-wheel assembly cart (from Santoni and Webster, 2001).

Tingle et al., (2002) continued the work by Santoni and Webster (2001) on PP fibre reinforced medium and fine sand and concluded that fibres provided improvement in rut resistance and *CBR* value in two different sand types. Compared with 76 mm length fibres, 51

mm length fibres appeared in their study to be more appropriate for field use. The authors also pointed out that fibre reinforced sands were a viable alternative to traditional road construction materials for temporary or low-volume roads. In both studies, the fibres were mixed into the sand using four passes with a self-propelled rotary mixer used by U.S. Army Engineers. Similar field tests also conducted on PP fibre reinforced pavements described in Lindh and Eriksson (1992), in which the authors mixing the composite of sand, water and plastic fibres in a concrete mixing plant of the drum mixer type, and obtained a satisfactory mixing effect. Crockford et al., (1993) and Grogan and Johnson (1994) found that the rutting of a pavement decreased and the number of passes to failure in field road test increased with fibre addition.

2.3.2 Foundations

Maheshwari et al., (2011) conducted footing tests on unreinforced and PP fibre reinforced clay in order to verify laboratory test results, and a 2m×2m×3m test pit was excavated (Figure 2.8). Full scale load test on both the soil was conducted on square footing of size 1.0m at depth of 1.0m below ground level. The safe bearing capacity of unreinforced and reinforced soil were found to be 64 and 250 kN/m³ respectively, which matched the results obtained from laboratory tests. However, the authors did not provide more details about soil mixing method in the field.



Figure 2.8. Test arrangement for full scale footing test (from Maheshwari et al., 2011).

Nasr (2014) studied the potential benefits of reinforcing the active zone behind a model sheet pile wall by using polypropylene fibre and cement kiln dust. The test involved loading a rigid strip footing resting on the sand backfill surface in the active zone adjacent to the sheet pile wall in a steel test tank (Figure 2.9). It was found that the fibres in the cemented sand behind the sheet pile wall had a significant effect in decreasing the lateral deflection along the sheet pile wall. For a given fibre inclusion ratio, as the thickness of reinforced sand layer increased from 25 to 125 mm, the ultimate bearing capacity of the strip footing on fibre reinforced cemented sand in the active zone increased significantly.

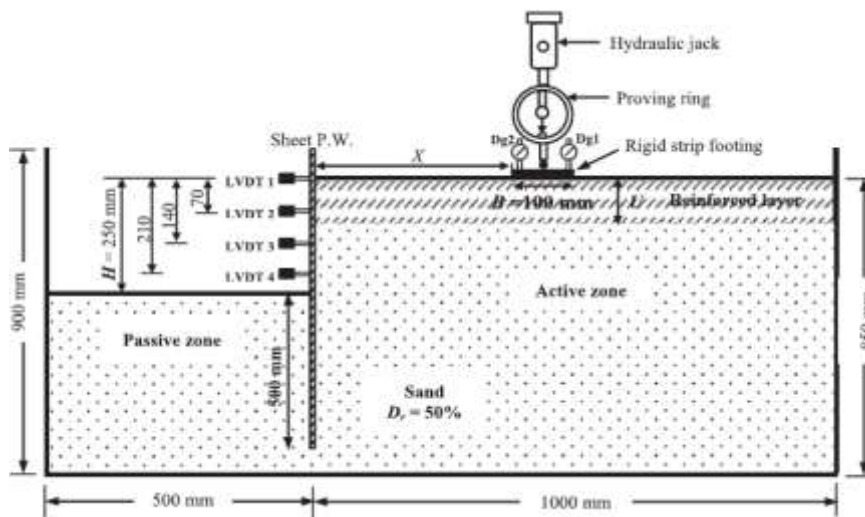


Figure 2.9. Schematic diagram of the model test configuration (from Nasr, 2014).

2.3.3 Embankments

Falorca et al., (2011) built a trial embankment 50 m long and 10 m wide in fibre reinforced silty sand in the campus of University of Beira Interior (Covilhã Portugal) to verify the feasibility of using PP fibre reinforcement in embankment engineering. The composite was prepared by spreading the soil and the fibres in a sandwich pattern: fibres were uniformly spread by hand over the surface, necessary amount of soil was then spread over the fibres, finally rotary tiller was driven along the composite to produce a homogeneous mixture. Plate-loading tests were carried out under repeated loading and unloading, the results

showed reinforced soil is more compressible than the unreinforced soil, but PP fibres can improve the elastic settlement of soils. The composite material was found to comply with the stiffness requirements for several construction applications, proving its practical suitability. Park and Tan (2005) built an unreinforced and a fibre reinforced retaining walls in PP fibre reinforced sandy silt to assess the contribution of fibre reinforcement to soil strength and stability of the soil. The soil and soil were mixed by a portable mixer. Both of the retaining walls were 22 m in length, 1.5 m in width and 2.4 m in height. It was found that fibres decreased the active earth pressure on and displacement of the wall, and led to an improved backfill material.

2.3.4 Seismic applications

The toughness and ductility of FRS are potentially beneficial for structures affected by seismic loading. According to Makiuchi and Minegishi (2001), two types of earth reinforcement techniques using synthetic fibres were already in use for earthquake resistance in Japan. In the first method, long polyester fibres were mixed with sandy soil and successful field applications of this method have been described by Leflaive (1988). The second technique was that of using short length fibres, but the authors did not provide further details and no relative literature can be found.

2.3.5 Summary

In conclusion, the feasibility of utilising fibres as reinforcement has been further proved by different full scale tests. Most of the full scale studies mentioned above concentrated on sandy soil, and the test results show that randomly distributed fibre can be a good material to reinforce sandy soil in pavement, embankment and foundation engineering. However, durability, one of the most important factors in this technique has not been investigated in full scale tests by researchers up to now. In addition, it is necessary to conduct more

comprehensive investigations via full scale tests on mixing method for different types of soils and fibres, because mixing large amount of the soil and fibres efficiently and homogenously is one of the most significant steps in engineering application.

2.4 Modelling fibre reinforced soil

While there is extensive literature on experimental studies of FRS, limited work has been done to take those studies and develop analytical and numerical models for predictive purposes. Clear understanding of the mechanisms leading to the observed mechanical properties of soil-fibre composites provides a consistent way of discussing and comparing various aspects of fibre reinforced soil, and gives guidance on further research and practical use. Below both analytical and numerical models available in the literature are discussed.

2.4.1 Analytical models of fibre reinforced soil

A comprehensive literature review shows that analytical models of the mechanical behaviour of FRS have been proposed by several investigators, each making their own set of assumptions to model a limited number of features, including confining stress, fibre inclusion ratio, fibre aspect ratio (fibre length and diameter), dilatancy effects, fibre orientation and distribution, fibre yielding and de-bonding.

Force equilibrium models

Gray and Ohashi (1983) proposed what they termed a “force equilibrium model” based on the results of a series of direct shear tests conducted on perpendicularly oriented fibre reinforced sands. In their model a fibre induced tension σ_R was defined as

$$\sigma_R = \left(\frac{4E_f \tau_f Z}{d_f} \right)^{0.5} (\sec \phi - 1)^{0.5} \quad (2.11)$$

where ϕ is the friction angle of the soil, E_f is the fibre modulus, τ_f is the interface frictional resistance along the fibre, d_f is the fibre diameter and z is the thickness of the shear zone.

Then, the mobilised tensile strength of fibres, t_R , is given by

$$t_R = \left(\frac{A_f}{A} \right) \sigma_R \quad (2.12)$$

where A_f and A are the areas of fibres cross the shear plane and the total shear plane respectively. The shear strength increase, ΔS , due to the fibre reinforcement is then determined from force equilibrium considerations, via the following equation if fibres are perpendicular to the shear plane.

$$\Delta S = t_R (\sin \theta + \cos \theta \tan \phi) \quad (2.13)$$

where θ is the angle between deformed fibre and vertical plane.

Maher and Gray (1990) further expanded this model to the condition of randomly-distributed fibres by using statistical concepts. The average embedment length for randomly distributed fibres is assumed to be $\frac{1}{4}$ of the fibre length on either side of the failure plane. So, the average number of fibres, N_s , intersecting a unit area of the shear plane can be obtained as

$$N_s = \frac{2 \times v_f}{\pi d_f^2} \quad (2.14)$$

where v_f is the volumetric fibre inclusion ratio, which can be defined as the ratio of volume of fibres to the total volume of the composite (Equation 2.15)

$$v_f = \frac{V_f}{V} \quad (2.15)$$

and the shear strength increase, ΔS developed by the presence of the fibres follows as

$$\Delta S = N_s \left(\frac{\pi d_f^2}{4} \right) \left[2(\sigma_n \tan \delta) \times \left(\frac{l_f}{d_f} \right) \right] (\sin \theta + \cos \theta \tan \phi) (\xi) \quad (2.16)$$

where σ_n is the confining stress acting on the fibres, δ is the surface friction angle of the fibres and ξ is an empirical coefficient depending upon sand granulometry (e.g. average grain size and particle sphericity) and fibre parameters (e.g. aspect ratio and surface friction angle). However, these two models are too idealised as the thickness of the shear zone is difficult to quantify in practice. Shukla et al., (2010) develops an analytical model for predicting the behaviour of fibre reinforced granular soils under high confining stresses also based on force equilibrium. Several important soil and fibre parameters are considered and pull-out of fibres is assumed not to take place. The effect of reinforcing with systematically oriented fibres is to introduce an apparent cohesion (c_R) to the granular soil and to increase the normal stress on the shear plane from σ to σ_{RS} , thereby increasing the shear strength of granular soil. Hence the shear strength of fibre-reinforced granular soil (S_R) is expressed as

$$S_R = c_R + \sigma_{RS} \tan \phi \quad (2.17)$$

the apparent cohesion and improved normal stress can be expressed as Equation 2.18 and 2.19 respectively.

$$c_R = \sigma_n \left[2 \left(\frac{A_f}{A} \right) \left\{ \frac{1 - \sin \phi \sin(\phi - 2i)}{\cos^2 \phi} \right\} \left(\frac{l_f}{d_f} \right) \tan \delta \sin i \cos \psi \right] \quad (2.18)$$

$$\sigma_{RS} = \sigma_n \left[1 + 2 \left(\frac{A_f}{A} \right) \left\{ \frac{1 - \sin \phi \sin(\phi - 2i)}{\cos^2 \phi} \right\} \left(\frac{l_f}{d_f} \right) \tan \delta \sin i \cos \psi \right] \quad (2.19)$$

where i is inclination of fibre to horizontal and ψ is the angle between deformed fibre and shear plane.

Model for soil reinforced with continuous threads

Di Prisco and Nova (1993) proposed a constitutive model for continuous threads reinforced sand by employing the conception of superposition. The threads reinforced soil is seen as a composite material and the stress of composite is derived by the superposition of stress of sand matrix and threads according to their volumetric contents.

$$\sigma_n A = \sigma_n' A_S + \sigma_n^R A_R \quad (2.20)$$

where A is the surface area of an elemental volume of reinforced sand. A_S and A_R are the area occupied by the sand and reinforcement, A_S is considered equal to A . σ_n is the normal stress acting on the surface and σ'_n and σ_n^R are the stresses taken by soil matrix and reinforcement. The strains of soil matrix, reinforcement and composite are assumed to be equal and the thread react only in radial direction in triaxial compression tests. The sand and the thread are assumed to behave both as elastic perfectly plastic materials. The constitutive law in the increment form of the reinforced material is

$$\begin{bmatrix} \dot{\varepsilon}'_a \\ \dot{\varepsilon}'_r \end{bmatrix} = \begin{bmatrix} 1/E_s & -2\nu/E_s \\ -\nu/E_s & (1-\nu)/E_s \end{bmatrix} \begin{bmatrix} \dot{\sigma}_a \\ -\rho E_t \dot{\varepsilon}_r \end{bmatrix} \quad (2.21)$$

where E_s and E_t are the Young's modulus of the sand and thread respectively, ν is the Poisson's ratio. ε_a and ε_r are the strain in axial and radial direction and σ_a is the stress in axial direction. ρ is the volumetric content of thread. However, the model neither considers the fibre distribution nor the post peak behaviour of the composite.

Energy-based homogenisation models

Michalowski and Zhao (1996) used what they call an “energy-based homogenisation” scheme to define the macroscopic failure stress of an isotropic fibre-sand composite. A piecewise closed-form failure criterion is derived. The internal friction angle of the soil (ϕ) is used to quantify the strength of the sand matrix, and the fibres are characterised by fibre volumetric concentration v_f (Equation 2.15), aspect ratio η_f (Equation 2.2), yield point $\sigma_{f,ult}$, and the fibre-soil interface friction angle δ . The energy dissipation rate of soil during plastic deformation of soil conforming to the Mohr-Coulomb failure condition and associative flow rule is zero. The model considers only energy dissipation due to fibre-soil slippage and fibre tensile rupture. The work rate of stress of the composite is equated to the energy dissipation rate in a representative volume (V) of the composite:

$$\sigma_1 \dot{\varepsilon}_1 + 2\sigma_3 \dot{\varepsilon}_3 = \frac{1}{V} \int d \, dV \quad (2.22)$$

where σ_1 and σ_3 are the maximum and minimum principal stress, ε_1 and ε_3 are the corresponding strain. The energy dissipation rate, d , due to fibre slippage and extension in a single fibre oriented in direction θ is

$$d = \pi d_f s^2 \sigma_n \tan \delta \dot{\varepsilon}_\theta + 0.25\pi d_f^2 (1 - 2s) \sigma_{f,ult} \dot{\varepsilon}_\theta \quad (2.23)$$

where $\sigma_{f,ult}$ is the yield stress of the fibre material, while, s is the length of the portion of fibre over which slippage occurs, d_f is the diameter of fibre. The strain rate $\dot{\varepsilon}_\theta$ in the direction of the fibre equals zero if the fibre is in compression. The total energy dissipation rate per volume of the soil, D , is the integral of Equation 2.23 over the volume of the fibre soil composite. This is given by

$$D = \frac{v_f \sigma_{f,ult} M \left(1 - \frac{\sigma_{f,ult}}{4s \times p \tan \delta}\right) \dot{\varepsilon}_1}{3} \quad (2.24)$$

where p is the mean of the maximum and minimum principal stresses, δ is the surface friction angle of fibre and M can be obtained from the coefficient of passive earth pressure K_p as

$$M = K_p \sin \tan^{-1} \sqrt{\frac{K_p}{2}} = \left(0.5 + \frac{\phi}{\pi} + \frac{\cos \phi}{\pi}\right) \tan^2 \left(\frac{\pi}{4} + \frac{\phi}{2}\right) - 0.5 - \frac{\phi}{\pi} - \frac{\cos \phi}{\pi} \quad (2.25)$$

If pure slippage occurs with no yielding of fibres, Equation 2.24 can be simplified to:

$$D = \frac{1}{3} v_f \eta_f M p \tan \delta \dot{\varepsilon}_1 \quad (2.26)$$

where η_f is the aspect ratio of fibre. The model discussed is identified as a ‘‘composite model’’ because the prediction of the equivalent shear strength of the composite uses parameters obtained from characterisation of fibre reinforced soil specimens.

Discrete framework model

Zornberg (2002) proposed a “discrete” framework to predict the equivalent shear strength of a fibre-soil composite considering the mechanical properties of individual fibres and the soil, rather than the mechanical properties of the fibre-reinforced composite material as a whole. This model recognises that fibre reinforcement contributes to the increase of shear resistance by mobilising tensile stress within fibres and with this model the equivalent shear strength of a fibre reinforced soil, S_{eq} consist of the shear strength of unreinforced soil S and fibre induced tension t , as shown below

$$S_{eq} = S + \alpha t = c + \sigma_n \tan \phi + \alpha t \quad (2.27)$$

where α is an empirical coefficient between 0 and 1 that accounts for the partial contribution of fibres, t is defined as the tensile force per unit area induced in a soil mass by randomly distributed fibres. The authors utilised the conception of “critical normal stress ($\sigma_{n,crit}$)”, which is similar with Gray and Ohashi (1983) and already introduced in 2.2.1. When the normal stress acting on the shear plane σ_n is lower than critical normal stress $\sigma_{n,crit}$, failure is governed by the pull-out of the fibres, Equation 2.27 can be expressed as

$$S_{eq,p} = (1 + \alpha v_f \eta_f c_{i,c})c + \sigma_n (1 + \alpha v_f \eta_f c_{i,\phi}) \tan \phi \quad (2.28)$$

where $c_{i,c}$ and $c_{i,\phi}$ are interaction coefficients. If $\sigma_n > \sigma_{n,crit}$, Equation 2.27 can be expressed by the ultimate tensile strength of single fibre ($\sigma_{f,ult}$) as

$$S_{eq,t} = (c + \alpha v_f \sigma_{f,ult}) + \sigma_n \tan \phi \quad (2.29)$$

and the $\sigma_{n,crit}$ can be expressed by

$$\sigma_{n,crit} = \frac{\sigma_{f,ult} - \eta_f c_{i,c} c}{\eta_f c_{i,\phi} \tan \phi} \quad (2.30)$$

The above expressions yield a bilinear shear strength envelope, which is shown in Figure 2.10.

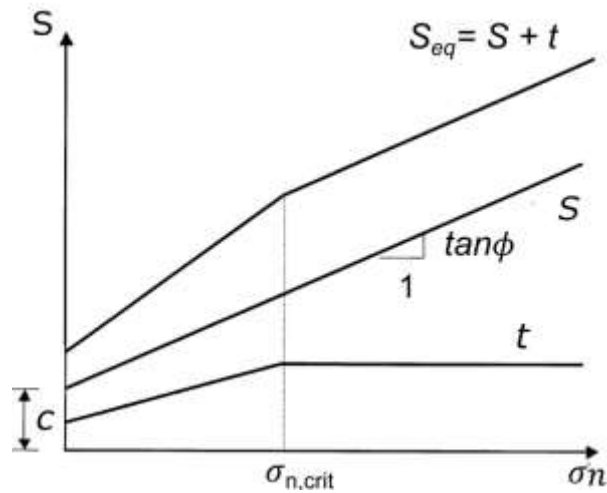


Figure 2.10. Representation of the equivalent shear strength according to the discrete approach (after Zornberg, 2002).

Two-phase model

Diambra et al., (2010) proposed an anisotropic model to express the stress-strain response of fibre reinforced sand by coupling the effects of fibres with the stress-strain behaviour of unreinforced sand. The two phases in the composite: fibres and soil were considered separately. Fibres behave linear elastically and the soil matrix obeys the Mohr-Coulomb failure criterion. The model is based on the basic rule of mixtures, as shown in Equation 2.31

$$\dot{\boldsymbol{\sigma}} = \nu_m \cdot \dot{\boldsymbol{\sigma}}_s + \nu_f \cdot \dot{\boldsymbol{\sigma}}_f \quad (2.31)$$

where ν_m and ν_f is the volumetric content of soil and fibre, $\dot{\boldsymbol{\sigma}}$ is the total stress increase of the composite, $\dot{\boldsymbol{\sigma}}_s$ is the stress increase in sand, $\dot{\boldsymbol{\sigma}}_f$ is the stress increase in fibres, and they can be expressed as in terms of mean effective stress and deviator stress of soil and fibres:

$$\dot{\boldsymbol{\sigma}}_s = [p', q]^T \quad ; \quad \dot{\boldsymbol{\sigma}}_f = [p'_f, q_f]^T \quad (2.32)$$

Based on Voigt's hypothesis, equality of stresses is assumed as

$$\dot{\boldsymbol{\sigma}} = \dot{\boldsymbol{\sigma}}_s = \dot{\boldsymbol{\sigma}}_f \quad (2.33)$$

Hence the constitutive model for the fibre reinforced sand is written in terms of stress and strain increments as

$$\dot{\boldsymbol{\sigma}} = \dot{\boldsymbol{\sigma}}_s + \nu_f \cdot \dot{\boldsymbol{\sigma}}_f = [M_m] \dot{\boldsymbol{\epsilon}} + \nu_f \cdot [M_f] \dot{\boldsymbol{\epsilon}} \quad (2.34)$$

M_m and M_f are stiffness matrices for sand and fibre respectively. Here the strain in the sand and in the fibres are assumed equal to the strain of the composite material. The authors also used a “sliding function”, f_b ($0 < f_b < 1$), to consider the imperfect interfacial bonding between fibre and soil. The function was proposed by Machado et al., (2002) for the model of municipal solid waste, as

$$f_b = k_e \left[1 - \exp\left(-C_s \frac{p'}{p_r}\right) \right] \quad (2.35)$$

where k_e is the efficiency coefficient of bonding, p_r is the reference pressure (0.1 MPa), C_s is the swelling index of the soil. The definition of the stiffness matrix for the fibres requires only the definition of the elastic modulus of the fibres, the sliding function and the fibre orientation distribution. In this model, the stress tensor characterising the fibre reinforcement effect ($\boldsymbol{\sigma}_f$) needs to be obtained through an integration which is dependent on the induced domain of tensile strains (Figure 2.11) and fibre orientation. For flexible fibres, only those fibres acting in tension contribute to the stresses of the composite. The limits of fibre inclination angle to horizontal plane (θ_0) for triaxial compression and tension conditions are shown in Figure 2.11.

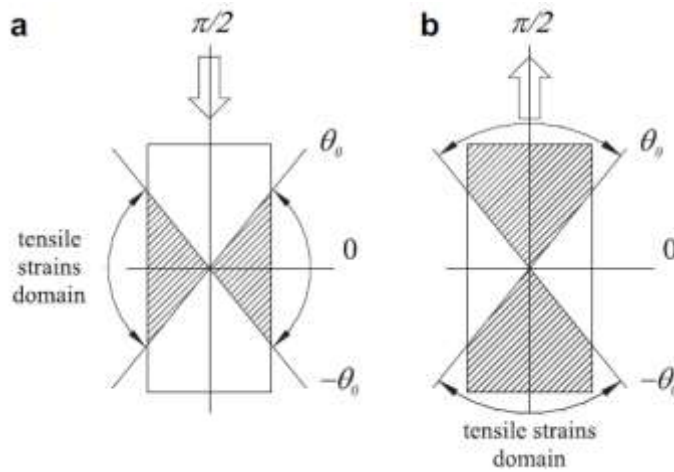


Figure 2.11. Domains of tensile strain orientations for compression (a) and extension (b) loadings (from Diambra et al., 2010).

A similar approach has been used in a constitutive model of fibre reinforced clay in Diambra and Ibraim (2014), where the model superimposes the stress contribution of fibrous elements to a Modified Cam Clay (MCC) like bounding surface model. The fibres are considered as one-dimensional elastic perfectly plastic elements with plastic threshold stress σ_f^p and strain ε_f^p (Figure 2.12), breakage of the fibre is also assumed if an elongation breakage limit ε_f^b is reached. After the breakage, the fibre becomes unstressed.

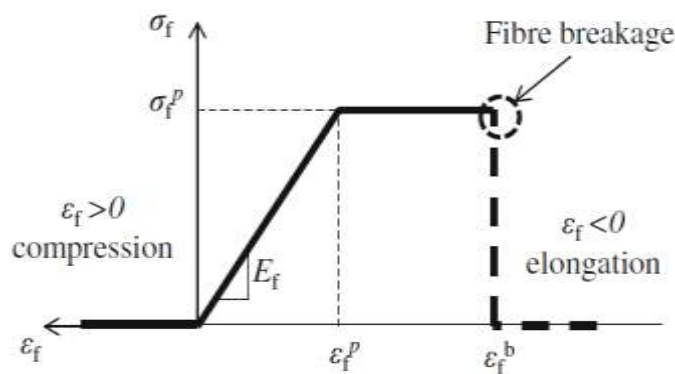


Figure 2.12. Assumed stress-strain relationship for a fibre in fibre reinforced clay (from Diambra and Ibraim, 2014).

The clay is assumed to obey an elastic-plastic incremental stress-strain relationship as shown in Equation 2.36.

$$\begin{bmatrix} \dot{p}' \\ \dot{q} \end{bmatrix} = \begin{bmatrix} K & 0 \\ 0 & 3G \end{bmatrix} - \frac{\begin{pmatrix} K(2p' - p'_0) & \frac{6GKq(2p' - p'_0)}{M^2} \\ \frac{6GKq(2p' - p'_0)}{M^2} & \frac{36Gq^2}{M^4} \end{pmatrix}}{K(2p' - p'_0) + \frac{12Gq^2}{M^4} + H} \begin{bmatrix} \dot{\varepsilon}_{mp} \\ \dot{\varepsilon}_{mq} \end{bmatrix} \quad (2.36)$$

where K and G are the bulk modulus and shear modulus of the soil matrix, p'_0 is effective consolidation stress, H is hardening modulus to control the bounding surface size. $\dot{\varepsilon}_{mp}$ and $\dot{\varepsilon}_{mq}$ are the plastic components of the incremental mean and deviatoric strains of the soil matrix. The stress state of the composite in terms of deviatoric (q^*) and isotropic (p^*) triaxial variables can be expressed as the combination of soil phase and fibre phase as the similar method with Equation 2.31:

$$p^* = v_m p' + v_f p'_f ; \quad q^* = v_m q + v_f q_f \quad (2.37)$$

and the stress relationship of composite at critical state can be expressed as

$$q^* = M(p^* - v_f p'_f) + v_f q_f \quad (2.38)$$

The expansion form and details of Equation 2.38 can be found in Appendix of Diambra and Ibraim (2014).

A failure criterion for fibre reinforced soil

Gao and Zhao (2012) presented a failure criterion for fibre reinforced sand based on the function proposed in Yao et al. (2004). The continuous function to characterise the failure envelope is given as

$$q = M_c g(\theta) [(p' + \sigma_0^u) + f_c] \quad (2.39)$$

where $g(\theta)$ is an interpolation function characterising the influence of the intermediate major principal stress magnitude on failure, θ is the *Lode angle*, M_c is the stress ratio ($\eta = q/p'$) at failure in triaxial compression, σ_0^u is the triaxial tensile strength of the soil without fibre reinforcement and f_c is a function describing the fibre reinforcement and soil-fibre bonding effect to the composite strength where

$$f_c = cp_r \left[1 - \exp \left(-\kappa \frac{p' + \sigma_0^u}{p_r} \right) \right] \quad (2.40)$$

In Equation 2.40, c and κ are two nonnegative material constants and p_r is the reference pressure (101 kPa). The proposed criterion can be applied to predict the strength of fibre reinforced sand with both isotropic and anisotropic fibre distributions, in both triaxial compression and extension tests. The failure curve of fibre reinforced soil in triaxial compression is shown in Figure 2.13. The predicted composite strength is zero at zero effective confinement state when $p + \sigma_0^u$ is zero.

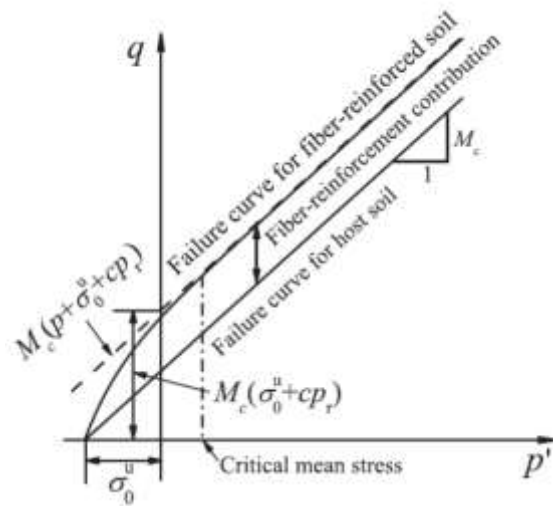


Figure 2.13. Failure curves for fibre reinforced soil in triaxial compression

(from Gao and Zhao, 2012).

Multiaxial model for fibre reinforced sand

proposed an anisotropic model for fibre reinforced sand under multiaxial loading conditions. In this model, the strain of FRS is dependent on the deformation of the sand skeleton. The fibre reinforcement affects the void ratio (e) and effective stress (σ_{ij}) of the soil skeleton, which governs the elastic properties, dilatancy and plastic hardening of the FRS. The failure criterion was based on Gao and Zhao (2012), which is shown in

$$q = M_c g(\theta) \left[(p'_{urs} + \bar{p}^f) \right] \quad (2.41)$$

where $g(\theta)$ is an interpolation function based on the *Lode angle* θ , \bar{p}^f is the stress contribution of the fibres at failure, which can be expressed by Equation 2.42

$$\bar{p}^f = \chi_r \phi(A) p_r \left[1 - \exp\left(-\kappa \frac{p'_{urs}}{p_r}\right) \right] \quad (2.42)$$

where χ_r is the model parameter and A is the anisotropic variable which characterises the relative orientation between the loading direction tensor n_{ij} and fibre orientation tensor F_{ij} as

$$A = \frac{F_{ij} n_{ij}}{F} \quad (2.43)$$

where $F = \sqrt{F_{ij} F_{ij}}$ is referred to as the degree of fibre orientation anisotropy. The effective stress of FRS, σ_{ij}^{frs} , can be expressed as Equation 2.44

$$\sigma_{ij}^{frs} = s_{ij}^{urs} + (p'_{urs} + p^f) \delta_{ij} \quad (2.44)$$

where s_{ij}^{urs} and p'_{urs} are the deviator stress tensor and mean effective stress of unreinforced soil, p^f is the strain-level dependent fibre reinforcement contribution and δ_{ij} is the Kronecker delta ($= 1$ for $i = j$ and $= 0$ for $i \neq j$). The void ratio of FRS, e^{frs} , is assumed have followed relationship with the void ratio of unreinforced soil (e):

$$e^{frs} = (1 + x\rho_f)e \quad (2.45)$$

where x is the model parameter and ρ_f is the ratio of fibre volume and dry sand volume. The yield function is proposed based on Li and Dafalias (2002), shown as follows

$$f = \frac{\sqrt{\frac{3 s_{ij}^{urs} s_{ij}^{urs}}{2 p'_{urs} p'_{urs}}}}{g(\theta)} - \Gamma \quad (2.46)$$

where Γ is the hardening parameter, the details of Γ can be found in Gao and Diambra (2020).

The elastic moduli are influenced by the fibre in the form of:

$$G = G_0 \frac{(2.97 - e^{frs})^2}{1 + e^{frs}} \sqrt{p_r p'_{frs}} ; \quad K = G \frac{2(1 + \nu)}{3(1 - 2\nu)} \quad (2.47)$$

where p'_{frs} is the mean effective stress of fibre reinforced soil and G_0 is a material constant, K and ν are the bulk modulus and Poisson's ratio respectively.

Equivalent confining stress models

On the basis of test results, Yang (1972) hypothesised that tensile restraint in the reinforcement induces an "equivalent confining stress" increase, $\Delta\sigma_3$ in a triaxial test.

Consequently, an increase in the effective value of the confining pressure leads to an increase in shear resistance of the soil, Δs (Figure 2.14). It can be seen that the value of Δs can be related to $\Delta\sigma_3$ by Equation 2.34 (Gray and Al-Refeai, 1986).

$$\Delta s = \frac{\Delta\sigma_3}{2} \times \tan\left(45^\circ + \frac{\phi}{2}\right) \quad (2.48)$$

where ϕ is the friction angle of the unreinforced sand.

However, no relationship between $\Delta\sigma_3$ and fibre properties is included in this early example of a model for FRS.

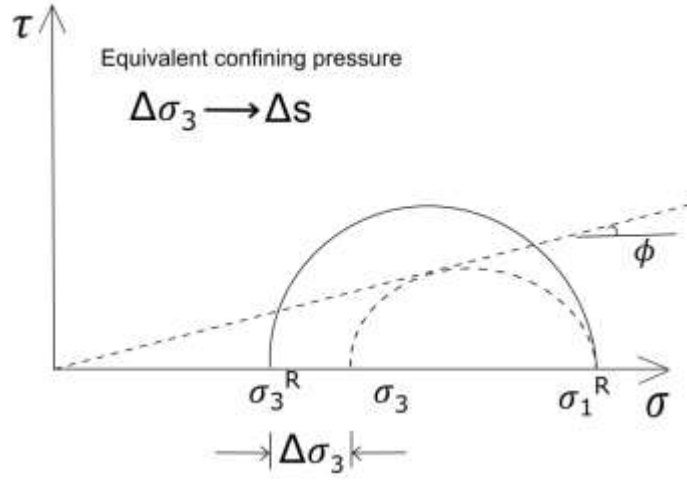


Figure 2.14. Equivalent confining stress concept displayed using Mohr circle axes (after Athanasopoulos, 1994).

Ajayi et al., (2016) analyses CD triaxial tests results on fibre reinforced gravel and links them to a model which uses the equivalent confining stress concept. The radial strain of the tested specimen was measured by image-based deformation measurement technique. The tensile stresses in fibres are assumed as effective confining stress directly act on the granular skeleton but not on the boundary of the specimen. The equivalent confining stress in proportion to the volumetric fibre ratio v_f , the Young's modulus of the fibres E_f and is dependent on the lateral strain ε_r . The equivalent confining effective stress σ_f' is assumed only to act in the horizontal direction and can be expressed as

$$\sigma_f' = \frac{\alpha \varepsilon_r E_f v_f}{(1 + e + v_f)} \quad (2.49)$$

where e is the void ratio of the soil and α is a fibre-grain interaction factor to account for the interface slip, α lies in the range 0 to 1 and is given as

$$\alpha = A_\alpha |\varepsilon_r|^{-\beta_\alpha} \quad (2.50)$$

where A_α and β_α are constants for a given soil and fibre type.

The parameters in Equation 2.50 were corrected by the stress-dilatancy relationship in Cam Clay model as follows

$$\eta = M + d \quad (2.51)$$

where d is the rate of dilation, and defined as ratio of volumetric strain increment to the shear strain increment.

Other models

Some investigators have taken semi-empirical approaches using regression analysis on test results to develop models that bring out the effect of fibre and soil factors on shear behaviour of fibre reinforced soil (Ranjan et al., 1996, Sivakumar Babu and Vasudevan, 2008, Maliakal and Thiyyakkandi, 2012). These models do not consider the mechanisms of fibre reinforcement and rely heavily on a simple set of experimental results. In addition to models for predicting shear strength behaviour of fibre reinforced soil, a few models focus on other behaviours of fibre-soil composites. For example, Zhu et al., (2014) proposed a tri-linear model to describe the pull-out process of a short fibre in the soil-fibre composite. Xiao and Liu (2016) proposed a model for estimating the tensile strength of fibre-cement-clay mixtures. These models are however not the main subject of this review and will not be further discussed.

2.4.2 Numerical models

In addition to the analytical models discussed above, numerical models have been developed although not to the same extent. Babu et al., (2008) performed both laboratory tests and numerical simulations (of triaxial tests) for the analysis of coir fibre reinforced sand using the finite difference code FLAC^{3D}. For the numerical simulation works, a triaxial specimen of 38mm diameter and 76mm height is generated using cylindrical elements. The domain is discretised into 1000 zones, organised in a radial pattern and randomly oriented coir fibres are

modelled as cable elements, which is a straight segment of uniform cross-sectional area between two nodal points. An elastic-perfectly plastic Mohr-Coulomb model is used to simulate the fibre reinforced sand behaviour. The simulation results indicate that presence of randomly distributed fibres in soils makes the stress concentration more diffuse and restricts the shear band formation (Figure 2.15). The authors also reported that simulation results are in good agreement with experiment results based on the triaxial tests on the same test conditions. However, no peak deviator stress of fibre reinforced soil is observed in numerical experiments, but in the simulation tests the deviator stress remains constant after reaching higher strain levels. In addition, apart from the simulation of triaxial tests, the numerical investigations did not provide further application of fibre reinforced sand (e.g. engineering design).

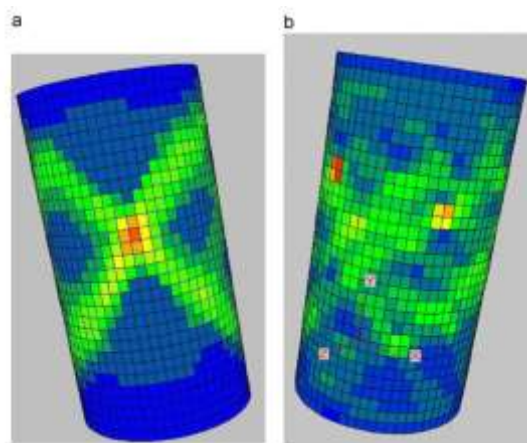


Figure 2.15. Failure pattern of the sample due to formation of shear band in (a) unreinforced soil and (b) reinforced soil (from Babu et al., 2008).

Neeraja et al., (2014) used similar method with Babu et al., (2008) to study the effect of fibre anisotropy on the strength of fibre reinforced soil. The simulation of materials is the same as Babu et al., (2008) and three different patterns of fibre orientation were simulated: all horizontal direction, all vertical direction and random orientation. The results show that distributions of fibres in which all were aligned horizontally offered a better stress-strain response compared to random fibre distribution and vertical fibres, being compressed cannot

contribute to strength improvement, the results thus verifying assumptions about fibre orientation by many researchers. Ibraim et al., (2018) utilised the discrete element method (DEM) to model the moist tamping of fibre reinforced sand to provide an insight into the local microscale mechanisms governing the fibre-grain interaction. The simulations reveal that during the tamping process, the fibres are mobilised in tension and then larger tensile stresses are mobilised at the end of the compaction stage. In addition, the simulations suggest that the fibre orientation is mainly controlled by the mixing and deposition phases of the mixtures rather than the formation stage (compaction or vibration). This seems to be in contradiction with conclusions on fibre orientation distribution in Diambra (2010).

Numerical simulations have also been used as a tool in the development of analytical and constitutive models of fibre reinforced soil. Bourrier et al., (2013) developed a numerical model of direct shear tests of root reinforced sandy soils based on the DEM to analyse the influence of the roots on the shear resistance of the soil, the soil being modelled as an assembly of locally interacting spheres and the roots modelled as deformable cylinders in the soil matrix (Figure 2.16). Simulations were made of frictional and cohesive materials in order to identify the different root-soil interaction mechanisms depending on the soil type. The results showed that the effect of the roots strongly depends on the shear strain. When the strain is small ($< 3\%$) the presence of roots leads to a slight decrease in the shear stress, for large strains values, a significant increase in the shear stress of the sample due to the fibres is observed. For a purely frictional material, an increasing shear strain induces progressively a pure tensile loading of the roots until there is slippage of the root-soil interface. For a purely cohesive material, tensile loading of the roots is followed by a progressive breakage of the adhesive root-soil links and by a complete slippage of the roots. The authors suggest that their results can be used in the calculation of slope stability when combining with other analytical approaches.

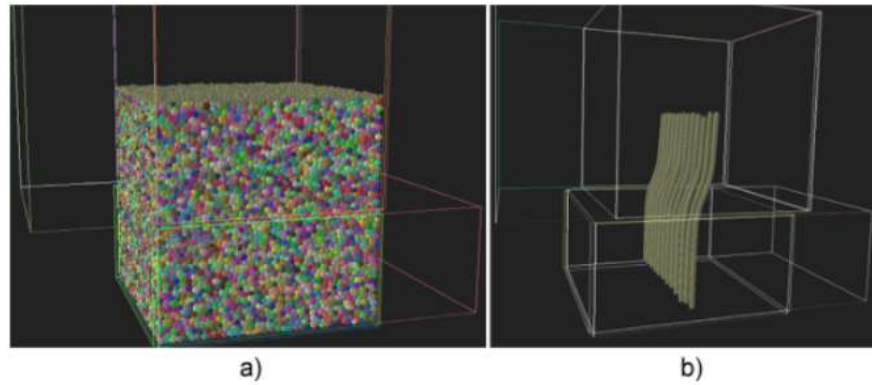


Figure 2.16. Example of the (a) numerical sample generated (b) deformed roots (from Bourrier et al., 2013).

Wang et al., (2019) developed a numerical analysis method to predict the shear strength of fibre reinforced clay based on equivalent confining stress concept which has already been introduced in Section 2.4.1. The fibres were assumed to be elastic-perfectly plastic, the soil-fibre bonding effect used the same sliding function as in both Machado et al., (2002) and Diambra (2010). The numerical analysis of the behaviour of fibre reinforced soils under triaxial compression was carried out via iterative calculation procedure, but the author did not provide the programming language type. The simulation results were then compared to the test results obtained by the authors and results by other researchers. The study shows that the proposed method slightly overestimates the internal friction angle and energy absorption capacity of fibre reinforced soil and is sensitive to volumetric fibre concentration and axial strain level. The reason posited is the bending of fibres induced by the consolidation stage produces a delayed mobilisation of equivalent additional stress.

In conclusion, several analytical and numerical models have been proposed by different researchers to explain the contribution to shear strength from randomly distributed fibres within soil matrix. According to these models, the shear strength of fibre reinforced soil can be expressed in different ways, using failure envelopes (Maher and Gray, 1990; Michalowski and Zhao, 1996) and stress-strain paths (Diambra et al., 2010). In addition to fibre inclusion

ratio and fibre aspect ratio, there are three main considerations raised these investigators: the constitutive model for the fibres, fibre orientation and distribution function and relative slipping (de-bonding) between fibres and the soil matrix. However, these models naturally have their own drawbacks as the hypotheses are in some place too idealised. In addition, parameters in some models are difficult to obtain from experimental tests and the influence of scale effects on the anisotropic mechanical properties of this complex composite material, due to the actual distributions of fibres were this material to be used in practice in engineering applications has not been fully investigated. Further constitutive model or numerical simulation studies based on these can help the technique to be used in engineering more accurately and reliable. However, limited studies can be found on constitutive models of fibre reinforced soil, and most of them focused on fibre reinforced sandy soil. Hence a constitutive model on fibre reinforced clay is worth to be studied. In the current study, based on previous work outlined in this chapter, a new model to predict the shear strength of fibre reinforced clayey soil will be proposed to exploit the strengths and minimise the weaknesses of these existing models. The model formulation will be described in Chapter 7, and calibrated by the data in Chapter 6.

2.5 Chapter summary

Review of the literature of fibre reinforced soil shows that there is a general consensus that fibre reinforcement (either natural or synthetic fibres) can improve soils' behaviours. Fewer investigations can be found on fibre reinforced clay comparing with fibre reinforced sand. According to the laboratory studies on fibre reinforced clay, the benefits of fibre reinforcement on clayey soil can be found generally in shear strength and tensile strength, , unconfined compressive strength, volumetric shrinkage and crack resistance. However, there is no agreement on the optimum inclusion ratio and aspect ratio of fibre for improving the properties of different soils. In addition, the test conditions in most of these research are not

close to the engineering condition (e.g. compacted clay). Full scale tests conducted on the fibre reinforced sand show that fibres are potentially effective reinforcement in various engineering projects. However, there is a potential application of fibres on clay soils when they are used as fill materials (e.g. road embankment), few full scale tests can be found on this so far. Analytical and numerical models of fibre reinforced soil also mainly concentrate on fibre reinforced sand, only a few models can be found on fibre reinforced clay. The stress-strain response and failure criterion of fibre reinforced clay can be predicted and expressed by these methods by considering important features like fibre inclusion ratio, fibre aspect ratio, fibre orientation and distribution, de-bonding of fibre. However, the existed models on fibre reinforced clay needs complicated calculations and extra tests on materials, a practical model of fibre reinforced clay for engineering purpose is necessary.

According to the review above, only a few numbers of published studies have been conducted on the utilisation of fibres to enhance the engineering properties and mechanical behaviour of high plasticity clay. To the date there has been no comprehensive study found on the fibre reinforcement effect on the engineering properties and mechanism analysis of London Clay, one of the most famous high plasticity soils in the world. Therefore, the primary aim of this study has been set to conduct a comprehensive investigation on engineering properties and mechanical behaviour of London Clay reinforced with polypropylene fibres, a mechanical model is also proposed in the study to predict the shear strength behaviour of fibre reinforced London Clay.

Chapter 3

3. Experimental testing programme

3.1 Introduction

In highway engineering, roadways are constructed through the compaction of materials to form road base, sub-base and surface paving layers. The sub-grade is also usually prepared through compaction, and depending upon the alignment requirements of the highway the sub-grade will either be in-situ soil exposed by the stripping of topsoil or will be composed of compacted fill if the road is constructed on an embankment. In either case the bearing capacity of the sub-base material is important to the stability and long term performance of the constructed roadway. High plasticity clays have been associated with low bearing capacities (Forster et al., 1994) and pose an additional problem due to their shrink swell potential which can lead to cycles of heave and subsidence, in turn leading to surface cracking. In Chapter 2 investigations are presented showing the potential of fibre additions to improve the mechanical behaviour of engineered soils for construction purposes, though research specifically on the effect of fibres in high plasticity soils in highway embankments is limited. This study therefore aims to address this research gap. To this end, a series of laboratory investigations have been conducted to investigate the properties of London Clay (a high plasticity soil) reinforced with polypropylene fibres. The laboratory testing programme comprised compaction tests, *CBR* tests, one-dimensional consolidation tests, linear shrinkage tests, desiccation cracking tests, direct tensile tests and triaxial tests, these tests were conducted on unreinforced and fibre reinforced soil. This chapter describes the materials used, the sample preparation methods employed and the detailed programme of tests in present research.

3.2 Materials

As stated above, the laboratory research was carried out on polypropylene (PP) fibres and London Clay. Polypropylene fibres were selected as they have already been used within the construction industry in concrete mixes and in the stabilisation of non-plastic soils. London Clay was selected as it represents a typical high plasticity soil that has been used in the construction of multiple embankments and other earth structures that form the highway and rail network in the south east of England.

3.2.1 London Clay

London Clay is found throughout the London Basin and ranges in thickness from a few meters to over 150 metres in places, it is predominantly argillaceous and mainly comprises bioturbated or poorly laminated, slightly calcareous, silty clay to very silty clay (BGS, 2004).

The mineral composition of London Clay are smectite, illite, chlorite and kaolinite but the composition ratios are various depending on location (Kemp and Wagner, 2006).

The London Clay used in this study was obtained from an excavation site for Crossrail project in Clapham, South-West of London, UK (Figure 3.1). After excavation and delivery to the laboratory, the soil was air dried at temperature below 35 °C and crushed with a mechanical crusher, then passed a 2 mm sieve to obtain consistent samples for testing. A series of classification tests were conducted as per BS 1377: 2 (BSI, 1990) to determine the particle size distribution, specific gravity and Atterberg limits. In order to ensure the representativeness of the results, each test was duplicated at least two times and the average values were calculated as the final results, the results of the classification tests are shown in Table 3.1.

In the testing programmes of desiccation crack testing (introduced in 3.4.5) and tensile strength tests (introduced in 3.4.6), soil specimens were prepared from a mixture containing

90% London Clay and 10% commercially available Wyoming bentonite (RS Minerals, 2015) by dry weight. Bentonite is a type of montmorillonite clay and has a much stronger ability to absorb water and a greater swelling potential with the increase of water content than other ordinary plastic clays. Bentonite was therefore employed in the research to make the soil more characteristic of expansive soil. Table 3.2 shows a comparison of the basic properties of London Clay (LC) and London Clay/bentonite composite (LB). In addition, the compaction characteristics of the LB were also determined and shown in Table 3.2, the procedure of the compaction tests is introduced in Section 3.4.1. It can be seen from Table 3.2 that after mixing with bentonite, the OMC, liquid limit (LL), plastic limit (PL) and plasticity index (PI) of the soil were increased, the MDD and D_{60} (particle size which 60% of the soil particles are finer than this) of the soil decreased. According to the BS standard classification system for fine soils (BS-5930, 1981), the soil was altered from a High Plasticity Clay (CH) to a Very High Plasticity Clay (CV). Also, the shrinkage potential of the soil was increased, making cracking more likely to occur during drying.



Figure 3.1 Position of London Clay in this study collected (Edina, 2019).

Table 3.1 Properties of London Clay used in study.

Soil Properties	Value
Specific Gravity	2.72
Liquid limit (%)	58.2
Plastic limit (%)	20.9
Plasticity index (%)	37.3
USCS classification	CH
<i>Grain size analysis</i>	
Sand (%)	13.8
Silt (%)	30.3
Clay (%)	55.9

Table 3.2. Comparison between London Clay and the composite mixed with bentonite.

Properties/ Soil Type	OMC (%)	MDD (Mg/mm ³)	D ₆₀ (mm)	LL (%)	PL (%)	PI (%)	BS classification
LC	22.4	1.581	0.003	58.2	20.9	37.3	CH
LB	25.7	1.535	0.002	72	25.6	46.4	VH

3.2.2 Fibres

Commercially available discrete polypropylene fibres were used as reinforcement in the research. There were two major reasons for choosing PP fibres: good mechanical properties and low cost. Also, polypropylene is a hydrophobic and chemically inert material which does not absorb or react with the moisture in soil. Due to the reasons above, PP fibres are the most common synthetic fibre material used in research of fibre reinforced soil. PP fibres can be divided into two categories: monofilament fibres (Figure 3.2a) and fibrillated fibres (Figure 3.2b). Fibrillated fibres are multifilament and remain in a bundle, this results in a stiffer fibre grouping that maintains the fibre's orientation. It was confirmed by the tests in this study that fibrillated fibres were hard to mix with soil homogeneously (Figure 3.3). Monofilament fibres are extremely fine single filaments and they are more flexible and soft than fibrillated fibres,

this leads to a better mixing effect with soil. Consequently, monofilament PP fibres were selected in this study. The fibres are produced by a construction fibres company named ADFIL (ADFIL, 2018), and the product name of the fibre is “Crackstop M”. Two different lengths of fibres (l_f) were used in the study to evaluate the effect of fibre length on reinforcing behaviour of fibres. Three fibre inclusion ratios (ρ_f) were adopted (0.3%, 0.6% and 0.9%) to evaluate the effect of fibre inclusion ratio on the reinforcing behaviour of fibres. The highest fibre inclusion ratio was set as 0.9% of the mass of dry soil because it was found that a higher fibre inclusion ratio might result in the accumulation of fibres and the formation of fibre lumps during mixing (Falorca and Pinto, 2011). The appearances of fibres at macroscopic and microscopic state are shown in Figure 3.4 and the chemical and physical properties of the PP fibres are given in Table 3.3.



(a)



(b)

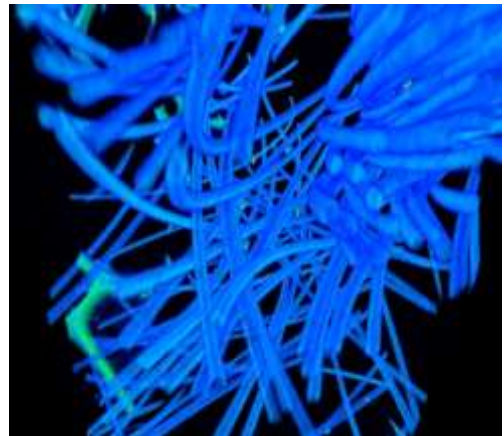
Figure 3.2 Two types of polypropylene fibres (a) monofilaments fibres (b) fibrillated fibres.



Figure 3.3. The accumulation of fibres in a fibrillated fibres-soil mixture (0.3% fibre inclusion ratio).



(a)



(b)

Figure 3.4 Appearance of fibres used in the study (a) macroscopic state (b) microscopic state (by 3D X-ray tomography).

Table 3.3 Properties of the PP fibre used in this study (ADFIL, 2019).

Fibre Properties	Value
Specific Gravity	0.91
Fibre Type	Monofilament
Length (mm)	6 & 12
Average Diameter (μm)	22
Tensile Strength (MPa)	416
Elongation at break (%)	43
Acid Resistance	High

3.3 Soil mixing

Laboratory investigations of soil behaviour require consistent test specimens to make the testing reproducible. Sample preparation in fibre reinforced soil is more complex than un-amended soil as besides the soil matrix and water, an additional material (fibre) is part of the mix. However, mixing procedures for soil-fibre composites have not been extensively discussed in existing literature and there is no standard method available for the preparation of fibre reinforced soil. The main concern in sample preparation is how to ensure fibres are evenly distributed and tangling is avoided. Sample preparation of fibre reinforced soil involves two stages: mixing and formation. The formation of the sample is dependent upon the eventual testing method and will be introduced in Section 3.4. A standardised mixing method has been developed which applies to all the laboratory experiments in this study and is described here. The mixing method of fibre-soil composite can be divided into two categories, wet mixing and dry mixing. In the wet mixing method, water is added to the dry soil and then mixed with fibres (Santoni et al., 2001, Tang et al., 2012, Patel and Singh, 2017), while in the dry mixing method, fibres are firstly added to the dry soil and then mixed with water (Estabragh et al., 2011, Cristelo et al., 2017, Anggraini et al., 2015).

The two mixing methods were compared and it was found that obvious fibre lumps were created in the wet mixing method (Figure 3.5). While no fibre lumps were observed and the fibre and soil mixed well when the dry mixing method was adopted (Figure 3.6). The dry mixing method resulted in less fibre lump formation because fibres are first coated by a layer of dry clay and then mixed well with water (Mirzababaei et al., 2012). Hence the dry mixing method was adopted in this study.



Figure 3.5 Fibre aggregation when fibres and soil were mixed using the wet mixing method.



Figure 3.6 Even distribution of fibres in dry mixing.

The whole process of fibre-soil mixture preparation is described below, this method was used for all the tests in this study. Designated masses of fibres were weighed and mixed with sieved, air-dried soil in small increments (10% of the fibre addition, e.g. 0.3%, 0.6% and 0.9%) by hand, making sure that a homogeneous composite was achieved without any visible aggregation of fibres. After fibre-soil mixing, distilled water was added to the mixture with a spray bottle until the target water content was achieved. According to sample preparation descriptions in existing literature, the mixing of fibre-soil composite was usually conducted by manual mixing or mechanical mixing. However, both of methods have been employed in this research in order to achieve a homogenous fibre-soil composite. Initial mixing of the wet material was performed by manually mixing with a pallet knife, this produced an even

distribution of water and prevented wet clay sticking to the mixer in the next step. The second step of the mixing was performed in a mechanical mixer. The mixer contains a stainless steel bowl and a hook-shape-blade which moves 139 revolutions per minute around the bowl. About 2 kg composite was put into the mixer each time and mixed for 3 minutes. After a 3-minute-mixing, no fibre cluster can be seen and fibres were randomly distributed, the final product can be considered homogenous. After the mixing was completed, the fibre-soil composite was stored in a sealed plastic bag for at least 24 hours until the sample formation for different tests. For the unreinforced soil, a similar process was adopted but without the step of adding fibres.

3.4 Testing program

There were seven groups of laboratory tests in this study and each test was conducted on both unreinforced and fibre reinforced soil. The procedure for these tests are introduced in this section and the whole laboratory test program is summarised at the end of the chapter.

3.4.1 Compaction tests

Light Proctor compaction tests were performed in accordance with BS 1377: 4 (BSI, 1990) to determine the compaction characteristics of unreinforced and fibre reinforced soil. The optimum moisture content (OMC) and maximum dry density (MDD) of the soil obtained from compaction tests determined the initial condition of the samples in further investigations in this study. An appropriate amount of prepared soil as stated in Section 3.3 was taken and compacted in three layers in the steel mould, each layer received 27 blows by a 2.5kg hammer falling from a height of 300 mm. The weight and water content of the samples were measured after compaction finished. The compaction tests were conducted on 35 samples in total for unreinforced soil and fibre reinforced soil and the programme of compaction tests is shown in Table 3.4.

Table 3.4. Programme of compaction tests.

Sample Type	Fibre inclusion ratio (%)	Fibre length (mm)	Number of samples
URS	-	-	5
FRSA	0.3	6	5
FRSB	0.6	6	5
FRSC	0.9	6	5
FRSD	0.3	12	5
FRSE	0.6	12	5
FRSF	0.9	12	5

* URS = unreinforced soil; FRS = fibre reinforced soil.

3.4.2 CBR tests

A series of laboratory California Bearing Ratio (*CBR*) tests were performed as per BS 1377: 4 (BSI, 1990) to evaluate the effect of fibre reinforcement on the bearing capacity of the soil. The samples were prepared at their OMC and MDD as determined from the compaction tests. This is to simulate the condition of the subgrade soil in road engineering. The tests were conducted in a soaked condition, the specimens were soaked in a water tank for 96 hours and a surcharge disc of 1 kg was added above the sample to simulate the effect of superimposed construction load (Figure 3.7a). After finish the swelling stage, the sample was allowed to be penetrated from both sides of the specimen respectively (Figure 3.7b), the penetration load and displacement were measured and the *CBR* value was calculated as per BS 1377: 4 (BSI, 1990). The average *CBR* value of two sides was adopted as the final result. Seven samples were conducted in total and the programme of *CBR* tests are shown in Table 3.5.



(a)



(b)

Figure 3.7. The process of *CBR* test (a) the sample during soaking (b) the sample during test.

Table 3.5. Programme of *CBR* tests.

Sample type	Fibre inclusion ratio (%)	Fibre length (mm)	Number of samples
URS	-	-	1
FRSA	0.3	6	1
FRSB	0.6	6	1
FRSC	0.9	6	1
FRSD	0.3	12	1
FRSE	0.6	12	1
FRSF	0.9	12	1

3.4.3 Consolidation tests

The oedometer test is usually used to investigate the stress-strain behaviour of a low-permeability soil (e.g. clay) in one-dimensional vertical compression and swelling (Powrie, 2004). In this study, oedometer tests were carried out as per BS 1377: 5 (BSI, 1990) to assess the consolidation characteristics of unreinforced and fibre reinforced London Clay. The

samples were prepared at their respective OMC and MDD and they were approximately 25 mm in diameter and 20 mm in height. The conventional methods of forming re-compacted oedometer samples are static compression or dynamic compaction. However, achieving a homogenous distribution of fibres in such small specimens is difficult, therefore the specimens for consolidation tests were cut from the middle part of *CBR* specimens as described in Section 3.4.2 with a circle ring cutter. In order to eliminate the interference from the penetration on the *CBR* samples, an extra unreinforced sample was cut from a soaked and unpenetrated *CBR* sample. By comparing the test results of consolidation samples cut from penetrated and unpenetrated *CBR* samples (results are shown in Chapter 4), it was found that there was no obvious difference between the consolidation behaviour of two samples. The process of consolidation test is described below. A seating load of 5 kPa was applied and once initial displacement under this load had ceased the samples were then allowed to undergo consolidation under a range of pressures (25, 50, 100, 200, 400 and 800 kPa), each pressure was applied for 24 hours and the vertical displacement of the sample was recorded as following periods of elapsed time : 0, 10, 20, 30, 40, 50 s, 1, 2, 4, 8, 15, 30 min, 1, 2, 4, 8, 24 h. After the final loading stage, the specimen was unloaded by pressure decrements (400, 200 and 50 kPa). Based on the tests results, the relationship between void ratio and normal pressure was obtained, the coefficient of consolidation and compressibility parameters were calculated according to related formula. Seven samples in total were subjected to consolidation tests and the programme is shown in Table 3.6.

Table 3.6. Programme of consolidation tests.

Sample type	Fibre inclusion ratio (%)	Fibre length (mm)	Number of samples
URS	-	-	1
FRSA	0.3	6	1
FRSB	0.6	6	1
FRSC	0.9	6	1
FRSD	0.3	12	1
FRSE	0.6	12	1
FRSF	0.9	12	1

3.4.4 Linear shrinkage tests

Linear shrinkage tests were carried out on unreinforced and fibre reinforced soil in order to evaluate the effect of fibre reinforcement on the linear shrinkage behaviour of soil. The tests were performed in accordance with BS 1377: 2 (BSI, 1990). To prepare this test, the soil was passed through a 425 μm sieve before mixing, then the fibre-soil composite was prepared as described in 3.3, and the water content of the specimen was controlled as the liquid limit of the soil (58.2%) to bring the composite into a slurry state. Then the composite was placed into a mould in the form of semi-cylindrical trough with 140 mm length and 25 mm diameter. The sample was dried firstly at room temperature (20 $^{\circ}\text{C}$) until the soil had shrunk away from the walls of the mould, then dried at 40 $^{\circ}\text{C}$ until shrinkage had largely ceased, and finally at 105 $^{\circ}\text{C}$ to complete the drying. After drying, the sample was removed carefully from the mould and the lengths of the top and bottom surfaces were measured, and the percentage linear shrinkage (*PLS*) was calculated using Equation 3.1, where L_1 is the final length of the specimen (average value) and L_0 is the initial length of the sample.

$$PLS = \left(1 - \frac{L_1}{L_0}\right) 100\% \quad (3.1)$$

As shown in Table 3.7, there are 21 samples in total for linear shrinkage tests and three specimens were tested for each sample type, and the average value of *PLS* was adopted as the final result.

Table 3.7. Programme of linear shrinkage tests.

Sample type	Fibre inclusion ratio (%)	Fibre length (mm)	Number of samples
URS	-	-	3
FRSA	0.3	6	3
FRSB	0.6	6	3
FRSC	0.9	6	3
FRSD	0.3	12	3
FRSE	0.6	12	3
FRSF	0.9	12	3

3.4.5 Desiccation cracking tests

As mentioned previously in Section 3.2.1, 10% bentonite by the dry weight of London Clay was added to the fibre-soil mixture and mixed as described in Section 3.3 for this test in order to achieve a more plastic soil. 1.555 kg of composite was compacted to a 200 mm × 200 mm × 20 mm metal container manually by a 2.5 kg hammer to achieve a dry density of 1.495 Mg/m³ with a water content of 30%. The dry density of the sample was set as 97% of MDD of the LB, this is to satisfy the requirement of subgrade fill for highways in the UK (Highways England, 2018). After compaction, the specimen was scraped carefully with a pallet knife to achieve a smooth surface. It is known that increased friction between soil and the base of container will promote crack initiation in shrinkage cracking experiments (Corte and Higashi, 1960, Groisman and Kaplan, 1994). Peron et al., (2009) increased the friction by using a container with a grooved base. In this study, a similar approach was taken where Medium-80

grade sandpaper (Oakey, 2019) was glued to the base of the container. The sand paper under the specimen was used to simulate the friction between the subsoil and the subgrade fill in a typical highway construction. The mould with sand paper is shown in Figure 3.8a, it can be observed that there are shadow areas at the edges of the mould, these can have a detrimental effect on digital image processing results. Therefore the specimens were placed under a lamp when photographed as the vertical light from the lamp can prevent the occurrence of shadow (Figure 3.8b).

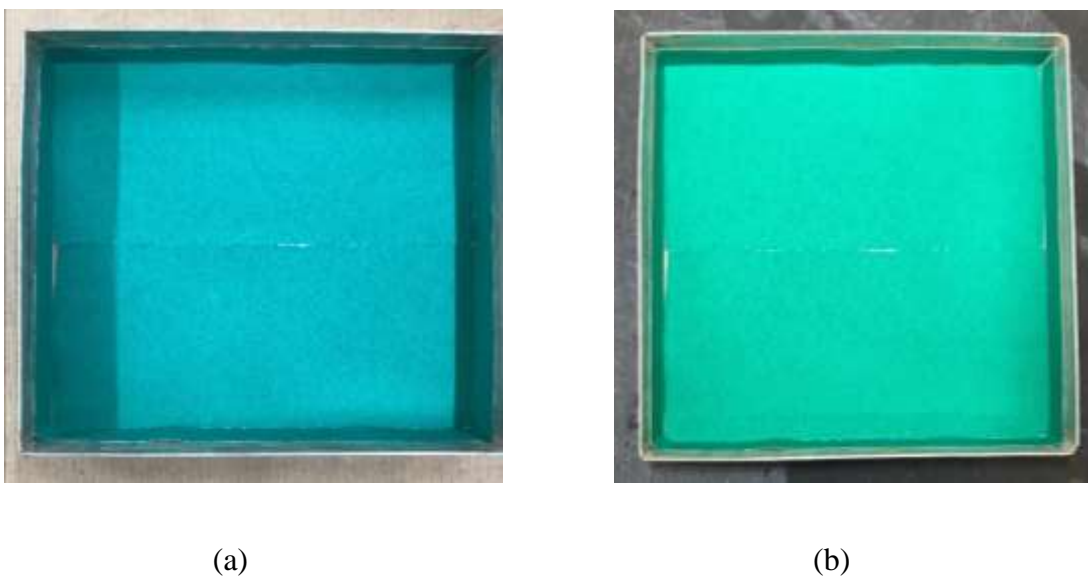


Figure 3.8. The mould used for desiccation cracking testing (a) without lamp light (b) with lamp light.

During the test, the specimen was placed in a temperature controlled oven at a temperature of 40 ± 1 °C for 24 hours to simulate high summer temperatures. The specimen was taken out of the oven and the mass of the specimen (with mould) was measured by a digital balance (with accuracy to 0.01 g) over certain time, which was set as 5, 10, 15, 20, 25, 30, 35, 40, 45, 50, 55, 60, 70, 80, 90, 105, 120, 150, 180, 210, 240, 300, 360, 420, 480, 600, 720 and 1440 minutes after the test started. In addition, an iphone-7 with 12 million pixels anti-shake lens with fixed position (250 mm above the specimen surface) was used as camera to record the appearance

of surface cracking. The specimen was put back in the oven immediately after measuring and photographing. A schematic diagram of the test setup is shown in Figure 3.9. A total of 14 samples were conducted on unreinforced soil and reinforced soil as per information presented in Table 3.8. Digital image processing software ImageJ (introduced in Chapter 5) was employed to monitor the development of the cracks and evaluate the crack resistance of the unreinforced and reinforced soil, the average results of two samples for each conditions were adopted.

Table 3.8. Programme of desiccation cracking tests.

Sample type	Fibre inclusion ratio (%)	Fibre length (mm)	Number of samples
URS	-	-	2
FRSA	0.3	6	2
FRSB	0.6	6	2
FRSC	0.9	6	2
FRSD	0.3	12	2
FRSE	0.6	12	2
FRSF	0.9	12	2

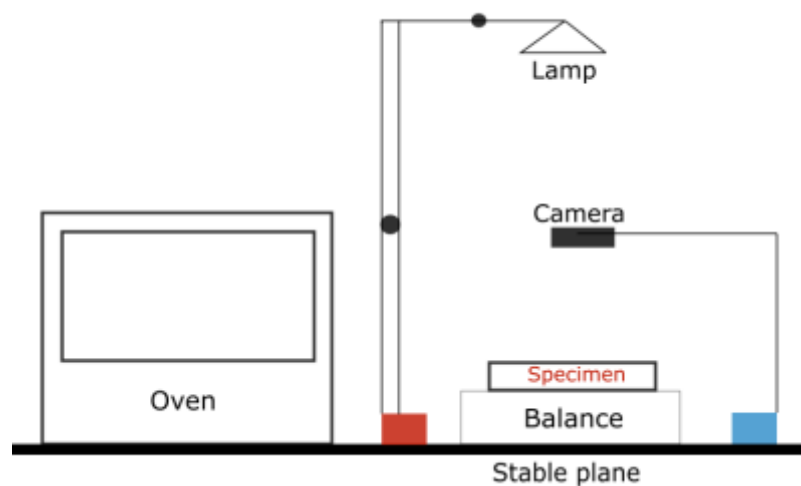


Figure 3.9. Schematic representation of the setup for the desiccation cracking test.

3.4.6 Direct tensile tests

A series of direct tensile tests were conducted on both unreinforced and reinforced samples to investigate the effect of fibre reinforcement on tensile behaviour of soil. The soil used in this test and the initial condition of the samples are the same as described in 3.4.5. The prepared soil was statically compressed in a “bow-tie”-shaped steel mould (Figure 3.10) in three layers as evenly as possible. The sample was then extracted carefully by dismantling the mould. Once free, the sample was then wrapped using cling film and stored for 24 hours before testing. Figure 3.11 shows the schematic drawing of a prepared specimen and its dimensions. The sample width is reduced from 34 to 17 mm to induce a failure at the centre section of the specimen and the total volume of samples is 70.5 ml. A novel adaptation of the direct shear apparatus proposed by Stirling et al., (2015) was employed in this study to conduct the direct tensile tests. Modifications to the standard test rig consist of two “bow-tie”-shaped PVC loading jaws to induce tension. PVC jaws (Figure 3.12a) gripped the mounted specimen during the test, with an interior jaw angle of 20°, which was greater than the potential dilatancy angle of soil tested (Arslan et al., 2008, Divya et al., 2013). This prevents the relative displacement of specimens with respect to the confining jaw surface during the test, and helps to achieve a uniform stress distribution (Divaya et al., 2013, Stirling et al., 2015). The modified direct shear apparatus shown in Figure 3.12b was used in this study, and the tests were conducted at a displacement rate of 1 mm/min. Horizontal load and displacement were continually measured by transducers and recorded by a data logger. The tensile stress was then calculated as follows:

$$\sigma_T = \frac{N}{A} \quad (3.2)$$

where N is the measured load and A is the cross-sectional area at specimen’s neck. Specimens shrank to different degrees due to desiccation, so the cross-sectional area of specimen was

measured before the test. After the test, the water content of each specimen was determined and total suction was measured by the chilled mirror dew point method in the form of a WP4C Soil water potentiometer from Decagon Devices (Decagon devices, 2015).

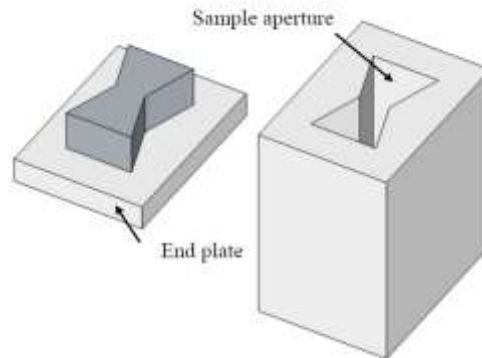


Figure 3.10. Mould used to form samples (from Stirling, 2014).

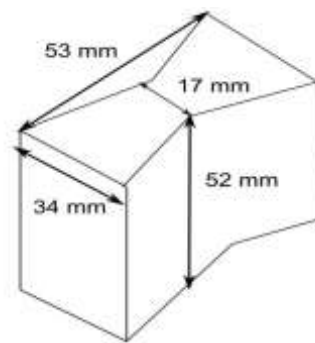


Figure 3.11. Size and shape of the specimen in tensile test.

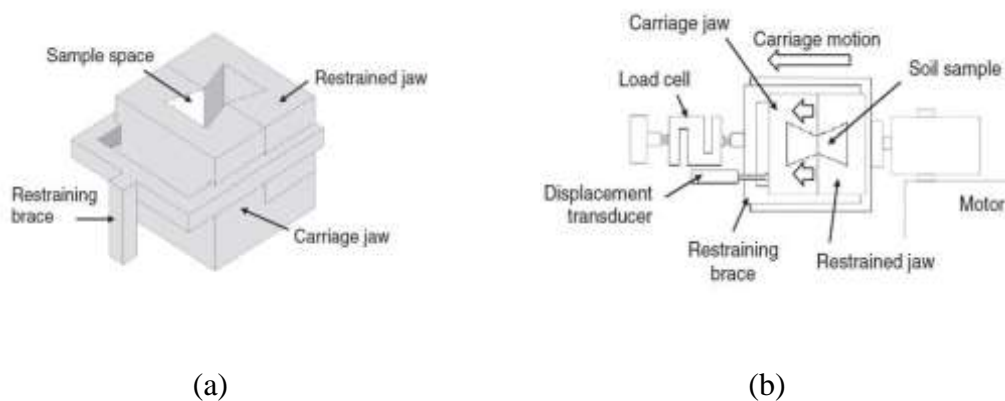


Figure 3.12. Tensile test equipment (a) loading jaws (b) schematic of testing rig (from Stirling et al., 2015).

As shown in Table 3.9, direct tensile tests were conducted on 105 samples in total for seven conditions. For each condition, 15 samples were prepared at initial gravimetric water content $w = 30\%$, three of the samples are tested at the initial water content and the remainder were allowed to air dry and tested at $w = 24\%$, 20% , 16% and 12% . Three parallel specimens were tested for each water content and 105 specimens in total were subjected to tensile test.

Table 3.9. Programme of tensile strength tests.

Sample type	Fibre inclusion ratio (%)	Fibre length (mm)	Water content (%)	Number of samples
URS	-	-	30, 24, 20, 16, 12	15
FRSA	0.3	6	30, 24, 20, 16, 12	15
FRSB	0.6	6	30, 24, 20, 16, 12	15
FRSC	0.9	6	30, 24, 20, 16, 12	15
FRSD	0.3	12	30, 24, 20, 16, 12	15
FRSE	0.6	12	30, 24, 20, 16, 12	15
FRSF	0.9	12	30, 24, 20, 16, 12	15

3.4.7 Triaxial tests

Consolidated-undrained (CU) tests were conducted on unreinforced and reinforced soil in accordance with BS-1377-8 (BSI, 1990) to investigate the effect of fibre reinforcement on undrained shear behaviour of the London Clay. The triaxial tests were conducted on a computer-controlled Wykeham Farrance Digital Tritech 50kN system (Figure 3.13).



Figure 3.13 Triaxial cell and loading frame.

A linear variable differential transformer (LVDT) was placed outside the cell to monitor axial strains and an internal submersible load cell was employed to measure the axial stresses in the specimen. In addition, two pressure transducers were utilised to measure the pore water pressures inside the sample and the back pressure in the cell respectively. These data were recorded using a data logger and saved in a computer. The unreinforced and fibre reinforced triaxial test samples were prepared at their own OMC and MDD. The samples were compacted in a 38 mm diameter \times 76 mm height cylindrical mould in three equal layers by the static compression method. Subsequently, the specimen was pushed out of the mould without disturbance and wrapped using cling film, after 24 hours the specimen was ready for testing. The specimen was back pressure saturated at 300 kPa back pressure and with 5 kPa difference between cell pressure and back pressure. The coefficient B was used to assess the completion degree of the saturation stage, it can be obtained from the following equation:

$$B = \frac{\Delta\sigma_3}{\Delta u} \quad (3.3)$$

If the B -value was greater than 0.95, the specimen was considered as saturated and ready for the next step, it took about 48 hours for the saturation stage. After saturation, the specimen

was isotropically consolidated at a predefined confining stress until no volume change, the confining stresses considered in this study were 50, 100 and 200 kPa. The drainage valves were closed after the completion of consolidation and the sample was sheared under undrained condition by applying the deviator stress. A constant axial displacement rate of 0.015 mm/min was selected giving an axial strain rate of 0.02% per minute. The shearing period lasted for about 17 hours to make the axial strain beyond 20%. A slow rate was chosen to ensure the equilibrium of pore water pressure throughout the sample during the test. The failed specimen was photographed after the test, and cross section area correction was calculated as

$$A_s = \frac{A_c}{1 - \varepsilon_a} \quad (3.4)$$

where A_s is the corrected cross section area, A_c is the initial cross section area and ε_a is the axial strain. The membrane barrelling correction was calibrated according to Figure 3.14 allow for the restraining effect of the membrane. Triaxial tests were conducted on 21 samples and the programme is shown in Table 3.10.

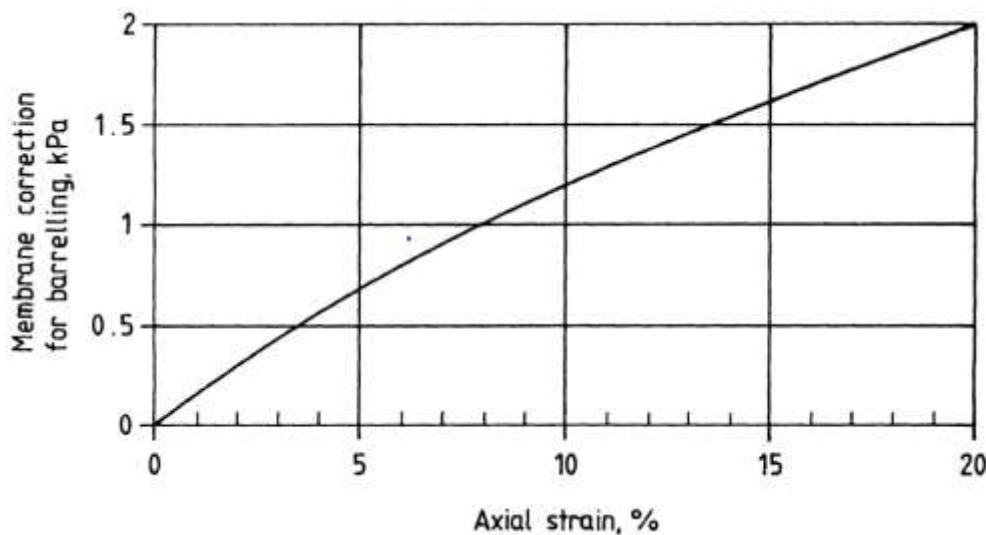


Figure 3.14. Membrane correction in triaxial test (from BS-1377-8, 1990).

Table 3.10. Programme of triaxial tests.

Sample type	Fibre inclusion ratio (%)	Fibre length (mm)	Cell pressure (kPa)	Number of samples
URS	-	-	50, 100, 200	3
FRSA	0.3	6	50, 100, 200	3
FRSB	0.6	6	50, 100, 200	3
FRSC	0.9	6	50, 100, 200	3
FRSD	0.3	12	50, 100, 200	3
FRSE	0.6	12	50, 100, 200	3
FRSF	0.9	12	50, 100, 200	3

3.4.8 Summary

The laboratory tests on unreinforced and fibre reinforced soil are summarised in Table 3.11, these seven types of tests are classified into three categories and will be discussed in Chapter 4, Chapter 5 and Chapter 6 respectively.

Table 3.11. Summary of the laboratory tests program in present research.

Test type	Chapter in the thesis	Soil type	Number of samples
Compaction tests	4	LC	35
CBR tests	4	LC	7
Consolidation tests	4	LC	7
Linear shrinkage tests	5	LC	21
Desiccation cracking tests	5	LB	14
Direct tensile tests	5	LB	105
Triaxial tests	6	LC	21

Chapter 4

4. Compaction and consolidation properties of fibre reinforced clay

The methodology of the laboratory research was introduced in the last chapter. In this chapter, the first part of the laboratory research in this study is presented, which includes a comprehensive study of the effect of fibre reinforcement on the compaction, *CBR*, and one-dimensional consolidation behaviour of London Clay. These investigations aim to understand the benefit of polypropylene fibre reinforcement in the application of embankment engineering. The tests results are reported and discussed as following.

4.1 Compaction tests

Compaction tests were conducted on unreinforced and fibre reinforced soil following the method described in 3.4.1, and the results are discussed in this section. The variations of moisture content and dry density of soil in the compaction tests are plotted in Figure 4.1, and the OMC and MDD of the unreinforced and reinforced soil are listed in Table 4.1. It is worth noting that compaction curves are the closest fit results to all data points. One can observe that there are gaps in data series FRSA and FRSB, but all the reinforced soil compaction curves show consistent trends generally, so the gaps are acceptable in this study. It can be seen that with the increase of fibre inclusion ratio from 0% (i.e. unreinforced soil) to 0.9%, the MDD of soil gradually decreases from 1.581 Mg/m³ for unreinforced soil to 1.546 Mg/m³ and 1.548 Mg/m³ for 6 mm and 12 mm FRS samples respectively. This trend is consistent with the conclusions found in other studies on different types of soil and fibre (see in Table 2.3). This decrease can be attributed partly to the decrease of the average unit weight of the solids in the soil fibre mixture, and the fibres preventing efficient particle packing. The OMC

is also observed to slightly decrease with the addition of fibres, this is believed to be due to the polypropylene fibres not being able to absorb moisture, and the disruption to the void structure caused by the inclusion of fibres (see also Harianto et al., 2008). These findings are in agreement with studies by Yaghoubi et al., (2018) and Plé and Le (2012). However, different conclusions can be found in other studies (detailed in Table 2.3). Khatri et al., (2016) and Viswanadham et al., (2009) found that OMC increased as fibre inclusion ratio increased in clay reinforced with coir and PP fibre respectively. Mohamed et al., (2013) investigated clay reinforced with hay fibres and found that OMC increases and then decreases with increases in fibre addition. Therefore, consensus has not been reached on the effect of fibre addition on the OMC of the soil based on the literature review. OMC of FRS is influenced by soil and fibre types rather than being consistent across all soil and fibre types. In addition, it can also be concluded from the results presented here that for the same fibre inclusion ratio, soil reinforced with longer fibres tends to have a higher MDD, though this phenomenon is less clear when the fibre inclusion ratio is increased to 0.9%. Fibre length is not seen to have a significant impact on OMC within the lengths investigated in this research (6 and 12 mm).

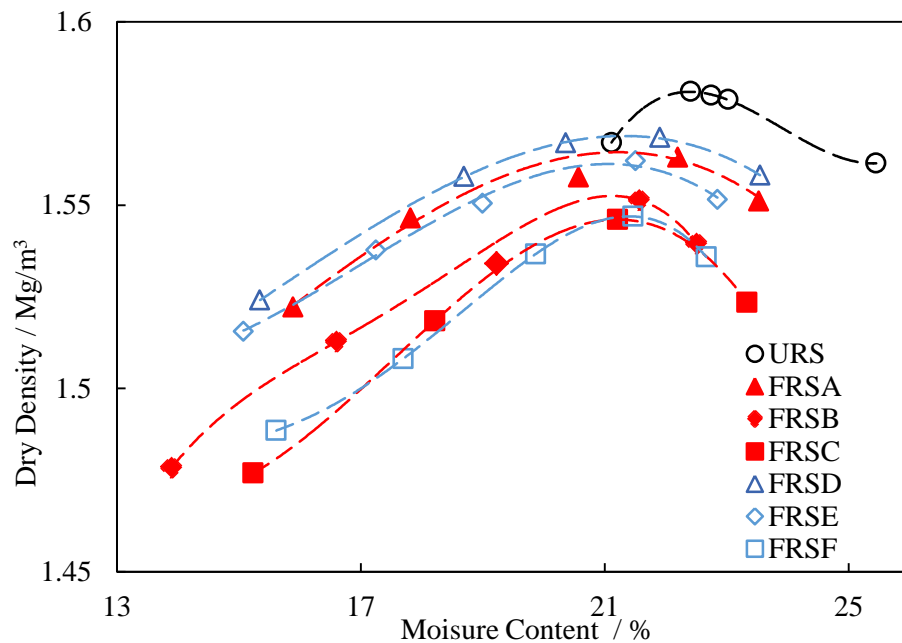


Figure 4.1. Compaction curves for unreinforced and reinforced soil.

Table 4.1. Compaction characteristics of unreinforced and reinforced soil.

Sample/Item	URS	FRSA	FRSB	FRSC	FRSD	FRSE	FRSF
MDD (Mg/m^3)	1.581	1.563	1.551	1.546	1.567	1.561	1.548
OMC (%)	22.4	22.3	21.5	21.3	22.1	21.6	21.5

4.2 CBR tests

CBR tests were conducted on unreinforced and fibre reinforced soil follows the method described in 3.4.2, and the results are discussed in this section. The *CBR* test results are shown in Figure 4.2, and demonstrate that the addition of fibres to London Clay results in a significant increase in *CBR* value. For a given fibre length, the improvement in *CBR* values appears to be roughly proportional to the increase in the percentage of fibre. The largest improvements occur for an inclusion ratio of 0.9% with 6 mm length fibre, where the *CBR* values is double the value of the unreinforced soil sample. The improvement in *CBR* values is believed to be due to fibres interacting with the soil particles, consequently generating surface friction and tensile capacity which is not present in the unreinforced soil. However, the rate of increase in *CBR* values reduces as the fibre inclusion increases. In order to show the benefit on *CBR* improvement, here a dimensionless term California Bearing Ratio Index (*CBRI*), defined as the ratio of the *CBR* value of reinforced soil (CBR_r) to the *CBR* value of unreinforced soil (CBR_u) (Choudhary et al., 2010) is employed and the relationship between *CBRI* and fibre inclusion ratio is shown in Figure 4.3. It can be seen from Figure 4.3 that the increase in *CBRI* corresponds with the increase of the fibre inclusion ratio. When the fibre length is 6 mm, the *CBR* value of FRSA, FRSB and FRSC are 138%, 176% and 200% of the URS sample respectively. When the fibre length is 12 mm, the value of FRSD, FRSE and FRSF are 125%, 169% and 185% of the URS sample respectively. It is also found in Figure

4.3 that samples reinforced with shorter fibres have a higher *CBR* for the given fibre inclusion ratio, e.g. 6 mm long fibres produced a greater improvement in the *CBR* values of the London Clay than the 12 mm long fibres. A similar trend was shown by Chore et al., (2011) and Pradani et al., (2017). This could be attributed to the fact that the difference in fibre length is relatively small when compared to the overall sample size. Shorter fibres are twice as numerous as longer fibres when the masses are equal, leading to a more homogeneous distribution within the sample. Other studies have shown differing results. According to Marandi et al., (2008) and Choudhary et al., (2010), when the fibre length is relatively long (> 20 mm), the *CBR* values of FRSs increases effectively as fibre length increases. Maity et al., (2018) found that *CBR* values of FRS tended to increase with the increase of fibre length up to a maximum limit (10 mm) and after that exhibit reduction, similar trend was found in Masoumi et al., (2013). The deviation of results between the different studies suggests that the mechanisms through which fibres improve *CBR* values are not completely understood and may vary with soil type. This provides further justification for investigating fibre effects on particular problem soils like London Clay. *CBR* value is a very important index to guide the design of road pavements. Actually, the *CBR* value of subgrade soils have a significant influence on the subbase and capping design (Figure 4.4). A higher *CBR* value results in a reduced thickness of capping (between the subgrade and sub-base) and subbase. For example, in a sub-base only design, an increase from 4% to 15% of the *CBR* value of the subgrade soil can lead to a 110 mm reduction in the thickness of the subbase (from 260 mm to 150 mm) representing a significant saving in materials and handling costs. Table 4.2 presents the alternative designs for different soils tested in this research. It can be seen from Table 4.2 that where the greatest improvement of *CBR* value can be implemented (FRSC), the total thickness of the capping/sub-base design and sub-base only design are reduced by 75 and 70 mm respectively compared with that of unreinforced soil.

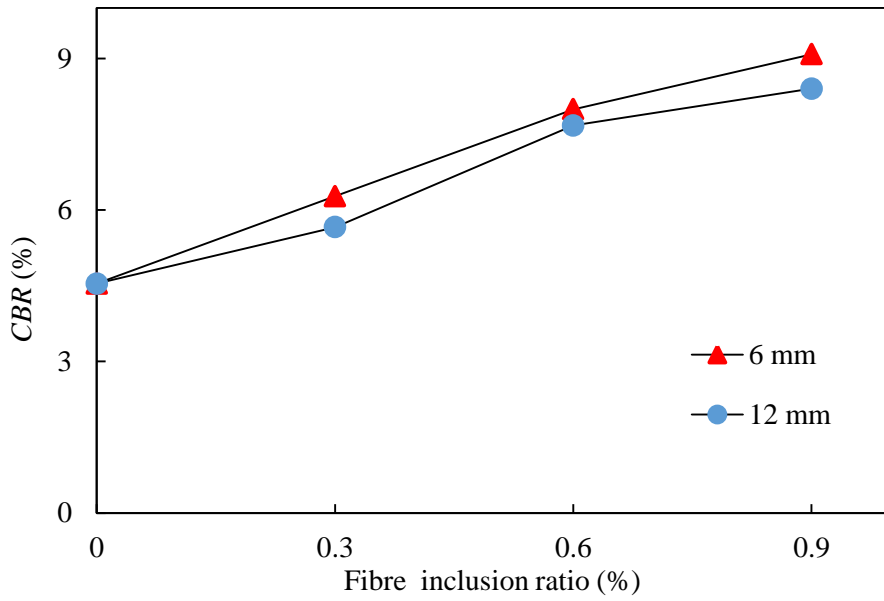


Figure 4.2. Variation of *CBR* value with fibre inclusion ratio at different fibre lengths.

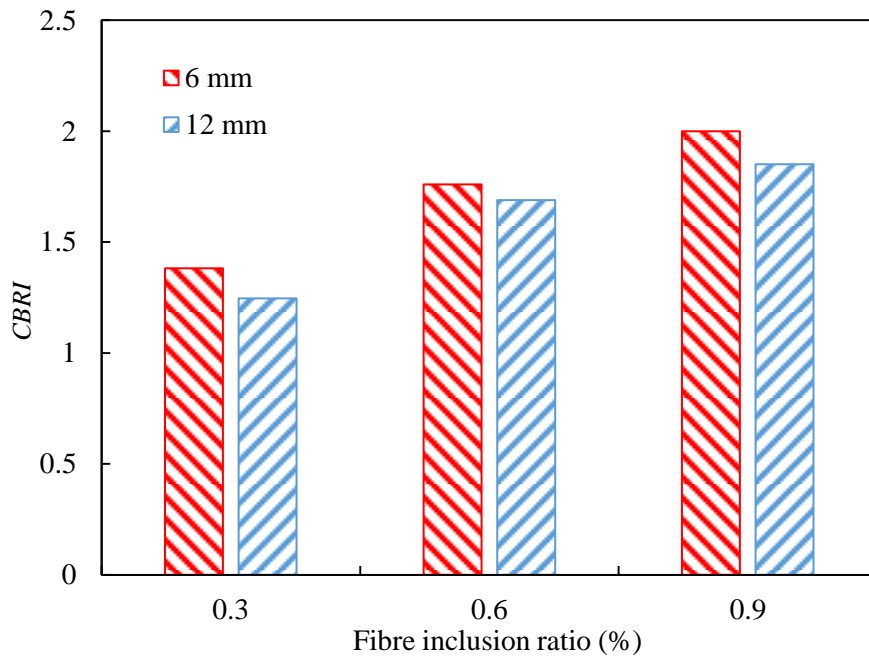


Figure 4.3. Variation of *CBRI* with various fibre inclusion ratio at different fibre lengths.

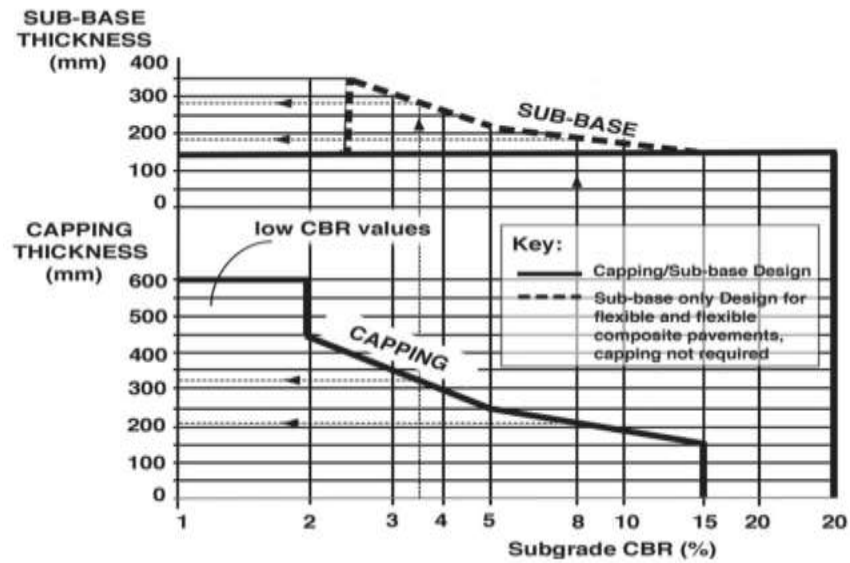


Figure 4.4. Capping and subbase thickness design (from HD 26/06, 2006).

Table 4.2. Pavement design alternatives for unreinforced and fibre reinforced soil.

Soil type	URS	FRSA	FRSB	FRSC	FRSD	FRSE	FRSF
<i>CBR (%)</i>	4.54	6.27	7.99	9.08	5.66	7.67	8.4
(1) Subbase (mm)	150	150	150	150	150	150	150
Capping (mm)	275	235	210	200	245	215	205
(2) Subbase (mm)	245	205	185	175	210	190	180

4.3 Consolidation tests

Consolidation tests were conducted on unreinforced and fibre reinforced soil following the method described in 3.4.3, and the results are discussed in this section. As mentioned in Chapter 3, consolidation samples were taken from the centre of previously tested *CBR* specimens. It was recognised that there was a risk of sample disturbance due to the *CBR* penetrometer compacting the material in the *CBR* mould during testing. In order to determine whether the *CBR* testing process may have changed the compressibility of the soil an extra

unreinforced sample was cut from an untested/unpenetrated *CBR* sample to check if the soil consolidation properties would be changed by the testing process alone. The void ratio-normal pressure curves of the two unreinforced specimens (previously *CBR* tested and not previously *CBR* tested) are shown in Figure 4.5. It can be seen from the two curves that in both compression and swelling stages, no obvious difference can be found between the two specimens. Hence cutting the consolidation samples from the middle of previously tested *CBR* samples is believed to be acceptable method in this research, and the test results are discussed as follows. The soil near the cut sample in the *CBR* specimens is used to measure the initial water content (w_0), by considering the sample is saturated (after soaked), the initial void ratio of the sample (e_0) is calculated as per Equation 4.1:

$$e_0 = w_0 G_s \quad (4.1)$$

where G_s is the specific gravity of soil.

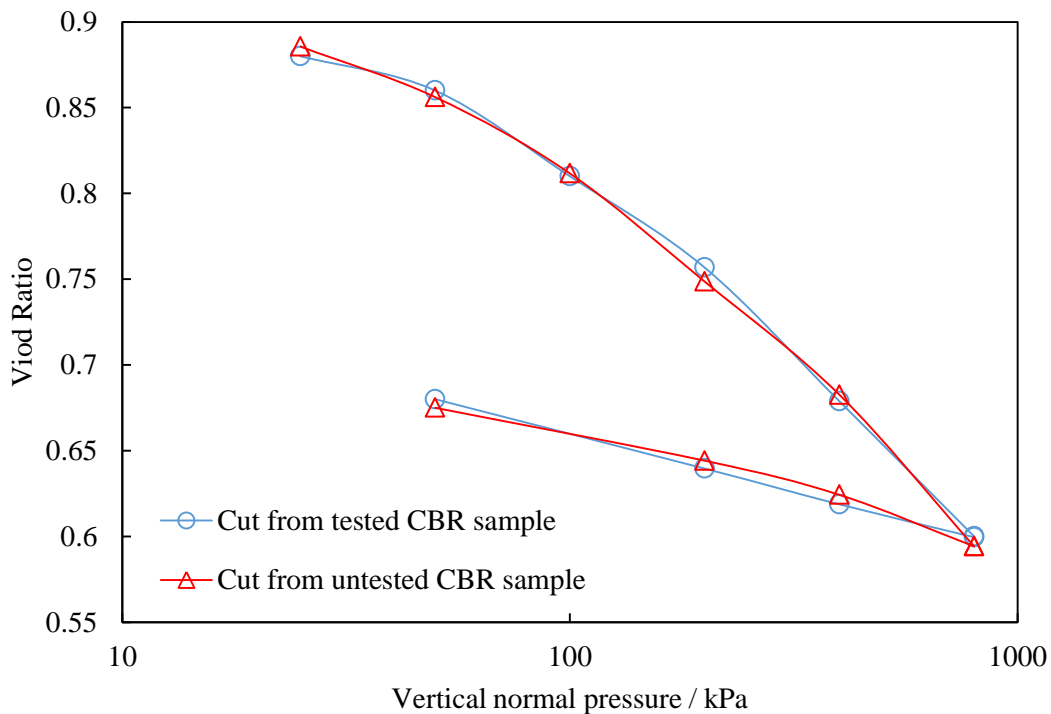


Figure 4.5. Comparison of two unreinforced sample cut from different conditions.

Void ratio-pressure relationship curves obtained from one-dimensional consolidation tests for unreinforced soil and FRS are shown in Figure 4.6. It can be seen from the figure that for a given pressure, the void ratio of the soil decreases with an increase in the percentage of fibre, which leads to the normal consolidation path of all reinforced samples lying below the unreinforced line. Similar trends can be found in Phanikumar and Singla (2016) and Kar et al., (2012) in which different soil and fibre types were investigated. It can be deduced that the mechanical effect of fibre is to constrain the compression and swelling of the soil, as might be expected. However, this trend seems contradiction with the conclusion obtained from compaction tests in Section 4.1, which fibres lead to a decrease in MDD and implying a higher void ratio. Hence, it is believed that the decrease in dry density of FRS might not come from the higher void ratio but a lower average unit weight of the fibres. At a given pressure level, the void ratio of samples decreases as the fibre content increases generally, and soil reinforced with 6 mm long fibres at 0.9% inclusion ratio shows the largest decrease. For instance, the void ratio at a pressure of 25 kPa reduces from 0.88 for the unreinforced soil to 0.75. Also, the void ratio of soil gets closer when the vertical normal pressure is higher, which indicates the one-dimensional NCL will converge at high pressure. This trend is consistent with Phanikumar and Singla (2016), but inconsistent with Kar et al., (2012), who reported a parallel NCL of URS and FRS at high pressure levels. However, the slope of NCL of the soil gets slower as the fibre inclusion ratio increases under the pressure of testing scale. The intersection of the two linear segments of the curves is used to determine the pre-consolidation pressure (p'_c) of the soil, the Compression Index C_c and Swelling Index C_s of URS and FRS are obtained from the linear portions of loading curves and unloading curves (see in Figure 4.6) for each soil and are plotted against the fibre inclusion ratio in Figure 4.7. It can be observed that both indices decrease with inclusion of polypropylene fibre for both fibre lengths investigated. Minimum C_c and C_s values are observed at fibre contents of 0.9%

when the fibre length is 6 mm. The decrease of C_c reduces when the fibre inclusion ratio is over 0.6%. This is more noticeable in samples with 12 mm long fibres. When the fibre inclusion is higher the volume occupied by the fibres is greater and some part of compression will be in the fibres themselves. It can be deduced from the above that the decrease of C_c will converge to a certain value, and this value is close to 0.9% according to the test results. Generally the behaviour of soil reinforced with different fibre lengths are similar, and samples reinforced with 6 mm long fibres exhibit a lower Swelling Index than 12 mm long fibres for the same given fibre inclusion ratio. The Swelling Index exhibits a similar trend to the compression index, a similar conclusion was reported by Kar et al., (2012). The decrease in Swelling Index can be attributed to the fibres locking the soil particles together preventing potential swelling. Figure 4.8 shows the effect of fibre addition on the pre-consolidation pressure of the soil. It can be seen that the pre-consolidation pressure generally increases with the increase of fibre inclusion pressure. This trend indicates that fibre reinforcement can expand the elastic zone of the soil, leading to a higher pressure induces soil yield. Fibre length does not have an obvious influence on the pre-consolidation pressure.

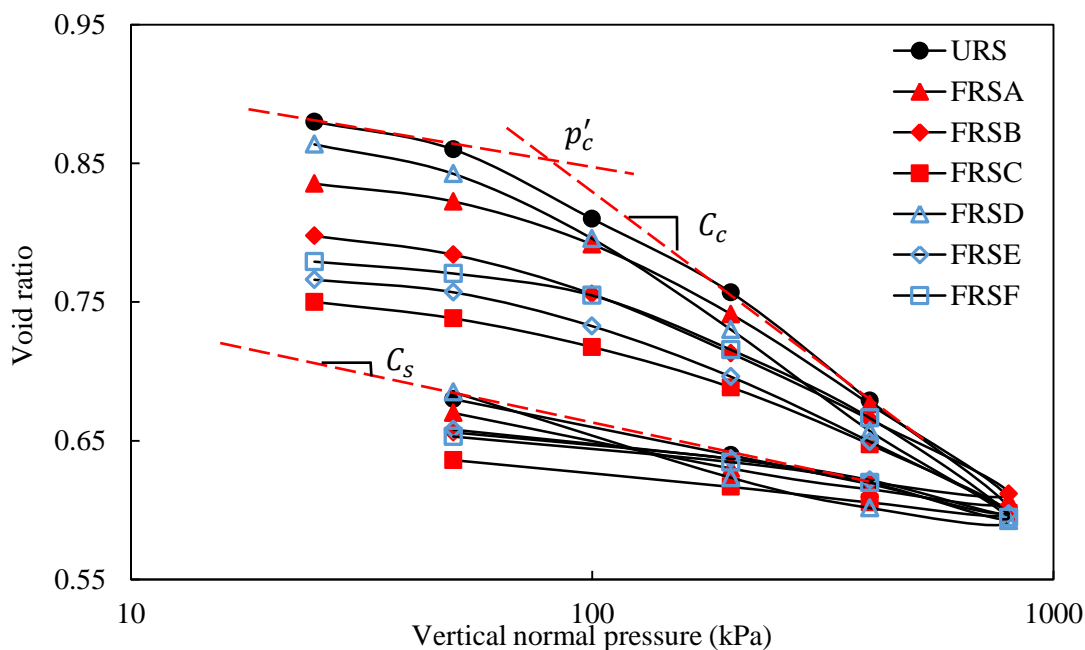


Figure 4.6. Void ratio-Pressure curves for unreinforced and reinforced soil.

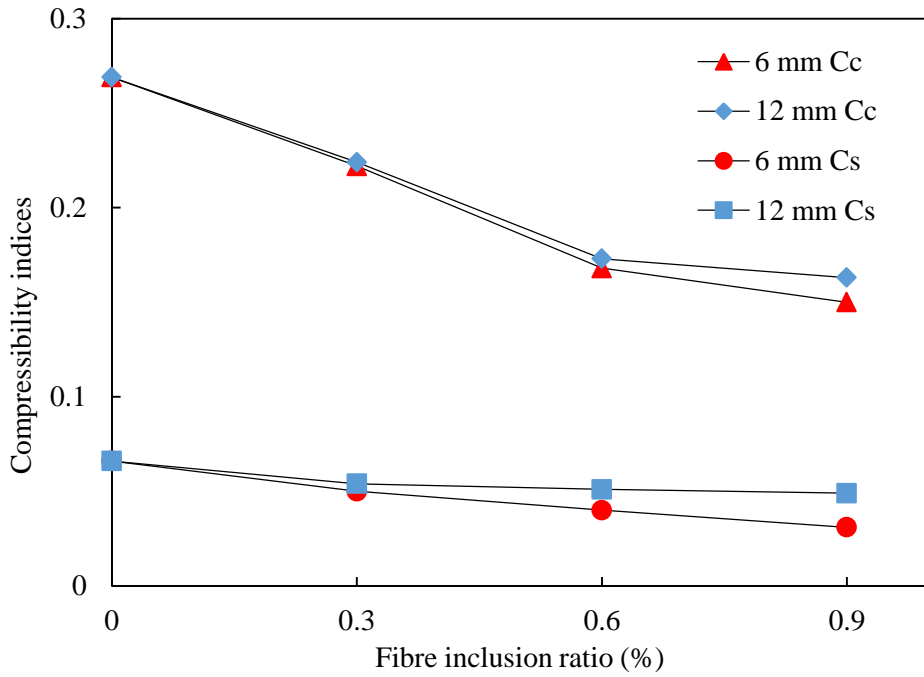


Figure 4.7. Variation of compressibility indices with fibre inclusion ratio and fibre length.

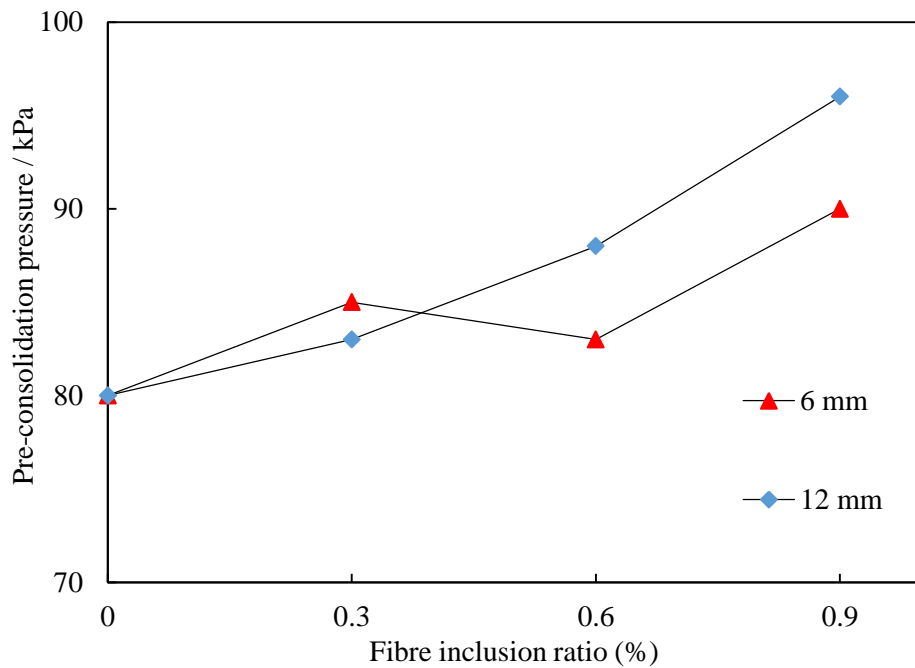


Figure 4.8. Variation of pre-consolidation pressure with fibre inclusion ratio and fibre length.

Figure 4.9 shows the effect of fibre reinforcement on the Coefficient of Consolidation (c_v) of London Clay. It is observed that as the fibre inclusion ratio increases, the Coefficient of Consolidation of the soil increases in both fibre lengths, which indicates fibre reinforcement

leads to an increase in the rate of consolidation. For soil reinforced with 6 mm and 12 mm fibres, the maximum value of Coefficient of Consolidation is obtained at 0.9% fibre inclusion ratio, where the value of c_v increases to about two times that of unreinforced soil. The increase in Coefficient of Consolidation may be due to the fact that fibres in the specimens can provide more drainage paths and consequently accelerate the consolidation process. In addition, it can be seen that no obvious difference can be found between the two different fibre lengths on the increase in the c_v . The changes in observed consolidation behaviour have potential benefits in ground engineering. A lower Compression Index and Swelling Index would result in reduced settlement and heave in highway engineering projects (e.g. subgrade and pavement works). A higher Coefficient of Consolidation can reduce the duration of consolidation, which can reduce the differential settlement and leads to an improvement in the stability and bearing capacity of the engineering projects. However, a more rapid consolidation means the settlement of the road is quicker in the short term, this has implications for highway maintenance.

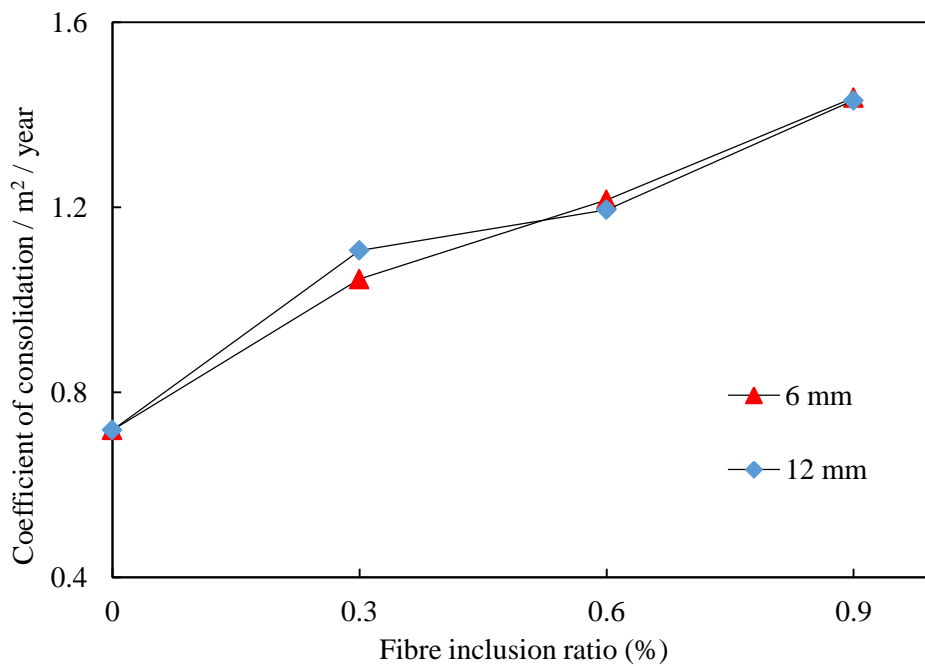


Figure 4.9. Variation of coefficient of consolidation with fibre inclusion ratio and fibre length.

4.4 Chapter summary

In this chapter compaction characteristics, bearing capacity and consolidation properties of unreinforced and fibre reinforced soil have been assessed based on the results of compaction tests, *CBR* tests and one-dimensional consolidation tests. The compaction test results indicate the OMC of the London Clay decreases slightly due to the addition of polypropylene fibres, and a reduction in MDD is found as fibre content increases in compaction tests. This can be explained by the reduction of average unit weight of solids in FRS. The *CBR* test results indicate that polypropylene fibres enhance the bearing capacity of the soil significantly. *CBR* value increase as the fibre amount increases and the fibre length decreases. The improvement in *CBR* values could be used to justify reducing the design thickness of subgrades with potential costs savings in materials and handling. The consolidation test results show that the addition of randomly distributed polypropylene fibres results in a reduction in compression and swelling of the clay soil. This conclusion is supported by the decreases in Compression Index and Swelling Index in fibre reinforced samples during testing. In addition, the Coefficient of Consolidation was observed to increase as the fibre inclusion ratio increased. The pre-consolidation pressure increase as the fibre inclusion ratio increases. The improvement in bearing capacity and the reduction in Compression Index and Swelling Index indicate that fibre reinforcement of clay soils would be beneficial in road embankment engineering.

Chapter 5

5. Desiccation cracking and tensile strength of fibre reinforced clay

In last chapter, the compaction, *CBR*, and one-dimensional consolidation behaviour of fibre reinforced soil has been discussed. This chapter presents the second part of the laboratory investigations in this study, which includes a comprehensive experimental study of the effect of fibre reinforcement on the linear shrinkage, desiccation cracking, and tensile strength behaviour of London Clay. These investigations aim to understand the benefit of polypropylene fibre reinforcement on the resistance of shrinkage and cracking of the soil, which are the potential problems occurring particularly in embankment engineering.

5.1 Linear shrinkage tests

Linear shrinkage tests were conducted on unreinforced and fibre reinforced soil as the experimental procedure described in 3.4.4, and the tests results are discussed in this section. Figure 5.1 shows the effects of PP fibres on linear shrinkage behaviour of London Clay. It can be observed that the Percentage of Linear Shrinkage (*PLS*) (see in Equation 3.1) of the soil reduces significantly with an increase of fibre inclusion ratio though the rate of decline decreases as the fibre inclusion ratio (ρ_f) increases. Taking the 6 mm case as an example, compared with the unreinforced sample ($PLS= 10.29\%$), when the fibre inclusion ratio is 0.3%, 0.6% and 0.9%, the *PLS* decreases to 7.09%, 4.47% and 3.99% respectively. When it comes to 12 mm length fibres, *PLS* of ρ_f at 0.3%, 0.6% and 0.9% is 6.26%, 4.42% and 3.95% respectively. It is notable that the 12 mm fibres are more effective than the 6 mm fibres in restricting samples' linear shrinkages when the ρ_f is relatively low. However, there is no

obvious difference between observed behaviour for the two lengths of fibres when the ρ_f increases above 0.6%. To formalise this here, the decrease in PLS due to the presence of PP fibres is measured using a dimensionless quantity termed the Linear Shrinkage Index (LSI), which is defined as the ratio of the displacement of a reinforced sample to that of an equivalent unreinforced sample as shown in Equation 5.1:

$$LSI = \frac{LS_R}{LS_U} = \frac{L_R - L_0}{L_U - L_0} \quad (5.1)$$

in which L_R and L_U are the final lengths of reinforced and unreinforced specimens respectively and LS_R and LS_U are the linear shrinkage strain of reinforced soil and unreinforced soil respectively. Figure 5.2 shows the variation of LSI with ρ_f at different fibre lengths (l_f). It can be seen that as fibre inclusion ratio increases from 0.3% to 0.9%, the linear shrinkage strains of the soil are approximately 65%, 43% and 38% of the shrinkage strain of unreinforced soil. The reduced strain is evident visually in Figure 5.3, which shows the samples in moulds at the end of the test. One can easily see the reduced length change from the smaller gap around the edge of the soil prism. The slight twist visible on the surface of the FRS sample is likely to be caused by uneven vertical strain as a result of the randomness of the fibres. The improvement in the linear shrinkage properties in the reinforced materials is likely due to the development of interaction between fibre surfaces and soil particles, with fibres acting as frictional and tension resistant elements in the mixture to prevent the shrinkage of the sample.

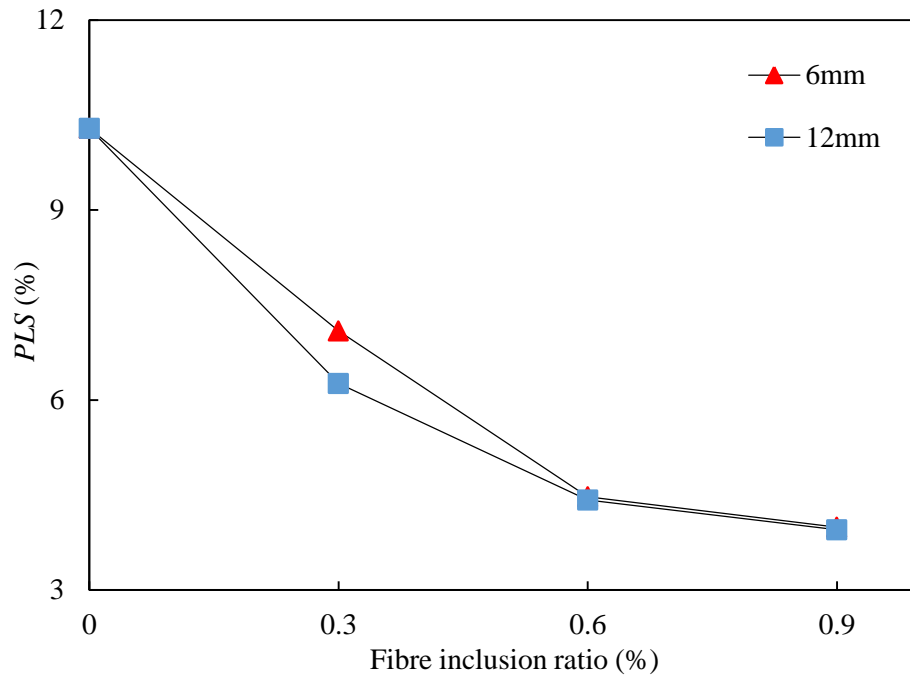


Figure 5.1. Variation of *PLS* with various fibre inclusion ratio at different fibre lengths.

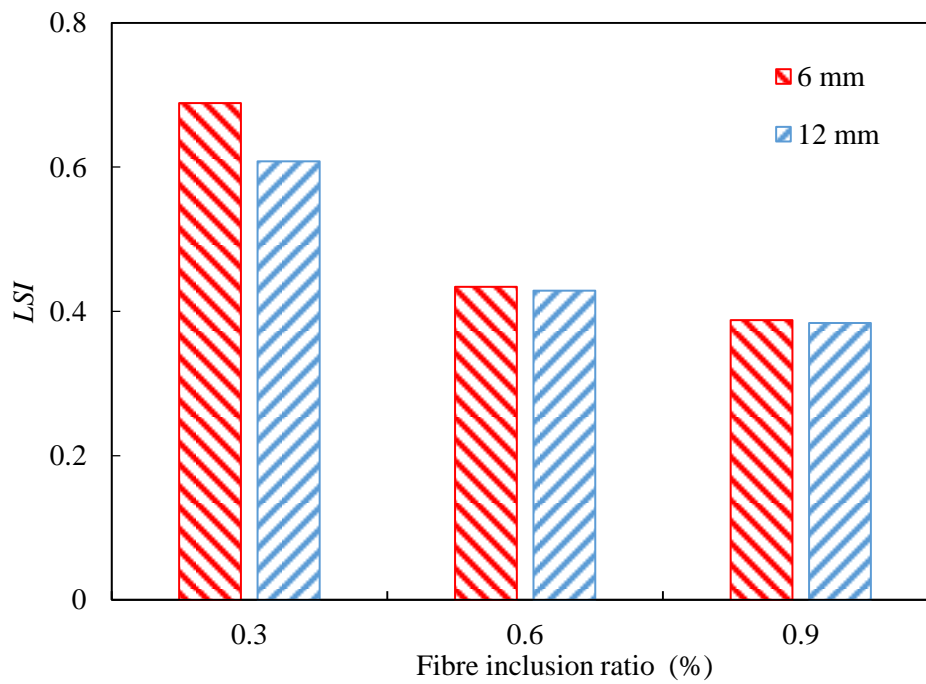


Figure 5.2. Variation of *LSI* with various fibre inclusion ratio at different fibre lengths.



(a)



(b)

Figure 5.3. The samples at the end of linear shrinkage test (a) URS sample (b) FRS sample ($\rho_f = 0.6\%$, $l_f = 6$ mm).

5.2 Desiccation cracking tests

Desiccation cracking tests were conducted on unreinforced and fibre reinforced soil as per the experimental method mentioned in 3.4.5. The details of image analysis techniques is introduced here and the desiccation cracking tests results are analysed in the form of crack intensity factor and crack initiation, crack development and crack pattern.

5.2.1 Image analysis processing

A desiccation crack network is usually irregular and difficult to measure using conventional quantitative methods, so here digital image analysis techniques were employed to investigate the desiccation cracking. The image analysis procedure can be described as follows. Firstly, the raw RGB image obtained from the camera (Figure 5.4a) was cropped into a core square image of 2350×2350 pixels (160 mm \times 160 mm) to eliminate boundary effects due to the adherence and frictional resistance of the soil to the side walls of the container (Figure 5.4b). Then the image was converted to a grayscale image using free image processing software,

ImageJ (Figure 5.4c). The grayscale image was then segmented and binarization (converting a pixel image to a binary image and extracting target information by threshold filtering) by thresholding using an ImageJ function, “Default”, and the cracked area was differentiated from the intact soil area in black and white respectively (Figure 5.4d). It should be mentioned that sometimes lighting and shadow effects on the irregular surface of specimens would result in dark spots, the area of these unwanted spots was determined to be less than 20 pixels² therefore the minimum size of crack area in ImageJ was set as 20 pixels² (0.06 mm²) in the analysis. The crack development was quantified by a Crack Intensity Factor (*CIF*) proposed by Miller et al., (1998), defined as the ratio between the area of cracks (A_c) and total area of the specimen (A_t), as shown in Equation 5.2:

$$CIF = \frac{A_c}{A_t} \times 100\% \quad (5.2)$$

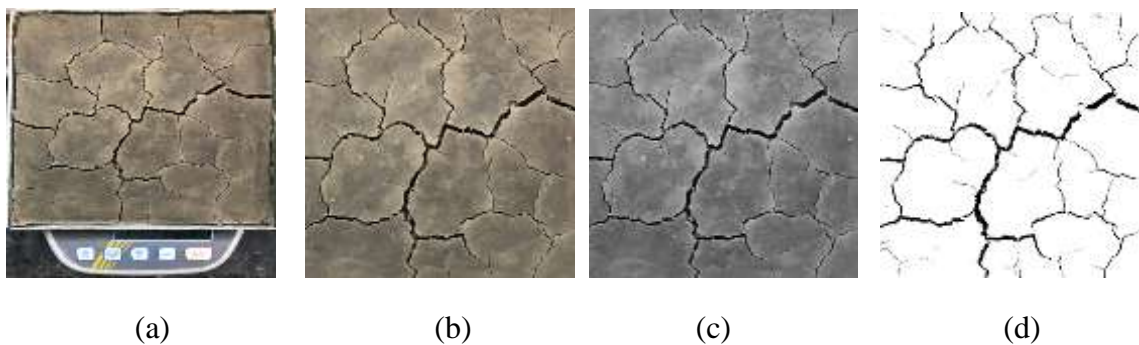


Figure 5.4. Procedure of digital image processing: (a) raw RGB image (b) cropped RGB Image (c) grayscale image (d) binary image.

5.2.2 Crack intensity factor and crack initiation

Of note during the tests was the phenomenon of crack closure during the latter part of drying. An explanation is attempted as follows. The observed crack propagation can be divided into two stages. In the first stage, water content in the upper part of the specimen reduces faster than in the lower part, which leads to differential stresses in the specimen and results in crack

generation. During the development of the cracks, the water contained in the lower part of the specimen reduces to that of the upper part of the sample and approaches equilibrium with the upper part, resulting in shrinkage in the lower part of the specimen. At this stage, the small cracks formed initially begin to close, as marked by red circles in Figure 5.5a, while the total shrinkage of the specimen increases, as shown by the black border in Figure 5.5b. The aperture that opens between the edge of the container and the soil is not included in the determined value of CIF but if it were to be considered as crack area then the value of CIF would continue to increase through this stage. In this study, the crack pattern was the major interest so here only the first stage will be discussed.

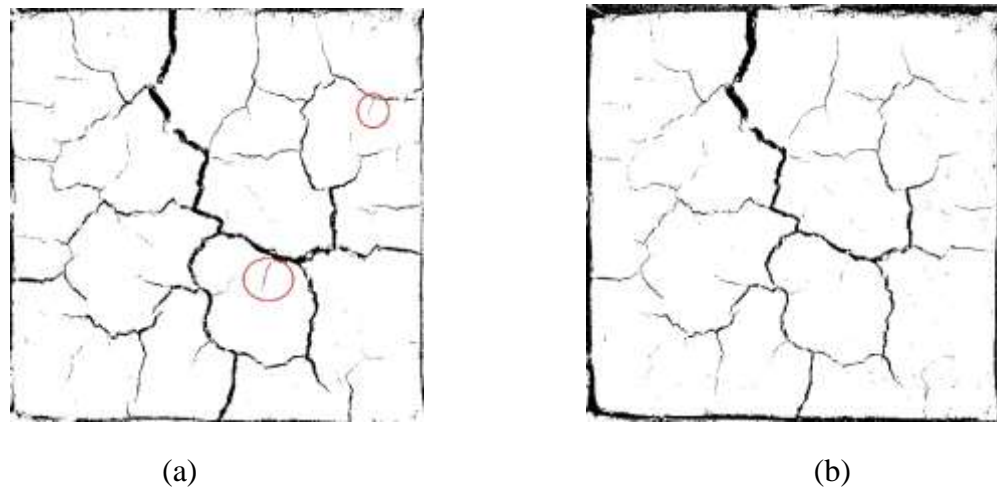


Figure 5.5. Total shrinkage of unreinforced specimen during the test: (a) after 6 hours (cracks in red circles closed at second stage) (b) after 12 hours.

The variation of CIF (i.e. average value of two replicated specimens) with gravimetric water content (w) for all specimens is shown in Figure 5.6 (note that the water content is plotted as reducing from left to right on the abscissa). During the process of crack propagation, the CIF of both URS and FRS increase with decreasing water content and finally reach stabilisation. It can be seen that fibre addition can effectively restrict crack development, expressed via the maximum CIF values of FRS which are much lower than that of unreinforced soil, and the slopes of the curves are shallower than that for unreinforced soil.

With an increase in the fibre inclusion ratio, the crack area decreases. The maximum *CIF* value reduces from 7.2% to approximately 3.8%, 1.9% and 0.9% for fibre inclusion ratios of 0.3%, 0.6% and 0.9% respectively. As for the influence of fibre length, it can be seen that 12 mm length fibres have a greater effect on crack resistance than 6 mm fibres at 0.3% fibre content. However, no obvious difference between the two kinds of fibres can be seen when the fibre inclusion ratio increases to 0.6% and 0.9%. To quantify the effect of fibre reinforcement on crack resistance of the soil, an index termed the Crack Reduction Ratio (*CRR*), proposed by Miller and Rifai (2004), is utilised here, and is defined as

$$CRR = \frac{CIF_u - CIF_f}{CIF_u} 100\% \quad (5.3)$$

where CIF_u and CIF_f are the crack intensity factors of unreinforced and fibre reinforced soil respectively. The *CRR* values for samples of fibre reinforced soil at the end of tests with different fibre inclusion ratios and lengths are plotted in Figure 5.7. It can be observed that for both fibre lengths, there is a reduction of approximately 45% to 88% of crack intensity as the fibre inclusion ratio increases from 0.3% to 0.9%. As in the discussion of the *CIF* results above, there is very little difference in the results for the two fibre lengths for the two higher values of ρ_f and in addition, the *CRR* increases less rapidly from $\rho_f = 0.6\%$ to $\rho_f = 0.9\%$ than from $\rho_f = 0.3\%$ to $\rho_f = 0.6\%$ for both fibre lengths. Figure 5.6 and 5.7 reflect fibre reinforcement can improve the cracking resistance of the London Clay, this can be attributed to the fact that fibres can increase the tensile strength of the soil, which will be discussed in 5.3. During the desiccation process, the water evaporation in the upper layer leads to the development of matrix suction, resulting in a higher tensile stress than the lower layer of the specimen. Once the tensile stress exceeds the tensile strength of the soil, desiccation cracks appear on the surface and develop as the further desiccation. On the one hand, the increased tensile strength due to the fibres in fibre reinforced soil can restrict the crack initiation. On the

other hand, the bonding effect and interface friction between fibres and soil matrix can restrict the tendency of development of the existed cracks.

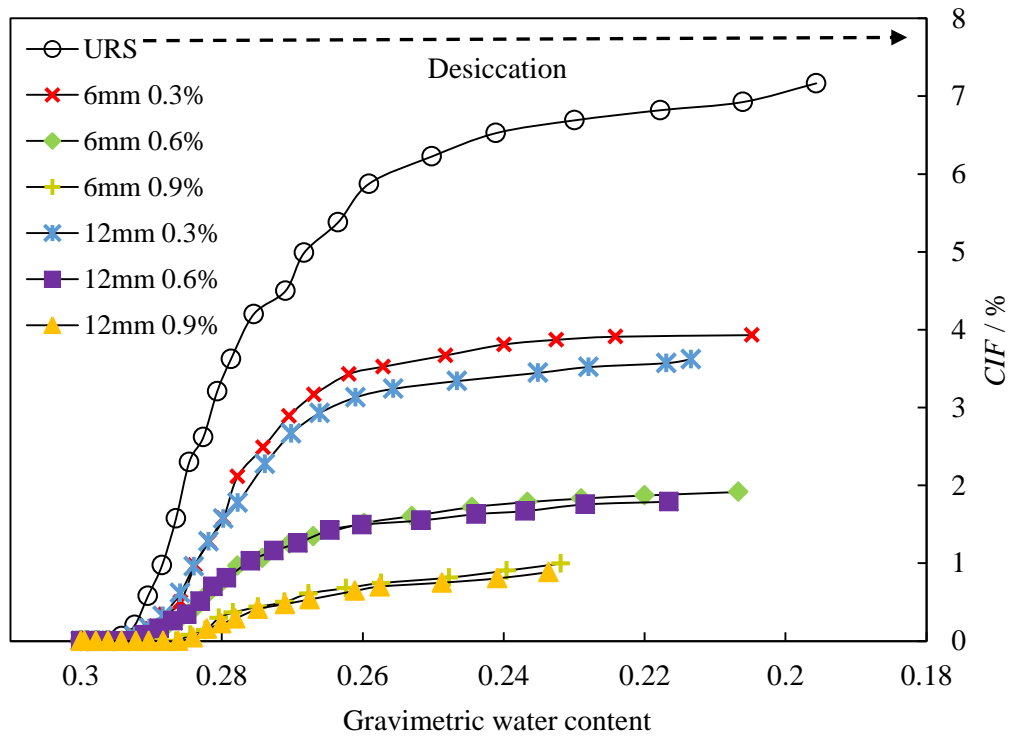


Figure 5.6. Variation of *CIF* with water content for different specimens.

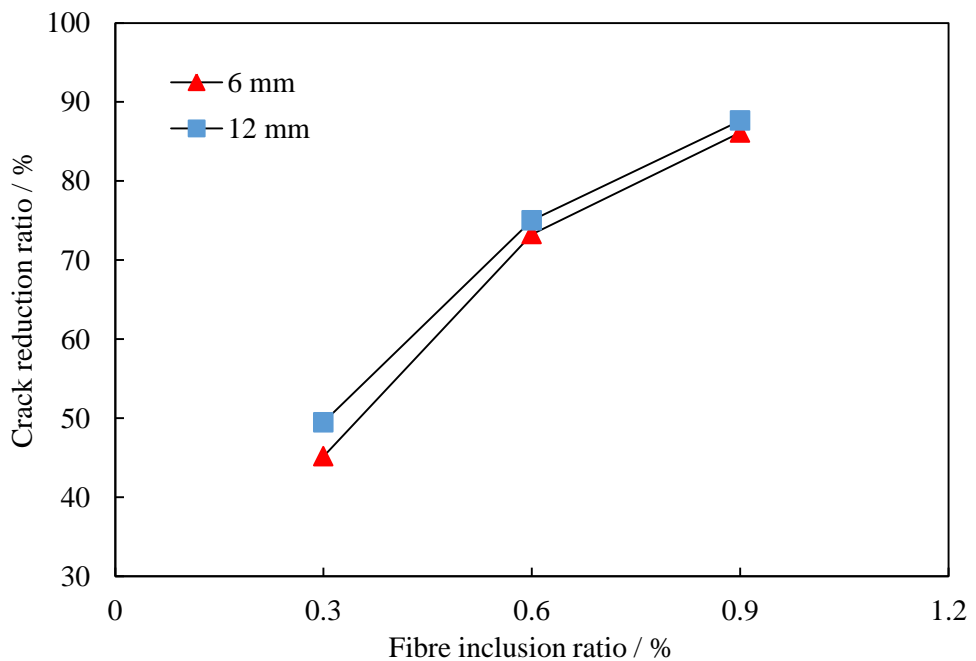


Figure 5.7. Variation of *CRR* with fibre inclusion ratio for different fibre lengths.

Figure 5.8 shows the variation of the time of occurrence of the first crack and the corresponding water content at that time for unreinforced and fibre reinforced specimens. It can be seen that the first cracking in the unreinforced specimen occurred 20 minutes after the test started. As the fibre inclusion ratio increased, for both fibre lengths, the first cracking started at 25 ($\rho_f = 0.3\%$), 30 ($\rho_f = 0.6\%$) and 45 ($\rho_f = 0.9\%$) minutes respectively. The water contents of the specimens at the occurrence of the first crack were also found to decrease as the fibre inclusion ratio increased. As mentioned above, the water in upper layer of the specimen evaporate quicker and results in cracking. However, the gravimetric water content measured in this study is the average water content of the whole specimen, because it is hard to measure the local water content near the cracks. For the reason that the testing environment of all the tested specimens is identical, the measured water content is still can be considered as an evaluation index of crack initiation, though it cannot truly reflect the surface water content of the soil at crack initiation. Based on the discussion above, it can be concluded that the occurrence of crack initiation is delayed with an increase in fibre inclusion ratio, and this is because the improved tensile strength of the soil due to the addition of fibres.

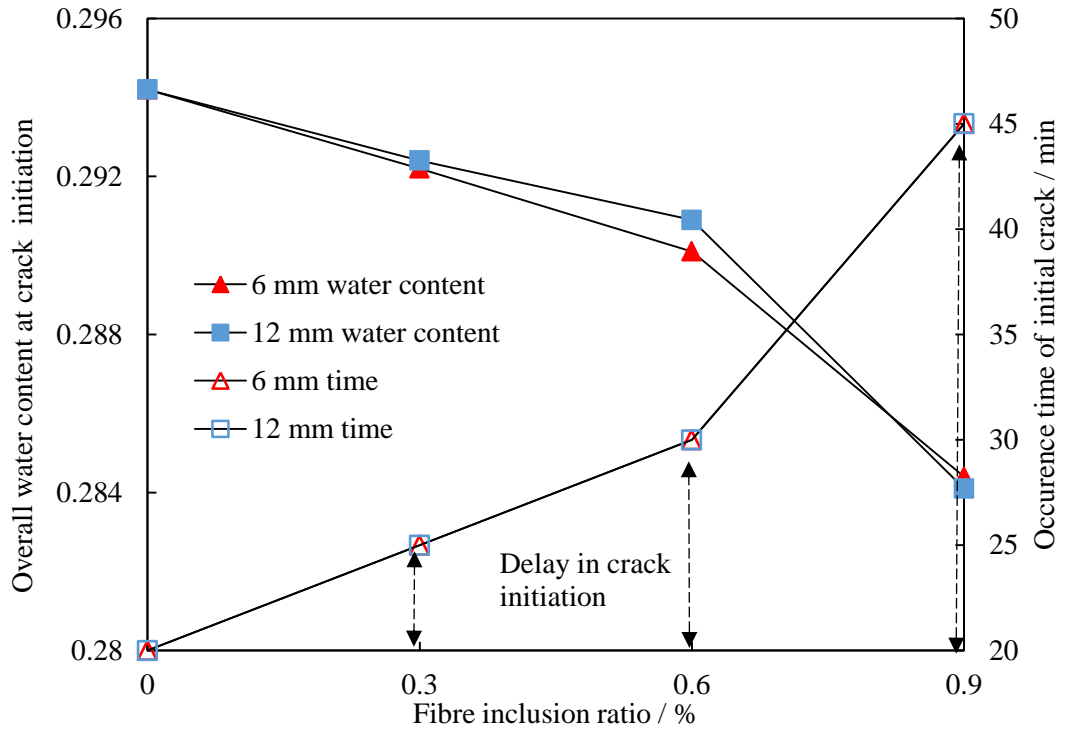


Figure 5.8. Variation of time and water content on crack initiation with fibre inclusion ratio and length.

5.2.3 Crack development and crack patterns

It is worthwhile to examine further the crack patterns witnessed in certain of the tests. In Figures 5.9 and 5.10, typical *CIF* curves of URS and FRS ($\rho_f = 0.6\%$, $l_f = 6$ mm) specimens are selected from Figure 5.6 and crack patterns at different water contents are linked to the corresponding points on the curves. It can be observed that for both URS and FRS specimens, initial cracks are small in both number and area (① in both figures). As the water content decreases, the initial cracks propagate and widen and many new cracks appear in random locations (② in both figures). Then, the URS and FRS specimens show different crack patterns. For URS specimens, the existing cracks become wider and some “sub-level” cracks occur based on these cracks, which leads to existing cracks connecting and intersecting (③ in Figure 5.9). Hardly any new cracks are generated and existing cracks get wider. In this stage,

the growth rate of cracking area slows down, was expressed by the decrease of the slope in the *CIF-w* curve. In addition, the cracks in the URS specimen appeared to propagate through the depth of the soil and divide the specimen along the thick cracks (④ in Figure 5.9). For the FRS specimens, after ① and ②, new cracks still appear randomly as the water content decreases. Then new cracks still appear and existing cracks became wider until the maximum cracking area (④ in Figure 5.10). The cracks in FRS specimens do not appear to propagate much through the depth, this is because the fibres distributed in the specimen prevent cracking crossing the crack plane at some depth. Another different crack pattern can be found is the cracks distribution in FRS is not as homogenous as that in URS. Taking the selected FRS specimen as an example (③ in Figure 5.10), no obvious cracks can be found in the lower-left and upper-right regions of the specimen. This trend might come from the uneven fibre distribution in the specimen.

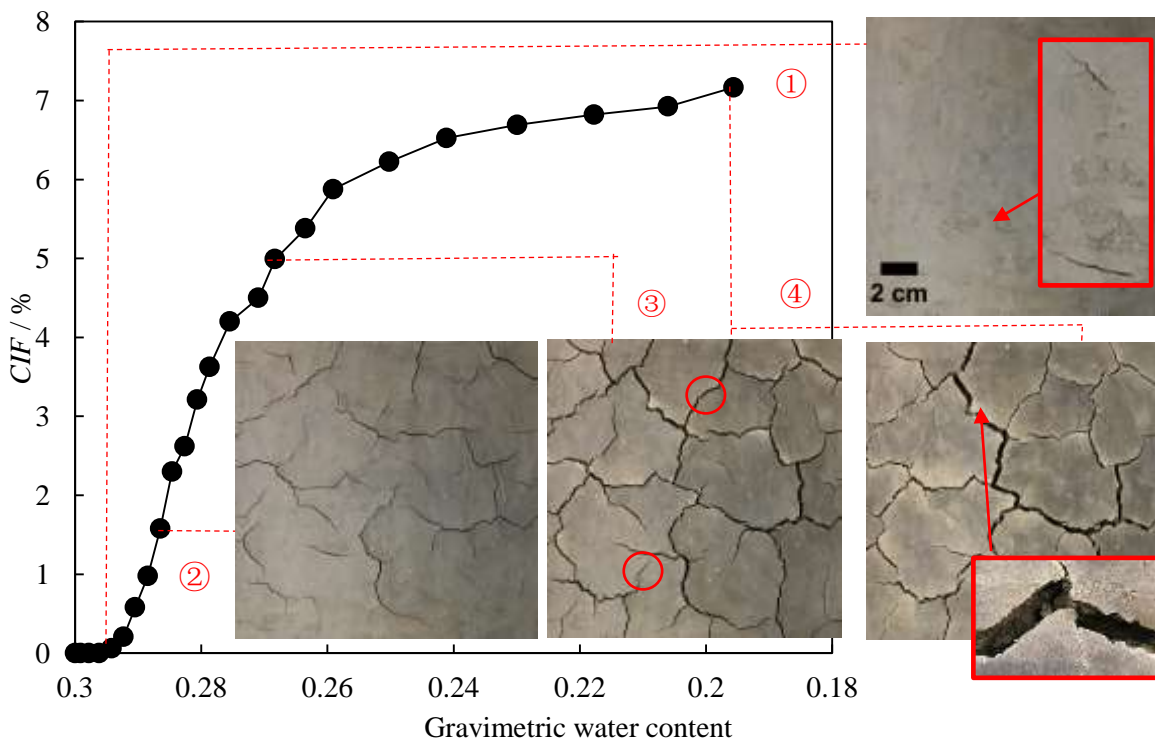


Figure 5.9. The development of desiccation cracking in a URS specimen.

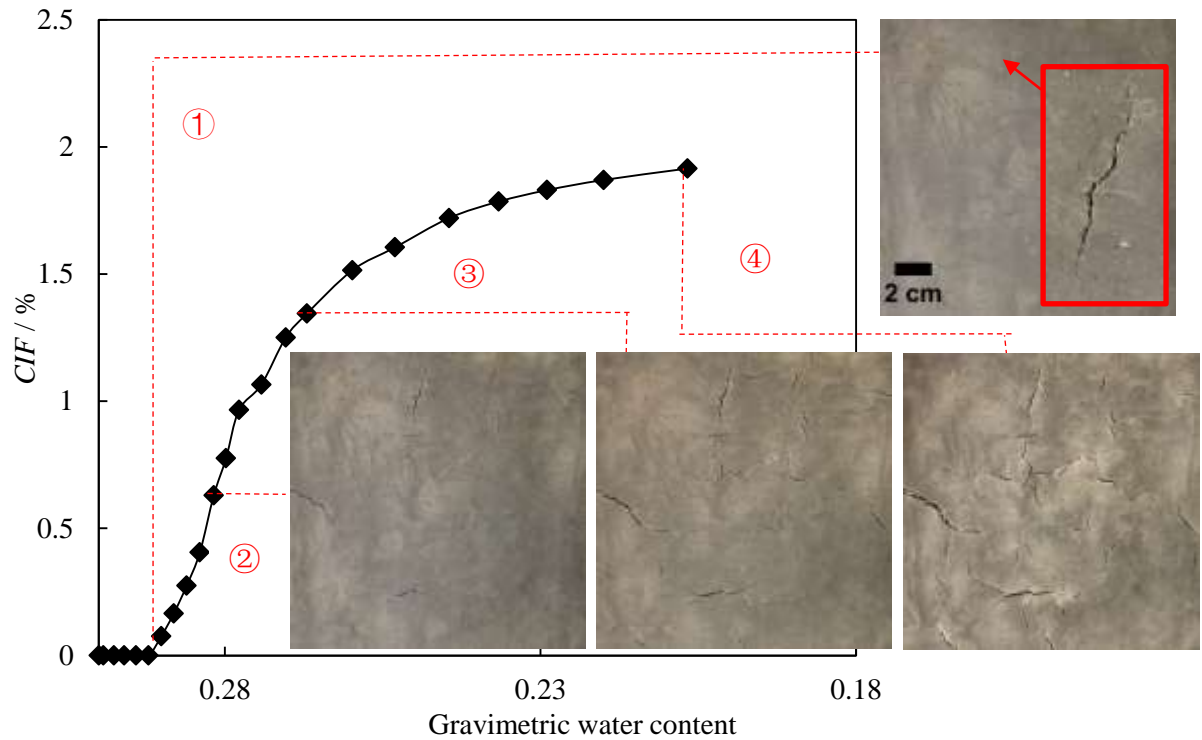
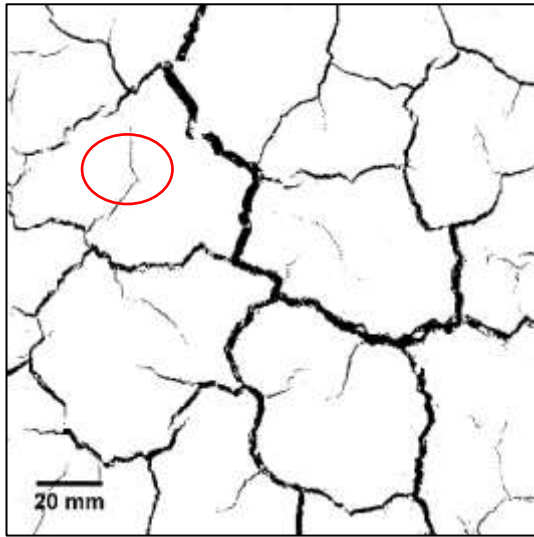


Figure 5.10. The development of desiccation cracking in a FRS specimen

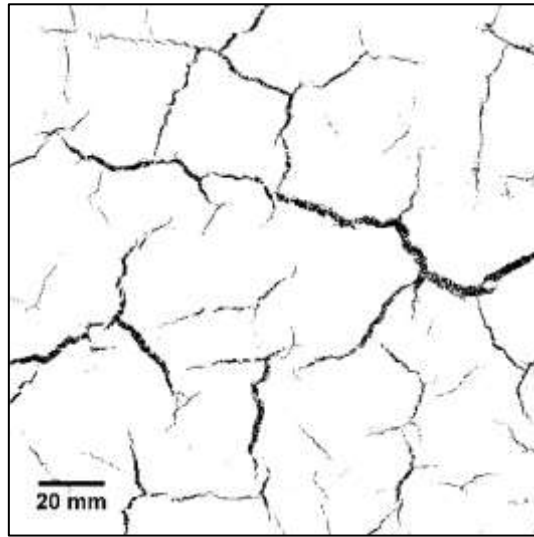
($\rho_f = 0.6\%$, $l_f = 6$ mm).

The final crack patterns of URS and FRS samples are shown in Figure 5.11. It can be seen that several wide cracks are found in the unreinforced sample (Figure 5.11a), while the number of wide cracks decreases and the number of fine cracks increases significantly in the reinforced sample at 0.3% fibre content (Figure 5.11b, Figure 5.11c). In addition, for the URS specimen, the intersection angles between any two cracks are mainly orthogonal, and cracks are interconnected in various directions forming closed (looped) crack paths. For the FRS specimens, a greater proportion of non-orthogonal cracks can be observed, and fewer closed crack paths are evident. These two features cause more ‘Y’ shape cracks and more ‘dead end’ cracks. Chaduvula et al., (2017) performed desiccation crack testing on polyester fibre reinforced clay and found a similar trend, and proposed that the presence of fibres may cause bifurcation or diversion of a single propagating crack. It can be seen in Figure 5.11d and Figure 5.11e that as fibre inclusion ratio increases from 0.3% to 0.6%, there are fewer long

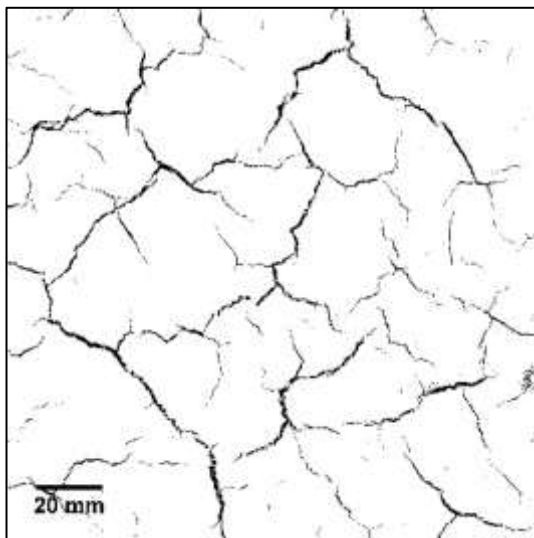
cracks and more individual short cracks. When the fibre content increases from 0.6% to 0.9%, fewer cracks can be seen on the specimens reinforced with both fibre lengths (Figure 5.11f and Figure 5.11g).



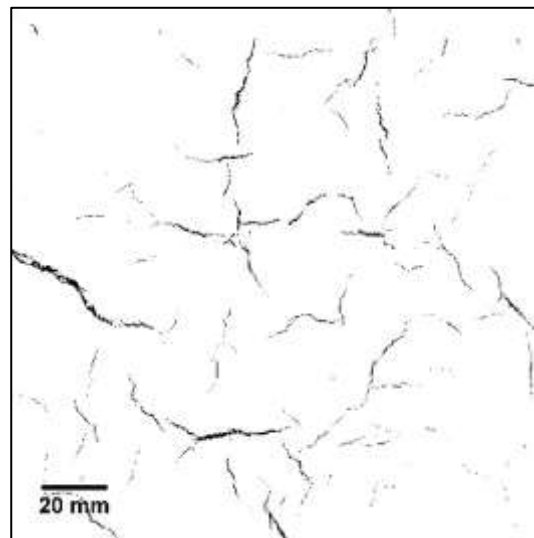
(a)



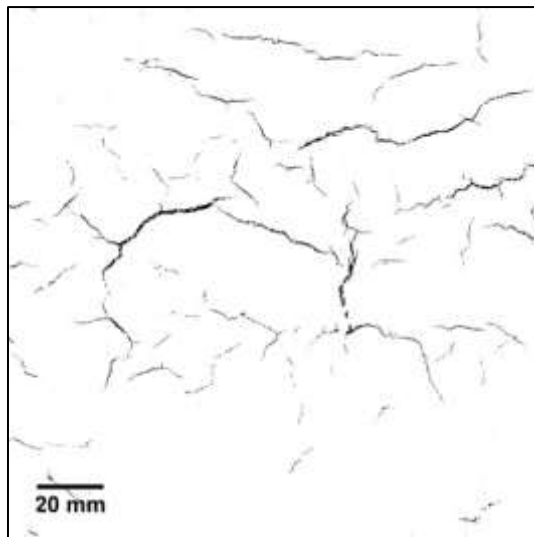
(b)



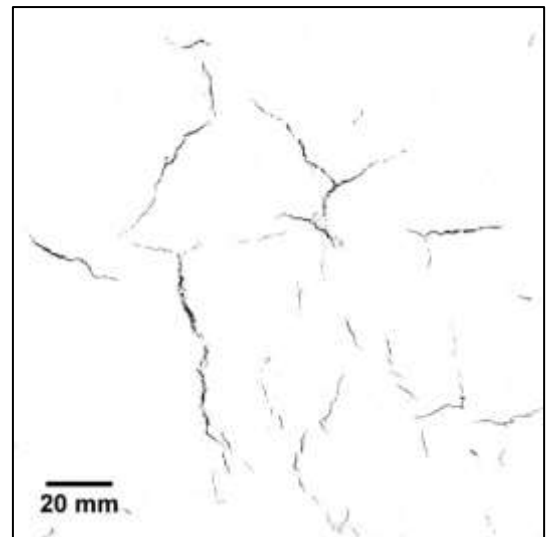
(c)



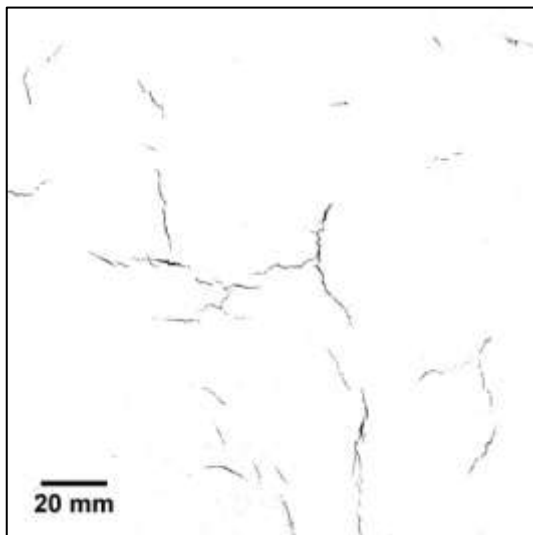
(d)



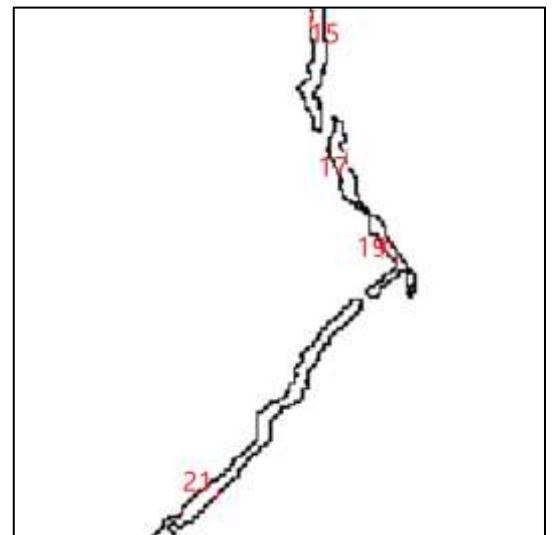
(e)



(f)



(g)



(h)

Figure 5.11. Final crack patterns of soil specimens (a) URS (b) $\rho_f = 0.3\%$, $l_f = 6$ mm (c) $\rho_f = 0.3\%$, $l_f = 12$ mm (d) $\rho_f = 0.6\%$, $l_f = 6$ mm (e) $\rho_f = 0.6\%$, $l_f = 12$ mm (f) $\rho_f = 0.9\%$, $l_f = 6$ mm (g) $\rho_f = 0.9\%$, $l_f = 12$ mm (h) crack counting and definition in ImageJ.

Quantitative analysis of crack patterns at the end of the tests shown in Figure 5.11 was conducted using ImageJ and the results are given in Table 5.1. In the quantitative analysis, the software will detect the boundary of the crack (black in binary figure) until a close outline is captured, and the crack will be counted automatically and its geometry information will be

saved. Figure 5.11f gives an example of analysis of the area with red circle in Figure 5.11a. It can be seen that Crack 17 and Crack 19 are disconnected so they are considered individually. It can be seen from Table 5.1 that numbers of cracks (both total and per unit area) increase when fibres are added and decrease as fibre inclusion ratio increases. The former phenomenon can be attributed to the presence of fibres reducing the number of large cracks and increasing the number of small cracks (Figure 5.11a to Figure 5.11b and Figure 5.11c), and the latter can be attributed to further restriction in crack development causing a reduction in total crack number (Figure 5.11d to Figure 5.11g). Another reason for this phenomenon could be that more small cracks occur in FRS specimens but are too small to be recognised by the software. When it comes to the areas of cracks, the total area and average area of cracks in reinforced specimens decrease significantly compared to that of unreinforced soil. Taking specimens with 0.3% fibre inclusion ratio as an example, the total area of crack reduces from 1984.6 mm² (unreinforced soil) to 1171 ($l_f=6$) and 424.9 ($l_f=12$) mm², while the average area of crack decreases from 7.43 mm² (unreinforced soil) to 1.80 mm² for 6 mm fibres and 1.67 mm² for 12 mm fibres respectively. The reduction in crack area is attributed to the increased tensile strength of the soil and the bridging effect coming from the fibres in FRS specimens. Figure 5.12 illustrates the latter point where fibres can be seen linking the separated soil mass to stop crack expansion.

Table 5.1. Quantitative analysis results on crack patterns at the end of tests.

Soil type	ρ_f (%)	l_f (mm)	Total crack number	Crack number per cm ²	Total crack area (mm ²)	Average crack area (mm ²)
URS	-	-	267	1.043	1984.6	7.43
FRSA	0.3	6	650	2.539	1171.0	1.80
FRSB	0.6	6	639	2.496	424.9	0.66
FRSC	0.9	6	390	1.523	187.2	0.48
FRSD	0.3	12	617	2.410	1027.9	1.67
FRSE	0.6	12	593	2.316	332.5	0.56
FRSF	0.9	12	345	1.348	151.8	0.44

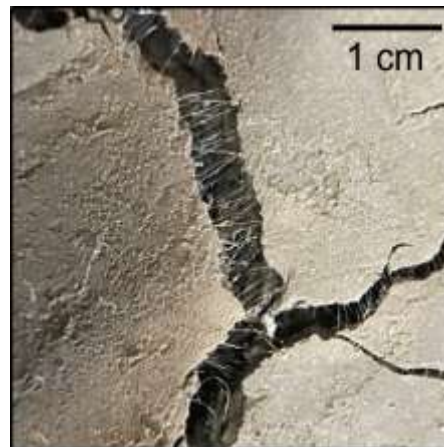


Figure 5.12. Bridging effect due to fibres in FRS specimen ($\rho_f=0.3\%$, $l_f=6$ mm).

In order to investigate the effect of fibre inclusion ratio and fibre length on crack patterns of the soil, two indices termed the Crack Number Ratio (N_R) and Average Crack Area Ratio (A_R) are introduced here, and defined as:

$$N_R = \frac{N_f}{N_u} 100\% \quad (5.4)$$

$$A_R = \frac{A_f}{A_u} 100\% \quad (5.5)$$

where N_u and A_u are the total crack number and average crack area of unreinforced soil, and N_f and A_f are the total crack number and average crack area of fibre reinforced soil.

The variations of N_R and A_R with fibre inclusion ratios for different fibre lengths are plotted in Figure 5.13. It can be seen that when the fibre inclusion ratio is 0.3%, the number of cracks observed by the software is more than two times of that of URS, while the average crack ratio is less than 25% of that of URS. This trend can be concluded as FRS shows a different crack pattern from URS, which reflects with more crack number and less crack area. As the fibre inclusion ratio further increases, N_f reduces as mentioned above, but the number of cracks is still more than that of the URS specimen ($N_f > 100\%$). On the other hand, A_R exhibits a rapid reduction from $\rho_f = 0.3\%$ to $\rho_f = 0.6\%$, followed by a slow decline from $\rho_f = 0.6\%$ to $\rho_f = 0.9\%$. It can be deduced that the average crack area of the FRS will converge to a certain value as the fibre inclusion ratio further increases.

In addition, it can be seen that compared with 6 mm length fibre reinforced specimens, 12 mm fibre reinforced specimens tend to have fewer cracks per unit area but greater Crack Number Ratios, coming from the fact that shorter fibres are twice as numerous as longer fibres when the masses are equal, leading to a finer crack pattern.

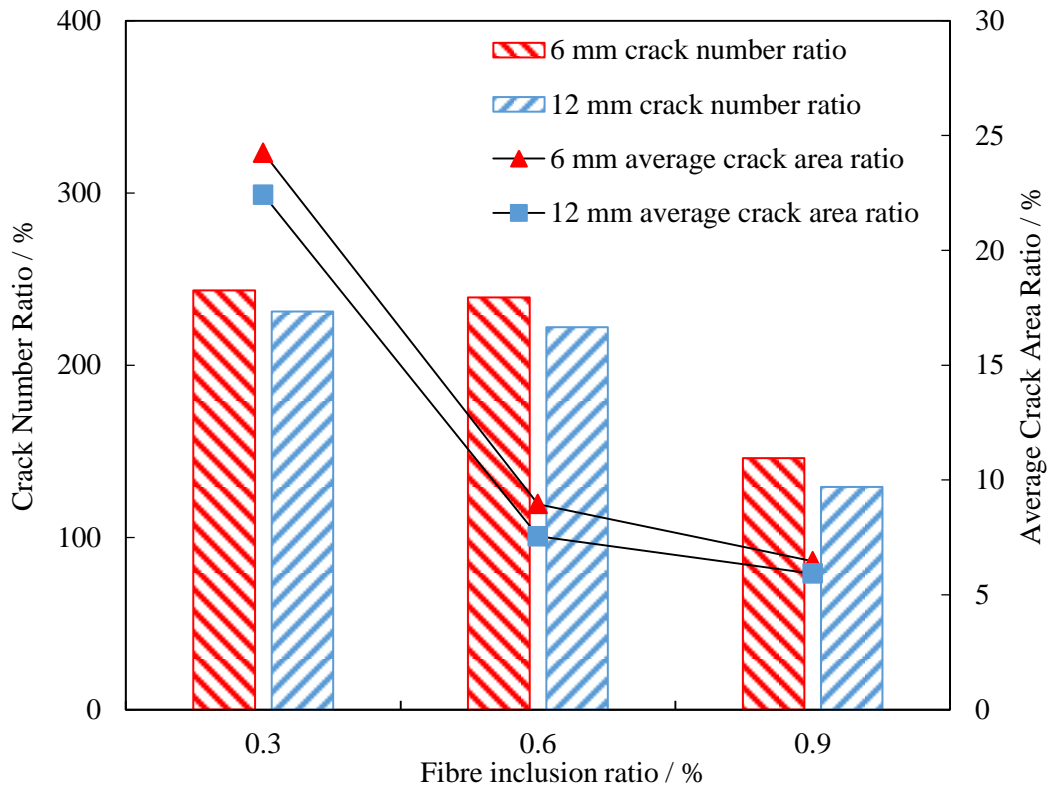


Figure 5.13. Variation of N_R and A_R with fibre inclusion ratio for different fibre lengths.

5.3 Direct tensile tests

Direct tensile tests were conducted on unreinforced and fibre reinforced soil as per experimental procedure outlined in 3.4.6. The effect of fibre reinforcement on the tensile strength improvement, stiffness behaviour, failure pattern and suction behaviour of the soil are discussed in this section.

5.3.1 Tensile strength improvement

The variations of tensile strength with gravimetric water content for URS and FRS specimens are shown in Figure 5.14. Generally, specimens reinforced with higher fibre inclusion ratios and longer fibres perform best in the sense of having higher tensile strengths and all curves in this plot are located to the top in the figure. For both unreinforced and reinforced soil, tensile strength (σ_t) varied exponentially with decreasing gravimetric water content (w) (fitted lines are only for visual guidance). This trend can be attributed to two sources: on the one hand, the

specimens are unsaturated soils and therefore the increase in water content decreases the capillary force (matrix suction) and hence the effective stress between particles (Fredlund and Rahardjo, 1993), leading to a reduction in tensile strength.

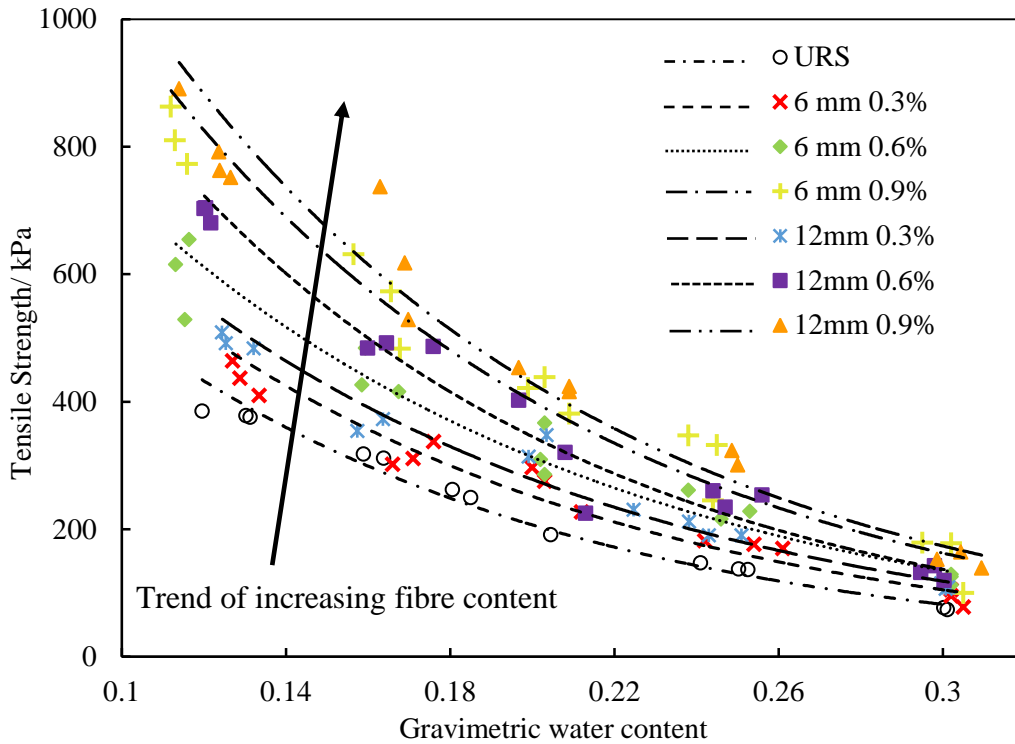


Figure 5.14. Variation of tensile strength of URS and FRS specimens with water content.

On the other hand, for the fibre reinforced soil, the increase in tensile strength can be attributed to the addition of fibres with a high tensile strength. The level of reinforcement is controlled by the pull-out resistance of the fibres as their own tensile strength exceeds the natural tensile strength of the soil, and the increase in water content causes a reduction in interfacial friction and adhesion between the fibres and the clay matrix, which leads to a decrease in pull-out resistance. This conclusion is supported by research conducted by Tang et al., (2010). The tensile strength of fibre reinforced soil (σ_{tfr}) comes from two major sources: tensile strength of unreinforced soil (σ_{tu}) and the benefit from fibre reinforcement ($\Delta\sigma_{tf}$), as shown in Equation 5.6

$$\sigma_{tfr} = \sigma_{tu} + \Delta\sigma_{tf} \quad (5.6)$$

So, in order to investigate the effect of fibre inclusion ratio and fibre length on tensile strength improvement, the benefit from fibre reinforcement ($\Delta\sigma_{tf}$) in different conditions are evaluated. According to Equation 5.6, $\Delta\sigma_{tf}$ at a given water content can be calculated as the difference between the tensile strength of the FRS (σ_{tfr}) and unreinforced soil (σ_{tu}) at the same water content. Values of σ_{tfr} and σ_{tu} have been obtained from the fitted curves in Figure 5.14 in order to compare at identical water contents. Figure 5.15 shows the variation of $\Delta\sigma_{tf}$ with water content at different fibre inclusion ratios and lengths.

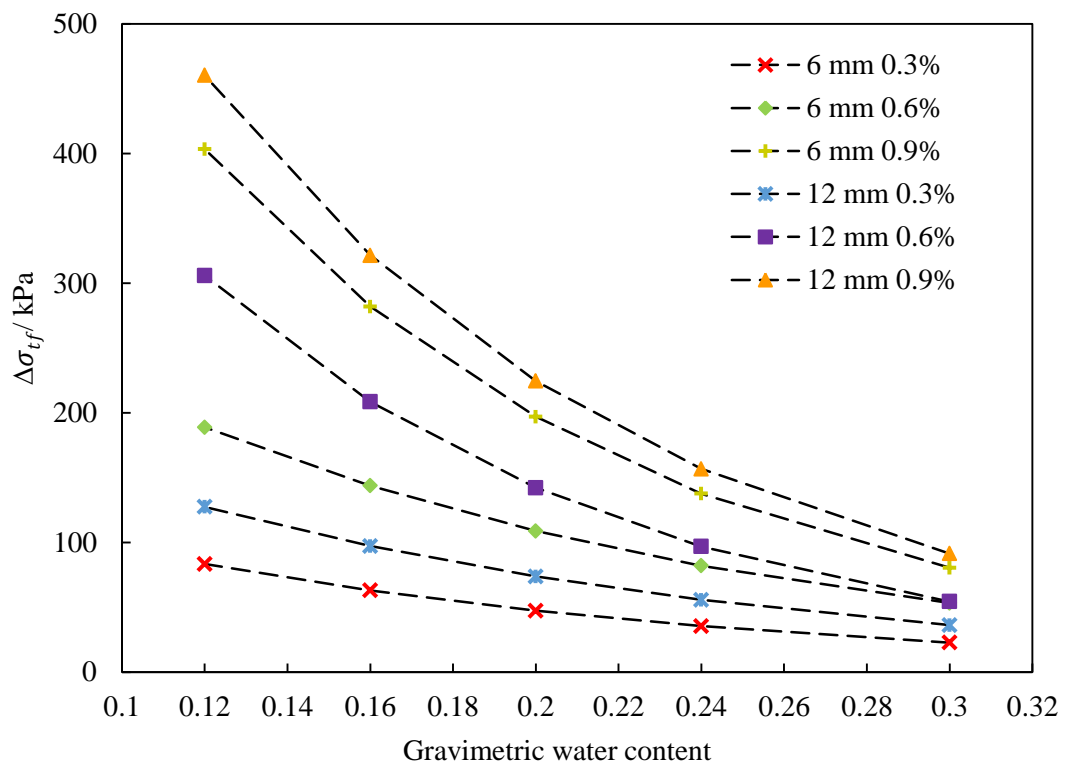


Figure 5.15. Variation in benefit from fibre reinforcement on tensile strength with water content.

It can be seen that for all five water contents in the study, $\Delta\sigma_{tf}$ increases as fibre inclusion ratio increases from 0.3% to 0.9%, and fibre length increases from 6 mm to 12 mm. Another conclusion that can be drawn from Figure 5.15 is that the $\Delta\sigma_{tf}$ induced by fibres also increases with decreasing water content. For example, as the fibre content increases from 0 to

0.3% at 6 mm fibre length, $\Delta\sigma_f$ is 22.8 kPa when water content is 30% and increases to 83.4 kPa when water content is 30%. The variation of $\Delta\sigma_{tf}$ with ρ_f at a selected water content ($w=24\%$) is shown in Figure 5.16, and the CRR values (introduced in 5.2.2) of unreinforced and fibre reinforced soil at $w=24\%$ are also calculated and included. As mentioned above, both $\Delta\sigma_{tf}$ and CRR increase with an increase of fibre inclusion ratio. The similar trends seen for these two factors supports the conclusion that the benefit of fibres to the tensile strength of soil is responsible for a reduction in cracking (Figures 5.6- 5.8). However, as the fibre inclusion ratio increases from 0.6% to 0.9%, the CRR of specimens reinforced with both fibre lengths does not increase as much as seen for $\Delta\sigma_{tf}$. This might be because the fibre distribution in $\rho_f=0.9\%$ is not as uniform as that for the lower fibre inclusion ratio in the cracking specimens.

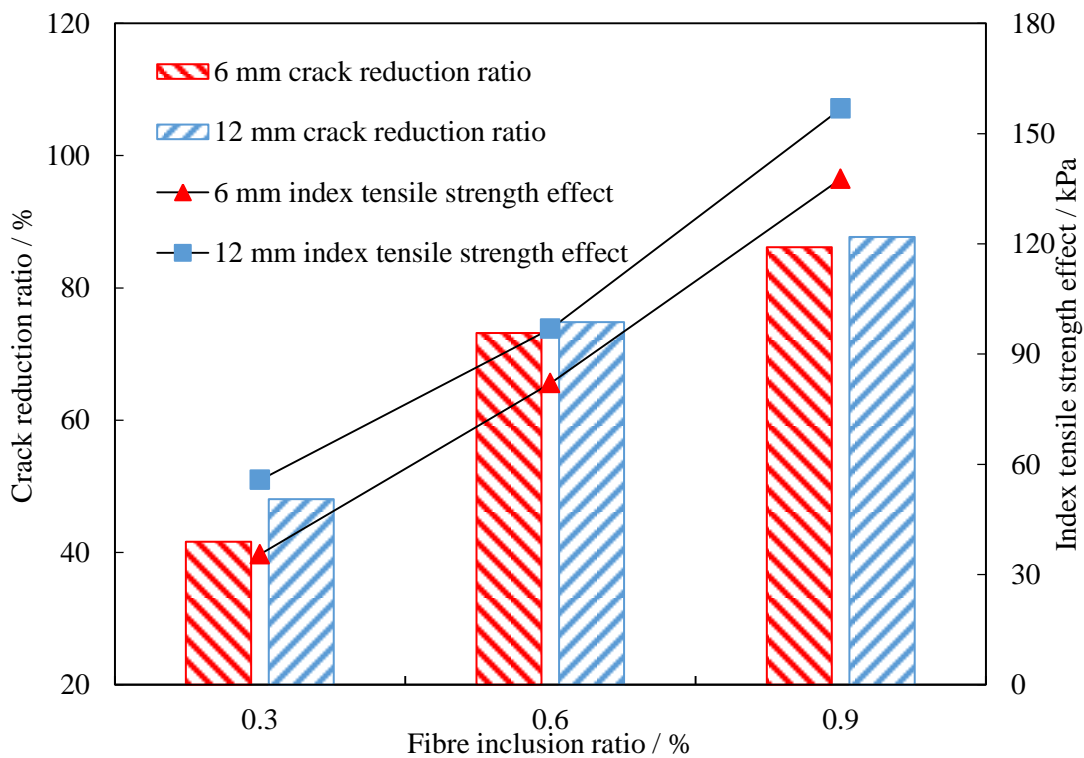


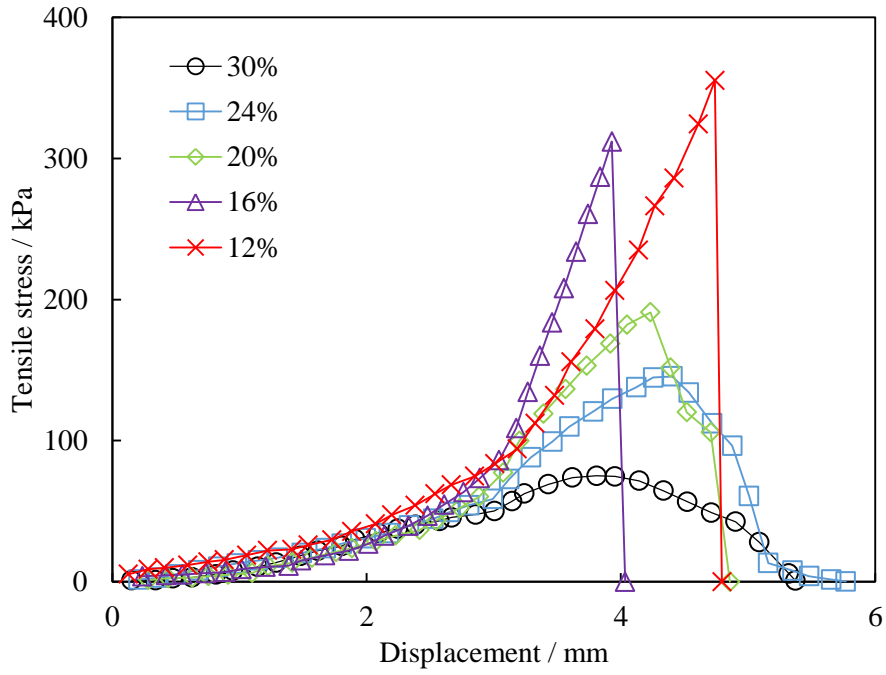
Figure 5.16. Variation of $\Delta\sigma_{tf}$ and CRR with fibre inclusion ratio for different fibre lengths at

$w=24\%$.

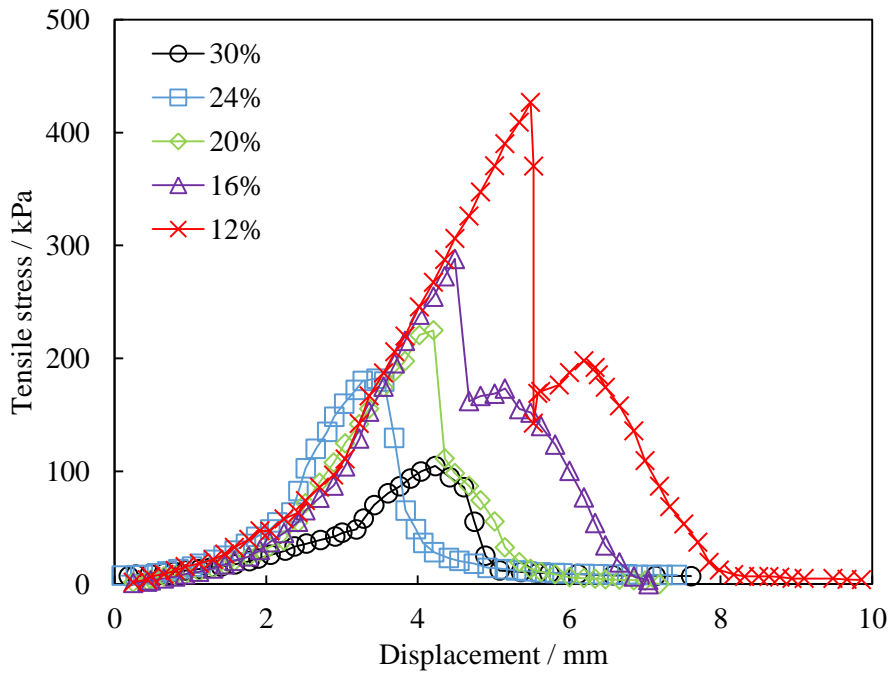
5.3.2 Stiffness behaviour

Effect of water content

Figure 5.17 shows typical stress-displacement curves of URS and FRS ($l=6\text{ mm}$, $\rho_f=0.3\%$) specimens at different water contents. For the URS specimens (Figure 5.17a), when the water content is 30%, the tensile stress drops to zero within approximately 1.5 mm displacement after a peak value. As the water content decreases, the displacement needed of the stress dropping from peak to zero decreases. When the specimen is in relative dry condition ($w=16\%$, 12%), the tensile stress drops to zero directly after peak value. It can be concluded that the unreinforced soil show a transition from ductile behaviour to brittle behaviour as the water content decreases. As for FRS specimens (Figure 5.17b), when the specimen is in a relatively wet condition ($w=30\%$, 24%), the soil shows a ductile behaviour and the tensile stress decreases gradually to zero, which is similar with URS specimens. However, when the specimens were relative dry ($w=16\%$, 12%), the tensile stress of FRS specimens drops from the peak value to a lower value, followed by a slight upward trend to a secondary peak value. This could be attributed to the redistribution of the tensile load between the fibres and soil matrix after the failure, so the combined maximum bond strength of the embedded fibres was mobilised after the cracking occurred (Divya et al., 2013 observed a similar phenomenon.). Then the tensile stress decreases gradually to zero. Generally, the displacement to reach the tensile strength increases as the decreasing water content, but the displacement from the failure to the end of the test is independent from water content. Compared with the unreinforced specimens, the fibre reinforced specimens show a more ductile behaviour in the same water content when the soil is relative dry. So it can be concluded that the failure brittleness of the London Clay is reduced due to the presence of PP fibres.



(a)



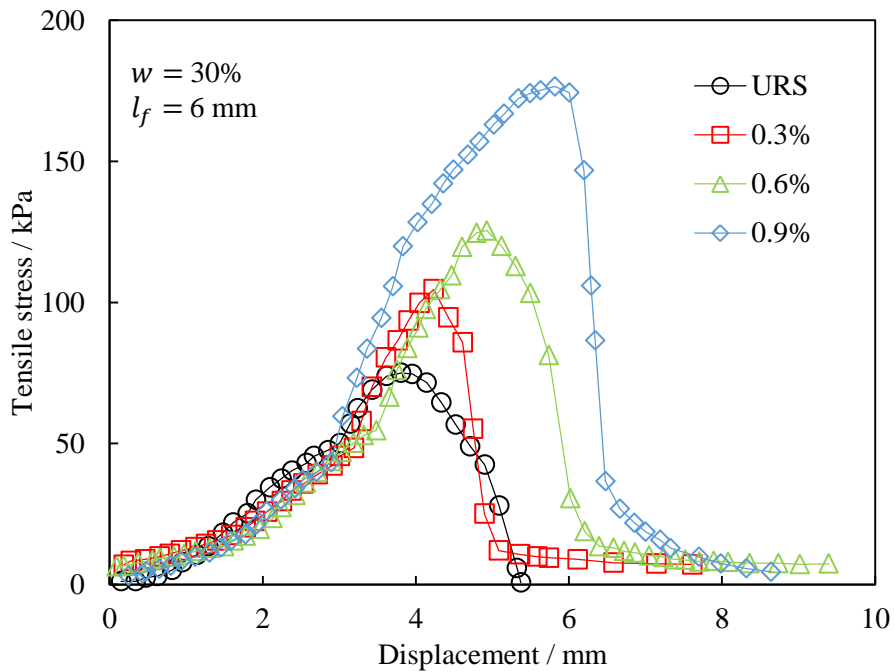
(b)

Figure 5.17. Plots of tensile stress against displacement in direct tensile testing of specimens with different w : (a) URS (b) FRS ($l_f = 6$ mm, $\rho_f = 0.3\%$).

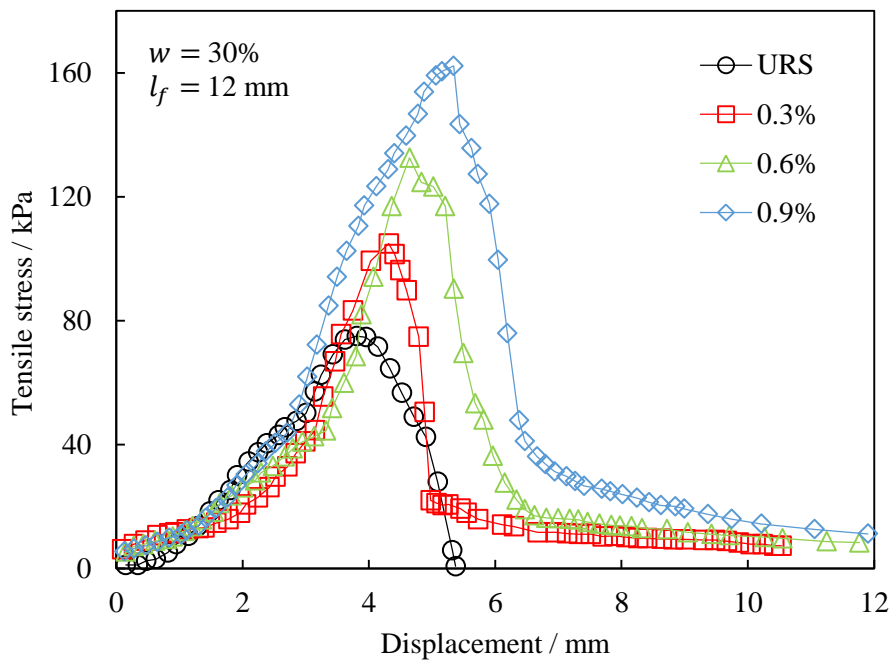
Effect of fibre inclusion ratio and fibre length

Figure 5.18 displays typical stress-displacement curves from direct tensile testing of URS and FRS specimens at two different water contents ($w=12\%$, 30%). It is clear that for both fibre lengths, the peak tensile strength increases as fibre inclusion ratio increases. The displacement before failure also increases with the increasing ρ_f , reflected in crack initiation in specimens and will be further discussed in 5.3.3. The delay in occurrence of peak stress also increases the energy absorption capacity (determined as the area under the stress-strain curve), which can be viewed as an improvement of the soil's toughness (Divya et al., 2013). However, the addition of fibres has no influence on the stiffness (slope of the beginning part of stress-displacement curves) of the soil. As mentioned in last section, the tensile stress carried by unreinforced specimens declines immediately after the peak stress in the wet condition (Figures 5.18a and 5.18b). In contrast, curves of FRS specimens display a "tail" after the stress drop to a post-cracking stress (defined as the stress of the point after the peak stress), and experienced a strain for fibre pull out distance simultaneously. This post-cracking stress is also called as "residual stress" in Chebbi et al., (2017) and Tang et al., (2016). Since the stress decreases gradually but not a steady value so the term "residual" is not adopted herein. It can be seen that the post-cracking stress of FRS specimens increases with an increase in either ρ_f and l_f . For example, when $\rho_f=0.3\%$, an increase in fibre length from 6 mm to 12 mm increases the post-cracking stress by 223% and 162% for water contents $w=30\%$ and $w=12\%$, respectively. Also, the 12 mm FRS has a longer post-peak displacement, which could come from the fact a longer embedded length has a greater pull out distance. Two major conclusions can be drawn from Figures 5.17 and 5.18. Firstly, FRS specimens exhibit different post-peak patterns than URS specimens, and their post-peak behaviour depends upon water content. Secondly, the post-peak patterns of FRS specimens are independent of fibre inclusion ratio and fibre length, certainly at the testing scale. In the most geotechnical

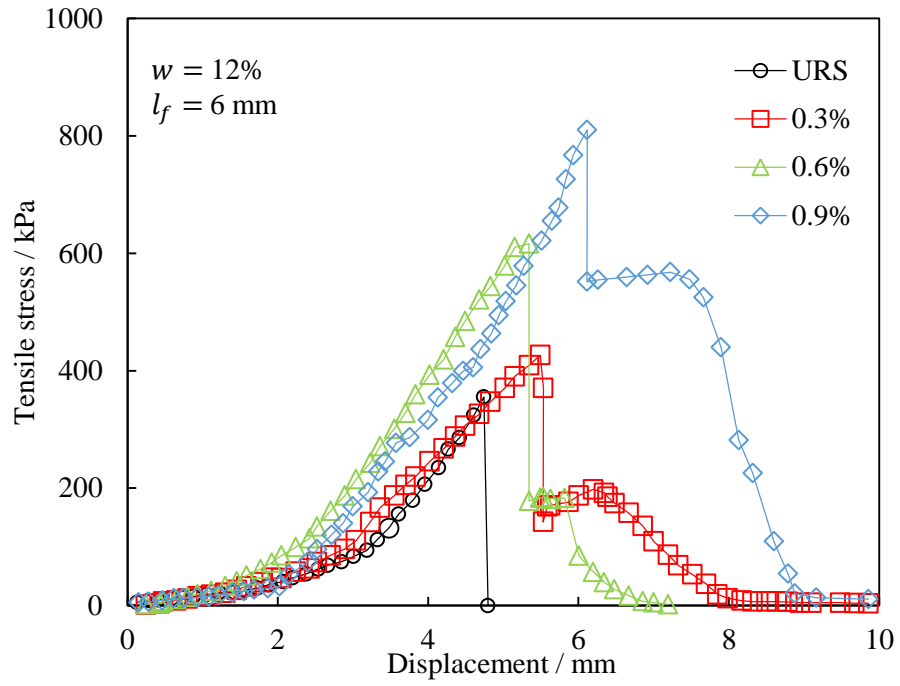
engineering projects, the designing is related to the first peak stress (tensile strength) of the soil. However, the secondary peak value of fibre reinforced soil can provide a new idea and perspective for improving soil's behaviour in large strain problems (e.g. seismic engineering).



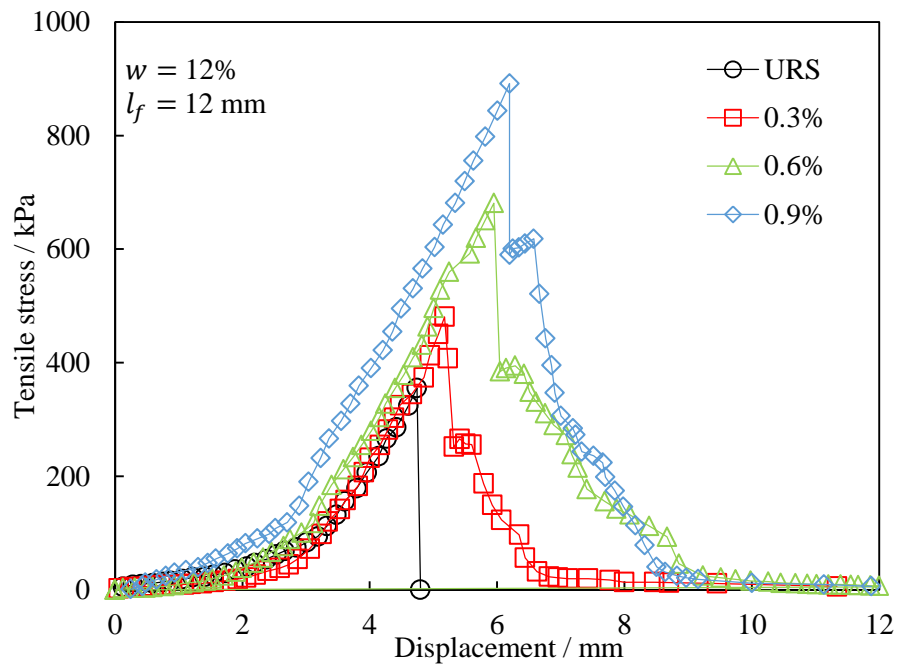
(a)



(b)



(c)



(d)

Figure 5.18. Plots of tensile stress against displacement in direct tensile testing of specimens with different ρ_f : (a) $l_f = 6$ mm, $w = 30\%$; (b) $l_f = 12$ mm, $w = 30\%$; (c) $l_f = 6$ mm, $w = 12\%$; (d) $l_f = 12$ mm, $w = 12\%$.

5.3.3 Failure patterns

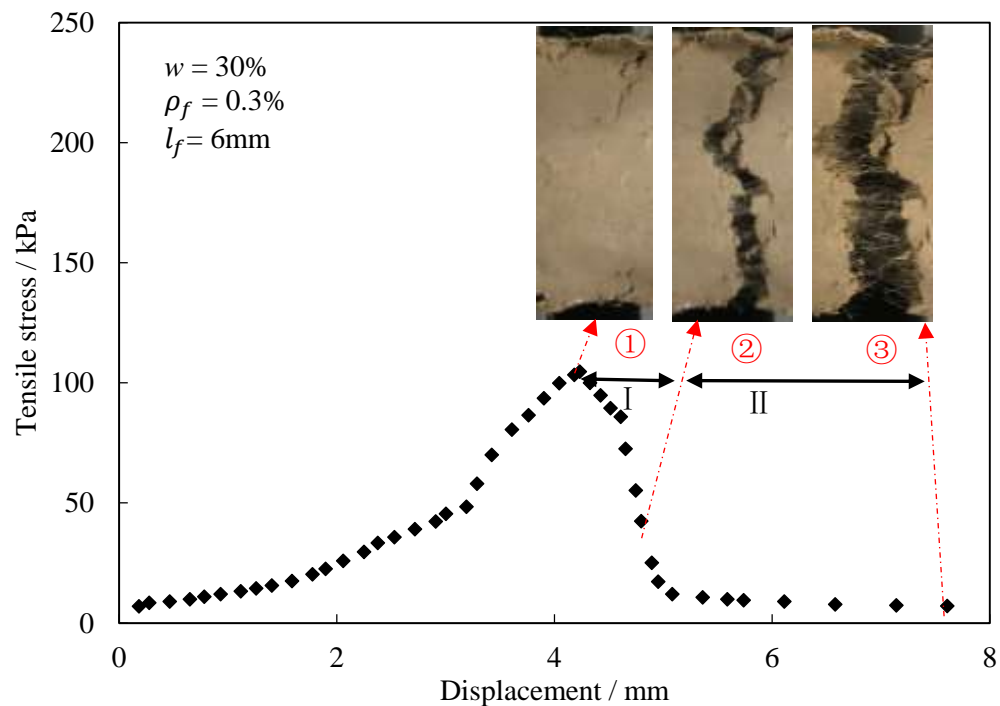
Based on the results presented so far, it is useful to classify the post-cracking period of wet samples and dry samples into two and three stages respectively. Figure 5.19 shows failure stages of the selected FRS specimens ($\rho_f = 0.3\%$, $l_f = 6$ mm, $w = 12\%$, 30%) by illustrating failure cracks initiation and propagation captured on the top surface of the specimens (as described in 3.4.6). It can be seen in Figure 5.19a that when the specimen is at a wet condition, the tensile stress increases as displacement increases and reaches a peak value.

Simultaneously, an initial crack occurs at the edges of specimen (① in Figure 5.19a). After this point, the tensile load drops rapidly as tensile resistance transfers completely to the fibres, and a more complete crack, which is perpendicular to the tensile load direction, can be seen on the surface (② in Figure 5.19a). This is stage I of the failure process; the majority of fibres were pulled out during this stage. At failure stage II, the crack expands with increasing displacement of the jaws and the rest of the fibres are pulled out. These fibres have a longer embedded distance and have not been pulled out totally in stage I due to the rough and uneven rupture plane. A continuous reduction of the load is recorded during this stage and until the end of the test. It can be seen from ③ in Figure 5.19a, at the end of test, almost all fibres on the failure plane only connect with one end of the sample.

Moving to the dry condition, it can be seen from Figure 5.19b, there are three stages in the failure process. Firstly, when the specimen reaches peak tensile stress, several separate micro cracks are observed (① in Figure 5.19b). This was a frequently observed phenomenon in the experimental testing undertaken with dry samples. After the stress drops to a post-cracking value, as mentioned above, the FRS specimens experience a second, lower peak stress and cracks develop as shown in ② in Figure 5.19b. This is the stage I for the dry condition.

Observation of a second peak stress is another frequent phenomenon for FRS when the water

content of the sample is low. As already discussed previously, here the maximum bond strength of the embedded fibres is mobilised. The mobilisation of fibres can also happen in the wet condition, but the pull-out resistance of fibres in the soil matrix depends strongly on the soil particle rearrangement and rotation. In a wet condition, bonding and interlock forces between particles are reduced, the latter as a result of lower suction. This might explain the different failure modes observed in wet and dry conditions. After the second peak load, the test shows a similar trend to that seen in the wet condition: a relatively rapid reduction (stage II), followed by a gradually decrease in load (stage III). It is worth mentioning that at stage II and stage III, cracks would develop along the path which has least tensile resistance, so a major crack develops (③ in Figure5.19b) and finally splits the specimen into two parts (④ in Figure5.19b). Specimens reinforced with 12 mm length fibres show similar behaviour.



(a)

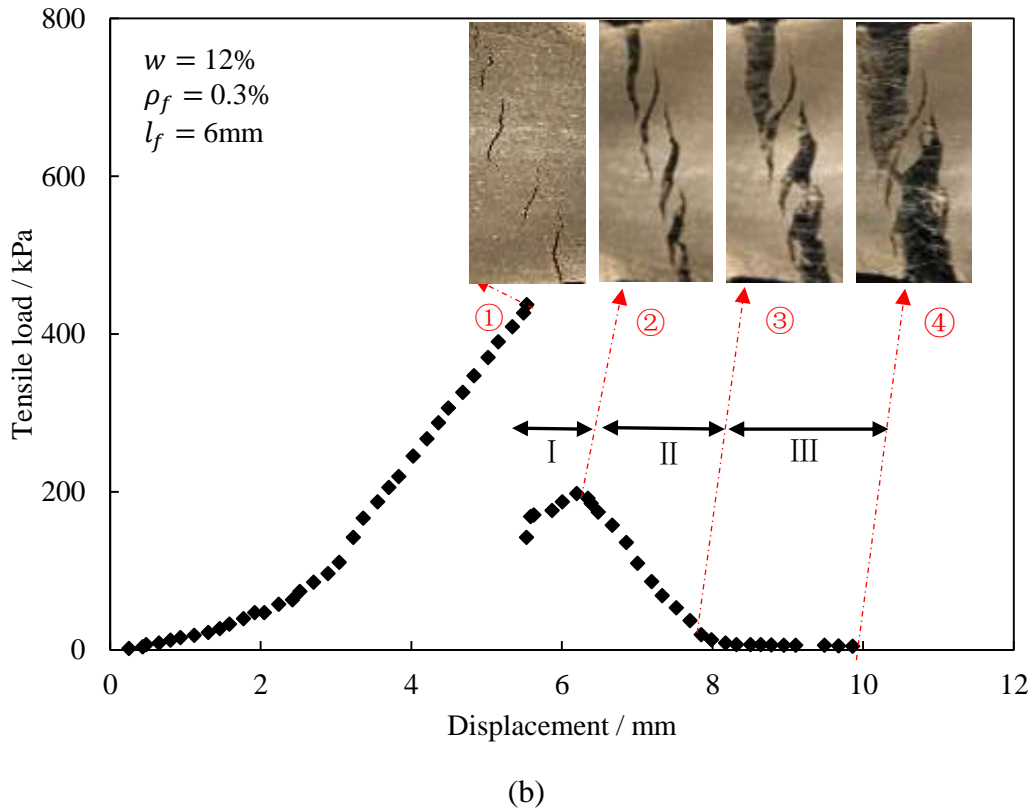


Figure 5.19. Typical failure patterns of FRS in (a) wet condition; (b) dry condition.

5.3.4 Suction behaviour

The suction measurement method in direct tensile tests has already been introduced in 3.4.6. The relationships between gravimetric water content and total suction for URS and FRS samples are presented in Figure 5.20. It can be seen that for both unreinforced and reinforced soil, suction increases as the water content decreases as expected. At a given water content, suctions for FRS samples are close to those for the unreinforced samples showing that fibre addition appears not to have an obvious influence on soil suction. It is known that soil suction depends on water content and porosity of soil matrix. The compaction and consolidation results in Chapter 4 have already shown that fibres might have an influence on void ratio of soil. However, the results presented in Figure 5.20 shows that fibres have no influence on water retention response of soil, which is therefore an unexpected result. However, due to the size difference between fibres and clay particles it is believed that the changes to the pore size

distribution are limited to macro pores, which can be defined as the magnitude of the fibre diameter (22 μm) in this study. With smaller pores, associated with higher suctions unaffected. Also, one would expect that the influence of fibre addition might change the air entry value (defined as the matric suction value that must be exceeded before air recedes into the soil pores) of suction, leading to an influence on the initiation of cracks. The air entry value is usually measured as the intersection point between the linear part of the water retention curve (Figure 5.20) and complete saturation ordinate. Although one cannot obtain the air entry value of URS and FRS in this study because of the lacking of saturation part of the water retention curves, it can be deduced from Figure 5.20 that fibre won't has influence on air entry value of soil. Hence, the delay of the crack initiation in Figure 5.8 is affected by the higher tensile strength comes from the fibres. Based on the discussion in 5.3.3 and 5.3.4, it can be concluded that the fibre reinforcement benefit to the tensile strength behaviour of soil is not in the form of suction improvement, but due to the pull out resistance of fibres.

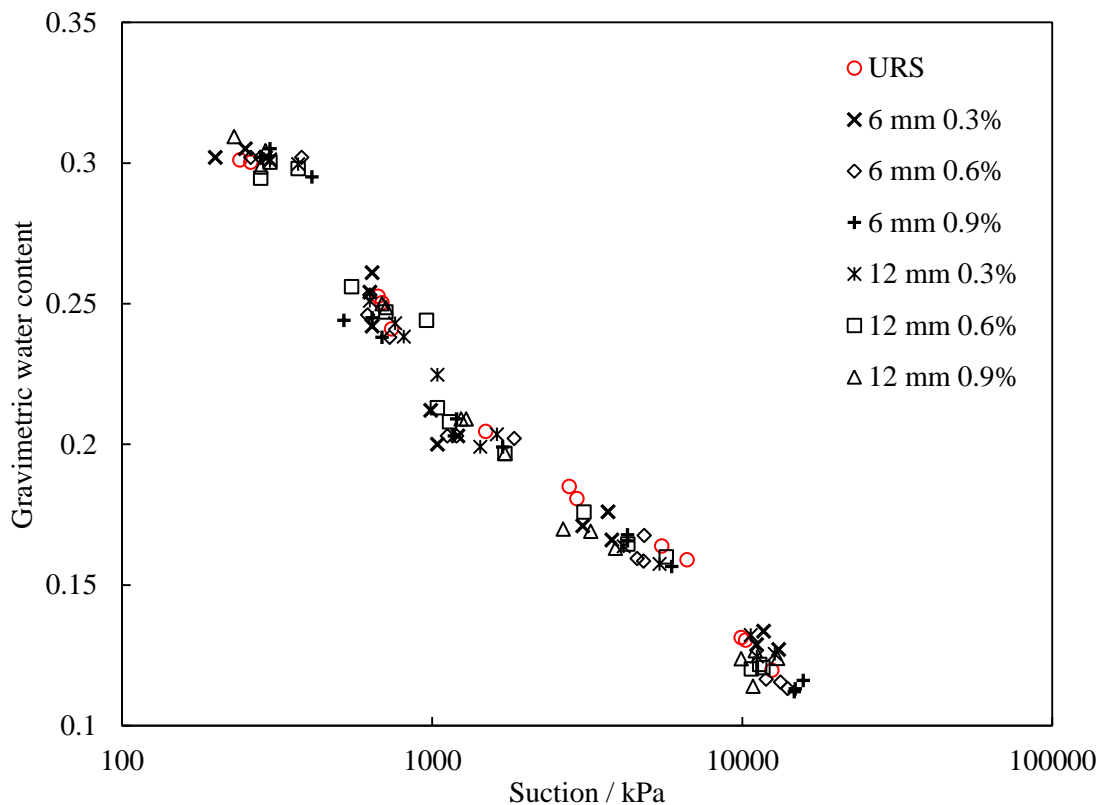


Figure 5.20. Relationship between gravimetric water content and suction for URS and FRS.

5.4 Chapter summary

A shrinkage and desiccation crack is likely to appear when the tensile stress of the soil reaches its tensile strength. Cracks on the surface of engineering projects can increase the permeability of the soil consequently let the water flow into the projects and reduce the shear strength of soil. As a high plasticity clay, London Clay has significant shrink-swell potential when the water content changes. Hence many engineering problems will be caused due to the shrinkage and cracking problems mentioned above when such soil is used as backfill in road embankment engineering. In this chapter, the linear shrinkage, desiccation cracking and tensile strength behaviours of PP fibre reinforced London Clay are discussed based on experimental test results. The conclusions are drawn as follows:

- (1). Fibre reinforcement can significantly improve the desiccation behaviour of London Clay. The improvement can be found in both desiccation shrinkage and desiccation cracking, this benefit comes from the increased tensile strength due to the fibre addition.
- (2). Linear shrinkage strain of the soil decreases significantly with PP fibre addition, which is only 38% of the unreinforced soil when the fibre inclusion ratio is 0.9%.
- (3). Fibre reinforcement can restrict the initiation and development of desiccation cracking. The crack intensity factor of soil is significantly reduced and initial crack occurrence is delayed as fibre inclusion ratio increases.
- (4). Fibres also change the crack pattern by reducing the size of main cracks and increase the number of small cracks. More closed crack paths are found in URS specimens, while cracks in FRS specimens are more individually and unevenly distributed.
- (5). Fibres can significantly increase tensile strength and ductility of the London Clay, the increased tensile strength is because of the pull out resistance of the fibres, and independent of soil's suction. The benefit of fibre reinforcement on tensile strength decreases as the water content increases.

(6). For the FRS specimens, the process after cracking can be generally described in two stages for wet soil and three stages for dry soil. 12 mm length fibres cause more tensile strength improvement than 6 mm length fibres do, which leads to a better effect in desiccation behaviour of the soil, especially when the fibre inclusion ratio is relatively low.

These results and conclusions indicate that fibre reinforcement is a potential soil improvement method in geotechnical constructions using clay fills such as road embankments, slopes and other engineering practices in which tension cracks would be encountered.

Chapter 6

6. Shear strength behaviour of fibre reinforced clay

The first and second part of the laboratory tests in this study have already been discussed in Chapter 4 and Chapter 5. In this chapter, the results of the third part of the laboratory investigations, comprising consolidated undrained triaxial tests, is discussed and the shear strength behaviour of unreinforced and fibre reinforced soil are analysed and evaluated based on the results. Three fibre inclusion ratios ($\rho_f = 0.3\%$, 0.6% and 0.9%), two fibre lengths ($l_f = 6$ mm and 12 mm) and three cell pressures ($\sigma_3 = 50$ kPa, 100 kPa and 200 kPa) were selected as variables. All specimens were prepared with their own OMC and MDD by static compression method as mentioned in Section 3.4.7. The stress-strain relationship, stress path behaviour and failure mode of the soil are discussed.

6.1 Data processing

Consolidated undrained triaxial tests were conducted on unreinforced and fibre reinforced soil in accordance with the experiment procedure described in 3.4.7. The raw data were collected and processed before analysis. Figure 6.1 shows the stress-strain curves for both unreinforced (URS) and fibre reinforced soil (FRS) ($\rho_f = 6$ mm, $l_f = 0.6\%$) at 50 kPa and 100 kPa cell pressure.

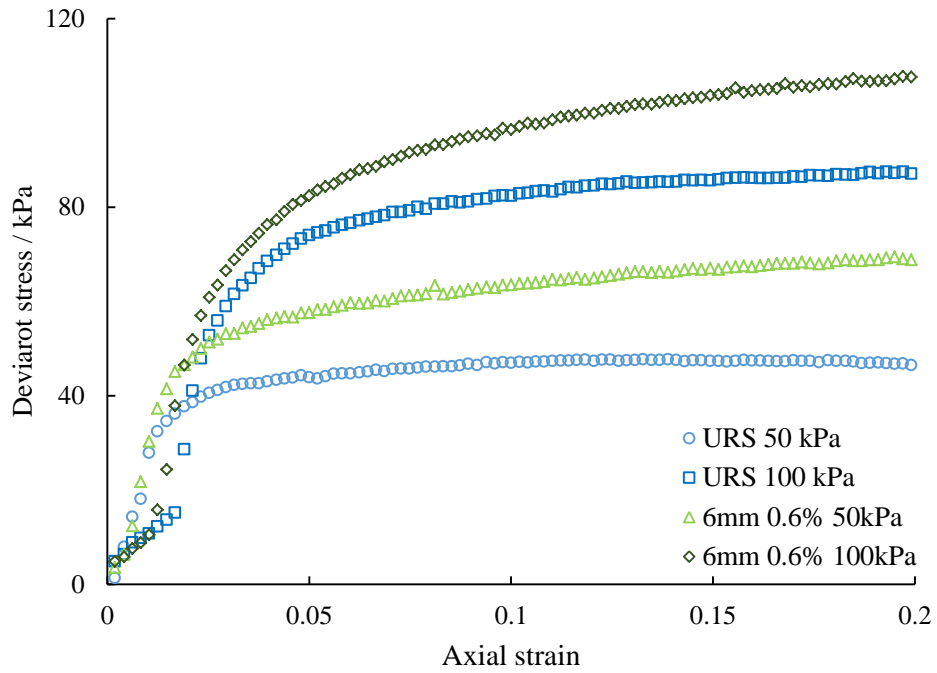


Figure 6.1. Stress-strain curves of unreinforced and reinforced soil.

It can be seen that for both URS and FRS samples, the stress-strain curves exhibit irregular fluctuation at the start of the tests, especially when the cell pressure is relatively high (100 kPa). The explanation for this is that the top cap and the loading system are connected via a mental marble (Figure 6.2), which can slide within the pit of the top cap when the top cap and the loading ram are not perfectly aligned. This experimental arrangement is used to prevent eccentric pressure being applied to the specimen, but can also generate fluctuations in load readings at the commencement of shearing. At higher cell pressures it can take longer for the end of the loading ram and the top cap pit to achieve good alignment. In order to make the stress-strain relationship of the soil more obvious and clear, it is necessary to smooth the initial section of the stress-strain curves for all specimens. The smooth process consists of removing the data points in the 0-1% axial scale (see in Figure 6.3). The post smoothing curves are shown in the following sections. This smoothing does not impact the accuracy of the data presented and the following discussion.



Figure 6.2. The connection between top cap and the load ram.

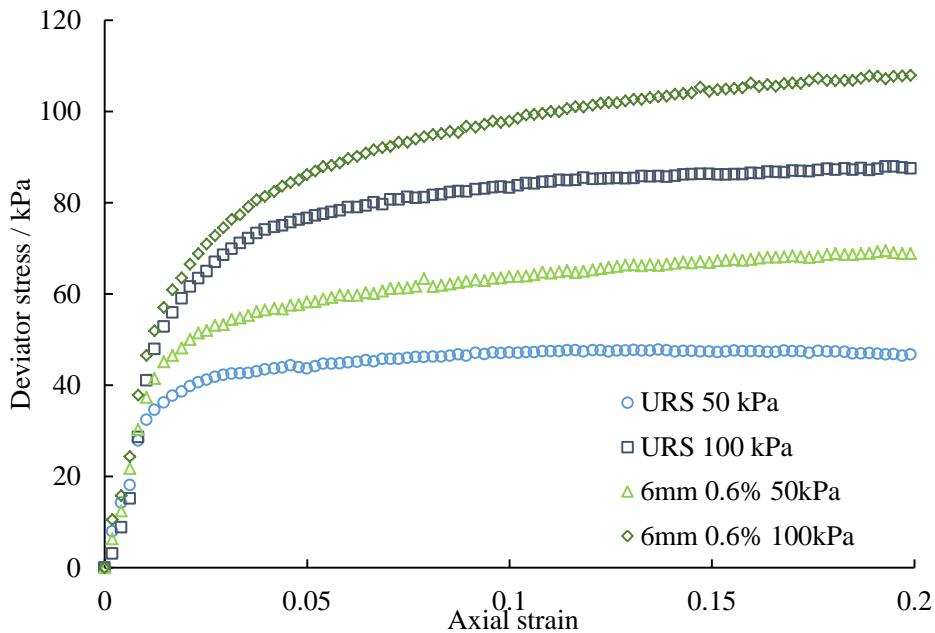


Figure 6.3 Stress-strain curves of unreinforced and reinforced soil after filtering.

Unreinforced and reinforced soil samples were prepared at their own optimum moisture content and maximum dry density. Although there is not big difference in OMC and MDD between different types of soil (see Section 4.1), it was felt necessary to do an extra test to determine the potential additional increment of shear strength resulting from lower initial water content of the samples. Consequently, an unreinforced sample was prepared at an initial

water content of 21.3%, which is same to the 6 mm 0.9% FRS sample. The dry density of this sample was kept the same as the other unreinforced samples (MDD of URS = 1.581Mg/m³), so these two samples have same initial void ratio. A comparison of the stress-strain curves at 50 kPa cell pressure between this sample, a 6 mm 0.9% fibre reinforced sample and a standard unreinforced sample is shown in Figure 6.4. It can be seen that two unreinforced samples show similar stress-strain behaviour, the sample with initial water content $w=21.3\%$ even shows lower deviator stress when the strain gets greater. The FRS samples prepared at $w=21.3\%$ shows a much higher deviator stress than the unreinforced samples, this confirms that the increase in shear strength is a result of the fibre reinforcement rather than the different initial water content.

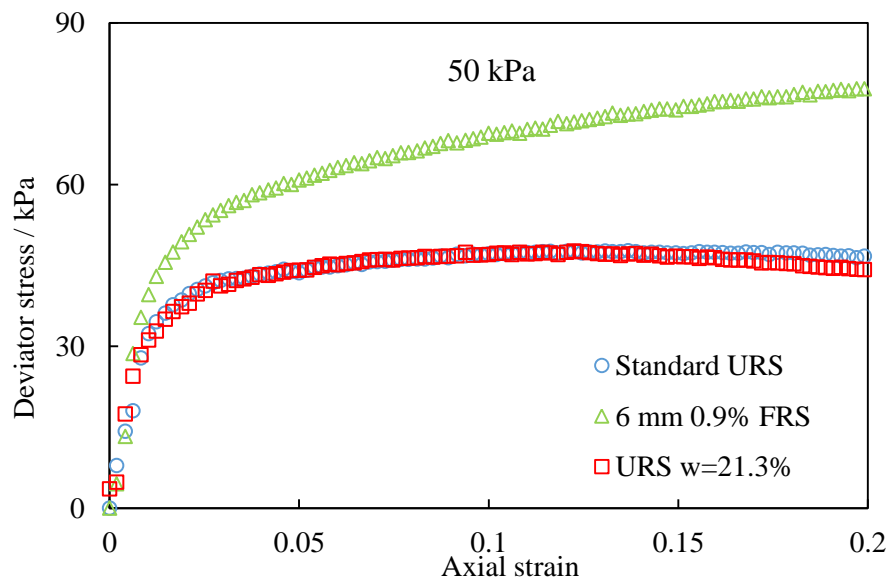


Figure 6.4. Stress-strain curves of controlled samples and tested samples at 50 kPa cell pressure.

The key information about the tests which includes fibre inclusion ratio (ρ_f), fibre length (mm), cell pressure (σ_3), void ratio before consolidation (e_0), void ratio after consolidation (e_1), deviator stress at the end of the tests (q) are concluded in Table 6.1, and they will be introduced and discussed in the follow sections.

Table 6.1. Key information about the triaxial tests.

Sample name	ρ_f (%)	l_f (mm)	σ_3 (kPa)	e_0	e_1	q (kPa)
URS50	0	0	50	1.049	0.920	46.5
URS100	0	0	100	1.049	0.851	87.3
URS200	0	0	200	1.049	0.773	169.2
FRSA50	0.3	6	50	1.003	0.885	63.9
FRSA100	0.3	6	100	1.027	0.842	99.4
FRSA200	0.3	6	200	1.006	0.762	180.5
FRSB50	0.6	6	50	0.995	0.881	69.7
FRSB100	0.6	6	100	0.993	0.824	180.3
FRSB200	0.6	6	200	0.984	0.756	187.3
FRSC50	0.9	6	50	0.969	0.868	77.8
FRSC100	0.9	6	100	0.970	0.808	123.5
FRSC200	0.9	6	200	0.966	0.747	214.6
FRSD50	0.3	12	50	0.994	0.885	71.3
FRSD100	0.3	12	100	1.011	0.843	112.2
FRSD200	0.3	12	200	0.997	0.765	185.4
FRSE50	0.6	12	50	0.992	0.874	78.4
FRSE100	0.6	12	100	0.987	0.835	116.2
FRSE200	0.6	12	200	0.983	0.764	192.4
FRSF50	0.9	12	50	0.969	0.867	82.9
FRSF100	0.9	12	100	0.961	0.811	133.8
FRSF200	0.9	12	200	0.969	0.755	206.6

6.2 The effect of fibre on deviator stress and pore water pressure behaviour of soil

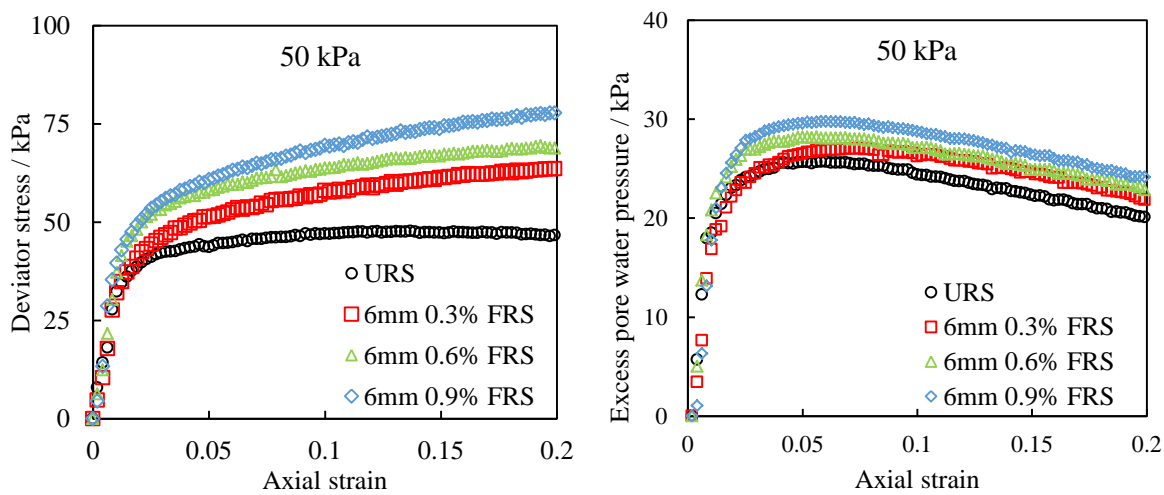
There are three variables in the triaxial tests, fibre inclusion ratio (ρ_f), fibre length (l_f) and cell pressure (σ_3). The influences of these variables on the deviator stress and pore water pressure behaviour of unreinforced and fibre reinforced soil are discussed in the following section.

6.2.1 Effect of fibre inclusion ratio

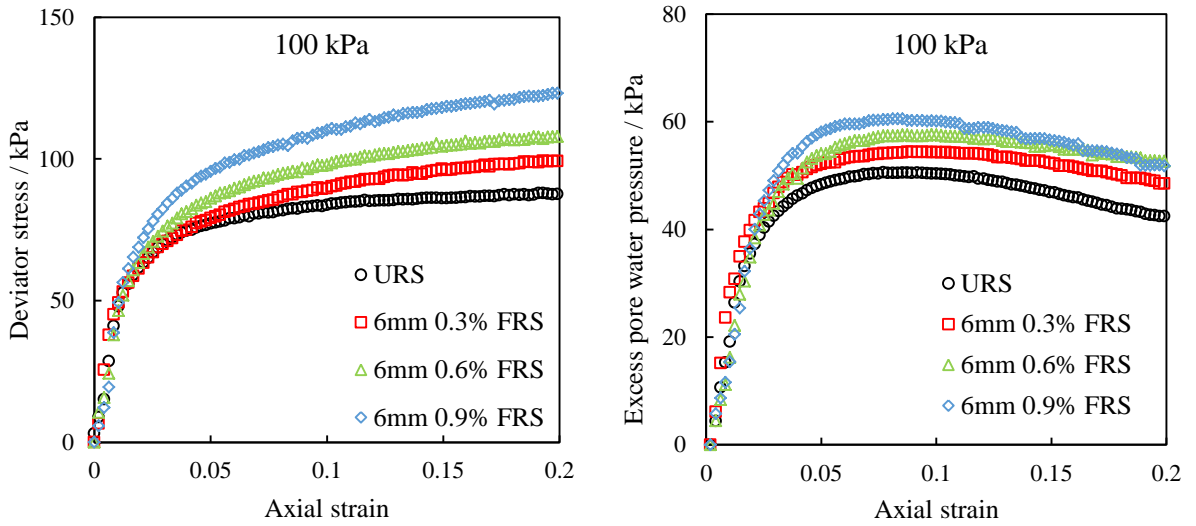
Figures 6.5 and 6.6 show the variations of deviator stress (q) and excess pore water pressure (u) with axial strain (ϵ_1) at different cell pressures for the unreinforced and fibre reinforced soil. It can be seen from Figures 6.5 and 6.6 that for the unreinforced soil, the deviator stress of the soil increases until approximately 5%, 10% and 15% axial strain at 50, 100 and 200 kPa cell pressure respectively, and then no obvious change has been found until a

serviceability failure criterion (at 20% axial strain, below the word “failure” and subscript “ s_f ” refer to this state). For the fibre reinforced soil with different fibre lengths and inclusion ratios, no peak values are observed in deviator stress-strain plots until 20% axial strain. Similar trends have been observed by Ranjan et al., (1996), and Maliakal and Thiyyakkandi (2013). It can be also observed that for a given fibre length, the deviator stress of soil increases with the increasing ρ_f at all three tested cell pressures. For example, the serviceability failure stress (at 20% axial strain) of unreinforced soil is 46.7 kPa at 50 kPa cell pressure, and it increases with increasing fibre inclusion ratio up to 63.6, 68.8 and 77.8 kPa for 6mm length fibre in $\rho_f = 0.3\%$, 0.6% and 0.9% respectively. The maximum increase in deviator stress for both fibre lengths are found at $\rho_f = 0.9\%$ for all three cell pressures. As for the excess pore water pressure-strain relationship, it can be observed in Figures 6.5 and 6.6 that for all specimens, the excess pore water pressure initially increases, peaks at the range of $\varepsilon_1 = 5\% - 10\%$, and then decreases gradually to different degrees. This trend has also been reported by Özkul and Baykal (2007), Ekinici (2016) and Mirzababaei (2012). The reduction in excess pore water pressure is a product of the tendency of dilation of the specimens. By comparing the excess pore water pressure-strain curves of unreinforced and fibre reinforced specimens, two conclusions can be made as follows. Firstly, for a given fibre length and cell pressure, the excess pore water pressure (both peak and serviceability failure) increases with the increasing ρ_f . It is believed that with the increasing fibre inclusion ratio, fibres distribute the stresses within the structure of the soil specimen and restrain the dilative deformation tendency of the soil specimen, which then leads to an increase in excess pore water pressure. This trend and conclusion is supported by the results presented by Estabragh et al., (2011) and Li (2005). Mirzababaei (2012) attributed the increase in pore water pressure to the change in the void ratio of the fibre reinforced soil specimen, the reduction in maximum dry density leads to an increased in void ratio in the specimens. Hence, specimens with more fibres

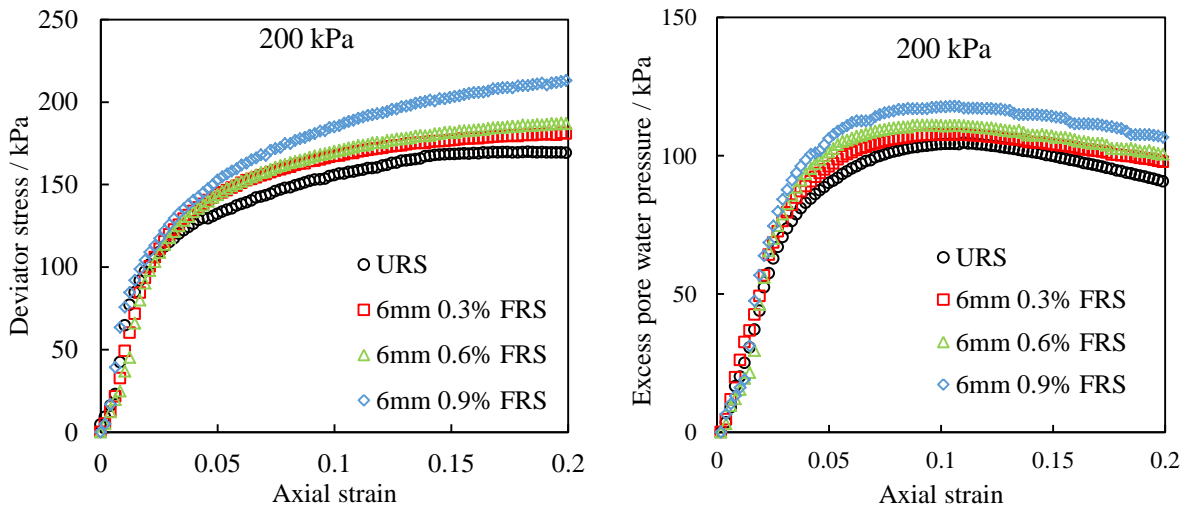
contain more water filled voids after saturation. This explanation is in agreement with the test conditions and results of this study. However, the state of specimens' voids during triaxial testing cannot be monitored by conventional techniques, so further investigations should be conducted to confirm this conclusion. Secondly, it can be found that the increase in ρ_f leads to a reduction in the post peak loss of the excess pore water pressure, because more fibres have a greater effect in preventing the potential of soil's dilation. This phenomenon is more obvious in sample reinforced with 12 mm length fibres. The different effects in soil reinforced with two lengths of fibre can be related to the different soil-fibre interaction of longer and shorter fibres during the deformation. The reduction in the post peak loss of excess pore water pressure also indicates that fibres can reduce the over consolidation ratio of the soil. From an engineering perspective, pore water pressure increased by fibre reinforcement is undesirable as it decreases the effective stress within the soil and leads to a reduction of the structural stability. However, considering the overall performance of the soil, the negative effects of fibre reinforcement on pore water pressure are outweighed by the observed increases of deviator stress and other engineering properties presented in Chapter 4 and Chapter 5.



(a)

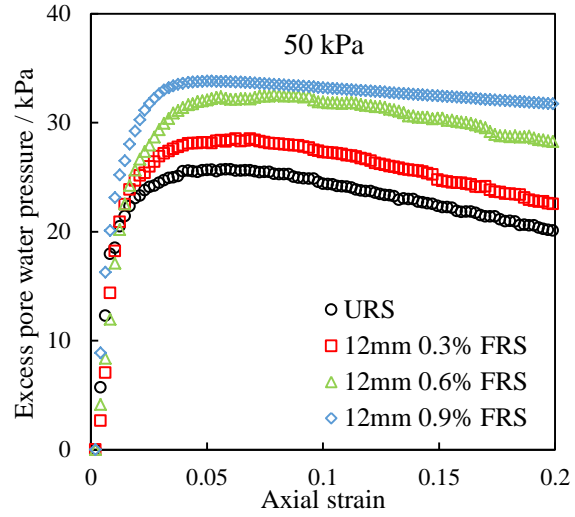
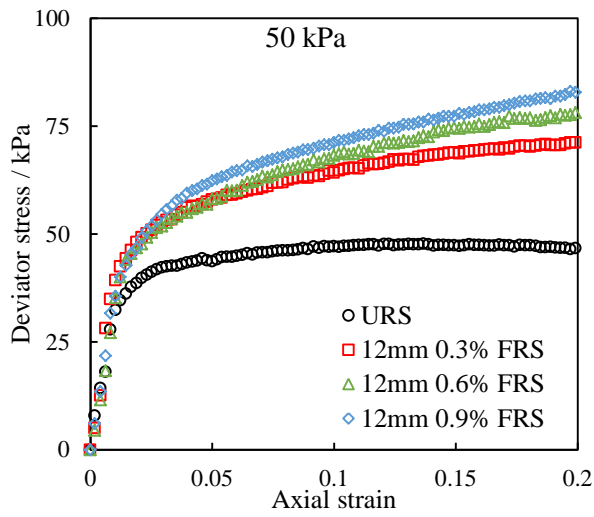


(b)

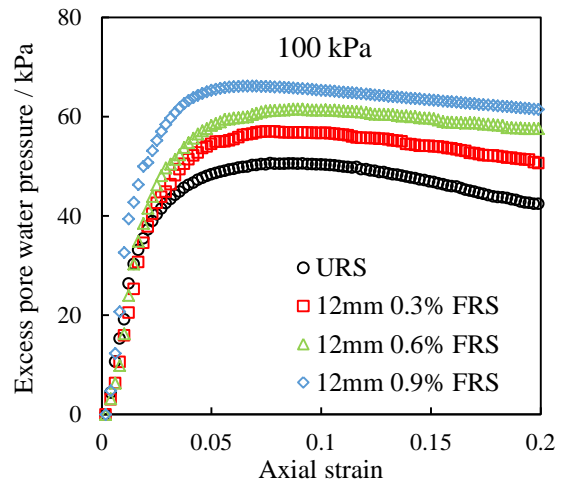
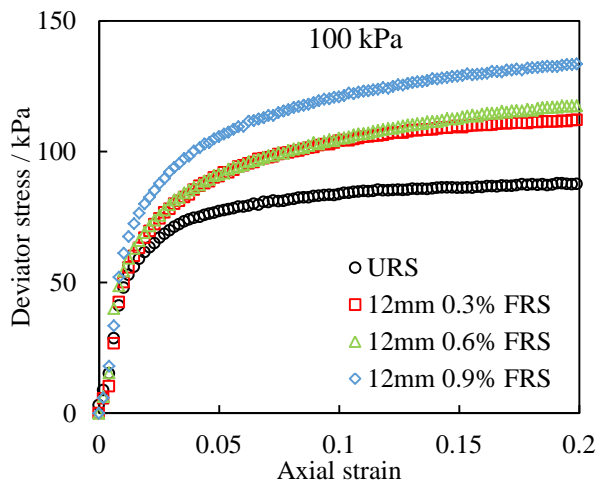


(c)

Figure 6.5. Deviator stress and pore water pressure versus axial strain at different cell pressures for 6 mm fibre reinforced soil (a) 50 kPa (b) 100 kPa (c) 200 kPa .



(a)



(b)

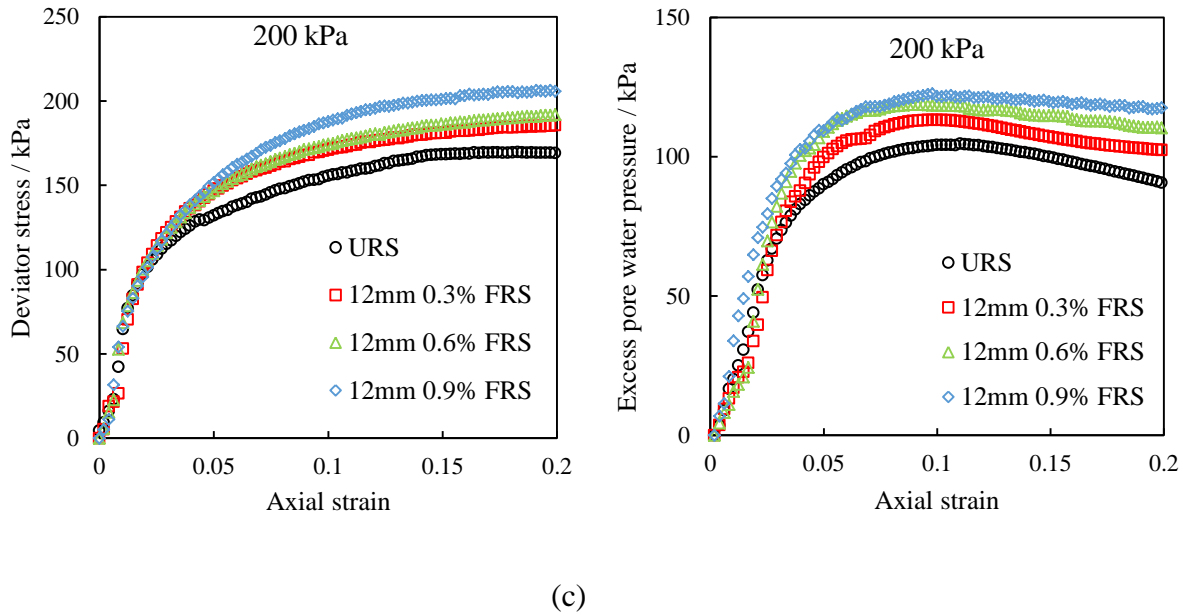


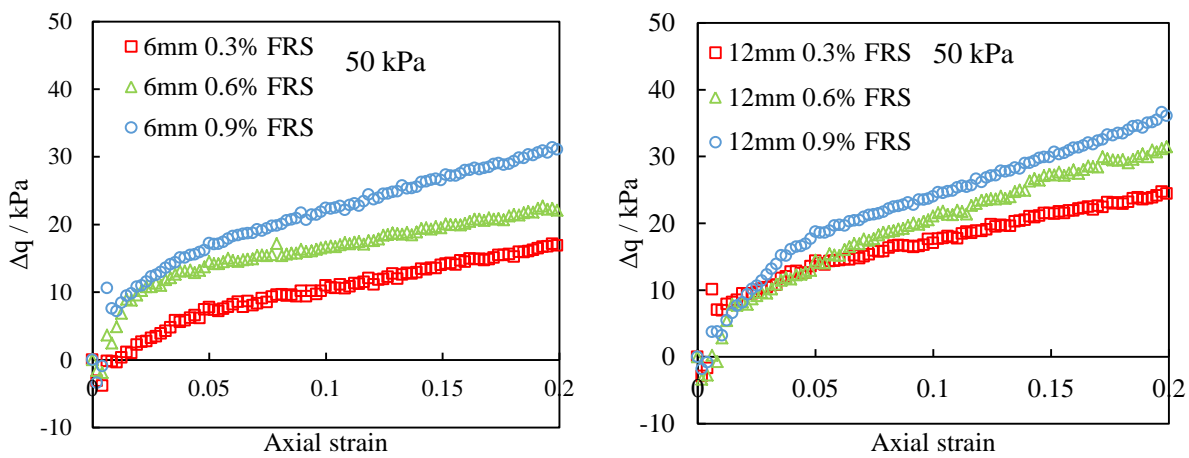
Figure 6.6. Deviator stress and pore water pressure versus axial strain at different cell pressures for 12 mm fibre reinforced soil (a) 50 kPa (b) 100 kPa (c) 200 kPa.

In order to evaluate the effect of fibre inclusion ratio on the deviator stress behaviour of the soil, a term named as “deviator stress increment” is introduced herein. For a given strain level, deviator stress increment (Δq) can be defined as

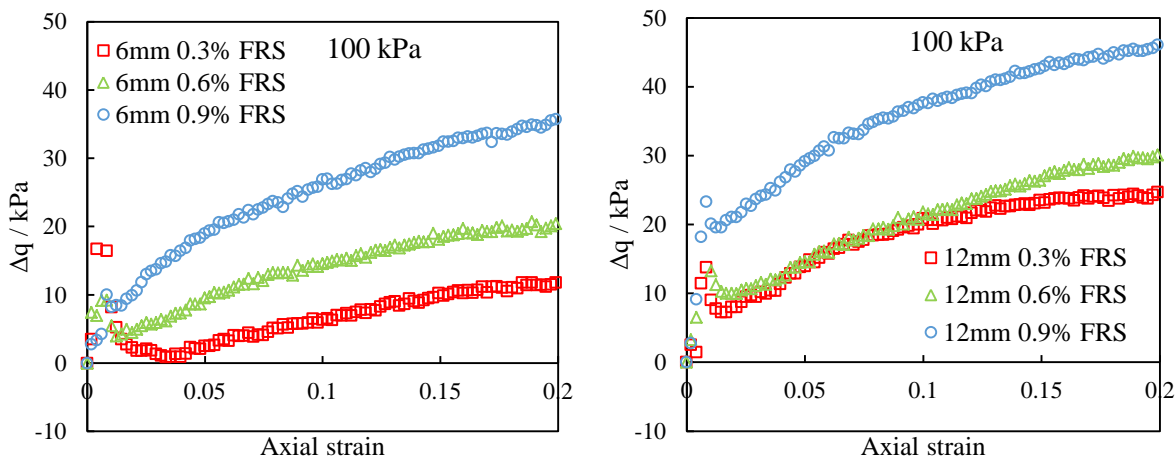
$$\Delta q = q_r - q_u \quad (6.1)$$

where q_r and q_u are the deviator stresses of the reinforced specimen and respective unreinforced specimen under the same test condition. Figure 6.7 shows the relationship between axial strain and Δq for different fibre reinforced specimens. It can be seen that variations of Δq do not follow an obvious pattern for all the specimens. In general, the Δq increases as the axial strain develops and the rate of increase reduces as the axial strain further increases. However, at the initial stage of shearing, the contribution of fibre reinforcement to deviator stress in different test conditions is irregular, and a negative value can be observed in some of the tests. The improvement of deviator stress of fibre reinforced soil comes from the tensile resistance of the fibres, which is induced by the tensile strain of the fibres. Before the

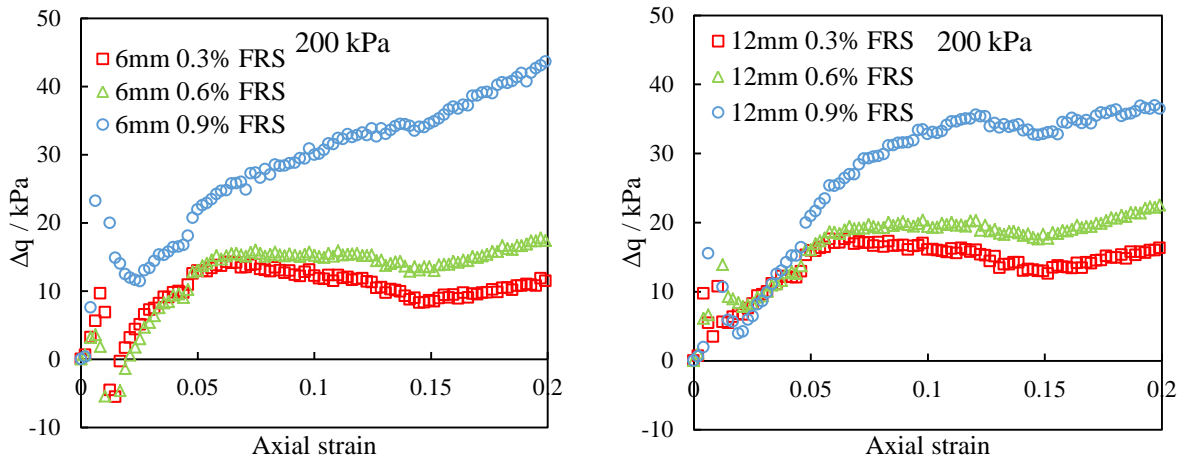
shearing, fibres in the composite are either bending or stretching due to compaction during sample preparation. Consequently, tensile resistance is only mobilised in the fibres after the sample has undergone some straining. The apparent negative values of Δq may be a product of small differences in initial sample density resulting from the sample preparation method and are considered acceptable in this study. The reduced increasing rate might come from increased relative sliding between soil particles and fibres. This trend will be described in the proposed model in Chapter 7.



(a)



(b)



(c)

Figure 6.7. Variations of deviator stress increment of fibre reinforced soil with different fibre inclusion ratios at (a) 50 kPa (b) 100 kPa (c) 200 kPa cell pressure.

In order to evaluate the effect of fibre inclusion ratio on deviator stress contributions more clearly, the deviator stress increment at the end of the tests Δq_{sf} of fibre reinforced soil with different ρ_f are selected and normalised by the Δq_{sf} when $\rho_f = 0.3\%$. The normalised results are plotted in Figure 6.8. It can be observed that for both fibre lengths and all three confining pressures, when the fibre inclusion ratio is doubled (from 0.3% to 0.6%), the deviator stress contribution does not increase to two times of the original value ($\rho_f = 0.3\%$). A similar trend can be observed for $\rho_f = 0.9\%$: generally when the fibre inclusion ratio is tripled (from 0.3% to 0.9%), the deviator stress contribution is not tripled. It can therefore be concluded that as the fibre inclusion ratio increases, the improvement of shear strength is not linear, the benefit obtained per unit fibre inclusion ratio decreases as ρ_f increases from 0 to 0.9%. This phenomenon will be considered in the proposed model in Chapter 7.

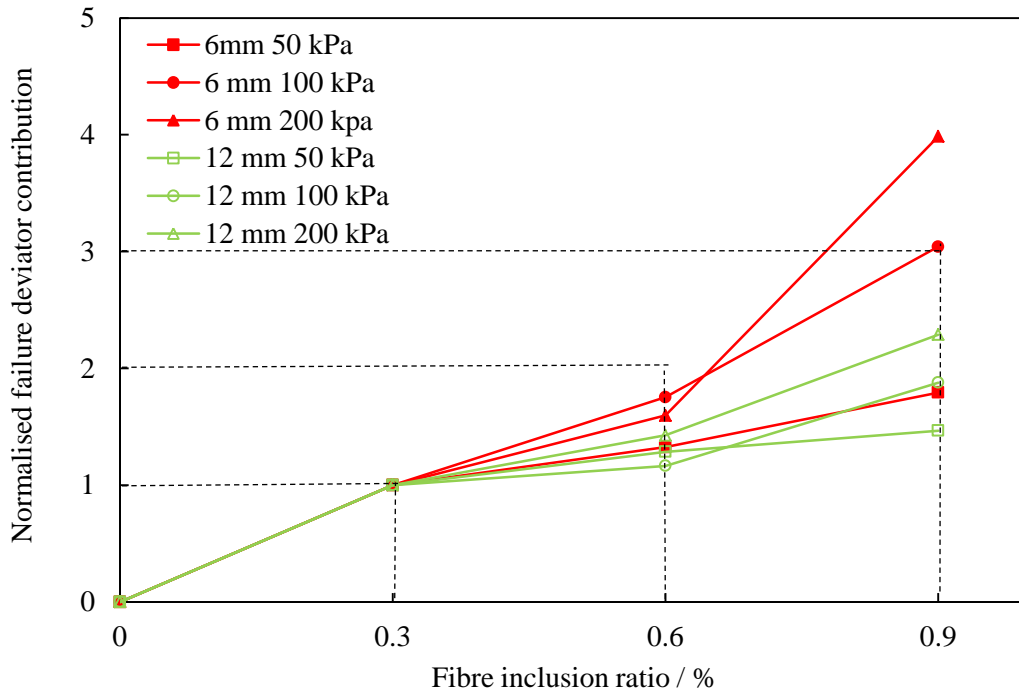


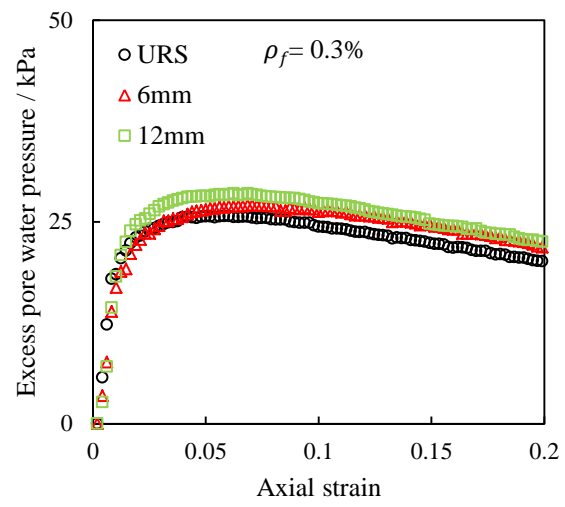
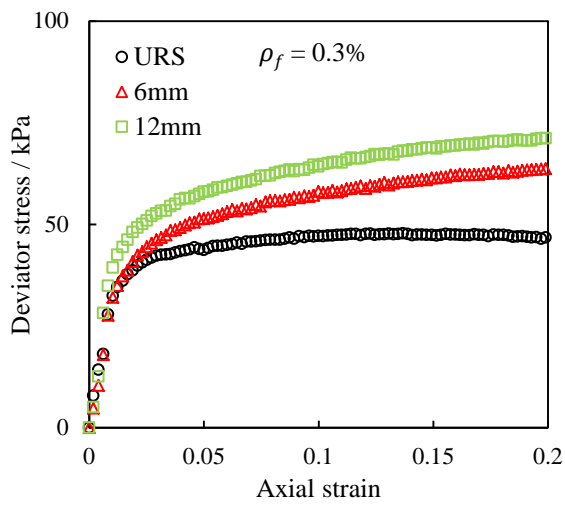
Figure 6.8 Variation of normalised failure deviator contribution (at 20% strain) with different fibre inclusion ratios.

6.2.2 Effect of fibre length

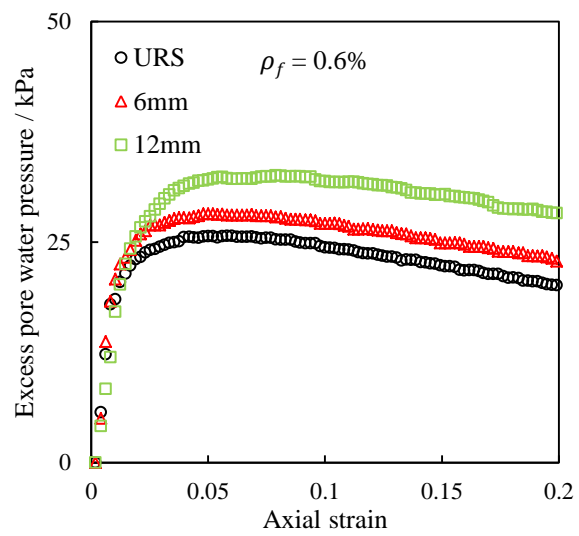
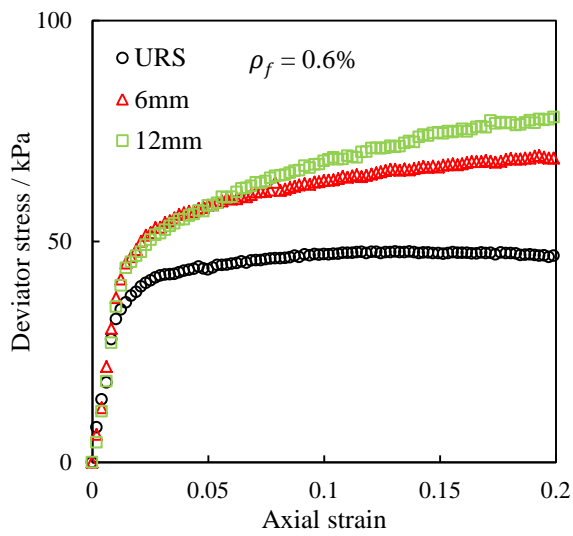
A comparison of deviator stress-strain and excess pore water pressure- strain relationships between specimens reinforced with different lengths of fibres is shown in Figures 6.9- 6.12. It can be seen that for a given fibre inclusion ratio and cell pressure, the specimens reinforced with longer fibres (12 mm) generally display higher deviator stress at the end of the test ($\epsilon_1 = 20\%$). This trend is also found on PP fibre reinforced sand in Li (2005). However, Li (2005) reported that peak deviator stress increases linearly with increasing fibre length, this trend was not observed in this study. It can be seen that the improvement in failure deviator stress from 0 (URS) to 6 mm is much higher than that from 6 mm to 12 mm. An exception occurs when the fibre inclusion ratio is 0.9% and cell pressure is 200 kPa, where the deviator stress of the specimen reinforced with 12 mm length fibres (205.8 kPa) is lower than that with 6 mm length fibres (213 kPa). The trend observed is believed to be due to the fact that the friction

between soil particles and fibres is mobilised along the length of the fibre and the tensile resistance provided by the fibre is proportionate to its length. Longer fibres also have longer embedded lengths which increase the overall pull out resistance. However, the probability of folding and bending of the fibres is higher when the fibre is longer, so additional increases in fibre length can lead to a reduction in deviator stress of the soil, this conclusion was stated in Petal and Singh (2019) and Falorca and Pinto (2011). In addition, the results also show that the increased fibre length leads to the improvement in both the peak and failure value of the excess pore water pressure. This can be attributed to the longer fibres having a greater effect in restricting the soil's dilation. Another interesting phenomenon can be found by comparing the difference in excess pore water pressure of 6 mm and 12 mm fibres from Figures 6.9- 6.11. For a given cell pressure, as the ρ_f increases, the difference of excess pore water pressure between 6 mm and 12 mm fibre length additions becomes greater. It can be concluded that longer fibres have a greater benefit in restricting soil's dilation when the fibre inclusion ratio is relatively high. The failure deviator stress of specimens reinforced with 6 mm and 12 mm length fibres is normalised by that of unreinforced soil at the same cell pressure and shown in Figure 6.12. It can be seen that as the ρ_f increases from 0 to 0.9%, the difference in the normalised failure deviator stress between 6 mm and 12 mm length fibre become smaller. This trend is opposite to the findings presented in Al-Refeai (1991), which were based on triaxial tests of fibre reinforced sand. The difference in findings might be a result of different interaction behaviour between fibre-sand soil and fibre-clay soil. It can also be found that when the cell pressure is 200 kPa, the difference between 6 mm and 12 mm fibres is much smaller than that at 50 and 100 kPa. This is due to the lateral strain of fibre reinforced soil being more restricted at the higher cell pressure, so the higher tensile strength of 12 mm fibre which comes from longer length cannot be fully mobilised. For both 6 mm and 12 mm length

fibre reinforced specimens, the maximum normalised value occurs at 50 kPa cell pressure when the fibre inclusion ratio is 0.9%.



(a)



(b)

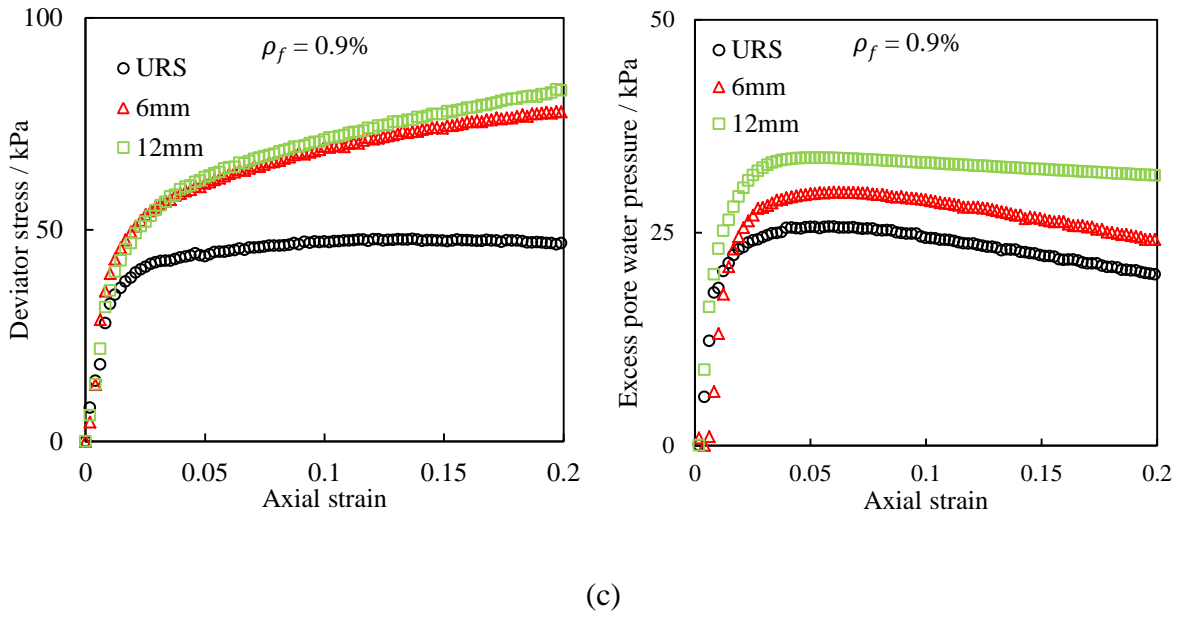
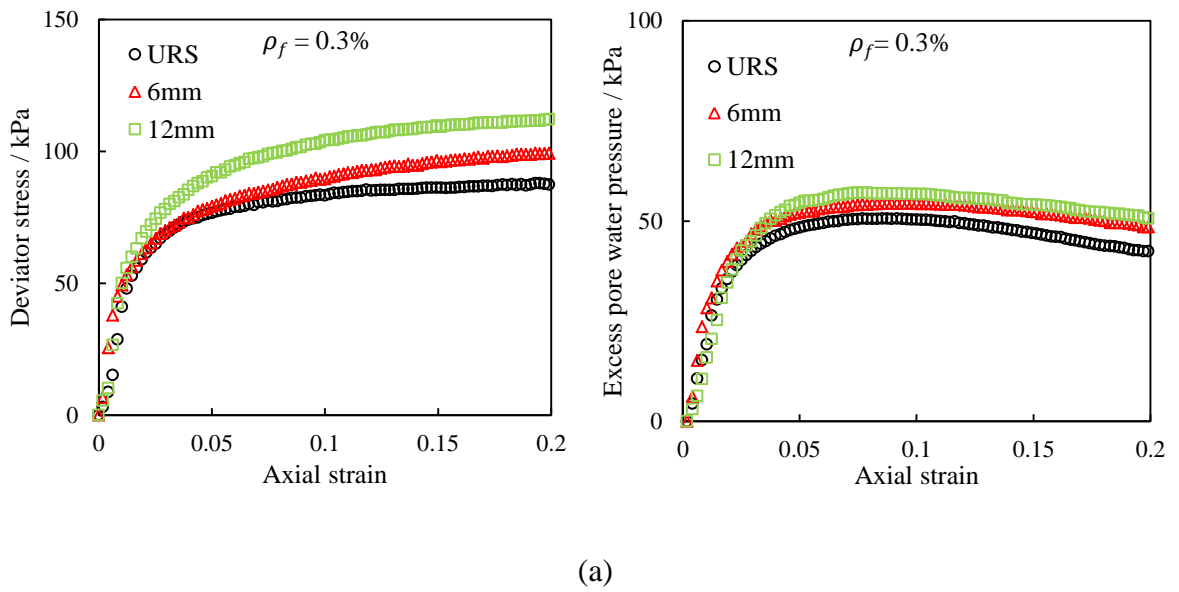
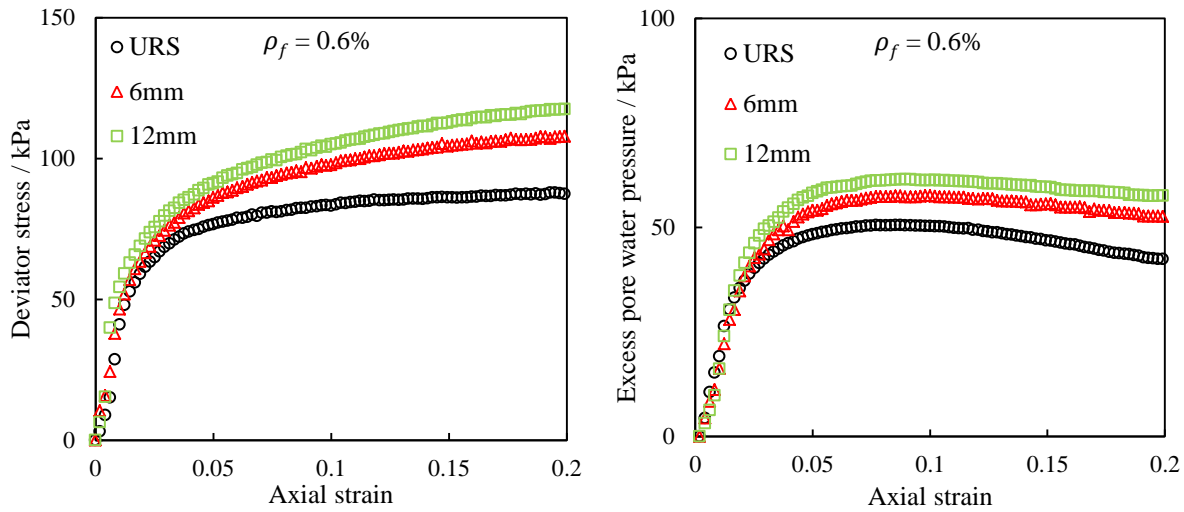
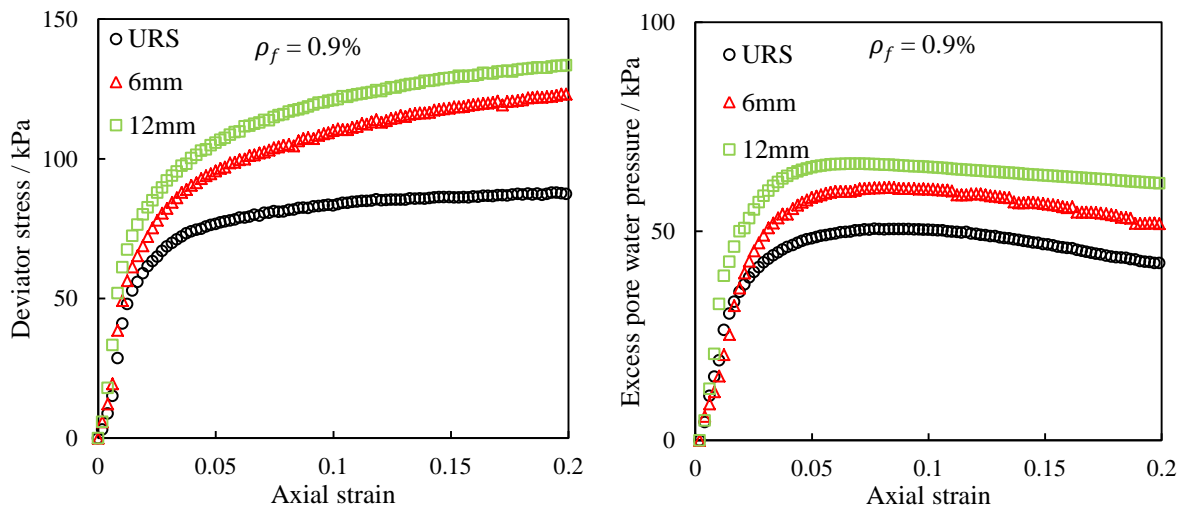


Figure 6.9. Deviator stress and excess pore water pressure versus axial strain at 50 kPa cell pressure for fibre reinforced soil (a) $\rho_f = 0.3\%$ (b) $\rho_f = 0.6\%$ (c) $\rho_f = 0.9\%$.



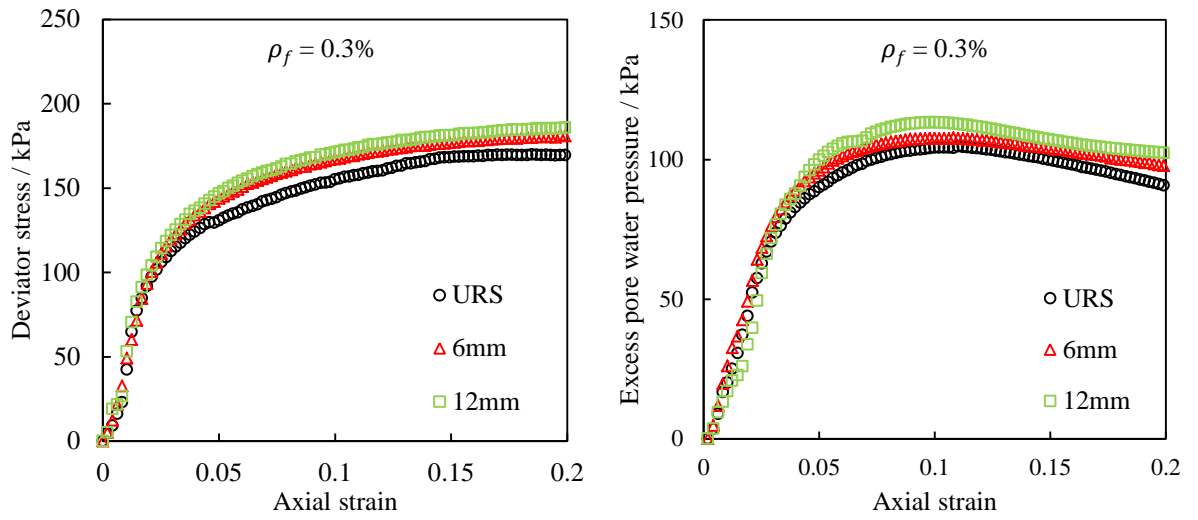


(b)

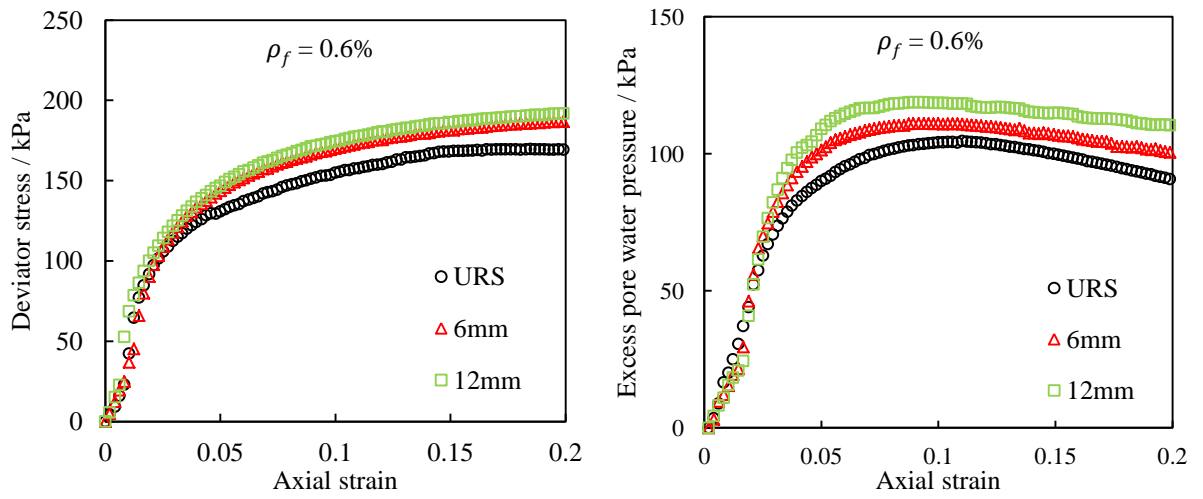


(c)

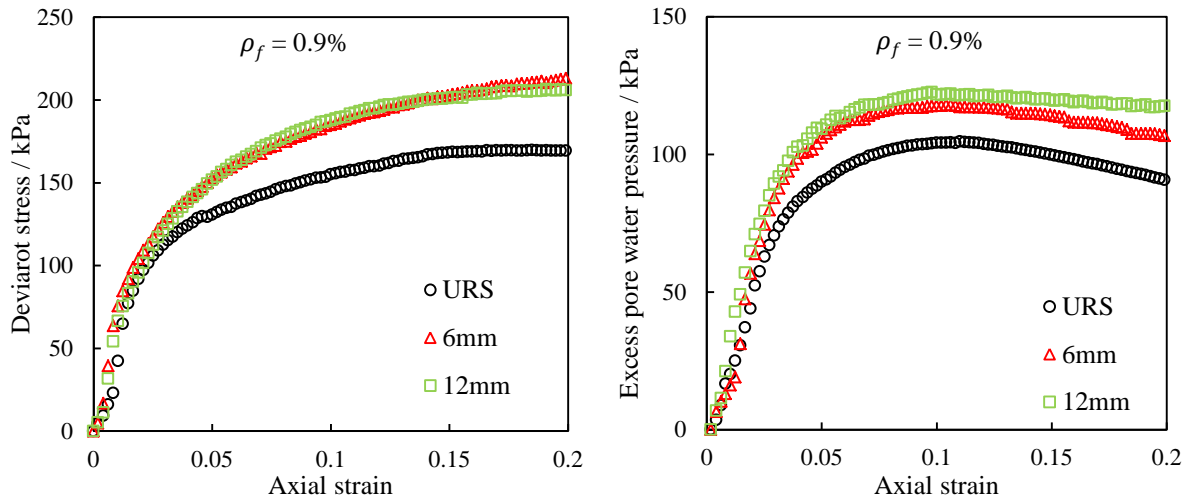
Figure 6.10. Deviator stress and excess pore water pressure versus axial strain at 100 kPa cell pressure for different fibre reinforced soil (a) $\rho_f = 0.3\%$ (b) $\rho_f = 0.6\%$ (c) $\rho_f = 0.9\%$.



(a)



(b)



(c)

Figure 6.11. Deviator stress and excess pore water pressure versus axial strain at 200 kPa cell pressure for different fibre reinforced soil (a) $\rho_f = 0.3\%$ (b) $\rho_f = 0.6\%$ (c) $\rho_f = 0.9\%$.

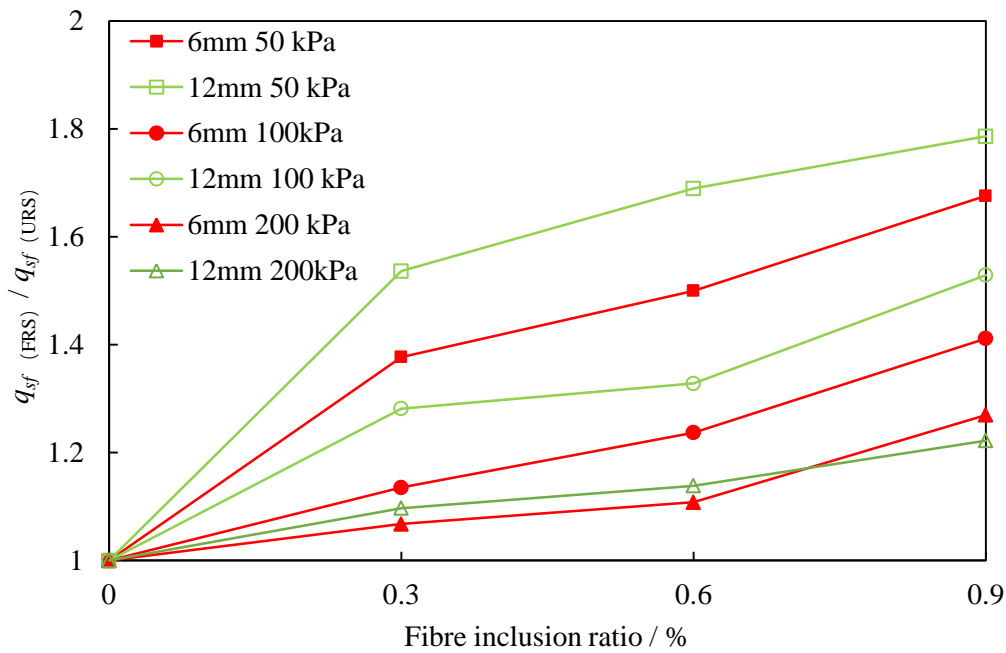


Figure 6.12. Normalised failure deviator stress (at 20% strain) of soil reinforced with 6 mm and 12 mm length fibres.

6.2.3 Effect of cell pressure

A comparison of deviator stress-axial strain and excess pore water pressure-axial strain relationships of URS and FRS at different cell pressures (50, 100 and 200 kPa) is shown in Figures 6.13- 6.15. It can be seen from Figure 6.13 that for the unreinforced specimens, the deviator stress increases as the axial strain develops and then generally stays constant after reaching a peak value. The axial strain corresponding to the peak deviator stress increases with increasing cell pressure. As for the fibre reinforced soil (Figure 6.14 and Figure 6.15), at all cell pressures tested, the deviator stress of the soil increases rapidly as the axial strain develops and then increases more slowly after reaching an “inflection point”, and does not reach a peak value in the 0- 20% strain range. It can be observed that the axial strain corresponding to the inflection point increases with increasing cell pressure. Figures 6.13-6.15 also shows that the excess pore water pressure of unreinforced and reinforced soil increases as the cell pressure increases. This is similar to the trends found in deviator stress. Strain corresponding to the peak excess pore water pressure increases as the cell pressure is increased. This trend attributes to a higher cell pressure holds the specimens tighter and restricts the lateral strain of the soil particles and fibres. More axial strain of the specimen is needed at high cell pressures to generate the lateral strain of soil particles and mobilise the tensile resistance of fibres. In order to compare the reinforcing effect of fibres at different cell pressures more clearly, the deviator stresses of specimens have been normalised by effective consolidation pressure (q/p'_0) and the results are shown in Figure 6.16. It can be seen that the normalised deviator stresses of unreinforced soil specimens converge to a unique path as the axial strain increases. In contrast, for fibre reinforced specimens, the normalised deviator stresses decrease as the cell pressure increases. It can be concluded that the benefit of fibre reinforcement is more significant at low confining pressures. A similar trend was observed by Özkul and Baykal (2007) and Patel and Singh (2019). This is due to the reason that at higher

confining pressure, the soil is already stiff and the effectiveness of fibre contribution is reduced (Maher and Ho, 1993). This trend will also be considered in the proposed model in Chapter 7.

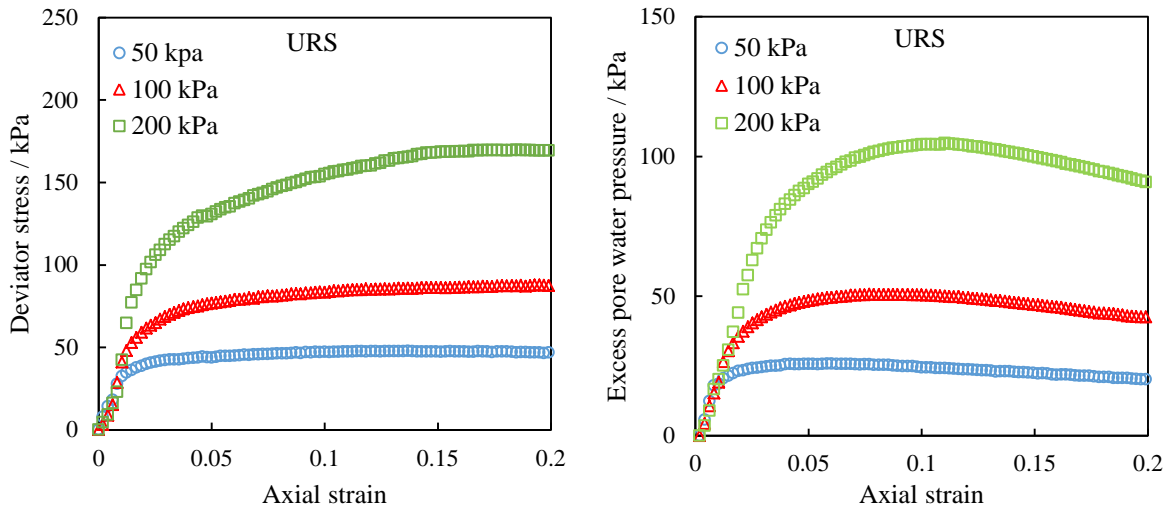
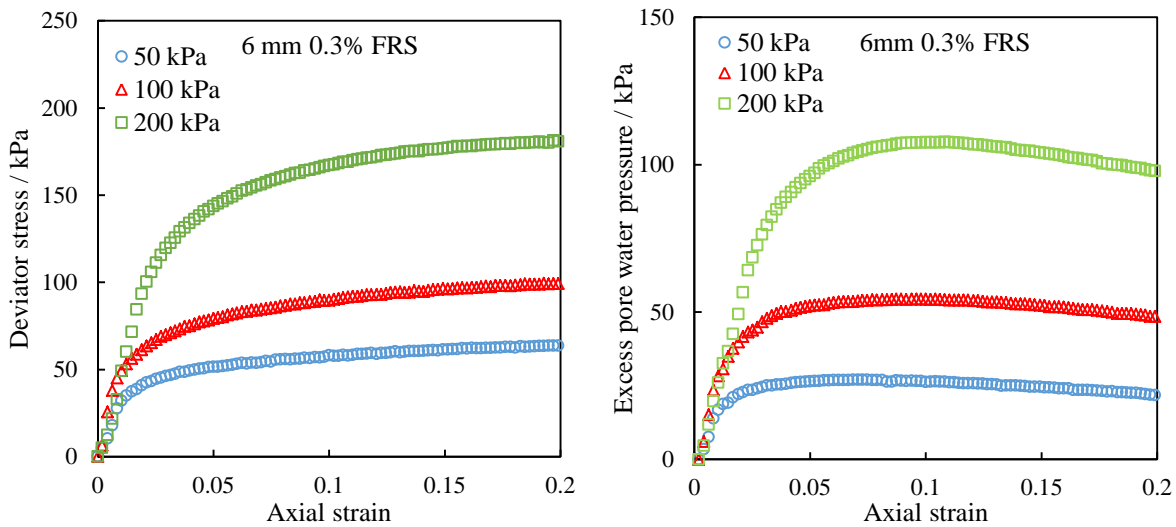
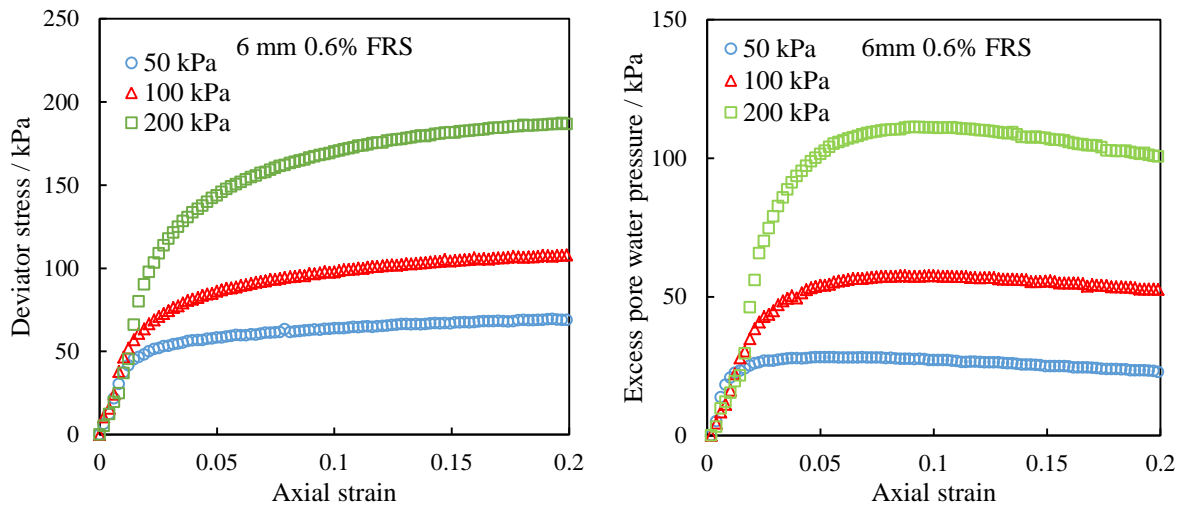


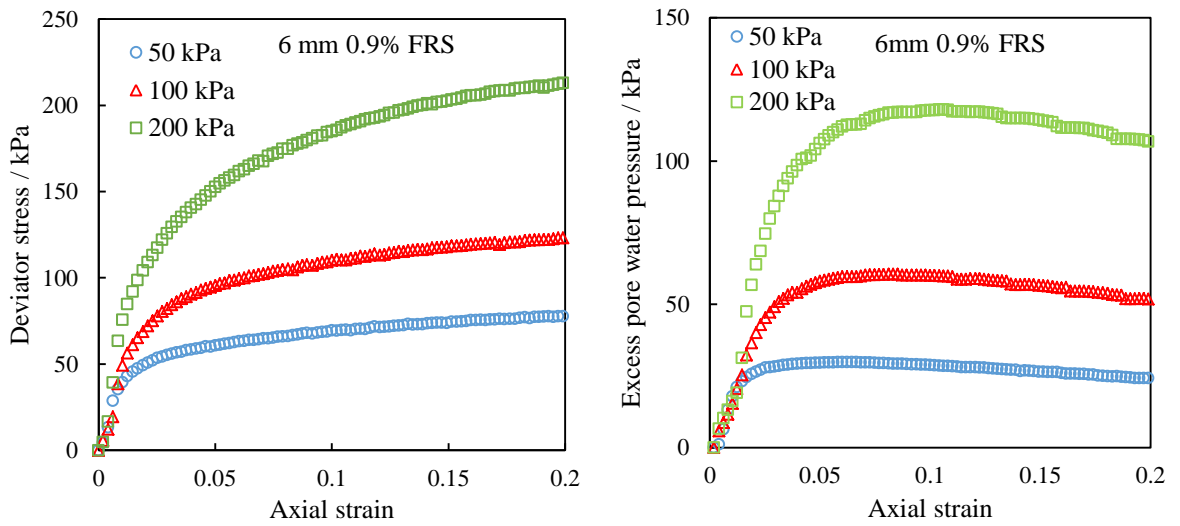
Figure 6.13. Deviator stress and pore water pressure versus axial strain at different cell pressures for unreinforced soil.



(a)



(b)



(c)

Figure 6.14. Deviator stress and pore water pressure versus axial strain at different cell pressures for 6 mm fibre reinforced soil (a) $\rho_f = 0.3\%$ (b) $\rho_f = 0.6\%$ (c) $\rho_f = 0.9\%$.

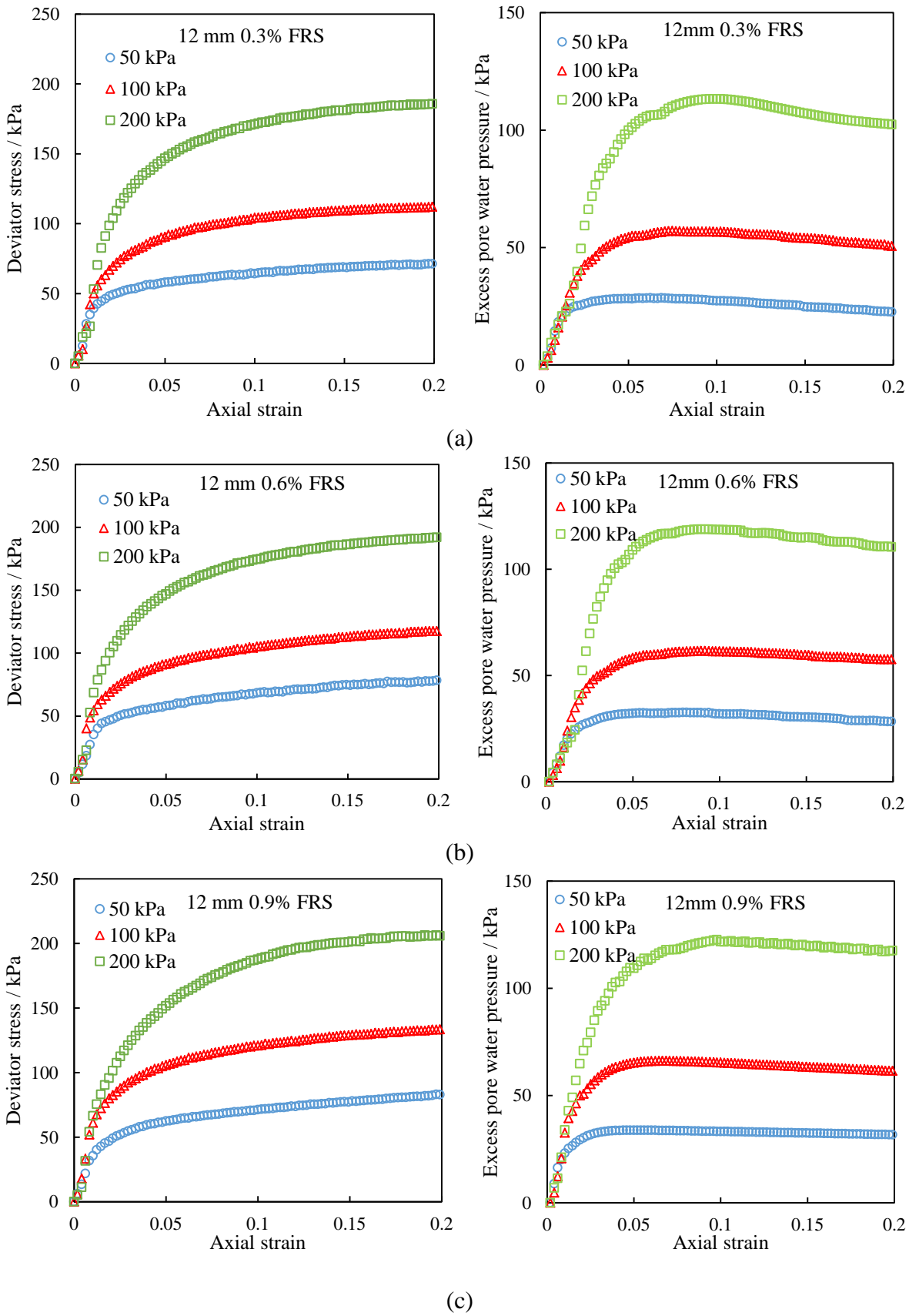
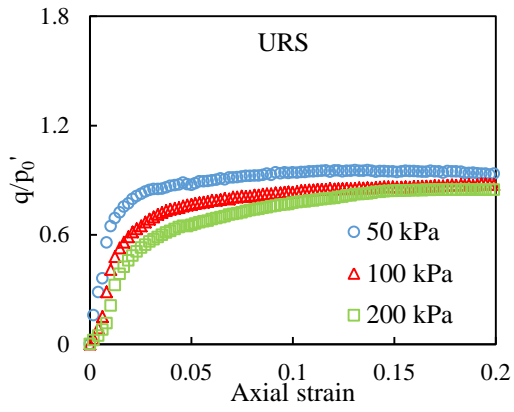
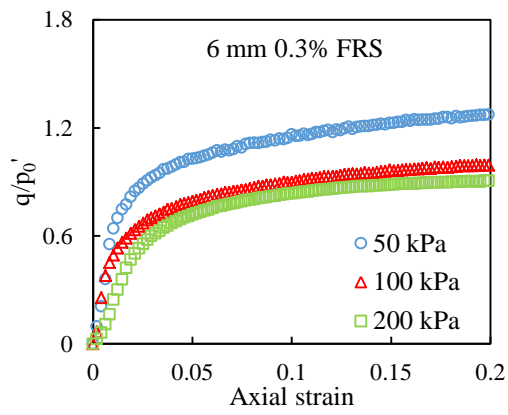


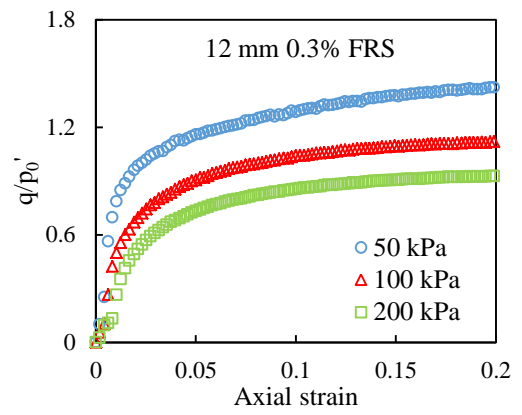
Figure 6.15. Deviator stress and pore water pressure versus axial strain at different cell pressures for 12 mm fibre reinforced soil (a) $\rho_f = 0.3\%$ (b) $\rho_f = 0.6\%$ (c) $\rho_f = 0.9\%$.



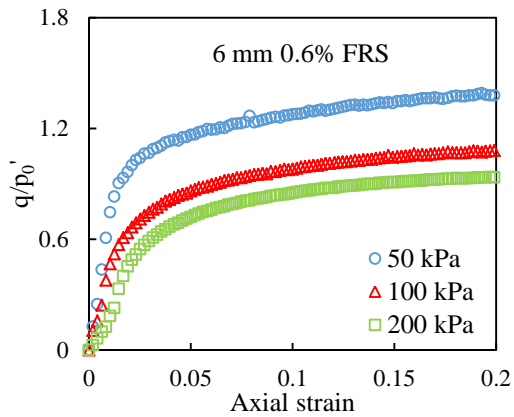
(a)



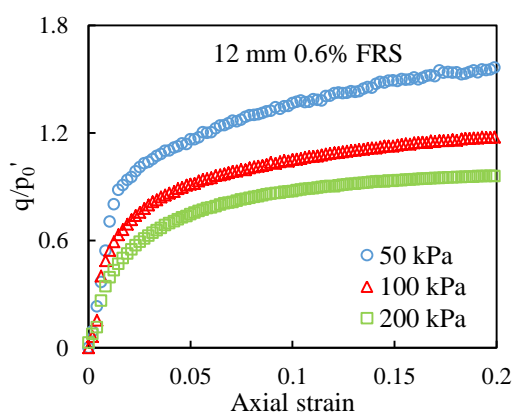
(b)



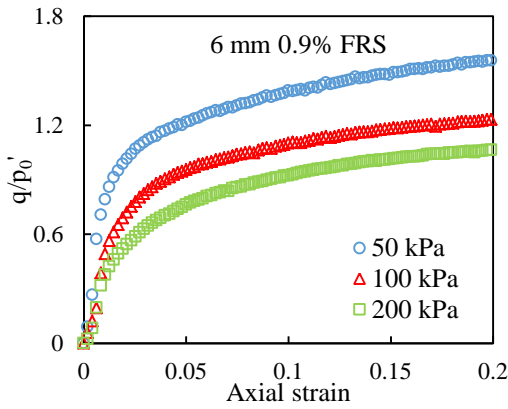
(c)



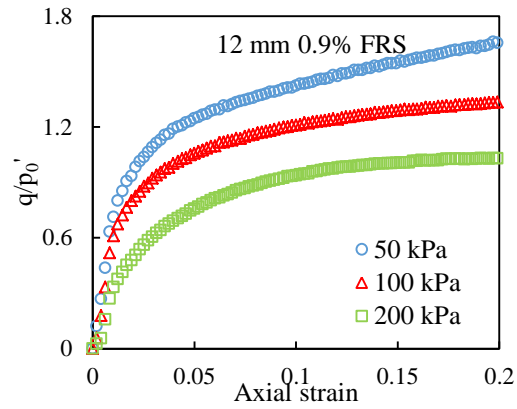
(d)



(e)



(f)



(g)

Figure 6.16. Normalised stress-strain curves of (a) unreinforced soil (b) $l_f=6$ mm, $\rho_f=0.3\%$ (c) $l_f=6$ mm, $\rho_f=0.6\%$ (d) $l_f=6$ mm, $\rho_f=0.9\%$ (e) $l_f=12$ mm, $\rho_f=0.3\%$ (f) $l_f=12$ mm, $\rho_f=0.6\%$ (g) $l_f=12$ mm, $\rho_f=0.9\%$.

6.3 The effect of fibre reinforcement on stress paths of soil

Stress paths reflect the variation of the stress state of an element in the soil during the triaxial loading period. An overview of the total and effective stress state of unreinforced and fibre reinforced soil during the test can be obtained by plotting the stress paths. To be consistent with the previous sections, the stress path behaviour of the soil is discussed in the context of changes in the cell pressure, fibre length and fibre inclusion ratio below.

6.3.1 Effect of cell pressure

The stress paths of unreinforced and fibre reinforced soil at different cell pressures are shown in Figures 6.17- 6.19. Notably, according to Figures 6.14 and 6.15, the excess pore water pressure of fibre reinforced soil are not at a steady value at the end of the test, which does not really meet the definition of critical state. Hence, the final state of the specimens presented here are “ultimate state”. However, for the purposes of this study the “critical state line” and “critical state parameter” in the following discussion are kept the original titles. The critical

state line in $p' - q$ plane is fitted based on the stress paths at different cell pressures and the critical state parameter M is also shown. According to the relationship between M and effective friction angle (ϕ') at ultimate state shown in Equation 6.2, the ϕ' of URS and FRS are also calculated and displayed.

$$M = \frac{6 \sin \phi'}{3 - \sin \phi'} \quad (6.2)$$

The stress paths for unreinforced and reinforced soil show a similar pattern: p' decreases and q increases at the first stage of shearing, so the stress paths plot to the top-left at first. Then the pore water pressure begins to drop and the deviator stress continues to increase (stays constant for URS), so the stress paths then plot to the top-right (right for URS). It can be seen from Figure 6.17 that the critical state line is well-fitted with stress paths of URS at different cell pressures and the critical state parameter M is 1. According to Figure 6.18 and Figure 6.19, for fibre reinforced specimens, the end of stress paths at 50 kPa cell pressure tend to lie above the fitted critical state line and stress paths at 200 kPa tend to lie below the critical state line. This also demonstrates that the reinforcing effect decreases as the cell pressure increases, which was mentioned in the previous section. A similar trend was reported in Consoli et al., (2007). It is worth mentioning that although a unique line is not a good fit result, for the purpose of model development a linear fit is considered and this will be explained in Chapter 7. The M values of reinforced specimens are higher than that of unreinforced soil, and the variation of M value with the change of fibre inclusion ratio and fibre length will be discussed in the following sections. Meanwhile, it can be seen that the effective friction angle ϕ' increases as the increase of fibre inclusion ratio and fibre length. The maximum value (36.9°) is achieved at 0.9% fibre inclusion ratio with 12 mm fibre length, which is much higher than that of unreinforced soil (25.4°). This is also a proof that fibre addition can significantly increase shear strength of London Clay.

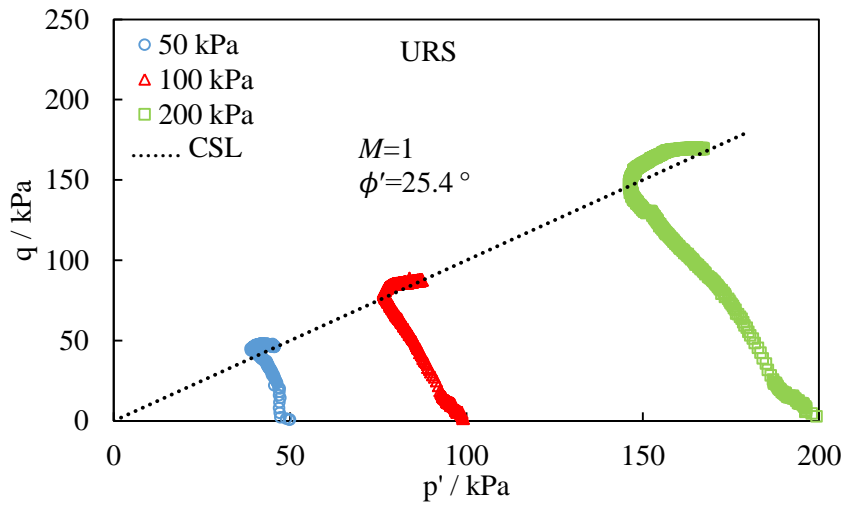
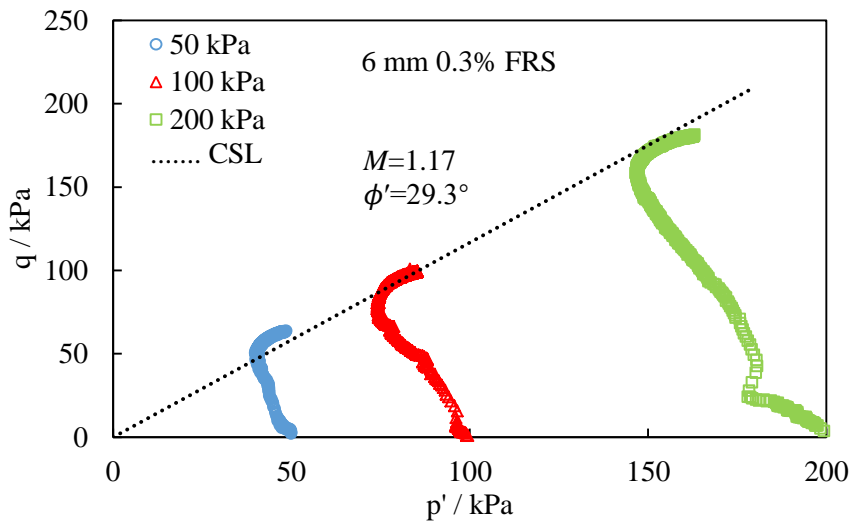
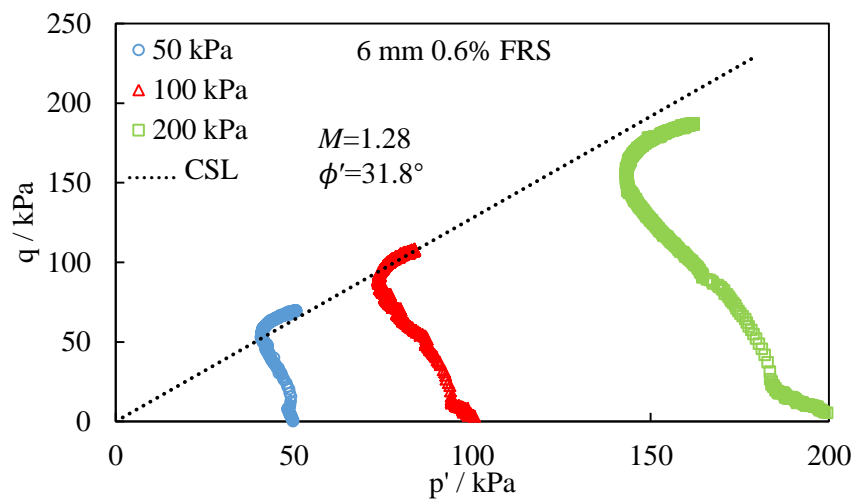


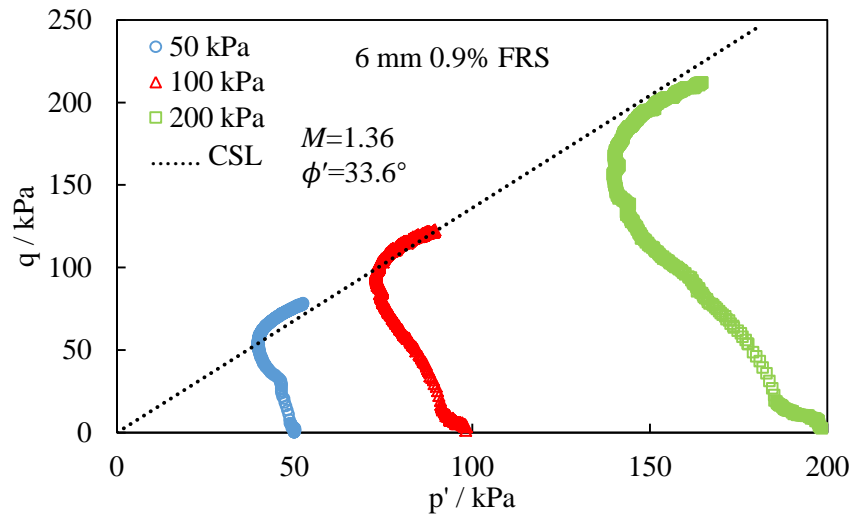
Figure 6.17. Stress paths of unreinforced soil at different cell pressures.



(a)



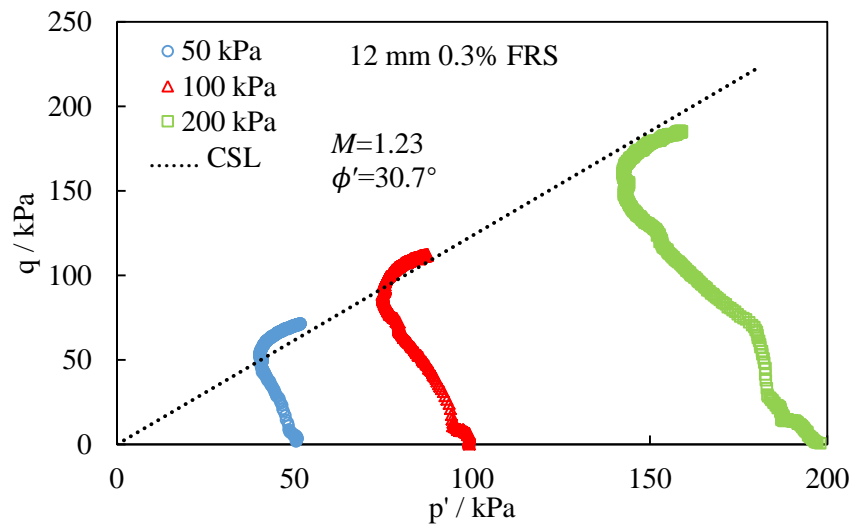
(b)



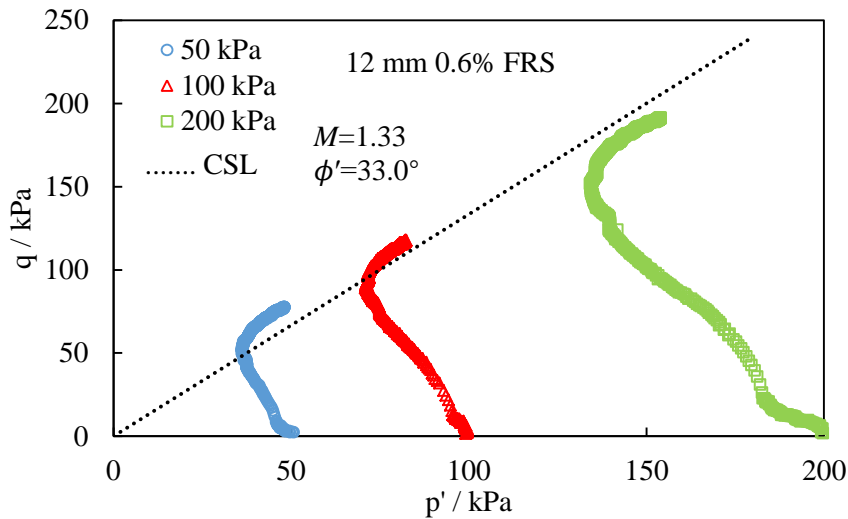
(c)

Figure 6.18. Stress paths of 6 mm fibre reinforced soil at different cell pressures

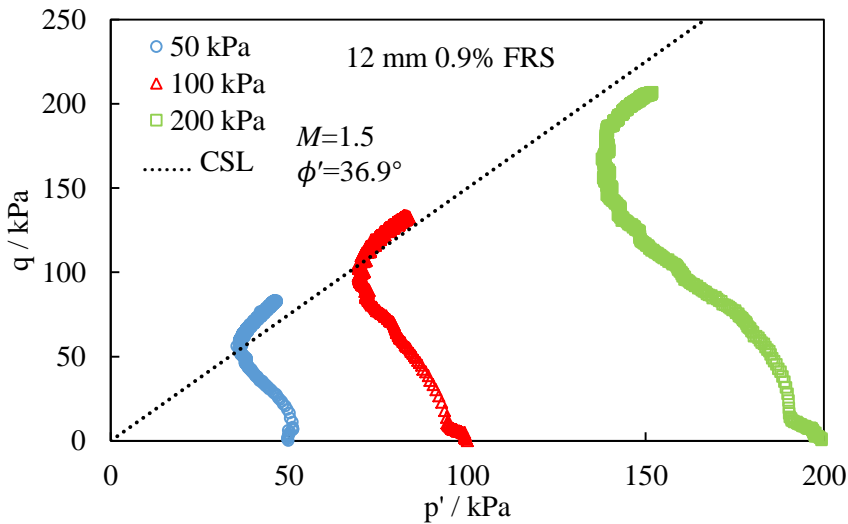
(a) $\rho_f = 0.3\%$ (b) $\rho_f = 0.6\%$ (c) $\rho_f = 0.9\%$.



(a)



(b)



(c)

Figure 6.19. Stress paths of 12 mm fibre reinforced soil at different cell pressures

(a) $\rho_f = 0.3\%$ (b) $\rho_f = 0.6\%$ (c) $\rho_f = 0.9\%$.

According to the void ratio of URS and FRS at different cell pressures (shown in Table 6.1), the isotropic NCL of URS and FRS are plotted in $e - \lg p'$ plane in Figure 6.20. During the shearing stage CU tests, the void ratio of specimen does not change and p' will gradually shift to the CLS. The ultimate state points ($\varepsilon_1 = 20\%$) at different cell pressures are also plotted. For

the distinguishable of the figure, here the data points of 12 mm, 0.9% reinforced soil (FRSF) and URS are selected. It can be seen from Figure 6.20 that the isotropic NCL of FRSF is below the NCL of URS, and the void ratio of two soil types at higher pressure level are closer. This trend is consistent with the conclusions obtained from one-dimensional consolidation tests (Chapter 4). In addition, it can be seen that for both URS and FRSF, the line of ultimate state is not parallel to their own NCL. According to the critical state soil mechanics, the CSL is parallel to the NCL in $e - \lg p'$ plane (Figure 2.4). Hence, this trend proves that the tested specimens do not reach the real critical state, as mentioned previously.

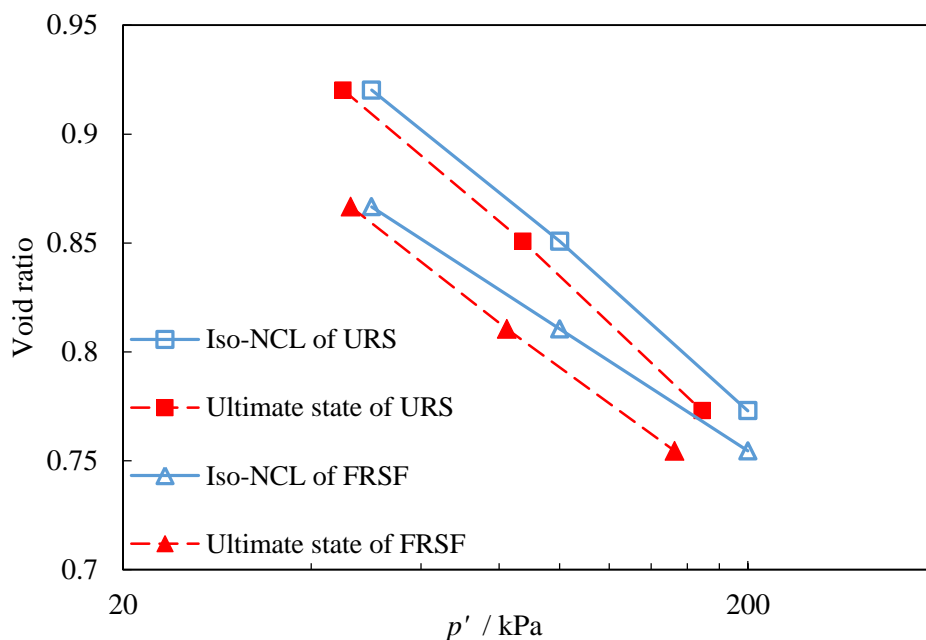
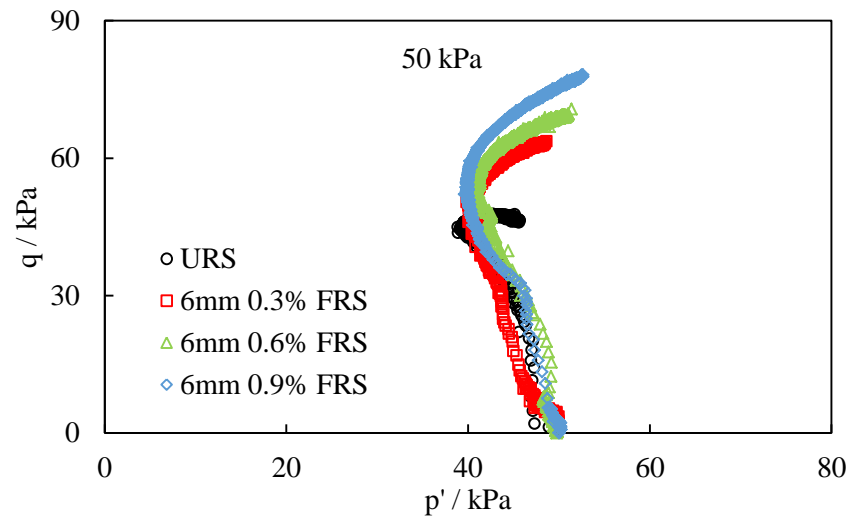


Figure 6.20. Isotropic NCL and ultimate state points for URS and FRSF.

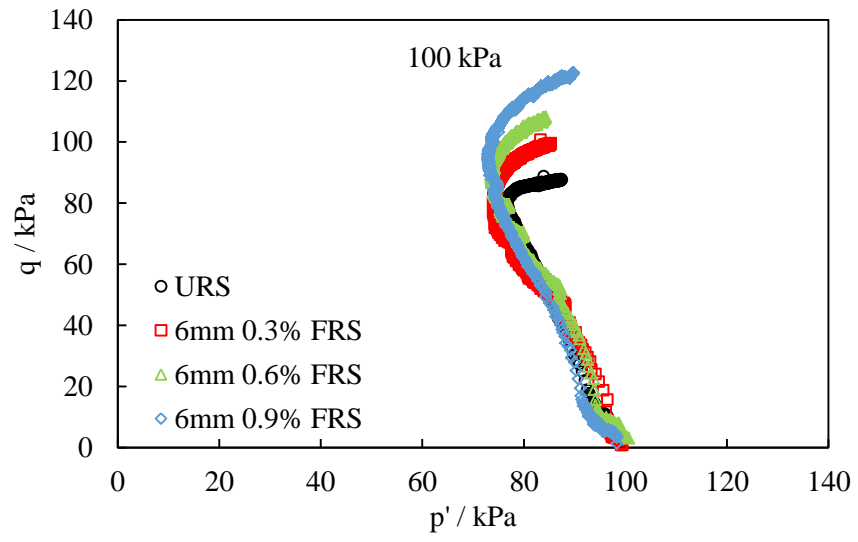
6.3.2 Effect of fibre inclusion ratio

Figures 6.21 and 6.22 display the stress paths of different fibre inclusion ratios at given fibre lengths and cell pressures. It can be seen that at all cell pressures and fibre lengths, the stress paths of reinforced soil are located above the one of unreinforced soil. The slope of the stress path (defined as the slope of the line between coordinate origin and end point of the stress path) increases with increasing fibre inclusion ratio, this also reflects the increase in ρ_f leads

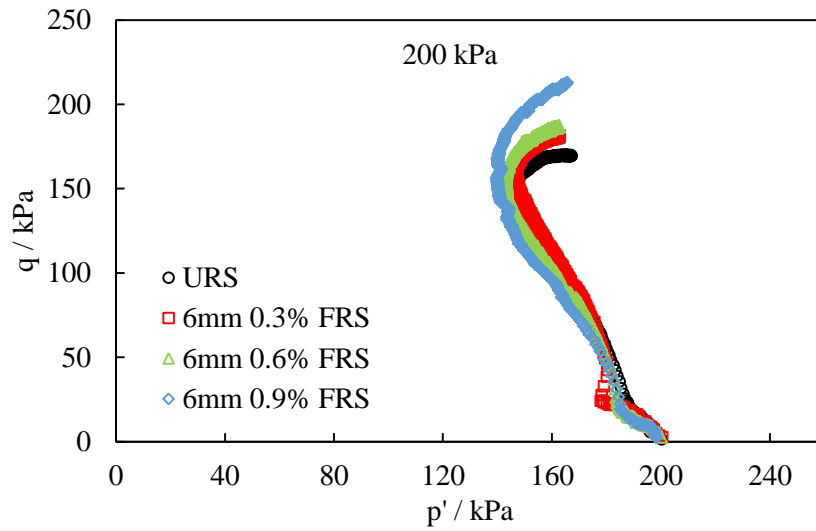
to an increase in deviator stress. Also, most of the stress paths of reinforced soil are located at the left of that of unreinforced soil, this is because more excess pore water pressure is generated in the reinforced specimens. When considered alongside Figures 6.5 and 6.6, one can observe that the stress paths of soil reinforced with different fibre inclusion ratios have a similar pattern at the beginning part of the tests (within 2%- 3% axial strain). A similar phenomenon was observed by Mirzababaei (2012). As the axial strain increases, specimens reinforced with lower fibre inclusion ratios tend to plot to the top-right because the excess pore water pressure of these specimens begins to drop. Specimens reinforced with higher fibre inclusion ratios tend to keep plot to the top-left until the excess pore water pressure begins to drop. After turning to the top-right, the slope of the reinforced soil is higher than that of unreinforced soil, this is because the deviator stress of the reinforced specimens continues increasing as the axial strain develops, while the deviator stress of the unreinforced specimens keep steady. Figure 6.23 shows the variation of M value with the change in ρ_f . It can be observed that for both fibre lengths, the M value increases with increasing fibre inclusion ratio. When the ρ_f increases from 0.3% to 0.9%, the M value is 1.17, 1.28 and 1.36 respectively for the 6 mm length fibre reinforced soil; and 1.23, 1.33 and 1.50 respectively when the fibre length is 12 mm. The maximum value of M for both two fibre lengths are obtained at 0.9% fibre inclusion ratio, the value is 1.36 and 1.50 times the value for the unreinforced soil respectively. So it can be concluded that increases in fibre inclusion can significantly increase the critical state parameter M of the soil.



(a)



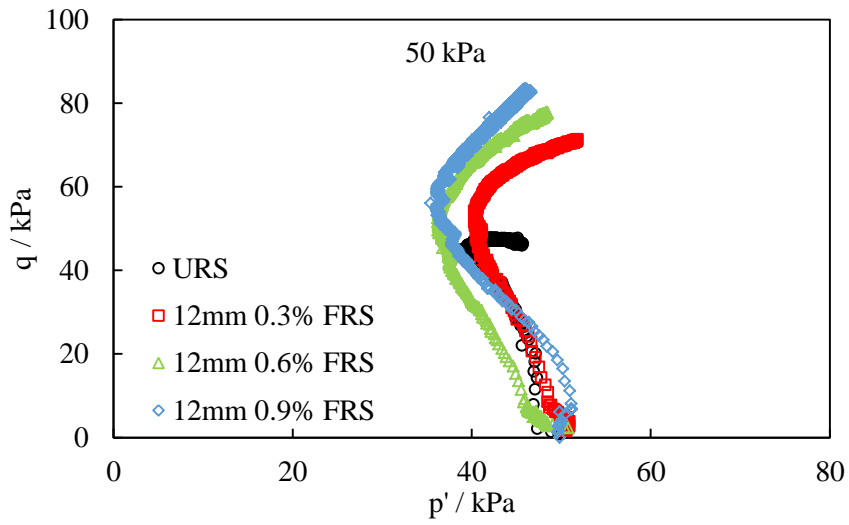
(b)



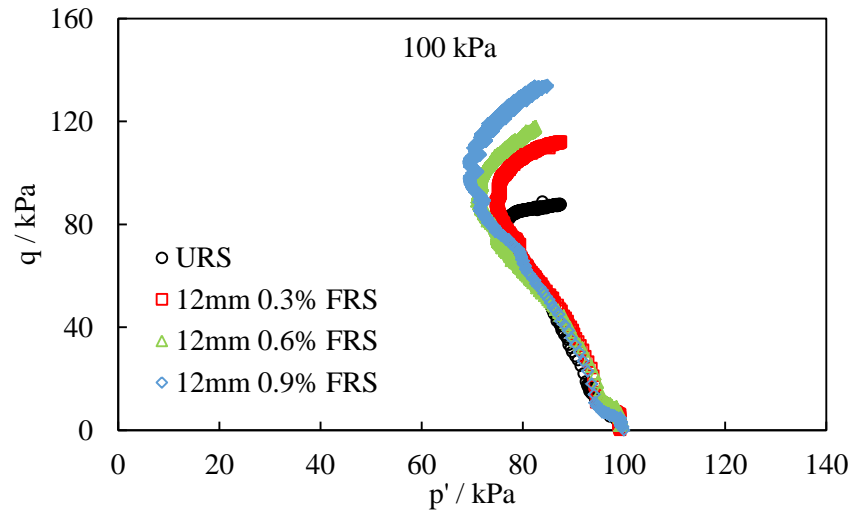
(c)

Figure 6.21. Stress paths of 6 mm fibre reinforced soil at different cell pressures

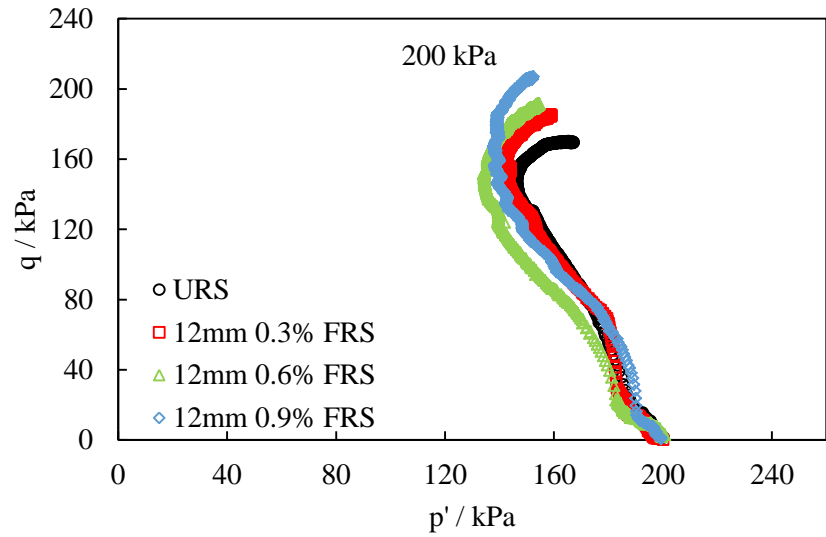
(a) 50 kPa (b) 100 kPa (c) 200 kPa.



(a)



(b)



(c)

Figure 6.22. Stress paths of 12 mm fibre reinforced soil at different cell pressures

(a) 50 kPa (b) 100 kPa (c) 200 kPa.

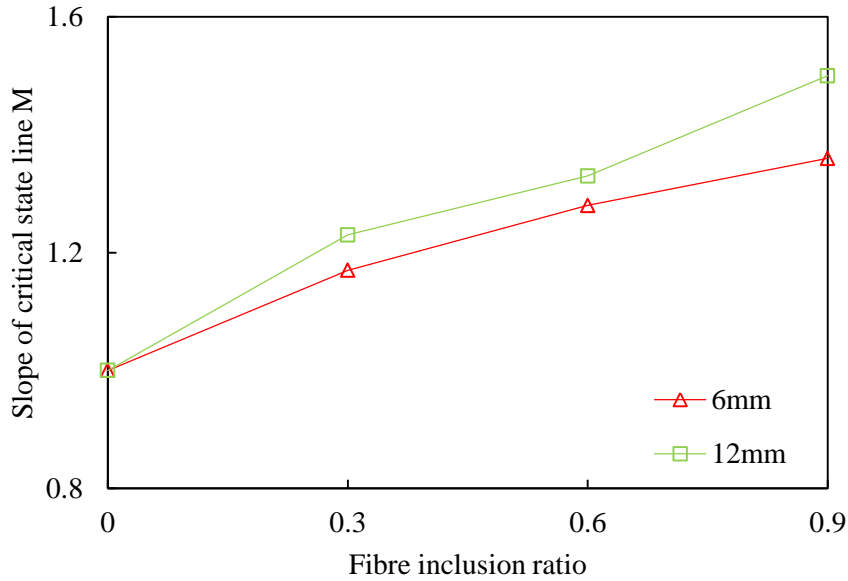
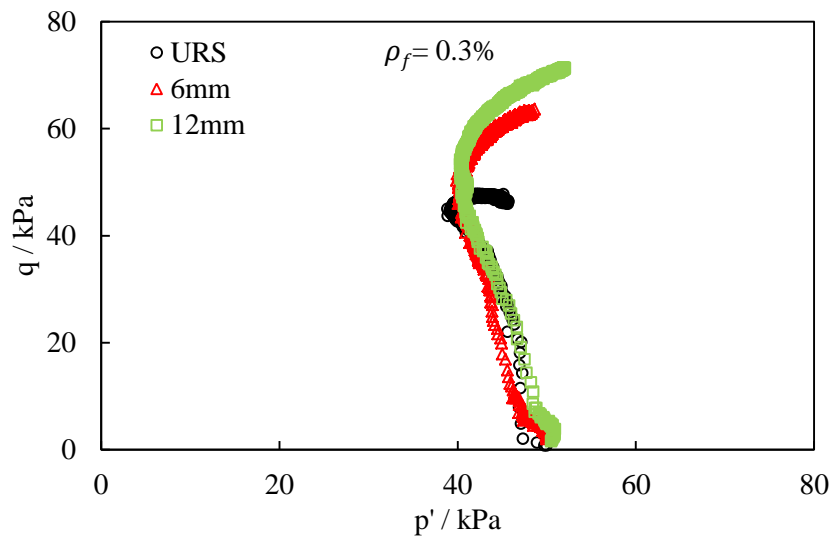


Figure 6.23. Variation of the M value with fibre inclusion ratio.

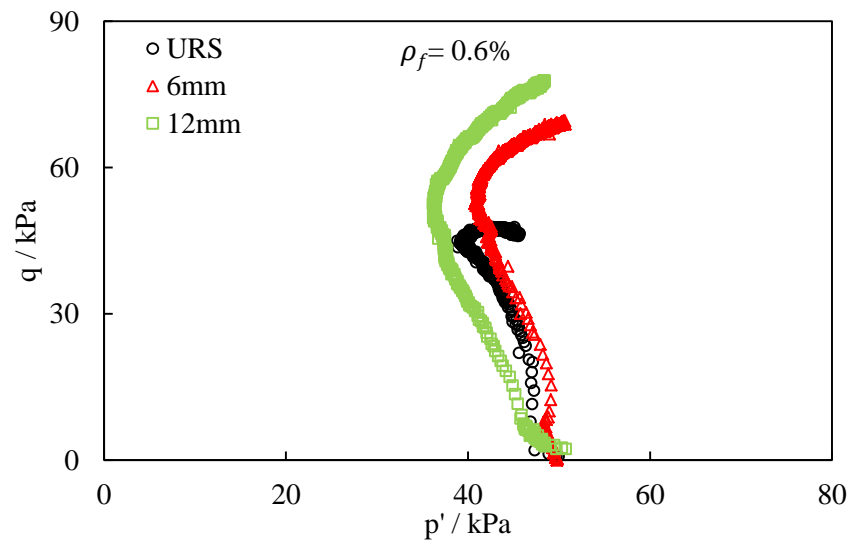
6.3.3 Effect of fibre length

The effects of fibre length on the stress paths of soil for different fibre inclusion ratios and cell pressures are shown in Figures 6.24- 6.26. It can be seen that for a given fibre inclusion ratio and cell pressure, the stress paths of soil reinforced with 12 mm fibres are located above those of soil reinforced with 6 mm fibres. However, when the fibre inclusion ratio is 0.9% and the cell pressure is 200 kPa, an opposite trend can be found because the deviator stress of 6 mm fibre reinforced soil is greater than 12 mm fibre reinforced soil, as discussed in Section 6.2.2. For a given cell pressure, the stress paths of 12 mm length fibre reinforced soil tend to be located to the left of that of 6 mm length fibre reinforced soil, and have a higher slope than that of 6 mm length fibre reinforced soil. As mentioned in Section 6.2.2, longer fibres have a greater benefit in deviator stress contribution. Also, the difference in excess pore water pressure generated between the two fibre lengths gets greater as the fibre inclusion ratio increases. Hence such a trend can be observed in the stress paths. Figure 6.27 shows the comparison of M value between fibre reinforced soil with 6 mm and 12 mm length fibres. It

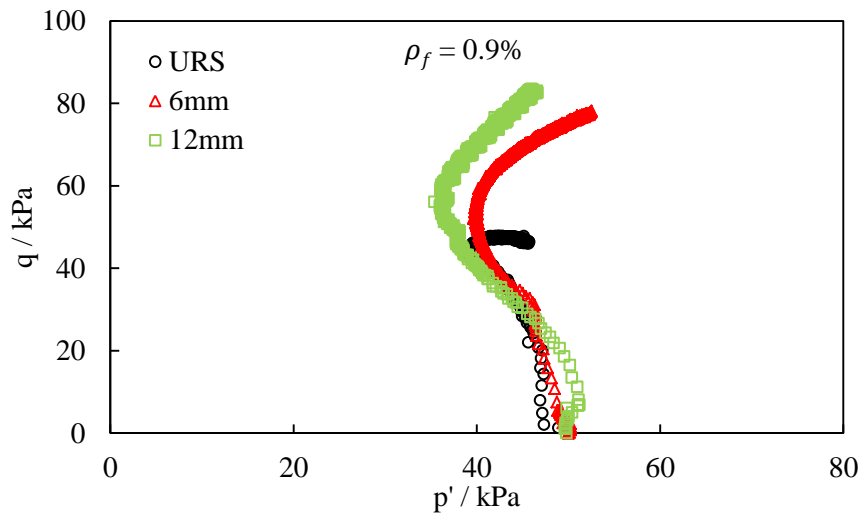
can be seen that for all three fibre inclusion ratios, soil reinforced with 12 mm fibres exhibits a greater M than that with 6 mm fibres.



(a)



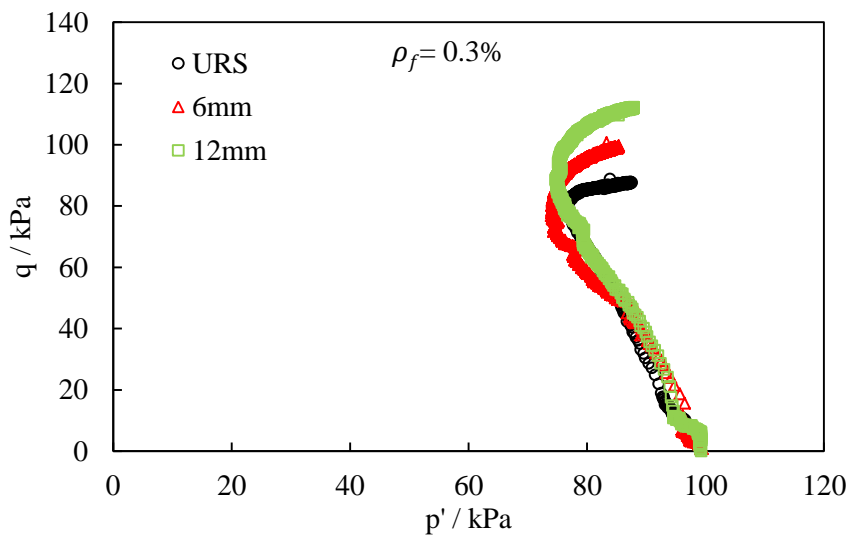
(b)



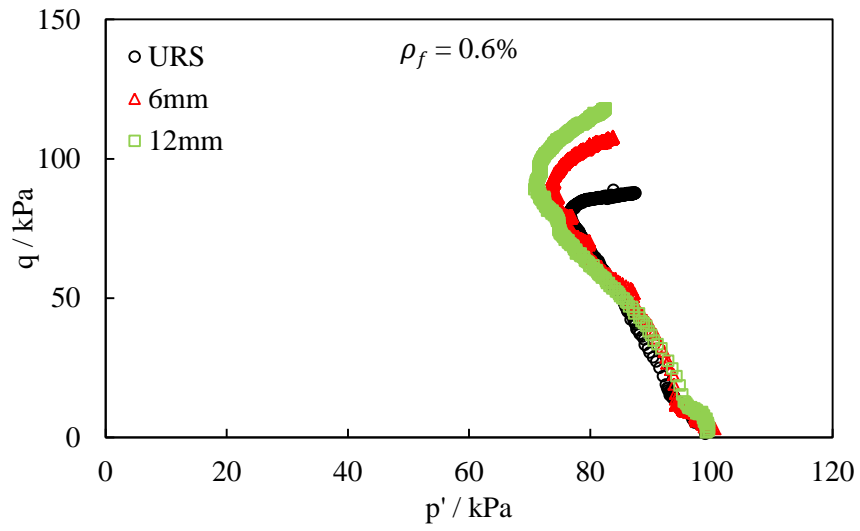
(c)

Figure 6.24. Stress paths of different fibre reinforced soil at 50 kPa cell pressure

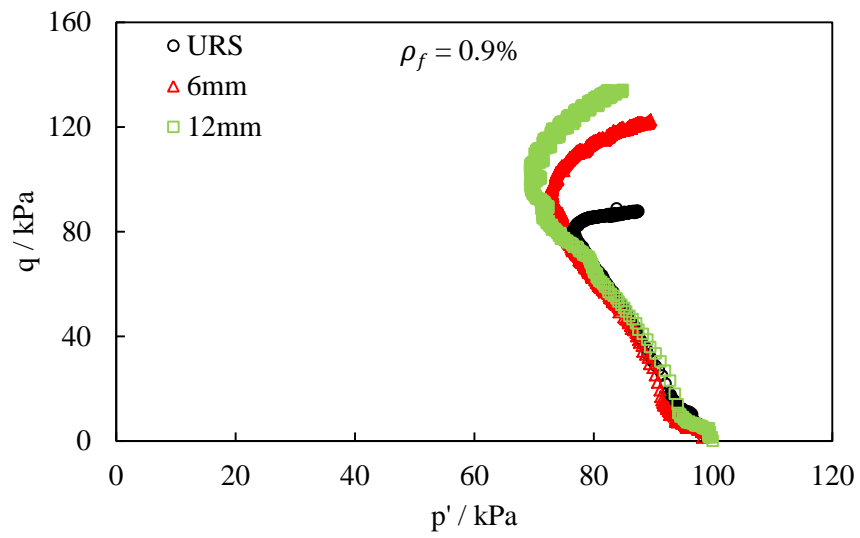
(a) $\rho_f = 0.3\%$ (b) $\rho_f = 0.6\%$ (c) $\rho_f = 0.9\%$.



(a)



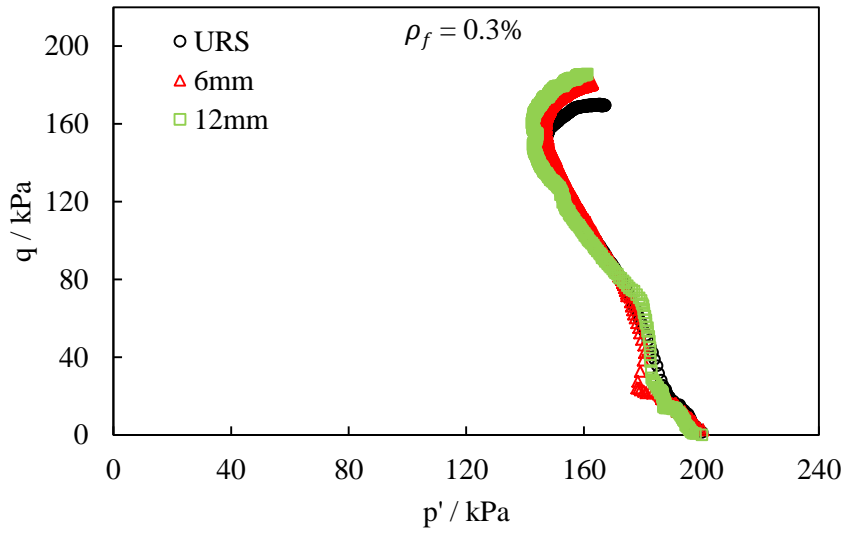
(b)



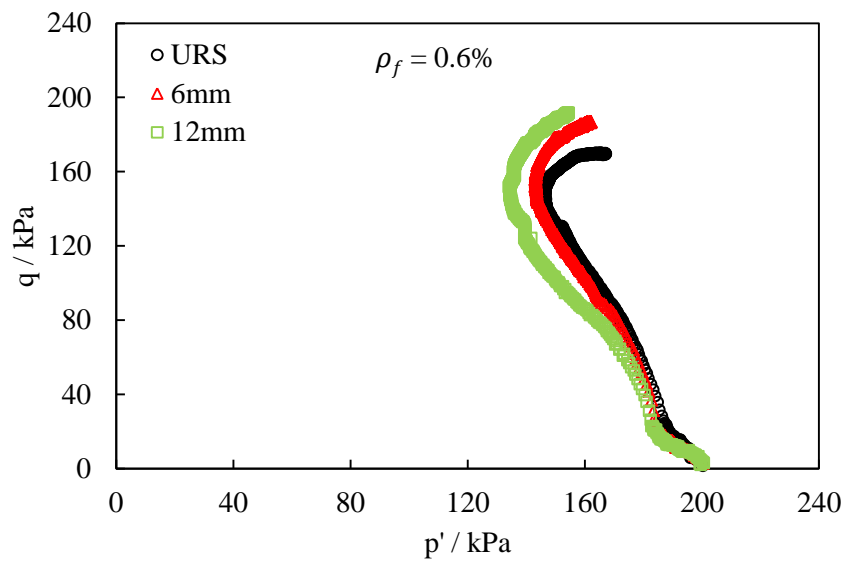
(c)

Figure 6.25. Stress paths of different fibre reinforced soil at 100 kPa cell pressure

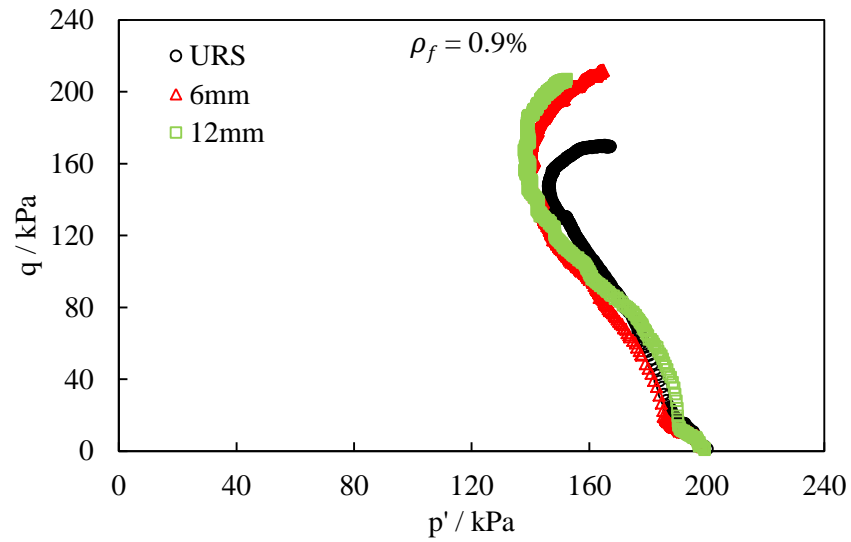
(a) $\rho_f = 0.3\%$ (b) $\rho_f = 0.6\%$ (c) $\rho_f = 0.9\%$.



(a)



(b)



(c)

Figure 6.26. Stress paths of different fibre reinforced soil at 200 kPa cell pressure

(a) $\rho_f = 0.3\%$ (b) $\rho_f = 0.6\%$ (c) $\rho_f = 0.9\%$.

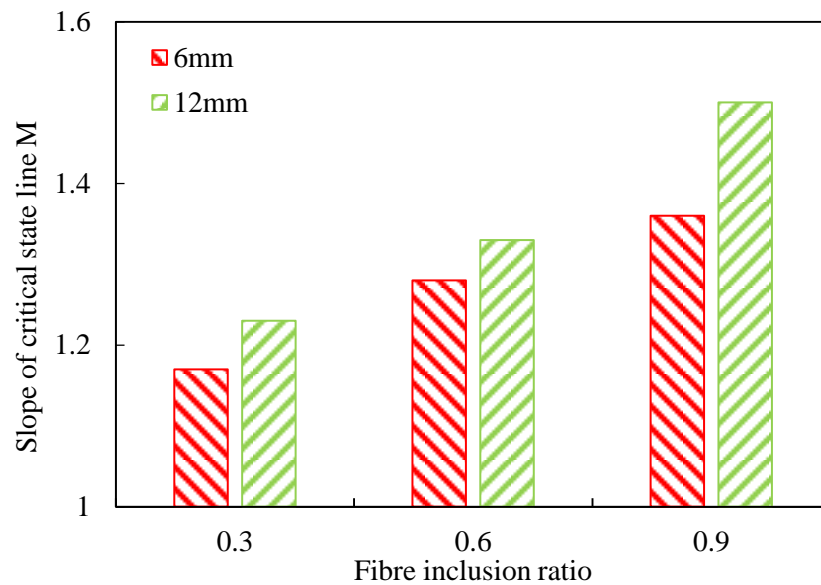


Figure 6.27. Comparison of M value between fibre reinforced soil with 6 mm and 12 mm.










6.4. The effect of fibre reinforcement on failure patterns of soil

After shearing, the specimens were photographed as mentioned in 3.4.7, and the failure patterns of these specimens are discussed here based on the pictures of failed samples shown

in Table 6.2. The specimens did not undergo any volume change in the undrained tests, but the shape and cross-sectional area of the specimens were changed to different degrees. In order to facilitate observation of the change of the specimens, the original shape is marked with a frame in red. It can be seen that unreinforced soil exhibits different failure patterns under different pressure levels. When tests were conducted at 50 kPa cell pressure, the unreinforced specimen shows a relatively clear shear band; when the specimen was tested at 100 kPa cell pressure, the shear band can hardly be observed; when the cell pressure increases to 200 kPa, no shear band can be seen on the specimen and sample exhibits a bulging failure mode. As for fibre reinforced soil, it can be seen that specimens at all three cell pressures generally show bulging failure and no shear band can be observed. This trend corresponds to the strain-hardening behaviour shown in Figures 6.5 and 6.6 (Chapter 6). An exception can be found at 12 mm length fibre reinforced soil at 0.9% fibre inclusion ratio. When the soil was tested at 200 kPa cell pressure (No.21 in Table 6.2) a shear band can be seen in the upper part of the specimen, and the curve corresponding to this specimen in Figure 6.6 shows the deviator stress keeps steady at the end of the test. In addition, the bulging in unreinforced specimen was along its entire length from the ends. (No.3 in Table 6.1). Compared with unreinforced specimen, the bulging behaviour of fibre reinforced soil specimens under 200 kPa cell pressure (No.6, 9, 15, 18 and 21) was not obvious in the ends of the specimens and the bulging behaviour reduces slightly with the addition of fibres. This is because soil particles are interlocked by the fibres and this interweaving of the fibres restricts the bulging of the sample. A similar trend can be found with respect to cell pressure, for a given fibre reinforcement condition, bulging behaviour of the specimens reduces slightly with increasing cell pressure. This trend is more obvious in 6 mm length fibre reinforced soil specimens. Apart from the restriction that comes from the higher cell pressure itself, fibres have a greater bonding effect and higher friction with the soil particles at a higher cell pressure. When it

comes to fibre length, it can be seen that the bulging behaviour in specimens reinforced with shorter fibres is more uniform, single-side-bulging can be observed in some specimens reinforced with 12 mm length fibres. This is due to the fact that shorter fibres are more evenly distributed than longer fibres.

Table 6.2. Sample failure patterns (at 20% axial strain level) in triaxial tests.

Cell pressure	50 kPa	100 kPa	200 kPa
Soil condition			
Unreinforced soil	 1	 2	 3
$\rho_f = 0.3\%$ $l_f = 6 \text{ mm}$	 4	 5	 6
$\rho_f = 0.6\%$ $l_f = 6 \text{ mm}$	 7	 8	 9

$\rho_f = 0.9\%$

$l_f = 6 \text{ mm}$



10



11



12

$\rho_f = 0.3\%$

$l_f = 12 \text{ mm}$



13



14



15

$\rho_f = 0.6\%$

$l_f = 12 \text{ mm}$



16



17



18

$\rho_f = 0.9\%$

$l_f = 12 \text{ mm}$



19



20



21

6.5 Chapter summary

Shear strength of soil is one of the primary parameters in embankment engineering design. The problems associated with constructing highway embankments over soil with insufficient shear strength (i.e. overall stability and uneven settlements) leads to the use of ground improvement techniques. The literature review has already shown that randomly distributed fibres can improve the shear strength of sandy soil. However, fewer investigations can be found on studying shear strength behaviour on fibre reinforced high plasticity clay. In this chapter, shear strength of polypropylene fibre reinforced London Clay has been discussed based on a series of consolidated undrained triaxial tests. The following conclusions can be drawn from the results and discussion presented in this chapter.

- (1) Fibre addition can change the stress-strain behaviour of the soil. As the axial strain increases, deviator stress of unreinforced soil tends to increase and then stabilise. For fibre reinforced soil, deviator stress increases throughout the test and does not show a peak value before the test is concluded (axial strain= 20%).
- (2) Fibre reinforcement can significantly increase shear strength of London Clay. The ultimate deviator stress increases with increasing fibre inclusion ratio. However, as fibre inclusion ratio increases from 0.3% to 0.9%, the normalised deviator contribution of fibre reinforced soil indicates that the benefit on shear strength improvement per unit ρ_f decreases.
- (3) During the shearing, the excess pore water pressure of both unreinforced and fibre reinforced soil increases to a peak value, then drops gradually until the end of the test. As fibre inclusion ratio increases, an increment in peak value and a decrease in post peak reduction can be found in the excess pore water pressure. This trend indicates fibre can restrict the tendency of the soil's dilation.
- (4) Longer fibres produce a greater improvement in the shear strength of soil than shorter fibres, which is reflected in a higher deviator contribution for a given fibre inclusion ratio and

cell pressure. Also, for a given fibre inclusion ratio and cell pressure, higher excess pore water pressure were generated in 12 mm length fibre reinforced soil than that of 6 mm length fibre.

(5) As fibre inclusion ratio increases and fibre length increases, critical state parameter M increases. The fitted critical state line lies below the stress paths of 50 kPa cell pressure and above the stress paths of 200 kPa cell pressure, which indicates that the fibre reinforcing effect decreases as the cell pressure increases. The results of normalised ultimate deviator contribution proves this conclusion.

(6) Unreinforced soil specimens exhibit shear bands at low cell pressure, fibre reinforced soil specimens show a bulging failure pattern at both low and high cell pressures, the bulging of specimens is reduced by increasing cell pressure and fibre inclusion ratio. Bulging appeared in specimens reinforced with shorter fibres are more uniform than that of longer fibres.

Consolidated undrained tests performed on polypropylene fibre reinforced London Clay have shown that the addition of fibre can significantly improve the shear strength behaviour of the soil. When such a composite is used as fill material in highway embankments, a higher shear strength of soil can lead to a higher stability. However, more studies are needed to develop more detailed guidelines for using such a material in embankment engineering. For example, it is necessary to evaluate the influence of soil's initial density on the shear strength behaviour of the fibre reinforced soil. Also, mobilised shear resistance of fibres leads to a higher ultimate deviator stress of fibre reinforced soil, which suggests that randomly distributed fibres could be a potential reinforcement in large strain engineering problems (e.g. seismic engineering). A deeper understanding of this needs further comprehensive investigations.

Chapter 7

7. Towards a predictive model of the shear strength behaviour of fibre reinforced clay

The proposed models for fibre reinforced soil so far in the literature have generally focused on fibre reinforced granular materials, only a few studies can be found on models for fibre reinforced clayey soils. Also, some of these models are not convenient for the prediction of the shear strength of fibre reinforced soil, since they need extra experimentation to obtain material parameters (e.g. pull-out tests of the fibres). The shear strength of polypropylene fibre reinforced London Clay has been discussed in last chapter based on triaxial tests results. In this chapter, a speculative model is proposed based on the concept of equivalent confining stress (to be explained below) and, like other models in the existing literature, the proposed model is based on several assumptions, definitions and notations which are introduced here in Section 7.1. The process of developing the model is then given via several stages in Section 7.2 and the experimental results discussed in Chapter 6 are compared with the predicted results by the model in Section 7.3.

7.1. Basis of the model

7.1.1 Assumptions

For simplicity, the model proposed is based on the following key assumptions:

- Soil matrix and fibre reinforced soil material in the model are homogeneous and isotropic. Fibres are homogeneously distributed in the composite but have a non-uniform orientation distribution. The model is based on shear strength observed in a standard triaxial test therefore every point has an identical stress state.

- Fibres are modelled as one-dimensional mechanical elements. Fibres only participate in tension loading and not in compression loading and behave elastically with an elastic modulus E_f . The mobilised tensile stresses are assumed at the end of the fibres.
- Compatibility between fibres and the soil matrix is assumed, i.e. fibres share an identical strain with the adjacent soil matrix as well as the composite due to assumed strong bonding between the clay particles and fibres. Having said this, sliding between fibres and the soil matrix is considered at the end of the model development.
- The aim of the model application is to predict the stress-strain behaviour of FRS based on the experimental stress-strain behaviour of URS. The behaviour of the soil matrix is the one for the unreinforced soil which is taken from experimental results, while the effect of the fibre is added. Like the unreinforced clay soil, the stress-strain relationship of the fibre reinforced soil is assumed to follow the critical state framework.
- The radial component of the tensile stress mobilised by fibres is approximately assumed as same as the isotropic stress p , this will be introduced in 7.1.3.

7.1.2 Definitions

The definitions of some basic variables are shown as follows. The mass and volume relationships of fibres and the fibre-soil composite are summarised here as they are fundamental to the modelling procedure. In this study, the fibre inclusion ratio used in all the laboratory tests (Chapters 4 to 6) is the gravimetric fibre content, as already been defined in Chapter 2, i.e.

$$\rho_f = \frac{m_f}{m_s} = \frac{W_f}{W_s} \quad (7.1)$$

where m_f and m_s are the masses of the fibres and dry soil respectively, and W_f and W_s are the weights of the fibres and dry soil respectively. In order to facilitate overall mechanical

analysis of the composite, a volumetric fibre content is utilised in the model derivation as already defined in Chapter 2, i.e.

$$v_f = \frac{V_f}{V_t} \quad (7.2)$$

where V_f and V_t are the volumes of the fibres and composite respectively. The dry unit weight of the fibre-soil composite can be expressed as:

$$\gamma_{dFRS} = \frac{W_f + W_s}{V_t} \quad (7.3)$$

The specific gravity of the fibres can be expressed as:

$$G_f = \frac{W_f}{V_f \gamma_w} \quad (7.4)$$

where γ_w is the unit weight of water. The relationship between gravimetric fibre content ρ_f and volumetric fibre content v_f can be obtained by substituting Equations 7.1 to 7.3 into Equation 7.4, i.e.

$$v_f = \frac{\gamma_{dFRS} \rho_f}{(1 + \rho_f) G_f \gamma_w} \quad (7.5)$$

In addition, a single fibre is assumed to have the geometry of a cylinder with an average diameter d_f and an average length of l_f .

7.1.3 Equivalent confining stress in a CU triaxial test

As mentioned in Chapter 2, Yang (1972) hypothesised on the basis of his tests that tensile restraint in the reinforcement within a fibre reinforced soil induced an “equivalent confining stress”, $\Delta\sigma_3$. This increment of the confining stress due to the reinforcement can lead to an improvement of a soil’s shear strength (Δs), as introduced by Gray and Al-Refeai (1986):

$$\Delta s = \frac{\Delta \sigma_3}{2} \times \tan \left(45^\circ + \frac{\phi}{2} \right) \quad (7.5)$$

The function above is proposed based on the Mohr-Coulomb formulation for the strength of a sandy soil, however the authors did not give a clear, experimental available relationship between $\Delta \sigma_3$ and the properties of the fibre reinforcement.

Here the last point of assumptions is clarified. If we consider a CU triaxial compression test of a fibre reinforced soil, the compressive axial strains induce tensile radial strains in the specimen. The distributed fibres in the specimen are therefore subjected to tensile strain during shearing and fibre tensile stresses are mobilised. Assuming the fibres' preferred distribution is generally horizontal and that resistance can only be mobilised in tension, so the stress component acting on fibres in the axial direction is neglected as that would lead to compression. The activated tensile stresses in the fibres act in the radial direction of the specimen, i.e. components σ_{xx} and σ_{yy} (Figure 7.1), acting as a radial confining pressure. The specimen is compressed due to the fibre confining pressure just like a bottle compressed by hands, which leading to a vertical elongation. However, the specimen is restrained in the axial direction by the top-cap and the base, of which the stiffness are assumed infinite, and it will be compressed during triaxial test and not allowed to extend in axial direction. The sample will subject to a compressive stress in axial strain σ_{zz} . Assuming specimen follows the elastic behaviour with a Poisson's ratio $\nu = 0.5$, according to Equation 7.6:

$$\varepsilon_1 = \frac{1}{E} \left(\sigma_{zz} - \nu(\sigma_{xx} + \sigma_{yy}) \right) \quad (7.6)$$

when the specimen is restrained in vertical extending, one can obtain $\sigma_{zz} = \sigma_{xx} = \sigma_{yy}$, and the isotropic stress of fibre applying on the soil $p = (\sigma_{xx} + \sigma_{yy} + \sigma_{zz})/3$ is equal to the radial component of the fibre mobilised stress. Assuming the triaxial specimen to have the

same state of stress at all points, we can consider this effect as an equivalent confining pressure p_f due to activation of the fibres.

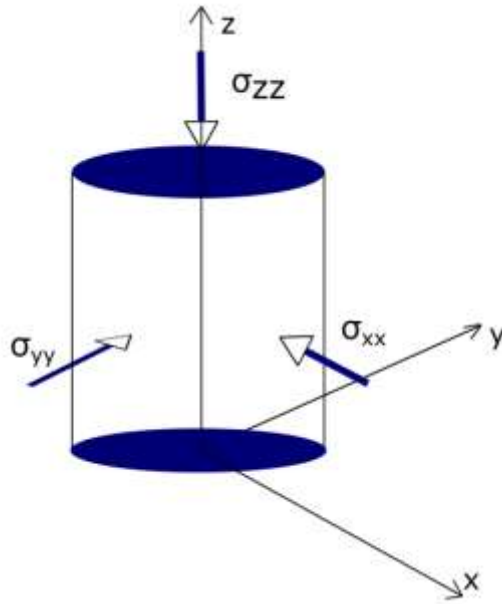


Figure 7.1. Schematic diagram of equivalent confining pressure in a triaxial specimen.

7.2 Model derivation

The model is introduced in three steps in this section. Firstly, the equivalent confining pressure is derived (7.2.1- 7.2.3). Secondly, the values obtained from the first step are calibrated (7.2.4). Finally, the shear strength of fibre reinforced soil is predicted by superposition of unreinforced soil and fibre reinforcement (equivalent confining pressure) (7.2.5).

7.2.1 The tensile force carried by a single fibre

The general expression for the axial tensile stress in a single fibre in a fibre reinforced soil specimen can be obtained as follows. For a single fibre inclined to the horizontal plane at an angle θ , the strain of a single fibre in the direction of the fibre axis ($\varepsilon_f^1(\theta)$) (assuming a

straight portion of fibre) can be decomposed into strains in the radial (ε_r) and axial directions (ε_a) as follows:

$$\varepsilon_f^1(\theta) = \varepsilon_a \sin^2 \theta + \varepsilon_r \cos^2 \theta \quad (7.7)$$

In a CU test, the volumetric strain, ε_v is zero so that

$$\varepsilon_v = \varepsilon_a + 2\varepsilon_r = 0 \quad (7.8)$$

$$\varepsilon_r = -\frac{1}{2} \varepsilon_a \quad (7.9)$$

Substituting Equation 7.9 into Equation 7.7 gives

$$\varepsilon_f^1(\theta) = \varepsilon_a \left(\sin^2 \theta - \frac{1}{2} \cos^2 \theta \right) \quad (7.10)$$

The stress of a single fibre in the fibre direction $\sigma_f^1(\theta)$ is

$$\sigma_f^1(\theta) = E_f \varepsilon_f^1(\theta) \quad (7.11)$$

where E_f is the elastic modulus of the fibre material. The contribution of a single fibre to the stress in the radial direction, $\sigma_{rf}^1(\theta)$, can be derived via a similar approach in Diambra (2010) by decomposing $\sigma_f^1(\theta)$ into terms associated with work done which can be expressed as

$$\sigma_{af}^1(\theta) \varepsilon_a + 2\sigma_{rf}^1(\theta) \varepsilon_r = \sigma_f^1(\theta) \varepsilon_f^1(\theta) \quad (7.12)$$

$$\sigma_f^1(\theta) \varepsilon_f^1(\theta) = \sigma_f^1(\theta) (\sin^2 \theta \varepsilon_a + \cos^2 \theta \varepsilon_r) \quad (7.13)$$

where $\sigma_{af}^1(\theta)$ and $\sigma_{rf}^1(\theta)$ are the stress of a single fibre in axial and radial direction respectively. So the stress decomposition in the radial direction is

$$\sigma_{rf}^1(\theta) = \sigma_f^1(\theta) \frac{1}{2} \cos^2 \theta = E_f \times \varepsilon_a \left(\frac{1}{2} \sin^2 \theta \cos^2 \theta - \frac{1}{4} \cos^4 \theta \right) \quad (7.14)$$

As mentioned above, only the stress in radial direction is considered. Then the tensile force carried by a single fibre in the radial direction ($F_{rf}^1(\theta)$) can be calculated by multiplying the stress in radial direction and the projected area of the fibre, i.e.

$$F_{rf}^1(\theta) = \sigma_{rf}^1(\theta) \frac{A_f^1}{\cos \theta} \quad (7.15)$$

where A_f^1 is the cross-sectional area of a single fibre.

7.2.2. Total tensile force of all fibres

Calculating the total tensile force carried by all fibres requires integration of all fibre forces. An approach similar to that proposed by Michalowski and Cermak (2003) is used here. The fibres are randomly distributed in the specimen (Fig. 7.2a), and the stress and strain conditions at every point in the triaxial specimen are assumed identical. The fibres are assumed to have a uniform distribution in horizontal plane (α). Hence the strains in fibres depend only on their inclination angle (θ) to the horizontal of fibre, and is independent of fibres' positions. So we can imagine that all fibres can be moved together, making the midpoints of fibres coincide (Fig. 7.2b), and spherical coordinates (Fig. 7.2c) are used as the integration space in order to calculate the contribution of all fibres in specimen. The volume of the sphere (V) is

$$V = \frac{4}{3} \pi \left(\frac{1}{2}l_f\right)^3 \quad (7.16)$$

the infinitesimal volume required to undertake the integration can be expressed by the fibre length l_f and the orientation of the fibre (α and θ)

$$dV = \frac{1}{3} \left(\frac{1}{2}l_f\right)^3 d\theta d\alpha \cos \theta \quad (7.17)$$

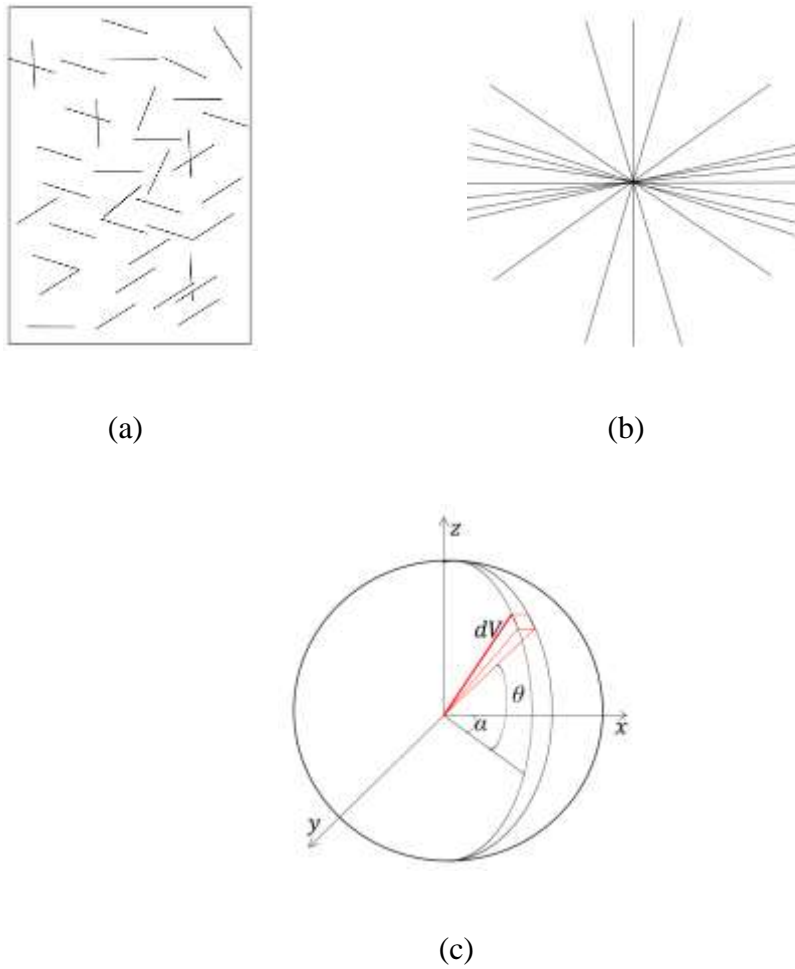


Figure 7.2. Transformation of randomly distributed fibres: (a) fibres in the specimen, (b) reassembled fibres, (c) integration space of spherical coordinates.

Since it is impossible to determine actual fibre arrangements in a given specimen here (as in other works) by considering the preferred sub-horizontal orientation of fibres, the distribution function proposed by Michalowski (1997), i.e.

$$\rho(\theta) = \frac{3}{2} \cos^2 \theta \rho_{ave} \quad (7.18)$$

where $\rho(\theta)$ represents the volumetric fibre content with an orientation angle θ above the horizontal plane in an infinitesimal volume dV (Figure 7.2c). ρ_{ave} is the average volumetric fibre content in the sphere, where

$$\rho_{ave} = \frac{V_f}{V} \quad (7.19)$$

Figure 7.3 shows a comparison between uniform fibre distribution and the chosen distribution function in this study.

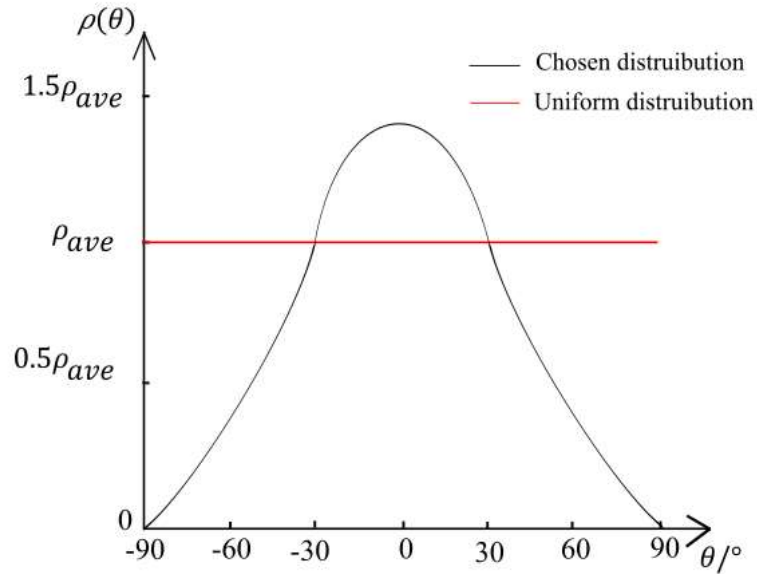


Figure 7.3 Variation of the volumetric fibre content with fibre inclination angle.

It is worth noting that for a given fibre reinforced soil specimen, ρ_{ave} is not the same as v_f in value because the volume of the specimen (V_t) is not the same as the volume of the integration space (V). The ρ_{ave} also depends on V_t . For a fibre reinforced specimen with a volume V_t , the relationship below can be obtained from Equations 7.18 and 7.19,

$$\frac{3}{2} \cos^2 \theta \rho_{ave} = \frac{3}{2} \cos^2 \theta \frac{V_f}{V_t} \times \frac{V_t}{V} = \frac{V_f^\theta}{dV} \times \frac{V_t}{V} \quad (7.20)$$

$$\rho(\theta) = \frac{V_f^\theta}{dV} \times \frac{V_t}{V} \quad (7.21)$$

where V_f^θ is the total fibre volume with an orientation angle θ above the horizontal plane in a fibre reinforced soil specimen. For all the fibres with an orientation angle θ above the

horizontal plane, the total tensile force in radial direction $F_{rf}(\theta)$ can be calculated using equilibrium as

$$F_{rf}(\theta) = \sigma_{rf}^1(\theta) \frac{A_f^1}{\cos \theta} N(\theta) \quad (7.22)$$

where $N(\theta)$ is the number of fibres at angle θ above the horizontal plane, which can be expressed as

$$F_{rf}(\theta) = \sigma_{rf}^1(\theta) \frac{A_f^\theta}{\cos \theta} = \sigma_{rf}^1(\theta) \frac{V_f^\theta}{l_f \cos \theta} \quad (7.23)$$

where A_f^θ is total cross sectional area of fibres at angle θ .

Substituting Equations 7.18 and 7.21 into Equation 7.23, one can obtain the following

$$F_{rf}(\theta) = \sigma_{rf}^1(\theta) \frac{\frac{3}{2} \cos \theta \rho_{ave} dV}{l_f} \quad (7.24)$$

Assuming the horizontal distribution (α in Figure 7.2c) of fibres in the specimen is homogenous, and the vertical distribution (θ in Figure 7.2c) of fibres in the specimen is followed, i.e. $\rho(\theta)$ in Equation 7.18, the total fibre tensile force in the radial direction in specimen is:

$$F_{rf} = \int_V \sigma_{rf}^1(\theta) \frac{\frac{3}{2} \cos \theta \rho_{ave} dV}{l_f} \quad (7.25)$$

and Equation 7.25 can be expanded to

$$F_{rf} = \frac{1}{l_f} \frac{\pi}{8} E_f l_f^3 \rho_{ave} \varepsilon_a \int_{-\frac{\pi}{2}}^{\frac{\pi}{2}} \left(\frac{1}{2} \sin^2 \theta \cos^4 \theta - \frac{1}{4} \cos^6 \theta \right) d\theta \quad (7.26)$$

As mentioned above already, in a triaxial compression test, only those fibres acting in tension contribute to generated confining stress. So that the integrations of Equation 7.26 should be

performed with upper and lower limits. According to Diambra (2010), the limit angle θ_0 (Figure.7.4) can be determined by decomposing the strain. According to a Mohr's circle for a strain increment, only the tensile zone ($d\varepsilon_\theta < 0$) should be considered. So by letting Equation 7.7 be zero, θ_0 can be obtained as

$$\theta_0 = \tan^{-1} \sqrt{-\frac{d\varepsilon_r}{d\varepsilon_a}} \quad (7.27)$$

Substituting Equation 7.9 to Equation 7.27, it can be shown that $\theta_0 = \tan^{-1} \sqrt{\frac{1}{2}} \approx \frac{\pi}{5}$

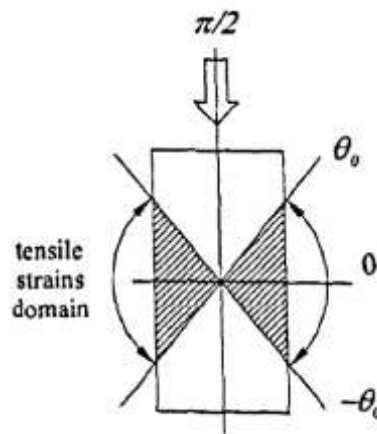


Figure 7.4. Domains of tensile strain orientations for triaxial compression test (from Diambra 2010).

So the integration part of Equation 7.26 can now be rewritten as

$$\int_{-\frac{\pi}{5}}^{\frac{\pi}{5}} \left(\frac{1}{2} \sin^2 \theta \cos^4 \theta - \frac{1}{4} \cos^6 \theta \right) d\theta \quad (7.28)$$

Equation 7.28 is a constant and can be obtained by numerical quadrature of the function curve, as shown in Figure 7.5. The hatched area is approximately 0.174.

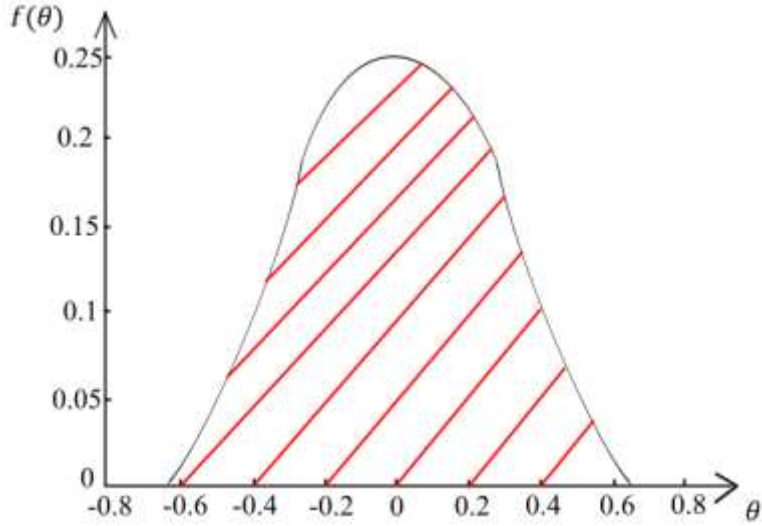


Figure 7.5. Function curve of the integration in Equation.7.27.

7.2.3 Total equivalent confining pressure

The radial component of total tensile force carried by all fibres has been obtained in 7.2.2. In a triaxial test, the equivalent confining pressure can be estimated by applying the total tensile force on the lateral surface (S_l) of the specimen, which can be expressed as

$$S_l = 2\pi RH \quad (7.29)$$

where R and H are radius and height of the specimen respectively.

So the equivalent confining pressure induced by the fibres is

$$p_f = \frac{F_{rf}}{S_l} = \frac{0.174 \frac{\pi}{8} E_f l_f^3 \rho_{ave} \varepsilon_a}{2\pi R H l_f} = \frac{0.065 R v_f E_f}{l_f} \varepsilon_a \quad (7.30)$$

It is worth mentioning that here isotropic stress p_f is assumed equal to the radial component of the fibre stress action on the specimen according to the last point of the assumptions (as clarified previously). Let $\frac{0.065 R v_f E_f}{l_f}$ be the parameter, P_f (kPa), Equation 7.29 can then be

expressed as

$$p_f = P_f \varepsilon_a \quad (7.31)$$

It can be seen from Equation 7.31 that for a given fibre reinforced soil specimen, the model developed above predicts equivalent confining pressure to increase linearly with the increasing axial compressive strain of the sample. Table.7.1 gives the relationship between P_f and fibre inclusion ratio v_f and fibre length l_f , as well as other parameters in the model. D_{50} in the table is the representative particle size of the soil (defined as 50 % of the soil particles are finer than this size), it will be introduced in the following paragraph.

Table 7.1. Input parameters and P_f for different fibre reinforced specimens.

Soil type	FRSA	FRSB	FRSC	FRSD	FRSE	FRSF
v_f (%)	0.53	1.05	1.58	0.53	1.05	1.58
l_f (mm)	6	6	6	12	12	12
D_{50} (mm)	0.0018	0.0018	0.0018	0.0018	0.0018	0.0018
E_f (MPa)	2000	2000	2000	2000	2000	2000
R (mm)	19	19	19	19	19	19
H (mm)	76	76	76	76	76	76
P_f (kPa)	2190.2	4380.5	6570.7	1095.1	2190.2	3285.3

As mentioned in Assumption (3) in 7.2.2, compatibility is assumed, i.e. the strain in the fibres is considered the same as in the surrounding soil matrix, but in reality there will be relative sliding between fibres and the surrounding soil particles. A modified parameter, α_f , is introduced in the form of Equation 7.32 to describe the sliding effect and take account of the various behaviours seen in the triaxial tests of fibre reinforced soils presented in Chapter 6. A number of material parameters are introduced as justified below and later, the triaxial results are used to provide calibration. After this, the model is used to predict strength behaviour, again with comparison to the triaxial test results.

$$\alpha_f = \left[(\varepsilon_a)^\alpha \left(\frac{\beta}{-\ln B_f} \right) \left(\frac{p_{ref}}{p'_0} \right)^\gamma \left(\frac{v_f}{v_f^{ref}} \right)^x \right] \quad (7.32)$$

$$B_f = \frac{l_f}{D_{50} \times 10^4} \quad (7.33)$$

where four new parameters are introduced to modify the model: sliding parameter (α), cell pressure parameter (γ), fibre inclusion ratio parameter (χ) and geometry parameter (β). p'_0 is the effective consolidation pressure and v_f is volumetric fibre content, they are normalised by the reference values p_{ref} (100 kPa) and v_f^{ref} (0.53% as the minimum fibre inclusion ratio in this study) respectively. B_f is introduced to eliminate the magnitude differences between D_{50} and l_f . α accounts for the sliding properties between fibre and soil particles.

7.2.4. Model calibration

The model is calibrated with the triaxial test results of 6 mm and 12 mm length fibre reinforced soil at $\rho_f = 0.3\%$, 0.9% and $\sigma_3 = 50, 100\text{kPa}$, and then verified with the results of fibre reinforced soil at $\rho_f = 0.6\%$ and $\sigma_3 = 200\text{ kPa}$. The process of calibration is introduced as follows. Sliding factor α accounts for the sliding effect and it is calibrated firstly. As discussed in Section 6.2, the shear strength improvement is nonlinear with respect to the axial strain and the rate of increase reduces with increasing axial strain due to the relative sliding. α is calibrated here separately by considering the Δq , as shown in Equation 7.34 (the details will be introduced in next section):

$$\Delta q = 3p_f = 3(\varepsilon_a)^\alpha P_f \varepsilon_a \quad (7.34)$$

and compared with the variation of Δq in Figure 6.7. The variation of the increasing rate of Δq with α is shown in Figure 7.6.

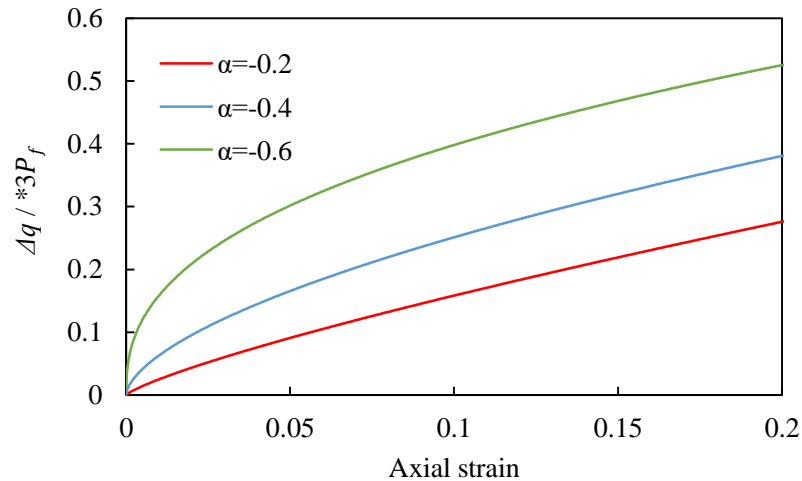


Figure 7.6. Variation of strength improvement trend with change of sliding parameter α .

It can be seen that when α is closer to 0, the relationship between strength improvement and axial strain is more linear. By considering the test results shown in Figure 6.7, α is set as -0.2 in the model. Geometry factor β accounts for this size effect of the materials and it is calibrated secondly by the results 6 mm and 12mm length fibre FRS with 0.3% fibre inclusion ratio at 100kPa cell pressure. They are selected because the third and fourth item in Equation 7.31 can be 1, and the fibre length effect can be calibrated. As mentioned in Section 6.2, the triaxial test results indicate that longer fibres have better behaviour in improving shear strength of the soil (Figure 6.11). In addition, although D_{50} is constant in this study, according to Michalowski and Cemark (2003), the reinforcement is more effective when the fibre length is large compared to the size of the grains. Hence D_{50} is introduced as a denominator and β accounts for this size effect of the materials. The influence of β on the predicted results and the comparison with experimental results are shown in Figure 7.7. It can be seen that the different between the benefit of 12 mm and 6 mm length fibre gets greater as β increase. β is set as 0.011 by considering the effect of fibre length.

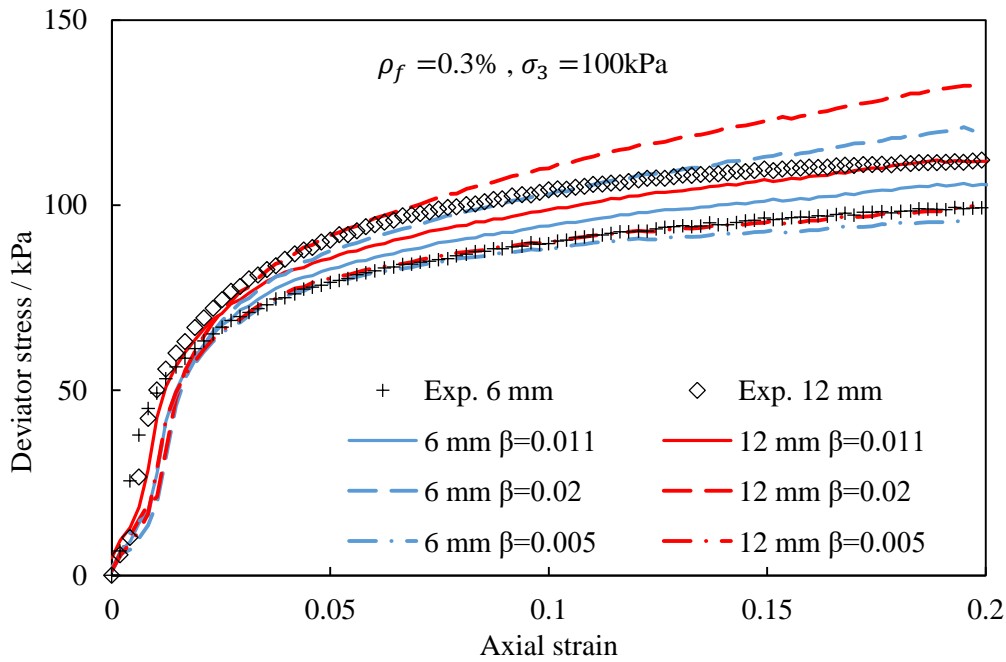


Figure 7.7. Influence of geometry parameter β on the predicted results.

Cell pressure parameter (γ) and fibre inclusion ratio parameter (χ) account for effects linked to the cell pressure and the fibre inclusion ratio, as observed in this study (and as discussed in Chapter 6), and they are calibrated by the test results of FRS ($\rho_f = 0.3\%$, $l_f = 6$ mm) with different cell pressures (e.g. 50 and 100 kPa) and FRS ($\sigma_3 = 100$ kPa, $l_f = 6$ mm) fibre inclusion ratios (e.g. 0.3% and 0.9%) respectively. The range of γ and χ is $0 \leq \gamma \leq 1$ and $-1 \leq \chi \leq 0$ and this is to satisfy the trends observed in the tests: as the fibre inclusion ratio and cell pressure increases, rate of increase of the shear strength reduces. The influence of these two parameters on the predicted results is shown in Figures 7.8 and 7.9 respectively. It can be seen from Figure 7.8 that the closer γ to 1, the increased reinforcing benefit at low cell pressure is more obvious. The predicted result at 100 kPa cell pressure is not influenced as 100 kPa is the reference pressure (p_{ref}). According to the degree of the trend of more reinforcing benefit at lower cell pressure, cell pressure parameter γ is set as 0.18. Similarly, it can be seen from Figure 7.9 that the closer χ to -1, the decreased reinforcing benefit at higher

fibre inclusion ratio is more obvious. According to the observed trend the fibre inclusion ratio parameter χ is set as -0.5.

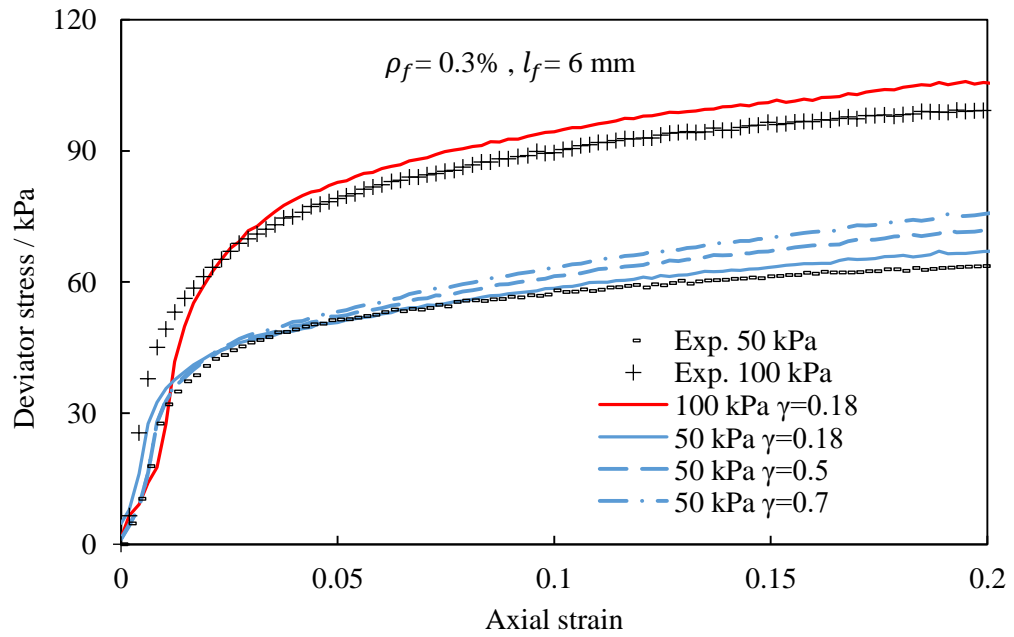


Figure 7.8. Influence of cell pressure parameter γ on the predicted results.

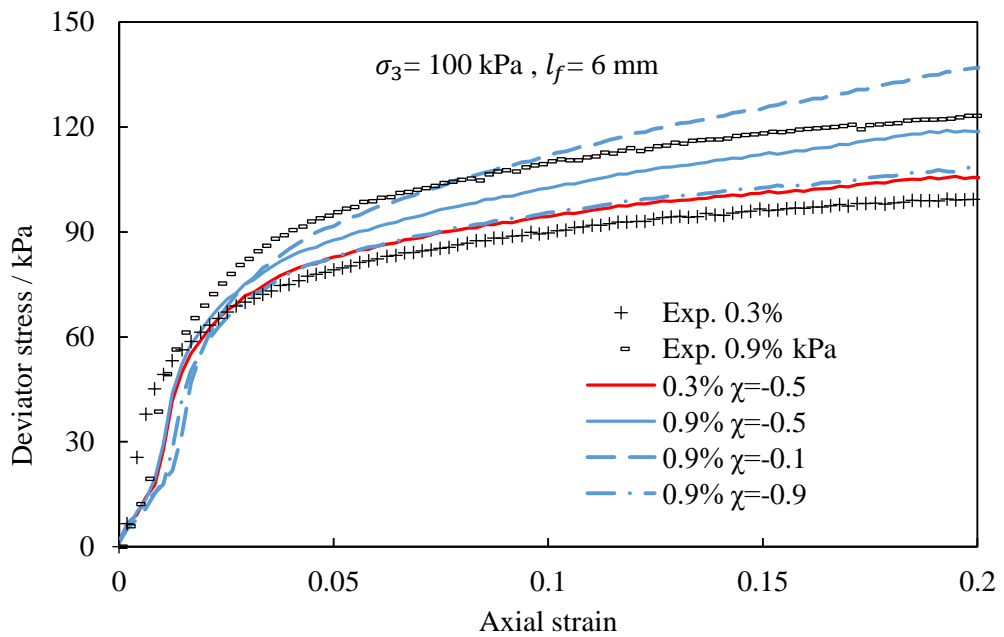


Figure 7.9. Influence of fibre inclusion ratio parameter χ on the predicted results.

The calibrated value of four parameters are shown in Table 7.2. The calibrated equivalent confining pressure can be expressed via Equation 7.35, and values of p_f^* at the end of shearing

($\epsilon_a = 20\%$) of different specimens are also calculated based on the calibration above and listed in Table 7.2.

$$p_f^* = \alpha_f P_f \epsilon_a \quad (7.35)$$

Table 7.2. Corrected parameters and p_f^* for fibre reinforced specimens.

Parameters		β	γ	χ	α		
Value		0.011	0.18	-0.5	-0.2		
Item	Soil type	FRSA	FRSB	FRSC	FRSD	FRSE	FRSF
p_f^* at $\sigma_3 = 50$ (kPa)		6.84	9.68	11.85	9.24	13.07	16.00
p_f^* at $\sigma_3 = 100$ (kPa)		6.01	8.56	10.48	8.18	11.56	14.15
p_f^* at $\sigma_3 = 200$ (kPa)		5.33	7.54	9.23	7.20	10.17	12.46

7.2.5. Predicting stress-strain behaviour using the model

An expression for the modified equivalent confining pressure p_f^* is obtained in 7.2.4, and the process of using this to predict the shear strength behaviour of the fibre reinforced soil is introduced as follows.

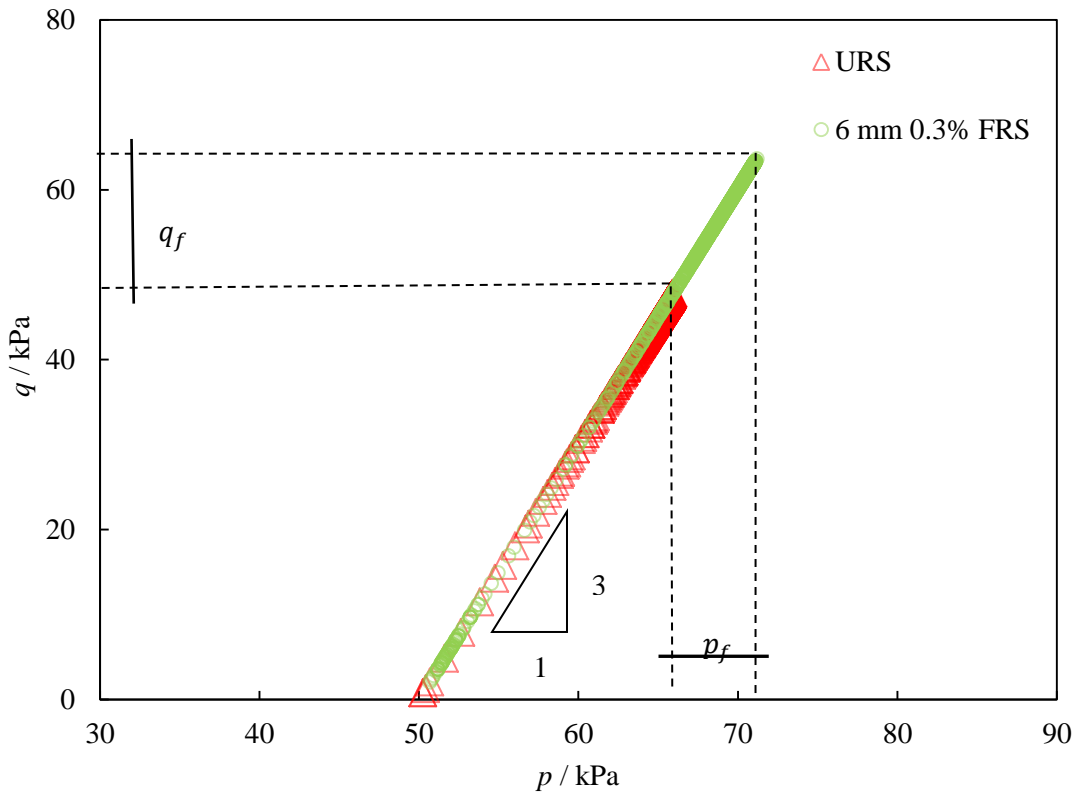


Figure 7.10. Equivalent confining pressure in $p - q$ plane.

Figure 7.10 illustrate this conception of equivalent confining pressure by experimental results of unreinforced and fibre reinforced soil. As mentioned above, the effect of fibre reinforcement is modelled as an equivalent confining pressure (p_f) acting on the specimen in the triaxial test. Figure 7.10 shows drained path results from unreinforced (red) and reinforced specimens (green) and there is a gap between the stress paths of the two materials. The mean stress difference is considered to be p_f for which there is a corresponding difference in final deviator stress (q_f). For the fibre reinforced soil, the mean stress (p_{frs}) and deviator stress (q_{frs}) of any point in the test can be considered as the combination of mean stresses in the unreinforced case and an effective confining pressure from the presence of fibre reinforcement, i.e.

$$p_{frs} = p_{urs} + p_f \quad (7.36)$$

$$q_{frs} = q_{urs} + q_f = q_{urs} + 3p_f \quad (7.37)$$

Clearly for a given sample p_{urs} and q_{urs} can be obtained from a triaxial test, so once the equivalent confining pressure is calculated, the model can deliver the total stress path for the same sample when fibre reinforced. According to Skempton (1954), the pore water pressure change for a saturated specimen during an undrained triaxial test can be expressed as

$$\Delta u = B[\Delta\sigma_3 + A(\Delta\sigma_3 - \sigma_1)] \quad (7.38)$$

where B is 1 and $\Delta\sigma_3$ is 0 during the CU test and A is the pore water pressure coefficient, which changes during the test and depends on the stress level. It can be expressed by the current slope of the $q - u$ curve (Figure 7.11). For the fibre reinforced soil, the excess pore water pressure generated during the tests (Δu_{frs}) can be considered as a combination of that which occurs in an unreinforced soil (Δu_{urs}) and a component due to the fibre reinforcement (Δu_f). Assuming the coefficient A of FRS is the same as that of URS and according to Equation 7.38, Δu_{frs} can be expressed as

$$\Delta u_{frs} = \Delta u_{urs} + \Delta u_f = \Delta u_{urs} + \frac{\Delta u_{urs}}{\Delta q_{urs}} \Delta q_f = \frac{\Delta u_{urs}}{\Delta q_{urs}} \Delta q_{frs} \quad (7.39)$$

A series of pore water pressure coefficients A can be calculated based on the test results of unreinforced soil at different cell pressures, and therefore the above relations can be used to predict the excess pore water pressures for a fibre reinforced soil can be obtained as per (7.39). The effective stresses can then be obtained following Terzaghi's principle.

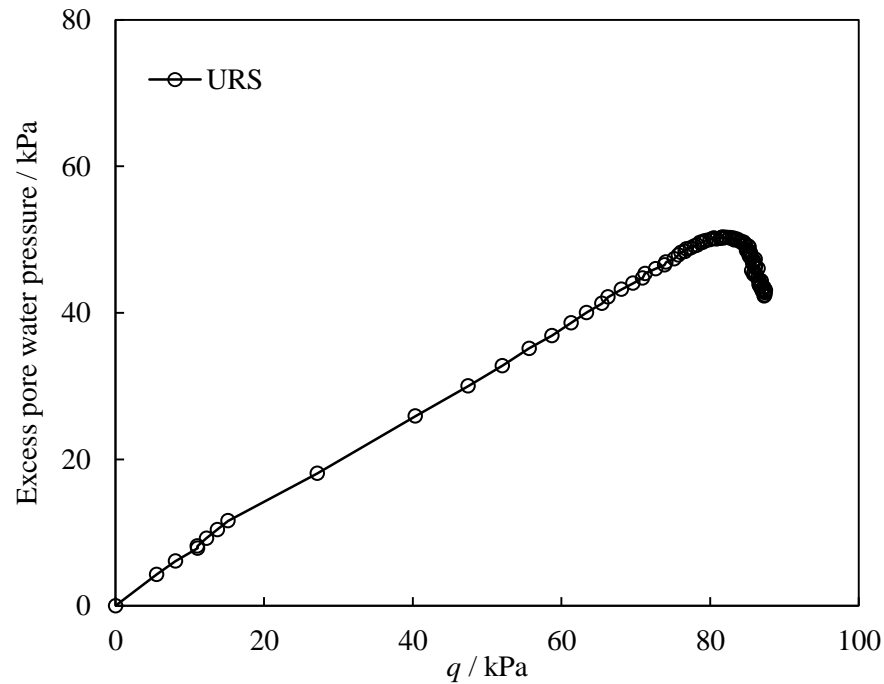


Figure 7.11. Variation of coefficient A at different stress states of unreinforced specimen at 100 kPa cell pressure.

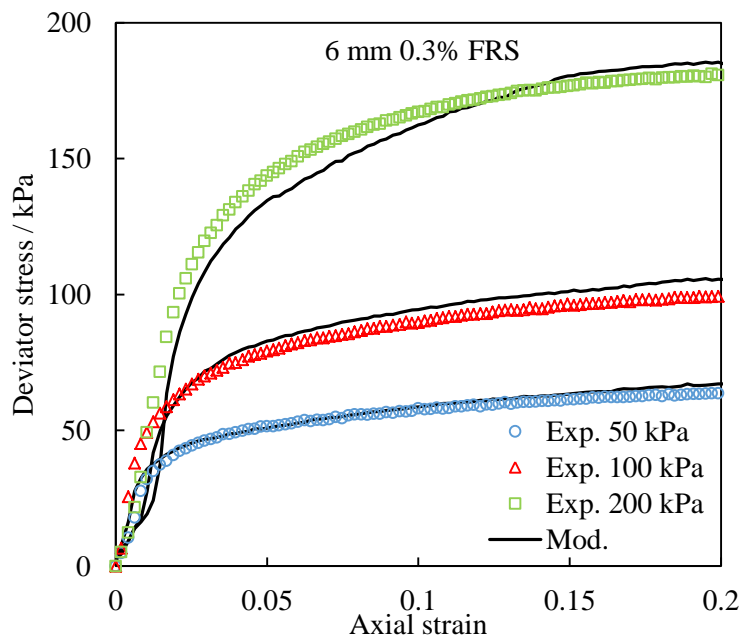
7.3 Comparison of predicted and experimental results

In this section, the model developed above is used to make predictions of stress/strain and excess pore pressure/strain behaviours in undrained triaxial tests. The predictions for the fibre reinforced soils are derived from the procedure described above applied to the unreinforced test results. The calibrated equivalent confining pressures have been obtained as shown in Table 7.2. The deviator stress (q_{fRS}), excess pore water pressure (u_{fRS}) and mean effective stress (p'_{fRS}) of fibre reinforced London Clay are then predicted using the approach mentioned in 7.2.4. The predicted results of both calibration group and verify group and experimental results are compared and discussed in this section.

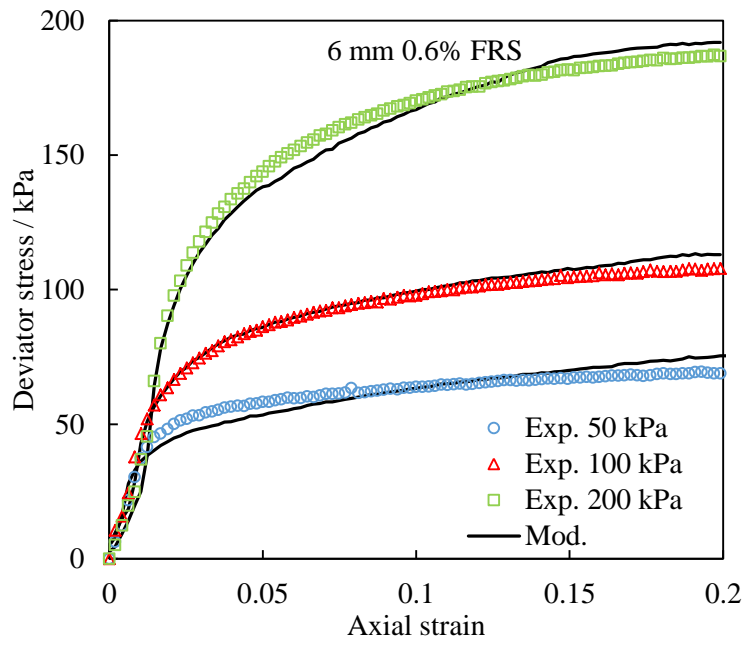
7.3.1 Stress strain behaviour

The measured and predicted deviator stress-axial strain curves of fibre reinforced soil with different fibre inclusion ratios, fibre lengths and cell pressures are shown in Figure 7.12.

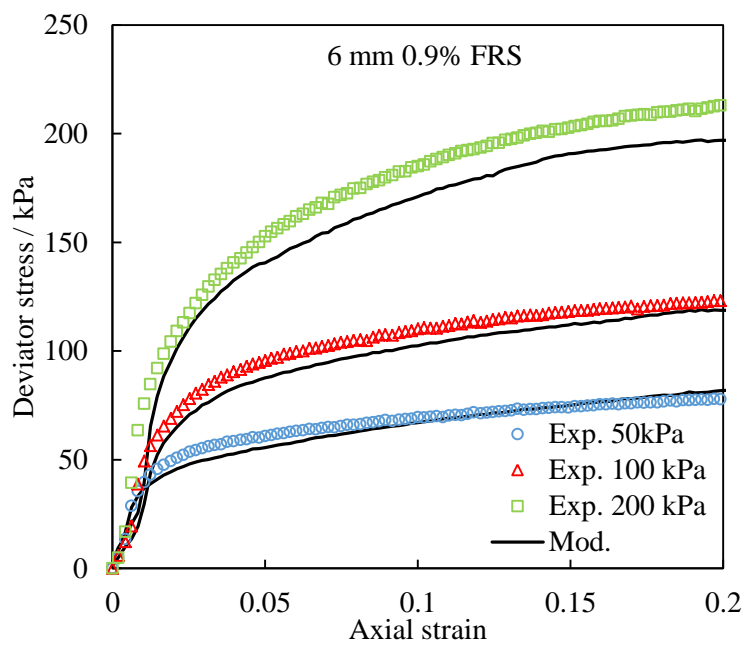
Generally, the model is capable of good predictions of the stress-strain relationship for the fibre reinforced soil at different cell pressures. An exception occurs when the soil is reinforced with 6 mm length fibres at 0.9% fibre inclusion ratio and tested at 200 kPa cell pressure, where the model underestimates the deviator stress of the soil during the whole process of shearing. Interestingly, the experimental results for this particular specimen ($\rho_f = 0.9\%$, $l_f = 6$ mm, $\sigma_3 = 200$ kPa) show it to be the only case where 6 mm length fibres lead to behaviour superior to the use of 12 mm fibres (see Figure 6.11c). However, the fibre length influence in the model is calibrated from a holistic perspective based on all tests, so this case is underestimated here and there could be further refinement needed in the model. For some of the predicted results, the fibre contribution to strength is slightly underestimated for axial strains from 2%- 10%.



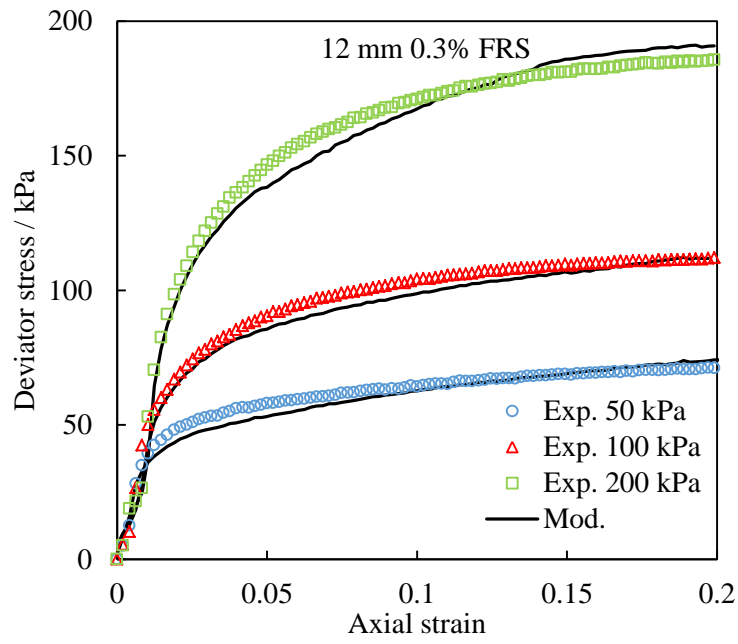
(a)



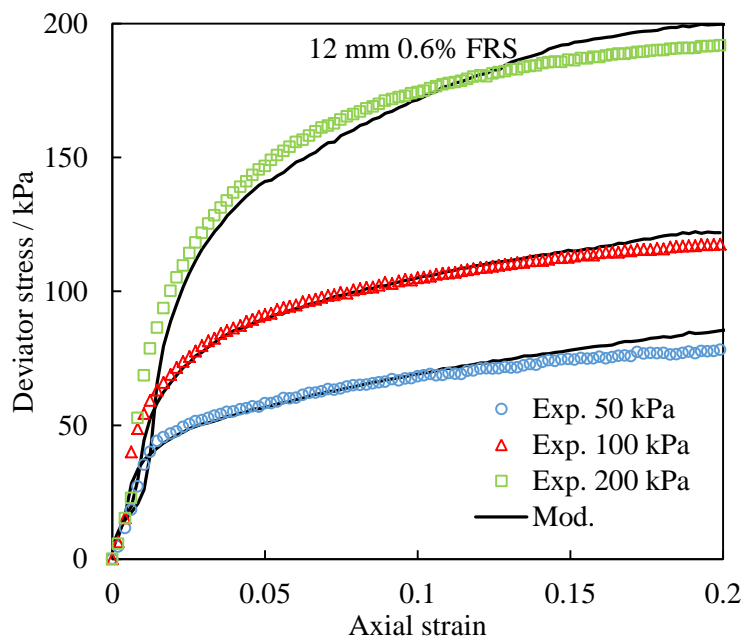
(b)



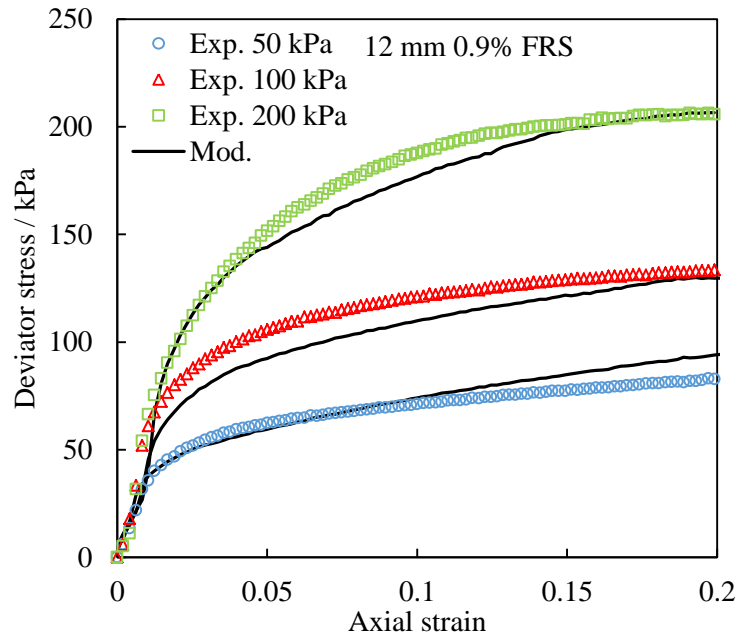
(c)



(d)



(e)



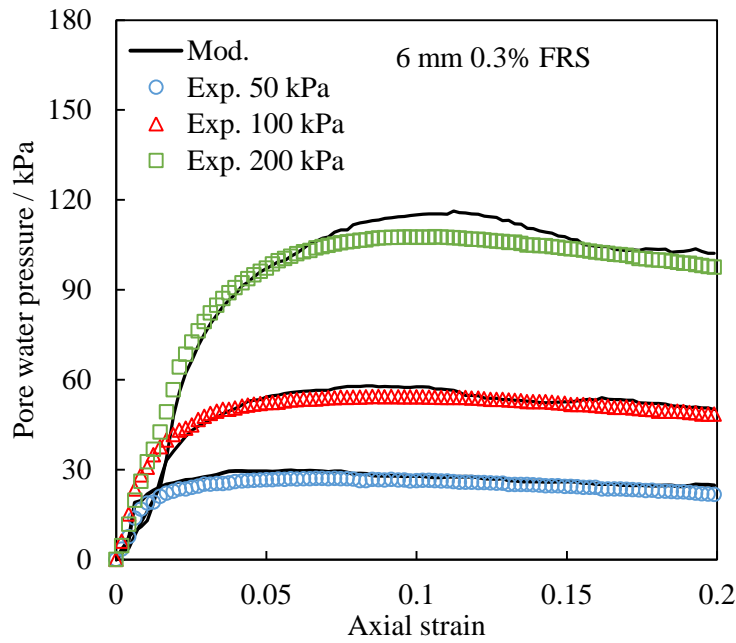
(f)

Figure 7.12. Experimental and predicted results of stress-strain relationships of fibre reinforced soil with $l_f=6$ mm (a) $\rho_f=0.3\%$ (b) $\rho_f=0.6\%$ (c) $\rho_f=0.9\%$; $l_f=12$ mm (d) $\rho_f=0.3\%$ (e) $\rho_f=0.6\%$ (f) $\rho_f=0.9\%$.

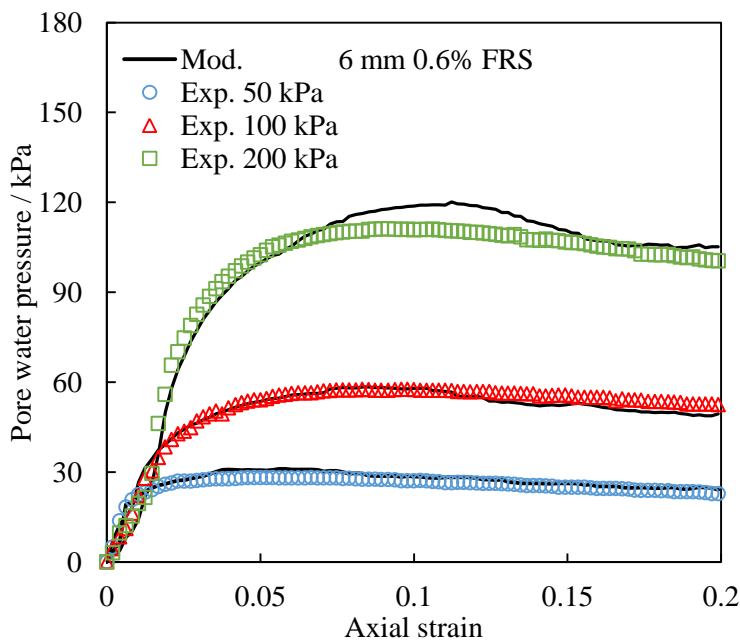
7.3.2 Pore water pressure behaviour

The measured and predicted pore water pressure- axial strain curves of fibre reinforced soil samples with different fibre inclusion ratios, fibre lengths and cell pressures are shown in Figure 7.13. It can be seen that when the cell pressures are 50 and 100 kPa, the model predicts the pore water pressure-strain relationship of the fibre reinforced soil to a good accuracy. When the cell pressure is 200 kPa, the model tends to overestimate pore water pressures for all fibre reinforced soil samples when the axial strain is in the range of 7% to 15%. In addition, all the predicted curves experience slight fluctuation, especially at higher strains (15% to 20%). This phenomenon may be attributable to coefficient A , which is obtained via the ratio of Δu_{urs} to Δq_{urs} . The fluctuation of the pore water pressure value leads to the value of A fluctuating around zero, and results in the fluctuation of predicted curves. However, in general

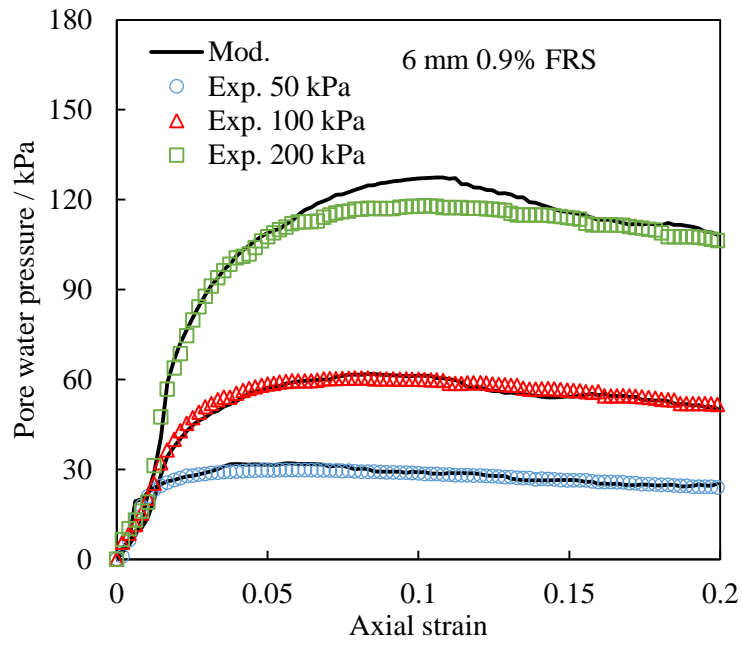
the predicted pore water pressure-axial strain relationships of the fibre reinforced soils are in close agreement with the experimental results. Clearly more repeats of tests could be conducted on unreinforced soil at the same cell pressure in order to have a more convincing value of A .



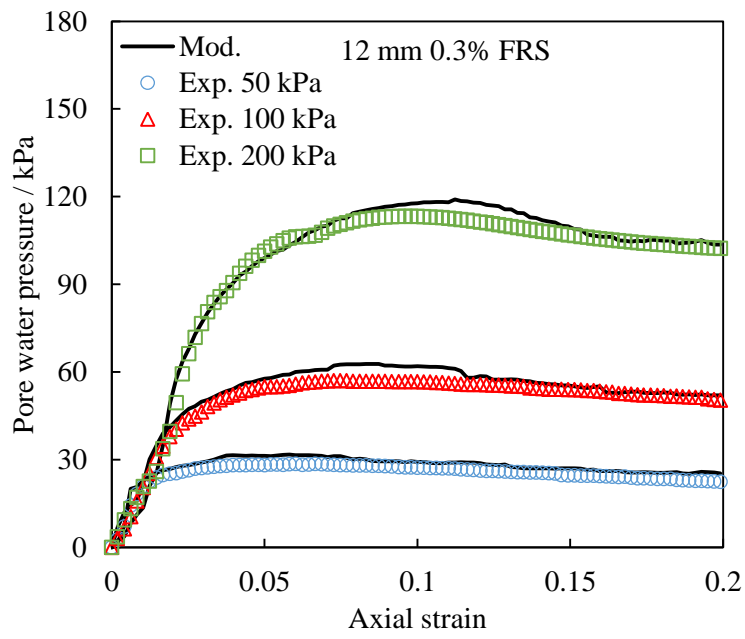
(a)



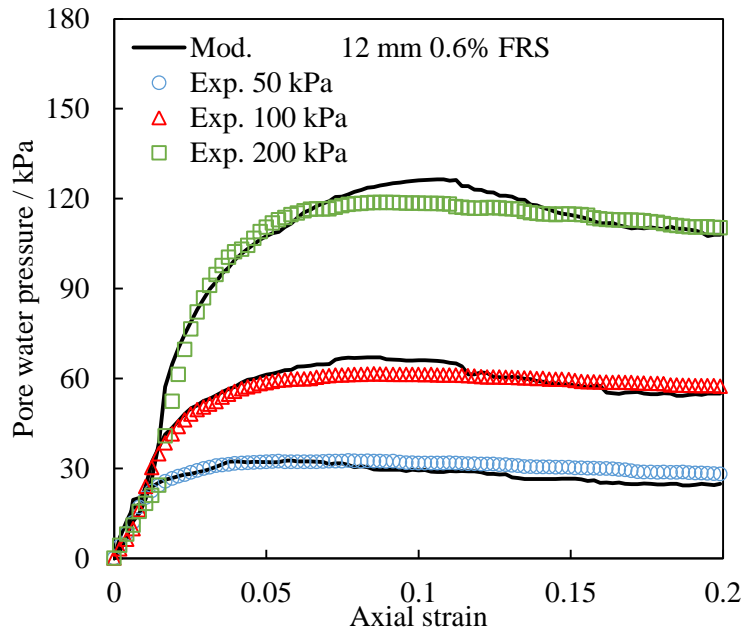
(b)



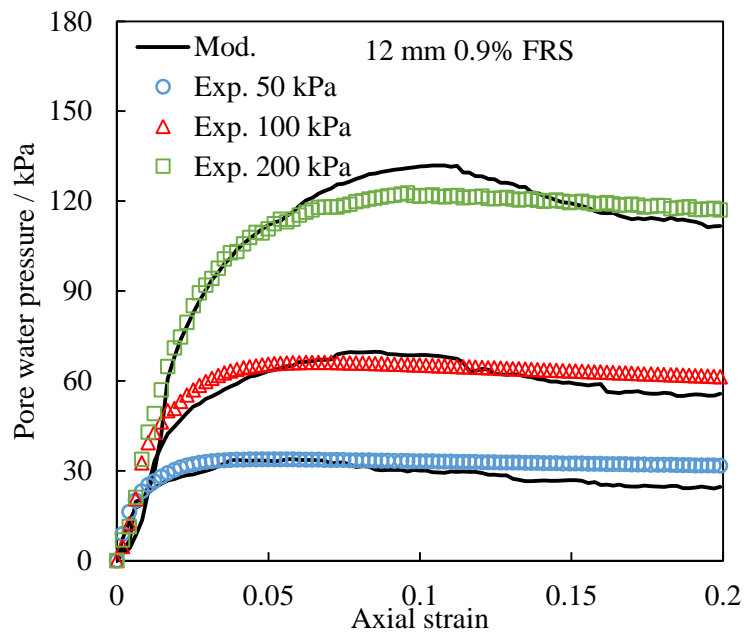
(c)



(d)



(e)

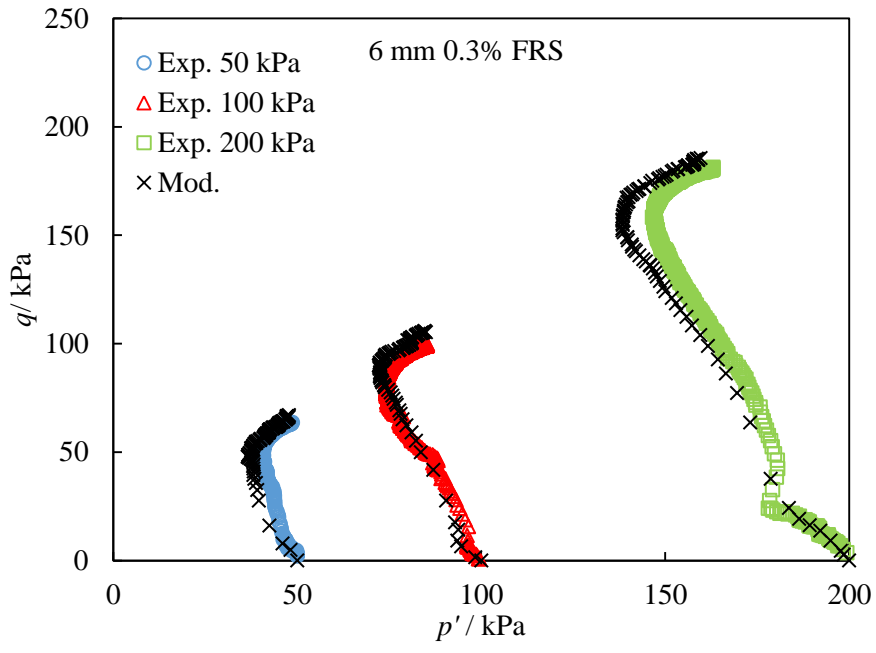


(f)

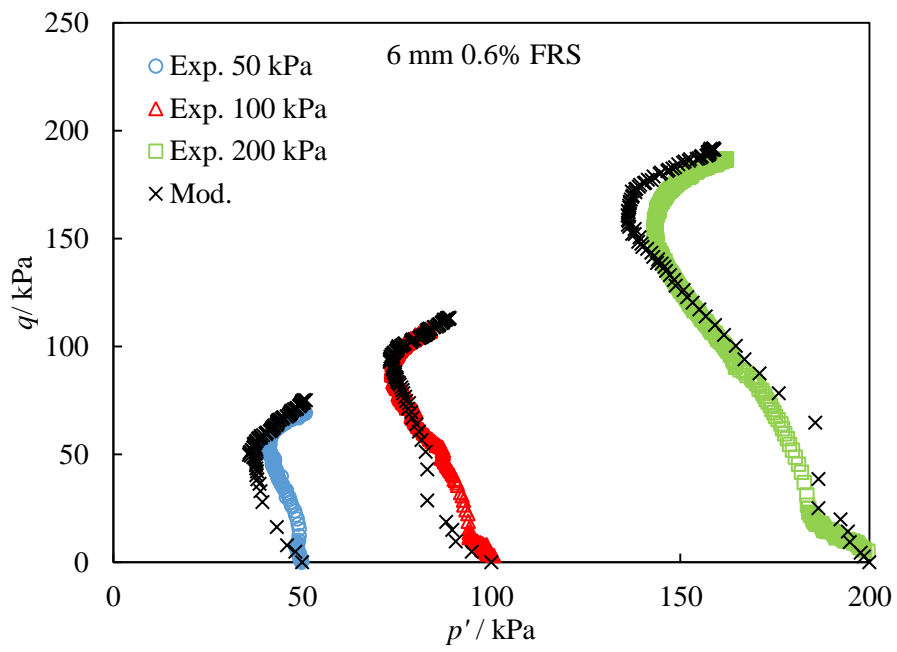
Figure 7.13. Experimental and predicted results of excess pore water pressure-strain relationship of fibre reinforced soil with $l_f = 6$ mm (a) $\rho_f = 0.3\%$ (b) $\rho_f = 0.6\%$ (c) $\rho_f = 0.9\%$; $l_f = 12$ mm (d) $\rho_f = 0.3\%$ (e) $\rho_f = 0.6\%$ (f) $\rho_f = 0.9\%$.

7.3.3 Stress path behaviour

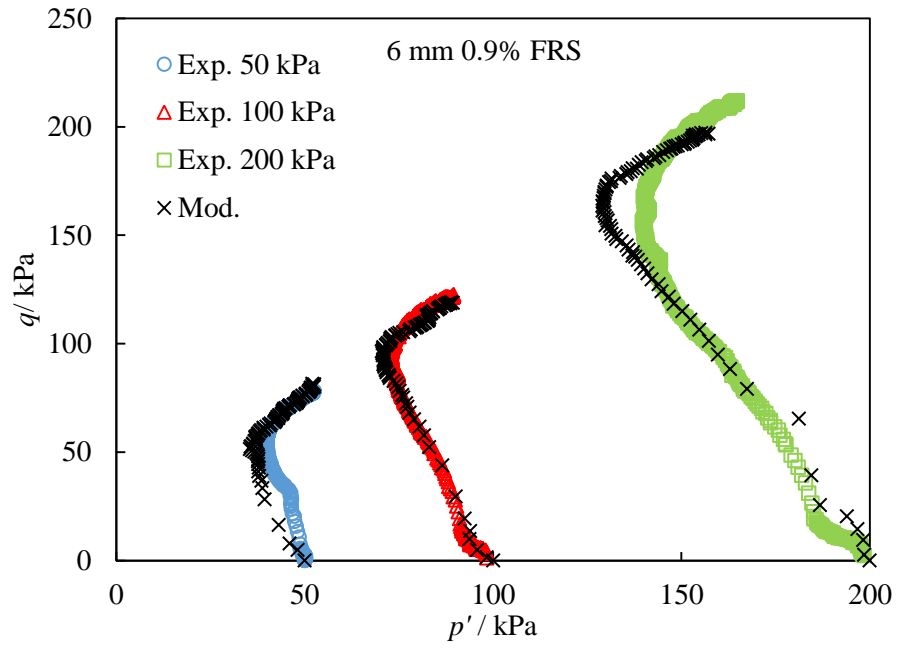
The final set of comparisons presented here are for effective stress paths in the tests, once again predicted following the model developed above. The measured and model predicted stress paths of fibre reinforced soils with different fibre inclusion ratios, fibre lengths and cell pressures are shown in Figure 7.14. It can be seen that in $p' - q$ plane the predicted results closely match the paths obtained from the experimental tests. For tests conducted at 50 and 100 kPa cell pressures, some of the predicted stress paths tend to lie to the left side of the experimental stress paths at the beginning. This trend implies that the model overestimates the deviator stress and pore water pressure of the fibre reinforced soil at these strains. The stress path of fibre reinforced soil with $l_f = 6$ mm and $\rho_f = 0.9\%$ at 200 kPa (the green curve in Figure 7.14c) shows obvious differences to the predicted results. The predicted curve lies below the tested curves at the end of the test, and is located to the left side in the middle of the test. The former probably comes from the underestimated deviator stress (mentioned in 7.3.1) and the latter from the overestimated pore water pressure (mentioned in 7.3.2). However, combining all three stress paths of every reinforcing condition, it can be concluded that the proposed model makes reasonable predictions of the stress paths followed in tests on fibre reinforced soils at different cell pressures. Consequently, one can predict the development of the stress state of selected fibre reinforced soil at a given consolidation pressure. Also, of the procedure allows one to estimate the critical state parameter M of a fibre reinforced soil by fitting a group of predicted stress paths, as an index of evaluating the shear strength of fibre reinforced soil.



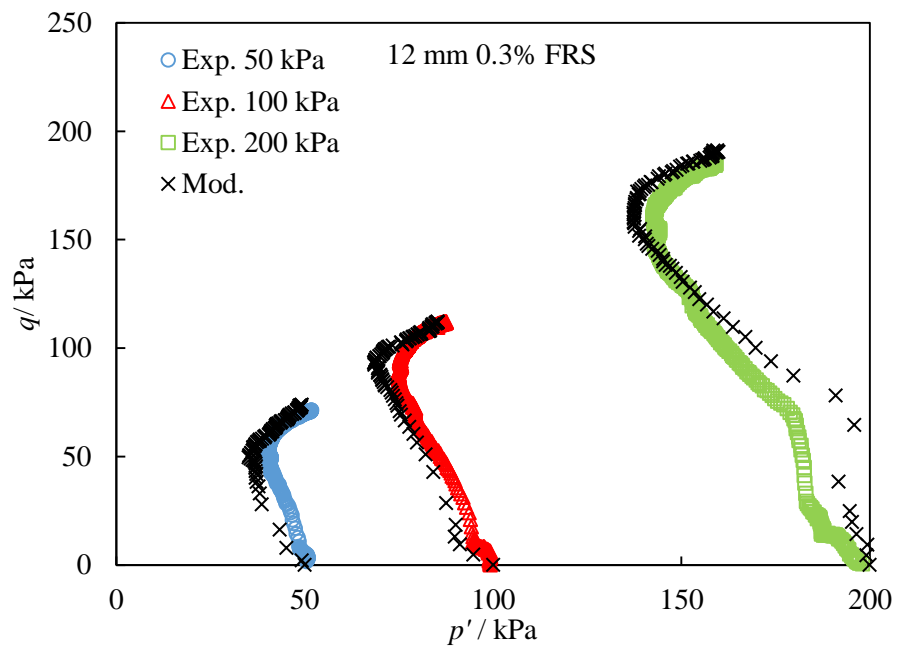
(a)



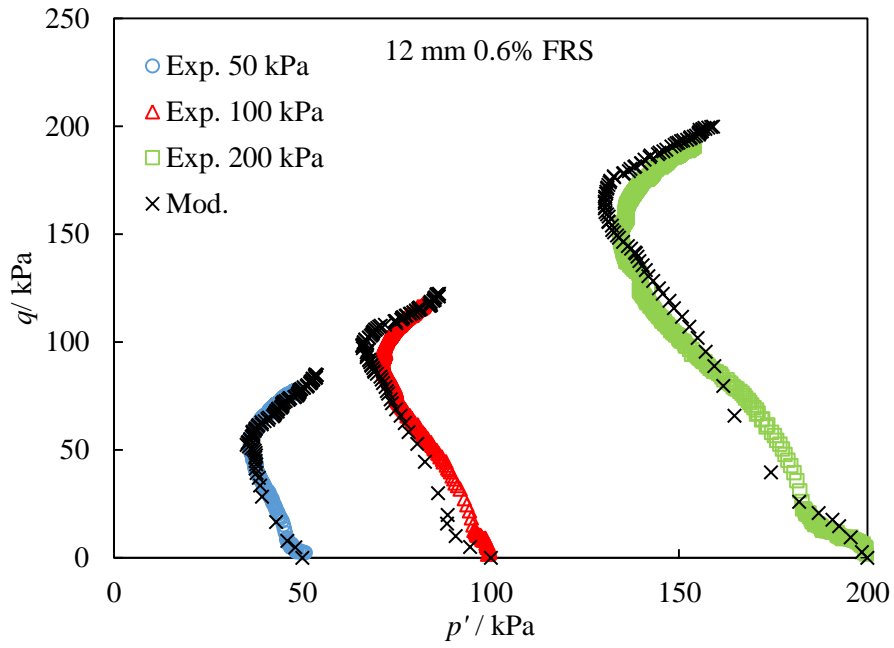
(b)



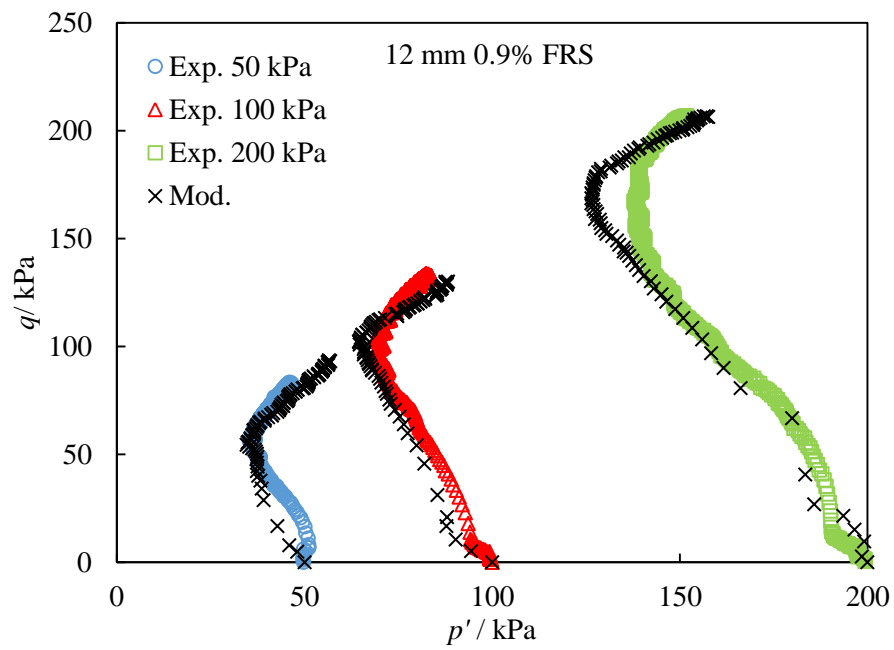
(c)



(d)



(e)



(f)

Figure 7.14. Experimental and predicted results of stress paths of fibre reinforced soil with $l_f = 6$ mm (a) $\rho_f = 0.3\%$ (b) $\rho_f = 0.6\%$ (c) $\rho_f = 0.9\%$; $l_f = 12$ mm (d) $\rho_f = 0.3\%$ (e) $\rho_f = 0.6\%$ (f) $\rho_f = 0.9\%$.

7.4 Chapter summary

A speculative model is proposed in this chapter to predict the shear strength behaviour of a fibre reinforced clay, where the model considers the effect of fibre reinforcement as an equivalent confining pressure which then leads to greater shear strength. Once the stress-strain-pore water pressure behaviours of unreinforced soil samples have been obtained, the corresponding behaviours of fibre reinforced soils can be predicted by the superposition of unreinforced soil and fibre contributions. According to the discussions above, although the model slightly underestimates the deviator stress in the axial strain of 2%- 10%, and overestimates the pore water pressure in the axial strain of 7- 15% (for 200 kPa cell pressure), it can be concluded that the model has a satisfactory performance in predicting the stress-strain, pore water pressure and stress path behaviour of this particular fibre reinforced London Clay. Compared to most of the existing models, the proposed model has two advantages. Firstly, the contribution of fibre reinforcement is considered separately from the soil matrix, which avoids extra experiments on fibre-soil composite samples to obtain material parameters. Secondly, the model is convenient to use. There are two parameters that account for the equivalent confining pressure and they depend on the materials involved. Two other parameters account for the fibre inclusion ratio effect and cell pressure effect in the tests. The model is however, speculative and forms a small part of the contribution of this thesis. It is perhaps a starting point for a comprehensive model of fibre reinforced clay. Clearly as it stands, there are limitations in this model. Firstly, the material parameters α and β need to be estimated via investigation of the characteristics of the fibres and soil matrix materials. More tests are clearly also needed on different fibre inclusion ratios and cell pressures to confirm the suggested ranges of γ and χ . The fibre distribution function used in this model might not be suitable for different conditions, for example, the fibre orientation might be different in the engineering application due to the mixing method. Therefore further research on fibre

distribution conditions could aid calibration of the model by using various other fibre distribution functions.

Chapter 8

8. Conclusions and recommendations

8.1 Thesis discussion and conclusions

Engineering problems occur in highway embankments related to shear strength, bearing capacity, compressibility and cracking resistance of the compacted clay of which they are constructed. The inclusion of randomly distributed fibres to improve the engineering properties of compacted clay is becoming a topic of increasing interest within geotechnical engineering projects. However, a comprehensive study on the engineering properties of fibre reinforced high plasticity clay is required to enable engineers to have confidence when designing new earth structures using this technique and soil. This research project has investigated the influence of fibre inclusion ratio and fibre length on the compaction, bearing capacity, one-dimensional consolidation, linear shrinkage, desiccation cracking, direct tensile strength and triaxial compression strength behaviour of London Clay. Laboratory results of unreinforced and fibre reinforced specimens from the tests mentioned above were analysed and interpreted in order to evaluate the potential benefit of high plasticity clay (CH) reinforced with polypropylene fibres in different conditions. The research also proposed a model for predicting the shear strength behaviour of fibre reinforced clay. A summary of the conclusions drawn from the results and discussions described in earlier chapters is presented below.

- *Compaction and bearing capacity properties.* As in many other studies, the MDD of the soil is observed to decrease as the fibre inclusion ratio is increased. The OMC of the soil also reduces slightly with the addition of fibres. The *CBR* value of the soil increases with the increasing fibre inclusion ratio.

- *One-dimensional consolidation behaviour.* As the fibre inclusion ratio increases, there is a reduction in C_s and C_c of the soil and an increase in c_v of the soil.
- *Desiccation behaviour.* During desiccation, fibres reduce the total crack area and the average area of the cracks in compacted specimens. Crack initiation time and crack number increase with fibre addition. In linear shrinkage tests, fibres are observed to significantly restrict the linear shrinkage strain of the specimens.
- *Strength and stiffness behaviour.* Fibre reinforcement can significantly increase the tensile and shear strength of the London Clay tested. However, fibre has no obvious influence on the stiffness of the soil.
- *Failure behaviour.* In triaxial tests, the failure pattern of specimens under low cell pressure changes from “shear band” type to “bulging” type. In tensile tests, the fibre reinforced soil specimens have a higher post-peak stress and change the failure type from brittle failure to the ductile failure.
- *Effect of fibre length.* Short fibres have a greater value of bearing capacity improvement of the soil for a given mass of fibres, longer fibres have a more pronounced influence on tensile strength and shear strength of the soil.
- *Effect of fibre inclusion ratio.* For all the tests in this study, the reinforcing effect has a positive correlation with the fibre inclusion ratio. However, as the inclusion ratio increases, the rate of improvement on soil properties reduces and this phenomenon is observed in all of the tests conducted.
- *Effect of other variables.* In triaxial testing, the benefit in deviator stress due to the fibre reinforcement reduces as the cell pressure is increased. In direct tensile tests, the benefit in tensile strength due to fibre reinforcement reduces as water content is increased.

8.2 Implications of the research in civil engineering applications

Today, soil reinforcement has been widely used in civil engineering projects across the world. The pursuit of reliable construction material engineering properties and efficiency savings in infrastructure projects has provided the impetus for research on randomly distributed fibre reinforced soil. Although this technique has been utilised in engineering construction for thousands of years it is only in the last few decades that a unified, scientifically based engineering approach has begun to be developed and to date this is still a work in progress. Based on the results and conclusions above, some suggestions can be made for the use of polypropylene in reinforcing clay soils for civil engineering projects today:

- When polypropylene fibres are to be used in reinforcing clay fill material in civil engineering projects, there is a tendency for the fibres to clump together when mixed with wet clay. More even distribution of fibres can be achieved if the clay fill is dried well below the plastic limit. However, it is acknowledged that drying clay fill may be difficult to achieve in the field. Further work is required on determining efficient means of mixing fibres with wet clay in order to facilitate economic construction using this technique.
- Higher bearing capacity of fibre reinforced soil leads to a reduction in the required thickness of subgrade layers. When the fibre inclusion ratio is 0.9%, the subgrade thickness can be reduced by around 25%. This would have significant potential benefits in reducing material costs for highway projects.
- When reinforcing a soil with low bearing capacity, shorter fibres are a better choice than longer fibres due to a greater improvement of *CBR* value. For the purpose of improving slope stability, longer fibres are more suitable than shorter fibres because of the increased benefit in improving shear strength and cracking resistance that longer fibres have shown.

- When the fibre inclusion ratio is over 0.6%, there is a reduction in reinforcing benefit per unit of fibre. Designers should be aware that using fibre inclusion ratios greater than 0.6% will produce progressively smaller benefits mechanically and may be economically unjustifiable.
- The addition of fibres might also bring disadvantages. The higher coefficient of consolidation produced by the addition of fibres could lead to a higher initial rate of settlement in the soil. Designers should be aware of this potential effect and situations where this may cause periods of differential settlement at the interface between fibre reinforced soil and other engineered structures should be considered on a project by project basis.
- As with other forms of reinforced soil some level of displacement (stretching) is required to mobilise tensile resistance in fibre reinforced soil. Fibre reinforced soil is therefore suitable to be used in the areas where large strains are anticipated (e.g. anti-seismic).
- According to the triaxial test results, fibre reinforcement is more effective at lower confining pressures. So this technique is more suitable to be employed in relative shallow soil layers.

8.3 Recommendations for future work

As mentioned above, the findings from this research project give a deeper understanding of the engineering behaviour of fibre reinforced high plasticity clay. However, due to time limits and other constraints the experimental research carried out by the author was restricted to London Clay reinforced with polypropylene fibres in three fibre inclusion ratios and two different fibre lengths only. Additionally, the model developed in Chapter 7 is speculatively proposed based on the results observed in a limited group of triaxial tests. In order to provide

more complete guidance for engineering design of fibre reinforced high plasticity clay further research is necessary, suggestions for additional research are presented below:

- The interaction between fibre and clay particles is difficult to measure and quantify. The initial dry density of the soil (for all tests), initial water content (in desiccation cracking test), drainage condition (triaxial test) and strain rate (triaxial tests and tensile test) may influence fibre/soil interaction. The influence of these variables on fibre/soil interactions and overall reinforced soil behaviour should be investigated further.
- The proposed model was based on the data of polypropylene fibre reinforced London Clay in limited test conditions. Further work to develop the model should focus on model calibration based additional testing involving different clay soils, different fibres and different test conditions. A database of material parameters for the model (α and β) can be built up based on these further tests. Additionally, as mentioned in the previous bullet point the interaction mechanism between fibres and clay particles is not fully understood. It is necessary to build the relationship between material parameters of the model and the relative characteristics of fibre and soil (e.g. fibre length, soil particle size).
- The triaxial and tensile test results reveal that fibre reinforcement can improve the strength of London Clay when the strain level is relative high. So reinforced soil can be a potential soil stabilisation technique in large strain problems (e.g. anti-seismic). The mechanical behaviour of fibre reinforced clay under dynamic loading condition should therefore be studied.
- When utilised in the field, fibre reinforced clay will be mixed in large quantities and mechanical mixing method will be used instead of the method used in this research (mentioned in Section 3.3). Hence, the fibre distribution condition might be different and the composite could be relatively anisotropic. An experimental field testing

programme should be carried out in order to establish the limitations of conventional soil mixing techniques when it comes to producing a homogenous fibre soil mix and to develop process for achieving greater homogeneity when mixing fibres with wet clay soil. The results from these field tests could be used to further verify the proposed models.

- Currently, the durability of the fibre reinforced clay is unknown. Although the polypropylene fibre itself has a high chemical and thermal stability, variations in environmental and engineering conditions (e.g. weather, loading conditions) might influence the bonding between fibre and soil, which would in turn effect the long term performance of the fibre soil composite. As a potential in-situ soil stabilisation method, it is recommended that the long term performance of fibre/clay soil composites are investigated under a variety of environmental and loading conditions.

REFERENCES

- Abdi, M.R., Parsapajouh, A. and Arjomand, M.A., 2008. Effects of random fiber inclusion on consolidation, hydraulic conductivity, swelling, shrinkage limit and desiccation cracking of clays. *International Journal of Civil Engineering*, 6(4), pp.284-292.
- Abou Diab, A., Sadek, S., Najjar, S. and Abou Daya, M.H., 2016. Undrained shear strength characteristics of compacted clay reinforced with natural hemp fibers. *International Journal of Geotechnical Engineering*, 10(3), pp.263-270.
- ADFIL, 2019. Product data. Available: [http:// www.adfil.com/products/micro-synthetic-fibres/monofilament-fibres](http://www.adfil.com/products/micro-synthetic-fibres/monofilament-fibres), (accessed 25/06/2019).
- A.E.M.K Mohamed., 2013. Improvement of swelling clay properties using hay fibers. *Construction and Building Materials*, 38, pp.242-247.
- Aggarwal, P. and Sharma, B., 2010, September. Application of jute fiber in the improvement of subgrade characteristics. In *Proceeding of International Conference on Advances in Civil Engineering*, Trabzon, Turkey. pp. 27-30.
- Ahmad, F., Bateni, F. and Azmi, M., 2010. Performance evaluation of silty sand reinforced with fibres. *Geotextiles and Geomembranes*, 28(1), pp.93-99.
- Ajayi, O., 2014. The effect of fibre reinforcements on the mechanical behaviour of railway ballast (Doctoral dissertation, University of Southampton).

- Ajayi, O., Le Pen, L., Zervos, A. and Powrie, W., 2016. A behavioural framework for fibre reinforced gravel. *Geotechnique*, 67(1), pp. 56-68.
- Alfaro, M.C., Miura, N. and Bergado, D.T., 1995. Soil-geogrid reinforcement interaction by pullout and direct shear tests. *Geotechnical Testing Journal*, 18(2), pp.157-167.
- Al-Refeai, T.O., 1991. Behavior of granular soils reinforced with discrete randomly oriented inclusions. *Geotextiles and Geomembranes*, 10(4), pp.319-333.
- Anggraini, V., Huat, B.B., Asadi, A. and Nahazanan, H., 2015. Effect of coir fibers on the tensile and flexural strength of soft marine clay. *Journal of Natural Fibers*, 12(2), pp.185-200.
- Arslan, H., Sture, S. and Batiste, S., 2008. Experimental simulation of tensile behavior of lunar soil simulant JSC-1. *Materials Science and Engineering A*, 478(1-2), pp.201-207.
- Arup., 2010. Highways Agency, A Risk-based framework for geotechnical asset management. Phase 2 Report, Issue 1.
- Athanasopoulos, G.A., 1994. On the enhanced confining pressure approach to the mechanics of reinforced soil. *Geotechnical & Geological Engineering*, 12(2), pp.122.
- Babu, G.S., Vasudevan, A.K. and Haldar, S., 2008. Numerical simulation of fiber-reinforced sand behavior. *Geotextiles and Geomembranes*, 26(2), pp.181-188.
- Baumann, V. and Bauer, G.E.A., 1974. The performance of foundations on various soils stabilized by the vibro-compaction method. *Canadian Geotechnical Journal*, 11(4), pp.509-530.

Bazne, M.O., Vahedifard, F. and Shahrokhbabadi, S., 2015. The effect of geonet reinforcement on bearing capacity of low-compacted soft clay. *Transportation Infrastructure Geotechnology*, 2(1), pp.47-63.

BBC News. Real concerns over cracks in A801 carriageway. 20/03/2018. Available: <https://www.bbc.co.uk/news/uk-scotland-tayside-central-43474149>, (accessed 24/02/2020).

Bhadriraju, V., Puppala, A.J., Enayatpour, S. and Pathivada, S., 2005. Digital imaging technique to evaluate shrinkage strain potentials of fiber reinforced expansive soils. In *Site Characterization and Modeling*, pp.1-12.

Bhardwaj, D.K. and Mandal, J.N., 2008. Study on polypropylene fiber reinforced fly ash slopes. *The 12th International Conference of International Association for Computer Methods and Advances in Geomechanics, India*, pp.3778-3786.

Bjerrum, L., Moum, J. and Eide, O., 1967. Application of electro-osmosis to a foundation problem in a Norwegian quick clay. *G éotechnique*, 17(3), pp.214-235.

Bouhicha, M., Aouissi, F. and Kenai, S., 2005. Performance of composite soil reinforced with barley straw. *Cement and Concrete Composites*, 27(5), pp.617-621.

Bourrier, F., Kneib, F., Chareyre, B. and Fourcaud, T., 2013. Discrete modeling of granular soils reinforcement by plant roots. *Ecological Engineering*, 61, pp.646-657.

Brandl, H., 1981. Alteration of soil parameters by stabilization with lime. In *Proceedings of the 10th International Conference on Soil Mechanics and Foundation Engineering, Volume 3*, Stockholm.

British Geological Survey (2004), *Memoirs of the Geological Survey of Great Britain, England and Wales*. Keyworth, Nottingham.

BSI (British Standards Institution), 1990. BS 1377-2 Methods of test for soils for civil engineering purposes- Classification tests.

BSI (British Standards Institution), 1990. BS 1377-4 Methods of test for soils for civil engineering purposes- Compaction-related tests.

BSI (British Standards Institution), 1990. BS 1377-5 Methods of test for soils for civil engineering purposes- Compressibility, permeability and durability tests.

BSI (British Standards Institution), 1990. BS 1377-7 Methods of test for soils for civil engineering purposes- Shear strength tests (total stress).

BSI (British Standards Institution), 1990. BS 1377-8 Methods of test for soils for civil engineering purposes- Shear strength tests (effective stress).

Butt, W.A., Mir, B.A. and Jha, J.N., 2016. Strength behavior of clayey soil reinforced with human hair as a natural fibre. *Geotechnical and Geological Engineering*, 34(1), pp.411-417.

Cai, Y. et al., 2006. Effect of polypropylene fibre and lime admixture on engineering properties of clayey soil. *Engineering Geology*, 87(3-4), pp.230-240.

Cetin, H., Fener, M. and Gunaydin, O., 2006. Geotechnical properties of tire-cohesive clayey soil mixtures as a fill material. *Engineering Geology*, 88(1-2), pp.110-120.

- Chaduvula, U, Viswanadham, BVS and Kodikara, J. 2017. A study on desiccation cracking behavior of polyester fiber-reinforced expansive clay. *Applied Clay Science*, 142, pp.163-172.
- Chaduvula, U., Manogaran, I., Viswanadham, B.V.S. and Kodikara, J., 2018. Some Studies on Desiccation Cracking of Fiber-Reinforced Expansive Clay Subjected to Drying and Wetting Cycles. In *PanAm Unsaturated Soils 2017*, pp. 361-370.
- Chandra, S., Viladkar, M.N. and Nagrale, P.P., 2008. Mechanistic approach for fiber-reinforced flexible pavements. *Journal of Transportation Engineering*, 134(1), pp.15-23.
- Chebbi, M., Guiras, H. and Jamei, M., 2017. Tensile behaviour analysis of compacted clayey soil reinforced with natural and synthetic fibers: effect of initial compaction conditions. *European Journal of Environmental and Civil Engineering*, 1, pp.1-27.
- Chore, H.S., Kumthe, A.A., Abnave, S.B., Shinde, S.S., Dhole, S.S. and Kamerkar, S.G., 2011. Performance evaluation of polypropylene fibers on sand-fly ash mixtures in highways. *Journal of Civil Engineering (IEB)*, 39(1), pp.91-102.
- Choudhary, A.K., Jha, J.N. and Gill, K.S., 2010. A study on CBR behavior of waste plastic strip reinforced soil. *Emirates Journal for Engineering Research*, 15(1), pp.51-57.
- Consoli, N.C., Heineck, K.S., Casagrande, M.D.T. and Coop, M.R., 2007. Shear strength behavior of fiber-reinforced sand considering triaxial tests under distinct stress paths. *Journal of Geotechnical and Geoenvironmental Engineering*, 133(11), pp.1466-1469.
- Consoli, NC, de Moraes, RR and Festugato, L., 2011. Split tensile strength of monofilament polypropylene fiber-reinforced cemented sandy soils. *Geosynthetics International*, 18(2), pp.57-62.

Corte, A. and Higashi, A., 1964. Experimental research on desiccation cracks in soil (No. RR-66). Cold Regions Research and Engineering Lab Hanover NH.

Cristelo, N., Cunha, V.M., Gomes, A.T., Araújo, N., Miranda, T. and de Lurdes Lopes, M., 2017. Influence of fibre reinforcement on the post-cracking behaviour of a cement-stabilised sandy-clay subjected to indirect tensile stress. *Construction and Building Materials*, 138, pp.163-173.

Crockford, W.W., Grogan, W.P. and Chill, D.S., 1993. Strength and life of stabilized pavement layers containing fibrillated polypropylene. *Transportation Research Record*, 1418 (1), pp.60-66.

Dang, L.C., Fatahi, B. and Khabbaz, H., 2016. Behaviour of expansive soils stabilized with hydrated lime and bagasse fibres. *Procedia Engineering*, 143, pp.658-665.

Dasaka, S.M. and Sumesh, K.S., 2011. Effect of coir fiber on the stress–strain behavior of a reconstituted fine-grained soil. *Journal of Natural Fibers*, 8(3), pp.189-204.

Dash, S.K., Rajagopal, K. and Krishnaswamy, N.R., 2001. Strip footing on geocell reinforced sand beds with additional planar reinforcement. *Geotextiles and Geomembranes*, 19(8), pp.529-538.

Dawson, R.J., Thompson, D., Johns, D., Wood, R., Darch, G., Chapman, L., Hughes, P.N., Watson, G.V., Paulson, K., Bell, S. and Gosling, S.N., 2018. A systems framework for national assessment of climate risks to infrastructure. *Philosophical Transactions of the Royal Society A: Mathematical, Physical and Engineering Sciences*, 376(2121), pp.20170298.

Deb, K. and Narnaware, Y.K., 2015. Strength and compressibility characteristics of fiber-reinforced subgrade and their effects on response of granular fill-subgrade system. *Transportation in Developing Economies*, 1(2), pp.1-9.

- Decagon devices Inc, 2015. WP4C Water Potential Meter. Available: <http://www.decagon.com/en/soils/benchtop-instruments/wp4c-water-potential-meter/>, (accessed 24/04/2019).
- Diambra, A., Russell, A.R., Ibraim, E. and Muir Wood, D., 2007. Determination of fibre orientation distribution in reinforced sands. *G éotechnique*, 57(7), pp.623-628.
- Diambra, A. and Ibraim, E., 2014. Modelling of fibre–cohesive soil mixtures. *Acta Geotechnica*, 9(6), pp.1029-1043.
- Diambra, A., 2010. Fibre reinforced sands: experiments and constitutive modelling (Doctoral dissertation, University of Bristol).
- Diambra, A., Ibraim, E., Wood, D.M. and Russell, A.R., 2010. Fibre reinforced sands: experiments and modelling. *Geotextiles and geomembranes*, 28(3), pp.238-250.
- Di Prisco, C. and Nova, R., 1993. A constitutive model for soil reinforced by continuous threads. *Geotextiles and Geomembranes*, 12(2), pp.161-178.
- Divya, P.V., Viswanadham, B.V.S. and Gourc, J.P., 2013. Evaluation of tensile strength-strain characteristics of fiber-reinforced soil through laboratory tests. *Journal of Materials in civil Engineering*, 26(1), pp.14-23.
- Edil, T.B., Acosta, H.A. and Benson, C.H., 2006. Stabilizing soft fine-grained soils with fly ash. *Journal of Materials in Civil Engineering*, 18(2), pp.283-294.
- Edina, 2019. Digimap of UK. Available: <https://digimap.edina.ac.uk/roam/download/os>, (accessed 25/03/2019).

Ekinci, A. and Ferreira, P.M.V., 2012, May. The undrained mechanical behaviour of a fibre-reinforced heavily over-consolidated clay. In ISSMGE Technical Committee TC 211 International Symposium on Ground Improvement, Brussels, Belgium.

Ekinci, A. and Ferreira, P.M.V., 2012. Effects of fibre reinforcement in the shrinkage behaviour of compacted clay. 3rd International Conference on New Developments in Soil Mechanics and Geotechnical Engineering, Nicosia, North Cyprus.

Ekinci, A., 2016. The mechanical properties of compacted clay from the Lambeth Group using fibre reinforcement (Doctoral dissertation, University College London).

England, H., 2018. Manual of Contract Documents for Highway Works. TSO.

Esna-Ashari, M. and Asadi, M., 2008. A Study on Shear Strength and Deformation of Sandy Soil Reinforced with Tire Cord Wastes. In Geosynthetics in Civil and Environmental Engineering, pp. 355-359.

Estabragh, A.R., Bordbar, A.T. and Javadi, A.A., 2013. A study on the mechanical behavior of a fiber-clay composite with natural fiber. *Geotechnical and Geological Engineering*, 31(2), pp.501-510.

Estabragh, A.R., Soltannajad, K. and Javadi, A.A., 2014. Improving piping resistance using randomly distributed fibers. *Geotextiles and Geomembranes*, 42(1), pp.15-24.

Estabragh, AR, Bordbar, AT and Javadi, AA. 2011. Mechanical behavior of a clay soil reinforced with nylon fibers. *Geotechnical and Geological Engineering*, 29(5), pp.899-908.

Falorca, I.M.C.F.G. and Pinto, M.I.M., 2011. Effect of short, randomly distributed polypropylene microfibrils on shear strength behaviour of soils. *Geosynthetics International*, 18(1), pp.2-11.

Falorca, I.M.C.F.G., Gomes, L.M.F. and Pinto, M.I.M., 2011. A full-scale trial embankment construction with soil reinforced with short randomly distributed polypropylene microfibrils. *Geosynthetics International*, 18(5), pp.280-288.

FIBRESAND Int, 2019. Product data. Available: <http://www.fibresand.com/products/fibresand>, (accessed 25/06/2019).

Fleming, I.R., Sharma, J.S. and Jogi, M.B., 2006. Shear strength of geomembrane–soil interface under unsaturated conditions. *Geotextiles and Geomembranes*, 24(5), pp.274-284.

Fletcher, C.S. and Humphries, W.K., 1991. California bearing ratio improvement of remolded soils by the addition of polypropylene fiber reinforcement. *Transportation Research Record*, 1295(1), pp.80-86.

Forster, A., Hobbs, P.R.N., Cripps, A.C., Entwisle, D.C., Fenwick, S.M.M., Raines, M.R., Hallam, J.R., Jones, L.D., Self, S.J. and Meakin, J.L., 1994. *Engineering geology of British rocks and soils: Gault clay* (Unpublished).

Freilich, B.J., Li, C. and Zornberg, J.G., 2010, May. Effective shear strength of fiber-reinforced clays. In 9th International Conference on Geosynthetics, Brazil, pp.1997-2000.

Freilich, B.J., Kuhn, J.A., Zornberg, J.G. 2008. Desiccation of fiber-reinforced highly plastic clays. *Proceedings of The First Pan American Geosynthetics Conference & Exhibition, Cancun, Mexico*, pp.32-241.

Gao, Z. and Diambra, A., 2020. A Multiaxial Constitutive Model for Fibre-reinforced Sand.

Geotechnique (In Press).

Gao, Z. and Zhao, J., 2012. Evaluation on failure of fiber-reinforced sand. *Journal of Geotechnical and Geoenvironmental Engineering*, 139(1), pp.95-106.

GDS, 2019. Introduction to triaxial testing. Available:

<https://www.gdsinstruments.com/information/white-paper-introduction-to-triaxial-testing>.

(accessed 25/08/2019)

Gelder, C. and Fowmes, G.J., 2015. Mixing and compaction of fibre-and lime-modified cohesive soil. *Proceedings of the Institution of Civil Engineers-Ground Improvement*, 169, pp.98-108.

George KP. 1970. Crack control in cement-treated bases. (Final Report, The University of Mississippi).

Ghavami, K., Toledo Filho, R.D. and Barbosa, N.P., 1999. Behaviour of composite soil reinforced with natural fibres. *Cement and Concrete Composites*, 21(1), pp.39-48.

Ghazavi, M. and Roustaei, M., 2010. The influence of freeze–thaw cycles on the unconfined compressive strength of fiber-reinforced clay. *Cold Regions Science and Technology*, 61(2-3), pp.125-131.

Gray, D.H. and Al-Refeai, T., 1986. Behavior of fabric-versus fiber-reinforced sand. *Journal of Geotechnical Engineering*, 112(8), pp.804-820.

Gray, D.H., 1978. Role of woody vegetation in reinforcing soils and stabilizing slopes. In *Proc. Symp. Soil Reinforcing and Stabilising Techniques*, Sydney, Australia, pp. 253-306.

Gray, DH and Ohashi, H. 1983. Mechanics of fiber reinforcement in sand. *Journal of Geotechnical Engineering*, 109(3), pp.335-353.

Grogan, W.P. and Johnson, W.G., 1994. Stabilization of high plasticity clay and silty sand by inclusion of discrete fibrillated polypropylene fibres for use in pavement. Final Report (No. Tech Rept CPAR-GL-94-2).

Groisman, A. and Kaplan, E., 1994. An experimental study of cracking induced by desiccation. *EPL (Europhysics Letters)*, 25(6), pp.415.

Guido, V.A., Chang, D.K. and Sweeney, M.A., 1986. Comparison of geogrid and geotextile reinforced earth slabs. *Canadian Geotechnical Journal*, 23(4), pp.435-440.

Harianto, T., Hayashi, S., Du, Y.J. and Suetsugu, D., 2008. Effects of fiber additives on the desiccation crack behavior of the compacted Akaboku soil as a material for landfill cover barrier. *Water, Air, and Soil Pollution*, 194(1-4), pp.141-149.

HD 26/06, 2006. Pavement design and maintenance-foundations, volume 7, design manual for roads and bridges (DMRB).

Hejazi, S.M., Sheikhzadeh, M., Abtahi, S.M. and Zadhoush, A., 2012. A simple review of soil reinforcement by using natural and synthetic fibers. *Construction and Building Materials*, 30, pp.100-116.

Highways England (2006) UK Design Manual for Roads & Bridges (DMRB). Highways England, Guildford, UK.

Hossain, M.A., Hossain, M.S. and Hasan, M.K., 2015. Application of jute fiber for the improvement of sub grade characteristics. *American Journal of Civil Engineering*, 3(2), pp.26-30.

Ibrahim, E., Camenen, J.F., Diambra, A., Kairelis, K., Visockaite, L. and Consoli, N.C., 2018. Energy efficiency of fibre reinforced soil formation at small element scale: Laboratory and numerical investigation. *Geotextiles and Geomembranes*, 46(4), pp.497-510.

Ibrahim, E., Diambra, A., Russell, A.R. and Wood, D.M., 2012. Assessment of laboratory sample preparation for fibre reinforced sands. *Geotextiles and Geomembranes*, 34, pp.69-79.

Iryo, T. and Rowe, R.K., 2005. Hydraulic behaviour of soil–geocomposite layers in slopes. *Geosynthetics International*, 12(3), pp.145-155.

Ivanov, V. and Chu, J., 2008. Applications of microorganisms to geotechnical engineering for bioclogging and biocementation of soil in situ. *Reviews in Environmental Science and Bio/Technology*, 7(2), pp.139-153.

Jayasree, P.K., Balan, K., Peter, L. and Nisha, K.K., 2014. Volume change behavior of expansive soil stabilized with coir waste. *Journal of Materials in Civil Engineering*, 27(6), pp.1-8.

Jiang, H., Cai, Y. and Liu, J., 2010. Engineering properties of soils reinforced by short discrete polypropylene fiber. *Journal of Materials in civil Engineering*, 22(12), pp.1315-1322.

Kalkan, E., 2011. Impact of wetting–drying cycles on swelling behavior of clayey soils modified by silica fume. *Applied Clay Science*, 52(4), pp.345-352.

Kaniraj, S.R. and Gayathri, V., 2003. Geotechnical behavior of fly ash mixed with randomly oriented fiber inclusions. *Geotextiles and Geomembranes*, 21(3), pp.123-149.

Kar, R.K., Pradhan, P.K. and Naik, A., 2012. Consolidation characteristics of fiber reinforced cohesive soil. *Electronic Journal of Geotechnical Engineering*, 17, pp.3861-3874.

Kemp, S.J.; Wagner, D.. 2006 The mineralogy, geochemistry and surface area of mudrocks from the London Clay Formation of southern England. Nottingham, UK, British Geological Survey (Unpublished).

Khan FH. 2016. Analysis of the influence of waste polymer on soil subgrade. *International Research Journal of Engineering and Technology*, 3(3), pp.1810-1817.

Khatri, V.N., Dutta, R.K., Venkataraman, G. and Shrivastava, R., 2016. Shear strength behaviour of clay reinforced with treated coir fibres. *Periodica Polytechnica Civil Engineering*, 60(2), pp.135-143.

Kolay, P.K. and Pui, M.P., 2010. Peat stabilization using gypsum and fly ash. *Journal of Civil Engineering, Science and Technology*, 1(2), pp.1-5.

Kumar, A, Walia, BS, Mohan, J. 2006. Compressive strength of fiber reinforced highly compressible clay. *Construction and Building Materials*, 20(10), pp.1063-1068.

Kumar, R., Kanaujia, V.K. and Chandra, D., 1999. Engineering behaviour of fibre-reinforced pond ash and silty sand. *Geosynthetics International*, 6(6), pp.509-518.

Leflaive, E., 1988. TEXSOL: Already more than 50 successful applications. In *Proceedings of the International Geotechnical Symposium on Earth Reinforcement*, 1, pp. 541-545.

- Leung M and Vipulanandan C. 1995. Treating contaminated, cracked and permeable field clay with grouts. In Proceedings of the Specialty Conference on Geotechnical Practice in Waste Disposal. New York. pp. 829-843.
- Li C., 2005 Mechanical response of fiber-reinforced soil (Doctoral dissertation, University of Texas at Austin).
- Li, C. and Zornberg, J.G., 2012. Mobilization of reinforcement forces in fiber-reinforced soil. *Journal of Geotechnical and Geoenvironmental Engineering*, 139(1), pp.107-115.
- Lindh, E. and Eriksson, L., 1991. T5/2 Sand reinforced with plastic fibres. A field experiment. In *Performance of reinforced soil structures*, pp. 471-473.
- Li, X.S. and Dafalias, Y.F., 2002. Constitutive modeling of inherently anisotropic sand behavior. *Journal of Geotechnical and Geoenvironmental Engineering*, 128(10), pp.868-880.
- Lo, K.W., Ooi, P.L. and Lee, S.L., 1990. Unified approach to ground improvement by heavy tamping. *Journal of Geotechnical Engineering*, 116(3), pp.514-527.
- Loehr, J.E., Axtell, P.J. and Bowders, J.J., 2000. Reduction of soil swell potential with fiber reinforcement. In *International Society for Rock Mechanics and Rock Engineering Symposium*. Melbourne, Australia.
- Machado, S.L., Carvalho, M.F. and Vilar, O.M., 2002. Constitutive model for municipal solid waste. *Journal of Geotechnical and Geoenvironmental Engineering*, 128(11), pp.940-951.
- Maher, M.H. and Gray, D.H., 1990. Static response of sands reinforced with randomly distributed fibers. *Journal of Geotechnical Engineering*, 116(11), pp.1661-1677.

Maher, M. H., and Y. C. Ho. 1993. Behaviour of Fibre-Reinforced Cemented Sand under Static and Cyclic Loads. *Geotechnical Testing Journal*, 16 (3), pp.330-338.

Maher, M.H. and Ho, Y.C., 1994. Mechanical properties of kaolinite/fiber soil composite. *Journal of Geotechnical Engineering*, 120(8), pp.1381-1393.

Maheshwari, K., Desai, A.K. and Solanki, C.H., 2011. Application and modeling of fiber reinforced soil. In *Proceedings of Indian Geotechnical Conference*, pp.15-17.

Maity, J., Chattopadhyay, B.C. and Mukherjee, S.P., 2018. Improvement of Characteristics of Clayey Soil Mixed with Randomly Distributed Natural Fibers. *Journal of The Institution of Engineers (India) Series A*, 99(1), pp.55-65.

Makiuchi, K. and Minegishi, K., 2001. Strain-induced toughness and shearing characteristics of short-fiber reinforced soils. In *Proceedings of the International Symposium on Earth Reinforcement*. Lisse, the Netherlands, pp. 83-88.

Malekzadeh, M. and Bilsel, H., 2012. Effect of polypropylene fiber on mechanical behavior of expansive soils. *The Electronic Journal of Geotechnical Engineering*, 17, pp.55-63.

Maliakal, T. and Thiyyakkandi, S., 2013. Influence of randomly distributed coir fibers on shear strength of clay. *Geotechnical and Geological Engineering*, 31(2), pp.425-433.

Mandolini, A., Diambra, A. and Ibraim, E., 2019. Strength anisotropy of fibre-reinforced sands under multiaxial loading. *G éotechnique*, 69(3), pp.203-216.

Marandi, S.M., Bagheripour, M.H., Rahgozar, R. and Zare, H., 2008. Strength and ductility of randomly distributed palm fibers reinforced silty-sand soils. *American Journal of Applied Sciences*, 5(3), pp.209-220.

Masoumi, E., Forooshani, S.M.A. and Nian, F.A., 2013. Problematic soft soil improvement with both polypropylene fiber and polyvinyl acetate resin. *Geotechnical and Geological Engineering*, 31(1), pp.143-149.

Mesbah, A., Morel, J.C., Walker, P. and Ghavami, K., 2004. Development of a direct tensile test for compacted earth blocks reinforced with natural fibers. *Journal of Materials in Civil Engineering*, 16(1), pp.95-98.

Michalowski, R.L., 1997. Limit stress for granular composites reinforced with continuous filaments. *Journal of Engineering Mechanics*, 123(8), pp.852-859.

Michalowski RL and Cermak J., 2003. Triaxial compression of sand reinforced with fibers. *Journal of Geotechnical and Geoenvironment Engineering*, 129(2), pp.125-136.

Michalowski, R.L. and Zhao, A., 1996. Failure of fiber-reinforced granular soils. *Journal of Geotechnical Engineering*, 122(3), pp.226-234.

Miller, C.J, Mi, H and Yesiller, N. 1998. Experimental analysis of desiccation crack propagation in clay liners. *Journal of the American Water Resources Association*, 34(3), pp.677-686.

Miller, C.J. and Rifai, S., 2004. Fiber reinforcement for waste containment soil liners. *Journal of Environmental Engineering*, 130(8), pp.891-895.

Mirzababaei, M.E.H.D.I., 2012. Reinforcement of clay soils using waste carpet fibres (Doctoral dissertation, University of Bolton).

Mirzababaei, M., Arulrajah, A., Haque, A., Nimbalkar, S. and Mohajerani, A., 2018. Effect of fiber reinforcement on shear strength and void ratio of soft clay. *Geosynthetics International*, 25(4), pp.471-480.

Mirzababaei, M., Arulrajah, A., Horpibulsuk, S. and Aldava, M., 2017. Shear strength of a fibre-reinforced clay at large shear displacement when subjected to different stress histories. *Geotextiles and Geomembranes*, 45(5), pp.422-429.

Mirzababaei, M., Miraftab, M., Mohamed, M. and McMahon, P., 2012. Unconfined compression strength of reinforced clays with carpet waste fibers. *Journal of Geotechnical and Geoenvironmental Engineering*, 139(3), pp.483-493.

Mirzababaei, M., Mohamed, M. and Miraftab, M., 2016. Analysis of strip footings on fiber-reinforced slopes with the aid of particle image velocimetry. *Journal of Materials in Civil Engineering*, 29(4), pp.1-14.

Mishra, AK and Ravindra V (2015) On the utilization of fly ash and cement mixtures as a landfill liner material. *International Journal of Geosynthetics and Ground Engineering*, 1(2), pp.17.

Mitchell, M (2019) Personal communication.

Naeini, S.A. and Sadjadi, S.M., 2008. Effect of waste polymer materials on shear strength of unsaturated clays. *The Electronic Journal of Geotechnical Engineering*, 13, pp.1-12.

- Nasr, A.M., 2014. Behavior of strip footing on fiber-reinforced cemented sand adjacent to sheet pile wall. *Geotextiles and Geomembranes*, 42(6), pp.599-610.
- Neeraja, V.S., Geetha Manjari, K. and Sivakumar Babu, G.L., 2014. Numerical analysis of effect of orientation of fibers on stress–strain response of fiber reinforced soil. *International Journal of Geotechnical Engineering*, 8(3), pp.328-334.
- Oakey, 2019. Product information. Available: <http://www.oakey-abrasive.co.uk/products/liberty-green/>, (accessed 25/03/2019).
- Oliveira, P.V., Correia, A.A.S., Teles, J.M.N.P.C. and Custódio, D.G., 2016. Effect of fibre type on the compressive and tensile strength of a soft soil chemically stabilised. *Geosynthetics International*, 23(3), pp.171-182.
- Omidi GH, Prasad TV and Thomas JC. 1996. Influence of amendments on the volumetric shrinkage and integrity of compacted clay soils used in landfill liners. *Water Air Soil Pollution*, 86, pp.263-274.
- Özkul, Z.H. and Baykal, G., 2007. Shear behavior of compacted rubber fiber-clay composite in drained and undrained loading. *Journal of Geotechnical and Geoenvironmental Engineering*, 133(7), pp.767-781.
- Park, S.S., 2011. Unconfined compressive strength and ductility of fiber-reinforced cemented sand. *Construction and Building Materials*, 25(2), pp.1134-1138.
- Park, T. and Tan, S.A., 2005. Enhanced performance of reinforced soil walls by the inclusion of short fiber. *Geotextiles and Geomembranes*, 23(4), pp.348-361.

- Patel, S.K. and Singh, B., 2019. Shear strength response of glass fibre-reinforced sand with varying compacted relative density. *International Journal of Geotechnical Engineering*, 13(4), pp.339-351.
- Peron, H., Hueckel, T., Laloui, L. and Hu, L., 2009. Fundamentals of desiccation cracking of fine-grained soils: experimental characterisation and mechanisms identification. *Canadian Geotechnical Journal*, 46(10), pp.1177-1201.
- Phanikumar, B.R. and Singla, R., 2016. Swell-consolidation characteristics of fibre-reinforced expansive soils. *Soils and Foundations*, 56(1), pp.138-143.
- Ple, O. and Lê T.N.H., 2012. Effect of polypropylene fiber-reinforcement on the mechanical behavior of silty clay. *Geotextiles and Geomembranes*, 32, pp.111-116.
- Powrie W., 2004. *Soil mechanics: concepts and applications*. Spon Press. Oxon, UK.
- Prabakar, J. and Sridhar, R.S., 2002. Effect of random inclusion of sisal fibre on strength behaviour of soil. *Construction and Building Materials*, 16(2), pp.123-131.
- Pradani, N, Irdhiani, Wibowo, J., 2017. Analysis of local sanded soil with coconut coir fiber reinforcement as subgrade on structural pavement. *International Journal of Civil Engineering and Technology*, 8, pp.787-795.
- Pradhan, P.K., Kar, R.K. and Naik, A., 2012. Effect of random inclusion of polypropylene fibers on strength characteristics of cohesive soil. *Geotechnical and Geological Engineering*, 30(1), pp.15-25.
- Punthutaecha, K. et al., 2007. Volume Change Behaviors of Expansive Soils Stabilized with Recycled Ashes and Fibers. *Journal of Materials in Civil Engineering*, 19(7), pp.616–617.

Punthutaecha, K., Puppala, A.J., Vanapalli, S.K. and Inyang, H., 2006. Volume change behaviors of expansive soils stabilized with recycled ashes and fibers. *Journal of Materials in Civil Engineering*, 18(2), pp.295-306.

Puppala, A.J. and Musenda, C., 2000. Effects of fiber reinforcement on strength and volume change in expansive soils. *Transportation Research Record*, 1736(1), pp.134-140.

Qu, J, Li, C, Liu, B, Chen, X, Li, M and Yao, Z. 2013. Effect of random inclusion of wheat straw fibers on shear strength characteristics of shanghai cohesive soil. *Geotechnical and Geological Engineering*, 31(2), pp.511-518.

Ranjan, G., Vasani, R.M. and Charan, H.D., 1994. Behaviour of plastic-fibre-reinforced sand. *Geotextiles and Geomembranes*, 13(8), pp.555-565.

Ranjan, G., Vasani, R.M. and Charan, H.D., 1996. Probabilistic analysis of randomly distributed fiber-reinforced soil. *Journal of Geotechnical Engineering*, 122(6), pp.419-426.

RS Minerals Ltd., 2015. Product information. Available: <https://www.rsminerals.co.uk/bentonite/>, (accessed 25/05/2019).

SAAD Suleiman S E, 2016. Mechanical behaviour of fibre reinforced unsaturated clay. (Doctoral dissertation, University of Bradford).

Sadek, S., Najjar, S.S. and Freiha, F., 2010. Shear strength of fiber-reinforced sands. *Journal of Geotechnical and Geoenvironmental Engineering*, 136(3), pp.490-499.

Sanger, F.J., 1968. Ground freezing in construction. *Journal of the Soil Mechanics and Foundations Division*, 94(1), pp.131-158.

- Santhi Krishna, K. and Sayida, M.K., 2010. Behaviour of black cotton soil reinforced with sisal fibre. On 10th National Conference on Technological Trends, pp.88-93.
- Santoni, R.L. and Webster, S.L., 2001. Airfields and roads construction using fiber stabilization of sands. *Journal of Transportation Engineering*, 127(2), pp.96-104.
- Santoni, R.L., Tingle, J.S. and Webster, S.L., 2001. Engineering properties of sand-fiber mixtures for road construction. *Journal of Geotechnical and Geoenvironmental Engineering*, 127(3), pp.258-268.
- Sarbaz, H., Ghiassian, H. and Heshmati, A.A., 2014. CBR strength of reinforced soil with natural fibres and considering environmental conditions. *International Journal of Pavement Engineering*, 15(7), pp.577-583.
- Savastano Jr, H., Warden, P.G. and Coutts, R.S.P., 2000. Brazilian waste fibres as reinforcement for cement-based composites. *Cement and Concrete Composites*, 22(5), pp.379-384.
- Şenol, A., 2012. Effect of fly ash and polypropylene fibres content on the soft soils. *Bulletin of Engineering Geology and the Environment*, 71(2), pp.379-387.
- Sharma, V and Kumar, A. 2017. Strength and bearing capacity of ring footings resting on fibre-reinforced sand. *International Journal of Geosynthetics and Ground Engineering*, 3(9), pp.1-17.
- Sherwood, P.T., 1962. Effect of sulfates on cement-and lime-stabilized soils. *Highway Research Board Bulletin*, (353),pp.98-107.
- Shukla, S.K., Shahin, M.A. and Abu-Taleb, H., 2015. A note on void ratio of fibre-reinforced soils. *International Journal of Geosynthetics and Ground Engineering*, 1(3), pp.1-5.

Shukla, S.K., Sivakugan, N. and Singh, A.K., 2010. Analytical model for fiber-reinforced granular soils under high confining stresses. *Journal of Materials in Civil Engineering*, 22(9), pp.935-942.

Singh, H.P. and Bagra, M., 2013. Improvement in CBR value of soil reinforced with jute fiber. *International Journal of Innovative Research in Science, Engineering and Technology*, 2(8), pp.3447-3452.

Sivakumar Babu, G.L. and Vasudevan, A.K., 2008. Strength and stiffness response of coir fiber-reinforced tropical soil. *Journal of Materials in Civil Engineering*, 20(9), pp.571-577.

Skempton, A.W., 1954. The pore-pressure coefficients A and B. *Géotechnique*, 4(4), pp.143-147.

Soltani, A, Taheri, A, Deng, A and Nikraz, H. 2018. Tyre rubber and expansive soils: Two hazards, one solution. *Proceedings of the Institution of Civil Engineers-Construction Materials* (published online ahead of print), pp.1-17.

Soltani-Jigheh, H. and Rasulifard, A., 2016. Assessing the Potential Improvement of Fine-grained Clayey Soils by Plastic Wastes. *Soils and Rocks*, 39(3), pp.333-339.

Sonthwal V and Sahni D, 2015. Subgrade Soil Improvement Using Jute Fiber. *International Journal of Emerging Technology and Advanced Engineering*, 5(6), pp.237-240.

Soriano, I., Ibraim, E., Ando, E., Diambra, A., Laurencin, T., Moro, P. and Viggiani, G., 2017. 3D fibre architecture of fibre-reinforced sand. *Granular Matter*, 19(4), pp.75.

Standard, B., 5930, 1981. Code of Practice for Site Investigations. British Standards Institution, London, pp.147.

- Stirling, R.A., 2014. Multiphase modelling of desiccation cracking in compacted soil (Doctoral dissertation, Newcastle University).
- Stirling, R.A., Hughes, P., Davie, C.T. and Glendinning, S., 2015. Tensile behaviour of unsaturated compacted clay soils- A direct assessment method. *Applied Clay Science*, 112, pp.123-133.
- Tang, C., Shi, B., Gao, W., Chen, F. and Cai, Y., 2007. Strength and mechanical behavior of short polypropylene fiber reinforced and cement stabilized clayey soil. *Geotextiles and Geomembranes*, 25(3), pp.194-202.
- Tang, CS, Shi, B, Cui, YJ, Liu, C. and Gu, K. 2012. Desiccation cracking behavior of polypropylene fiber–reinforced clayey soil. *Canadian Geotechnical Journal*, 49(9), pp.1088-1101.
- Tang, C.S., Wang, D.Y., Cui, Y.J., Shi, B. and Li, J., 2016. Tensile strength of fiber-reinforced soil. *Journal of Materials in Civil Engineering*, 28(7), pp.04016031.
- TDP.Ltd, 2019. Product information. Available: <https://www.tdpltd.com/our-products/concrete-and-screed-fibres>, (accessed 25/03/2019).
- TEXSOL.Ltd, 2019. Product information. Available: <http://www.eiffageinfrastructures.com/en/home/produits/texsol.html>, (accessed 25/03/2019).
- Thusyanthan, NI, Take, WA, Madabhushi, SPG and Bolton, MD., 2007. Crack initiation in clay observed in beam bending. *G éotechnique*, 57(7), pp.581-594.
- Tingle, J.S., Santoni, R.L. and Webster, S.L., 2002. Full-scale field tests of discrete fiber-reinforced sand. *Journal of Transportation Engineering*, 128(1), pp.9-16.

- Tran, K.Q., Satomi, T. and Takahashi, H., 2019. Tensile behaviors of natural fiber and cement reinforced soil subjected to direct tensile test. *Journal of Building Engineering*, 24, pp.100748.
- Velde, B., 1999. Structure of surface cracks in soil and muds. *Geoderma*, 93(1-2), pp.101-124.
- Vidal, H., 1969. The principle of reinforced earth. *Highway Research Record*, (282), pp.1-16.
- Viswanadham, B.V.S., Phanikumar, B.R. & Mukherjee, R. V., 2009. Swelling behaviour of a geofiber-reinforced expansive soil. *Geotextiles and Geomembranes*, 27(1), pp.73-76.
- Viswanadham, BVS, Jha, BK and Pawar, SN, 2010. Influence of geofibers on the flexural behavior of compacted soil beams. *Geosynthetics International*, 17(2), pp.86-99.
- Waldron, L.J., 1977. The shear resistance of root-permeated homogeneous and stratified soil 1. *Soil Science Society of America Journal*, 41(5), pp.843-849.
- Wang, M.C., Benway, J.M. and Arayssi, A.M., 1990. The effect of heating on engineering properties of clays. In *Physico-Chemical Aspects of Soil and Related Materials*, pp.139-158.
- Wang, Y., Guo, P., Lin, H., Li, X., Zhao, Y., Yuan, B., Liu, Y. and Cao, P., 2019. Numerical analysis of fiber-reinforced soils based on the equivalent additional stress concept. *International Journal of Geomechanics*, 19(11), pp.04019122.
- Wu, T.H., Beal, P.E. and Lan, C., 1988. In-situ shear test of soil-root systems. *Journal of Geotechnical Engineering*, 114(12), pp.1376-1394.
- Xue, Q, Hai-jun, L, Zhen ze, L. and Lei, L. 2014. Cracking, water permeability and deformation of compacted clay liners improved by straw fibre. *Engineering Geology*, 178, pp.82-90.

Yaghoubi, M., Shukla, S.K. and Mohyeddin, A., 2018. Effects of addition of waste tyre fibres and cement on the engineering behaviour of Perth sand. *Geomechanics and Geoengineering*, 13(1), pp.42-53.

Yang, Z., 1972. Strength and deformation characteristics of reinforced sand. (Doctoral dissertation, University of California).

Yao, Y. P., Lu, D. C., Zhou, A. N., and Zou, B., 2004. Generalized nonlinear strength theory and transformed stress space. *Science in China Series E Technological Sciences*, 47(6), pp.691-709.

Yesiller, N., Miller, C.J., Inci, G. and Yaldo, K., 2000. Desiccation and cracking behavior of three compacted landfill liner soils. *Engineering Geology*, 57(1-2), pp.105-121.

Yetimoglu, T. and Salbas, O., 2003. A study on shear strength of sands reinforced with randomly distributed discrete fibers. *Geotextiles and Geomembranes*, 21(2), pp.103-110.

Yong, R. N., and B. P. Warkentin. 1975. *Introduction to Soil Behavior: Soil Properties and Behaviour*. New York: Elsevier.

Zaimoglu, A.S. and Yetimoglu, T., 2012. Strength behavior of fine grained soil reinforced with randomly distributed polypropylene fibers. *Geotechnical and Geological Engineering*, 30(1), pp.197-203.

Ziegler, S, Leshchinsky, D, Ling, HI and Perry, EB. 1998. Effect of short polymeric fibers on crack development in clays. *Soils and Foundations*, 38(1), pp.247-253.

Zornberg, J.G., 2002. Discrete framework for limit equilibrium analysis of fibre-reinforced soil. *Géotechnique*, 52(8), pp.593-604.